# STUDY OF BLUE EMITTING ELECTROLUMINESCENT DEVICES

**SHAN CHUAN, LIEW**

A thesis submitted in partial fulfilment of the requirements of

The Nottingham Trent University for the degree of

Doctor of Philosophy

School of Engineering

Electrical and Electronic Engineering Divisions

The Nottingham Trent University

**February 2003**

## ABSTRACT

The main aim for this work is to enhance the luminescent efficiency of the blue emitting SrS:Cu,Ag thin films. The initial phase of the study was to establish suitable parameters for the fabrication of SrS:Cu,Ag thin films utilising the rf magnetron sputter deposition technique. Conventional thermal based post deposition annealing, although found capable of improving the photoluminescence properties of the resulting SrS:Cu,Ag films, was however not suitable for the electroluminescence study of these films. In order to avoid this high temperature process, extensive experiments of an alternative form of annealing utilising laser pulse irradiation was carried out. The laser utilized for the investigation was a KrF laser at the Central Laser Facility at the Rutherford Appleton Laboratory. Optimization of the laser annealing process found that the effect of laser annealing SrS:Cu,Ag thin films was highly dependant on the laser fluence and the number of laser irradiation pulses. Laser annealed devices were found to electrically luminesce by a factor of 3 over conventional thermally annealed devices. The study of improving the luminescent properties by structure modification was also carried out by incorporating a thin insulating layer within the phosphor layer of the ACTFEL structure. These barrier layer devices were found to enhance the overall luminance of the device by improving the impact ionization mechanism of SrS:Cu,Ag ACTFEL devices. The detailed study of laser annealing and barrier layer devices has lead to the potential commercial fabrication of an ACTFEL device with the benefit of barrier layer characteristic but without the need of incorporating the crucial thin insulating layer within the phosphor layer.

## ACKNOWLEDGEMENTS

The work described in this thesis was carried out during the tenure of a research studentship in the Electrical and Electronic Engineering division (School of Engineering) at the Nottingham Trent University.

I have benefited from the support of many individuals during the course of completing this thesis. In particular, my most sincere thanks go to the following member of the Electrical and Electronic Engineering division at the Nottingham Trent University.

Prof. Clive B. Thomas and Dr. Wayne C. Cranton, my supervisor, for giving the opportunity to undertake this stuffy and also countless hours of discussion together with their support and guidance.

Mr. Demosthenes C. Koutsogeorgis for his unending drive, enthusiastic discussion and particularly assistant in laser annealing.

Dr. Costas Tsakonas, Dr. Robert Ranson, Dr. Mark Craven, Dr. E.A. Mastion, Dr. S. Otero Barros, Dr. Murugesan Sethu and Mr Tae Sung Nam for their contribution and support.

Finally, the completion of this thesis would not have been possible without the unending love, support and encouragement from my family. My brother, Paul Liew for taking care of things back home, and my parents for their love and affection.

## LIST OF PUBLICATIONS

*Pulsed KrF laser annealing of blue emitting SrS:Cu,Ag thin films*

S.C. Liew, D.C. Koutsogeorgis, W.M. Cranton and C.B. Thomas
Electronic Letters, Vol. 38, No. 23, pp. 1466-8, Nov. 2002

*Thin film electroluminescent devices based on SrS:Cu,Ag.*

S.C. Liew, D.C. Koutsogeorgis, W.M. Cranton and C.B. Thomas
Proceedings of EL 2002, Ghent, Belgium, Sep. 2002

*Laser annealing of inorganic thin film phosphors.*

D.C. Koutsogeorgis, B. Nassuna, S.C. Liew, R.M. Ranson, W.M. Cranton and C.B. Thomas
Proceedings of EL 2002, Ghent, Belgium, Sep. 2002

*Pulsed KrF laser annealing of R.F. magnetron sputtered SrS:Cu,Ag thin films*

S.C. Liew, D.C. Koutsogeorgis, W.M. Cranton and C.B. Thomas
Proceedings of the 7th Asian Symposium on Information Displays, ASID'02, Singapore, Sep. 2002

*Miniature Transverse TFEL Displays*
W.M. Cranton, C.B. Thomas, D.C. Koutsogeorgis, R.M. Ranson, S.C. Liew, C. Tsakonas, M.Sethu.
Proceedings of the International Display Manufacturing Conference, seoul, 2002.

*Laser processing of thin film phosphors for flat panel displays*

W.M. Cranton, D.C. Koutsogeorgis, S. Liew, B. Nassuna, R. Ranson and C.B. Thomas
CLF Annual Report 2001/2002

*Optically transparent frequency selective window for microwave applications*

C. Tsakonas, S.C. Liew, C. Mias, D.C. Koutsogeorgis, R.M. Ranson, W.M. Cranton and M. Dudhia
Electronics Letters IEE, Vol. 37, No. 24, pp. 1464-6, Nov. 2001

*Materials processing and device Engineering for Laterally Emitting Thin Film Electroluminescent Miniature Displays.*

W.M. Cranton, C.B. Thomas, D.C. Koutsogeorgis, E. Mastio, M. Craven, R. Stevens, R. Ranson, M. Sethu, J. Rudiger, S. Barros, A. Liew, C. Tsaskonas and P. Theng
Proceedings of the SID Microdisplay Conference 2001, Colorado U.S.A., Aug. 2001

*Highly conductive ITO coating for Frequency Selective Structures,*
C. Tsakonas, C. Mias, S.C. Liew, C. Oswald, D.C. Koutsogeorgis, W. M. Cranton and M. Dudhia
Proceedings of Telematics Automotive 2001, Birmingham, pp. 3/10-3/15

*Optically transparent microstrip antennas*

C. Mias, C. Tsakonas, N. Prountzos, D.C. Koutsogeorgis, S.C. Liew, C. Oswald, R. Ranson, W.M. Cranton and C.B. Thomas
IEE colloquium on antennas for Automotives, Ref. No.00/002, pp. 8/1-6, 2000

## TABLE OF CONTENTS

**CHAPTER 2**

**TFEL TECHNOLOGY, NOVEL DEVICES & PROCESSING**



**CHAPTER 3**

**EXPERIMENTAL DETAIL**

**CHAPTER 4**

**GROWTH & CHARACTERISATION OF SrS THIN FILMS**

**CHAPTER 5**

**LASER ANNEALING OF SrS:Cu,Ag**



**CHAPTER 6**

**BARRIER LAYER SrS:Cu,Ag DEVICES**

**CHAPTER 7**

**CONCLUSIONS AND FUTURE WORK**



**CHAPTER 8**

**APPENDIXES**

## LIST OF ABBREVIATIONS

| | |
|---|---|
| °C | Degree Centrigate |
| Å | Angstroms |
| a.c. | Alternating Current |
| a.u. | Arbitrary Unit |
| ACTFEL | Alternating Current Thin Film Electro-Luminescent |
| Ag | Silver |
| Al | Aluminium |
| ALE | Atomic Layer Epitaxy |
| AMEL | Active Matrix Electro-Luminescent |
| Ar | Argon |
| Au | Gold |
| $BaAl_2S_4$:Eu | Europium activated Barium Thioaluminate |
| BL | Barrier Layer |
| BV | Brightness Voltage |
| CaS:Pb | Lead doped Calcium Sulphide |
| Ce | Cerium |
| Cd | candelas |
| CIE | Commission Internationale de I'Eclairage |
| $cm^{-2}$ | per Centimetre Square |
| CLF-RAL | Central Laser Facility of Rutherford Appleton Laboratory |
| CRT | Cathode Ray Tube |
| Cu | Copper |
| CVD | Chemical Vapour Deposition |
| DC | Direct Current |
| DMD | Digital Micromirror Device |
| E-Beam | Electron Beam |
| EL | Electroluminescence |
| EP | Electrophotography Printing |
| ETL | Electron Transport Layer |
| eV | electron Volts |
| FED | Field Emission Display |

| | |
|---|---|
| FPT | Flat Panel Display |
| $H_2S$ | Hydrogen Sulphide |
| HF-EL | High Field Electroluminescent |
| HMD | Head Mounted Display |
| HTL | Hole Transport Layer |
| Hz | Hertz |
| IT | Information Technology |
| ITO | Indium Tin Oxide |
| J | Joule |
| KrF | Kryton Fluoride |
| LA | Laser Annealing |
| LASER | Light Amplification by Stimulated Emission of Radiation |
| LCD | Liquid Crystal Display |
| LED | Light Emitting Diode |
| LETFEL | Lateral Emitting Thin Film Electro-Luminescent |
| lm | lumens |
| MBE | Molecular Beam Epitaxy |
| Mn | Manganese |
| mm | millimetre |
| $N_2$ | Nitrogen |
| NTU | Nottingham Trent University |
| ns | nano second |
| $O_2$ | Oxygen |
| OEL | Organic Electroluminescence |
| OLED | Organic Light Emitting Diode |
| PC | Personal Computer |
| PDP | Plasma Display Panels |
| PL | Photo-Luminescence |
| PLED | Polymer Light Emitting Diode |
| PM | Premature Emission |
| psi | pound per square inch |
| PVD | Physical Vapour Deposition |
| rf | radio frequency |
| RIA | Rapid Isothermal Annealing |

| | |
|---|---|
| RIE | Reactive Ion Etching |
| RTA | Rapid Thermal Annealing |
| s | second |
| SEM | Scanning Electron Microscope |
| Si | Silicon |
| $SiO_2$ | Silicon Dioxide |
| SID | Society of Information Display |
| SMLED | Small Molecule Light Emitting Diode |
| SrS | Strontium Sulphide |
| SrS:Ce | Strontium Sulphide doped with Cerium |
| SrS:Cu,Ag | Strontium Sulphide doped Copper and Silver |
| TDEL | Thick Dielectric Electroluminescene |
| TEE | Trailing Edge Emission |
| TNTU | The Nottingham Trent University |
| TFD | Thin Film Diodes |
| TFEL | Thin Film Electro-Luminescence |
| TI | Texas Instrument |
| Torr | Torricelli |
| TV | Television |
| UV | Ultraviolet |
| $V_{p-p}$ | Volt peak to peak |
| VFD | Vacuum Florescent Displays |
| W | watt |
| XeCl | Xenon Chloride |
| XRD | X-Ray Diffraction |
| $Y_2O_3$ | Yttrium Oxide |
| ZnS | Zinc Sulphide |
| ZnS:Cu | Zinc Sulphide Copper |
| ZnS:Mn | Zinc Sulphide doped with Manganese |

# CHAPTER 1

# INTRODUCTION

## 1.1 AIM AND OBJECTIVE

Flat Panel Display (FPD) technology is a 30 billion US dollar growth market, currently dominated by liquid crystal displays. Although over four decades old now, Thin Film Electroluminescene (TFEL) has been of commercial and scientific interest in the field of emissive flat panel display technology, attributed to it's ruggedness, solids state, high operation speed, wide operating temperature range, high contrast, high viewing angle and long lifetime. However until today, electroluminescent displays still occupy less then 1% of the total flat panel display market. This is mainly due to the lack of an efficient blue emitting phosphor, hence hampering the advancement of Thin Film Electroluminescene (TFEL) technology, typically in the realisation of full colour devices.

The aim of this PhD work is to investigate a mean for enhancing the luminescent efficiency of a suitable blue emitting electroluminescence phosphor to be utilised in TFEL display devices. A primary investigation into potential blue emitting phosphors was carried out. This has been followed by the determination of the most promising phosphor for the required application. A fabrication path utilising commercial favoured magnetron sputtering of the chosen phosphor thin film was determined and presented. Commissioning the necessary equipment plus the calibrations of the sputtering parameters of the thin films were undertaken. Devices were fabricated based on two proposed mechanisms for the improvement of the phosphor efficiency and device stability was examined. The results from the fabricated devices were compared with conventional devices.

Additional work was performed on identifying a suitable, and alternative, dry etching technique to be utilised in the fabrication of Lateral Emitting Thin Film Electroluminescent (LETFEL) displays. Such devices provide the only solid state display for head mounted operation with the image superimposed on the scene observed by the eye.

## 1.2 SUMMARY OF THESIS

The first chapter of the thesis is a general review chapter. It starts with a general overview of all display technology broken down into two main categories, emissive and non emissive display. This is followed by the author's prediction of the future trend for flat panel displays.

Chapter 2 is a review of TFEL technology and device improvement during the past twenty years.

Chapter 3 will describe the successful fabrication path and also the various post deposition techniques utilised for the fabrication of the blue emitting thin film devices. It will also detail the techniques used for characterisation of the fabricated device.

The parameters for the growth and fabrication of the chosen thin films will be discussed in chapter 4. This also includes the parameters for device improvement utilising conventional thermal based post deposition techniques.

Due to the requirement of high temperature post deposition techniques, novel laser annealing was employed in order to fabricate devices due to the absence of such high temperature processes. Chapter 5 will concentrate on the effect of various laser annealing parameters on the characteristic of the chosen blue emitting thin film devices.

Previous experiments from The Nottingham Trent University display group on manganese doped zinc sulphide has shown that by introducing an additional layer within the phosphor layer of TFEL devices, namely a barrier layer, can result in device performance improvement compared to conventional devices. Hence a similar layer had been introduced into the blue emitting TFEL devices. Chapter 6 will be describing the effect of such a layer on the blue emitting TFEL devices. In addition, the outcome of laser annealing various layer of the phosphor will also be presented in this chapter.

Finally, chapter 7 will provide a summary of the work, as well as achievement from the work performed. In addition, some possible future work is proposed in order to improve the overall performance of the blue emitting TFEL.

To facilitate continuity description of plasma etching of various films utilised in both TFEL and LETFEL devices is described in Appendix A.

## 1.3 OVERVIEW OF THE DISPLAY TECHNOLOGY

When we talk about display technology, most people think about computer screens or television. Yet we rely even more on displayed information for all our daily activities. From the first cup of coffee in the morning to the alarm we set before going off to sleep. In fact, there is no modern electronic device today that comes without a display. Before the invention of Cathode Ray Tube (CRT) and subsequently the Television (TV) in the late ninetieth century, displays were non emissive and non electronic. This constrained display technology to high luminance ambience, low speed and low information content. Reminiscences of such display are still available nowadays such as road signs, billing meters, posters, airport information panels and much more. However, with the arrival of the 21$^{st}$ century, current existing display technology can no longer satisfy the demand from the information hungry society. If truth be told, we live in an age in which displays are visually inadequate for many of the uses to which we put them. The invention of computers and the advancement in communication have been the main contributors for the creation of such an information hungry society. The power of today's computers rival those of yesterday's mainframes while communication has emerged from a few 'car phones' to a state whereby anybody can be contacted independent of their location. Twenty years ago, the CRT based display system had been more than adequate for the first rudiments of personal computers (PC). Today, only the best CRTs and liquid crystal displays (LCD) are reasonable for desktop computers but they are barely passable for application on laptop computers, personal digital assistants (PDA), and mobile phones. The display requirement for such modern tools can only barely be satisfied by the utilisation of flat panel display technology.

According to iSuppli/Stanford Resources[1] as shown in figure 1.1, the forecast is that the global display market is expected to reach over US$65 billion this year and is expected to have grown to over US$ 80 billion by the year 2005. Flat Panel Displays (FPDs) cover over 50% of the total display markets, with over US$ 35 billion in 2002 and is expected to grow to almost US$ 60 billion in the next 3 years time. Evidently, the FPD market is one of the fastest or even the only growing electronic business segment despite the burst of the Information Technology (IT) bubble.

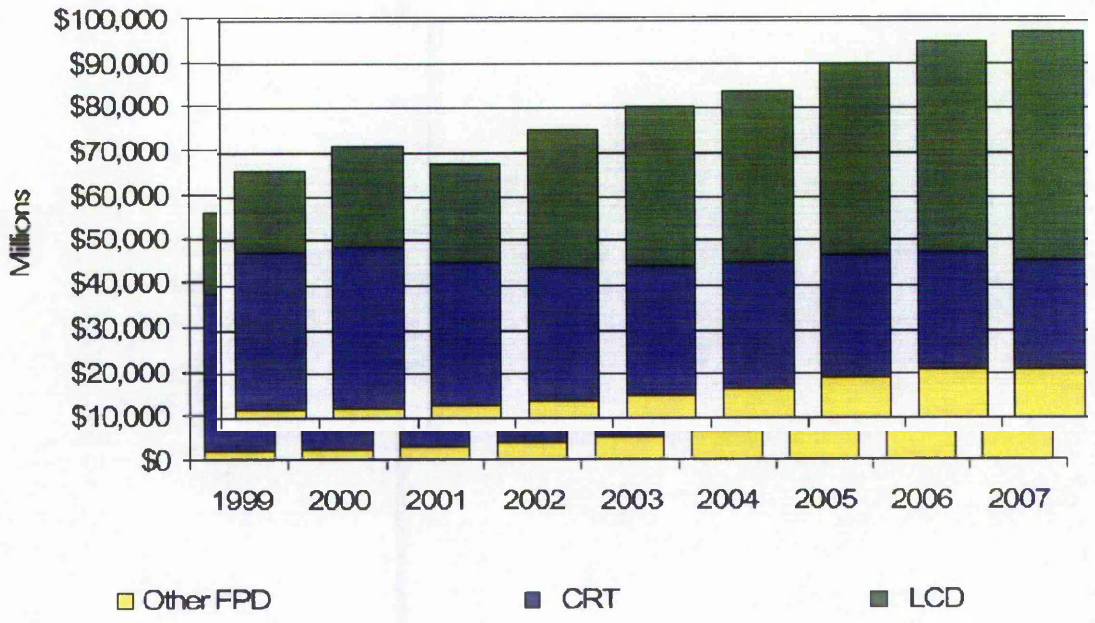


Figure 1.1: World Wide Display Market Forecast by Stanford Resources 9/2001

In addition, DisplaySearch[2] expected that for the very first time in history FPDs are also expected to surpass the CRTs revenues this year as illustrate in figure 1.2. This is mainly contributed by the demand of flat screen monitors and notebooks which evidently leads to boost of manufacturing capacity for device manufacture and also matureness of FPD fabrication.

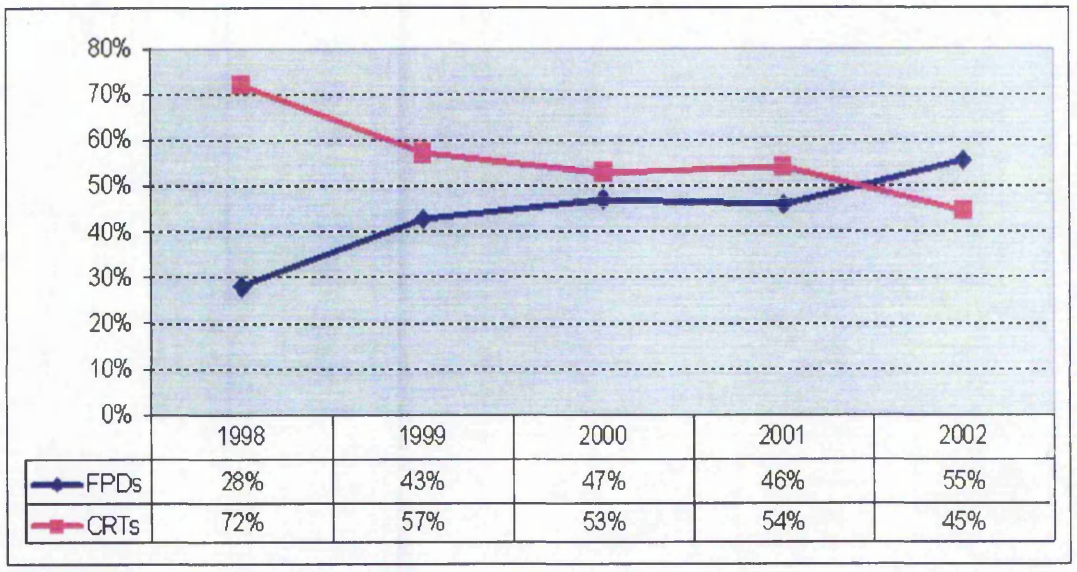


| | 1998 | 1999 | 2000 | 2001 | 2002 |
|---|---|---|---|---|---|
| FPDs | 28% | 43% | 47% | 46% | 55% |
| CRTs | 72% | 57% | 53% | 54% | 45% |

Figure 1.2: CRTs vs LCDs Revenue Forecast by DisplaySearch March 2002

The major components of the FPD market include: Liquid Crystal Display (LCDs), Plasma Display Panels (PDPs), Vacuum Florescent Displays (VFDs), Field Emission Displays (FEDs), Electroluminescent (EL) Displays, Thin Film Diodes (TFDs), Organic Light Emitting Dioides (OLEDs) and microdisplays. FPDs are utilised not only for PC based display but also as display devices for camera/camcorder, television, mobile phones, PDAs, automotives, and even as display units for the industrial instrument. Among all, LCD technology occupied over 85% of the total revenue mainly generated from sales of monitors and notebook PCs. According to the revenue share forecast of DisplaySearch[2] as shown in figure 1.3, this dominancy however, is expected to be sustained at least for the next few years.

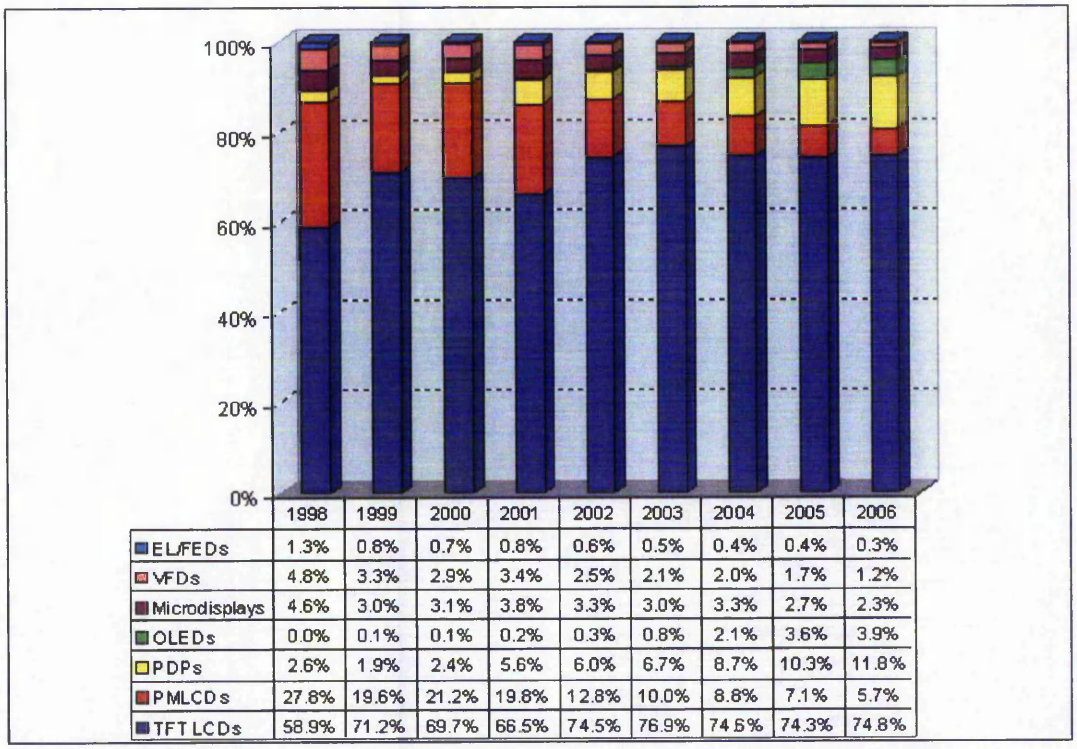


| | 1998 | 1999 | 2000 | 2001 | 2002 | 2003 | 2004 | 2005 | 2006 |
|---|---|---|---|---|---|---|---|---|---|
| EL/FEDs | 1.3% | 0.8% | 0.7% | 0.8% | 0.6% | 0.5% | 0.4% | 0.4% | 0.3% |
| VFDs | 4.8% | 3.3% | 2.9% | 3.4% | 2.5% | 2.1% | 2.0% | 1.7% | 1.2% |
| Microdisplays | 4.6% | 3.0% | 3.1% | 3.8% | 3.3% | 3.0% | 3.3% | 2.7% | 2.3% |
| OLEDs | 0.0% | 0.1% | 0.1% | 0.2% | 0.3% | 0.8% | 2.1% | 3.6% | 3.9% |
| PDPs | 2.6% | 1.9% | 2.4% | 5.6% | 6.0% | 6.7% | 8.7% | 10.3% | 11.8% |
| PMLCDs | 27.8% | 19.6% | 21.2% | 19.8% | 12.8% | 10.0% | 8.8% | 7.1% | 5.7% |
| TFT LCDs | 58.9% | 71.2% | 69.7% | 66.5% | 74.5% | 76.9% | 74.6% | 74.3% | 74.8% |

Figure 1.3: FPDs Revenue share by Technology (DisplaySearch March 2002)

Displays are generally categorised into two main groups, namely emissive and non emissive displays as shown in figure 1.4[3]. The main difference is that the non emissive display, as the name indicates, do not emit light themselves but operate in a transmissive mode which either utilises the ambient light or some form of backlighting and reflective devices.

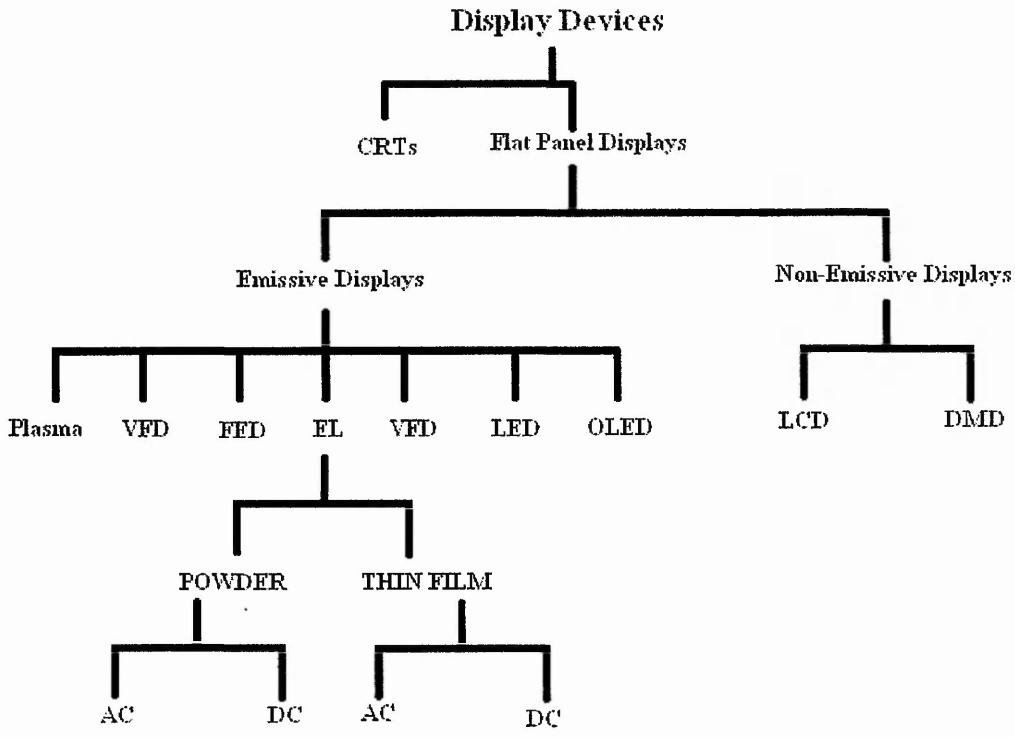


Figure 1.4: Display Devices Categories

### 1.3.1 EMISSIVE DISPLAY

Emissive displays are devices which emit light from a particular phosphor due to some form of excitation. There are wide varieties of display technologies utilising phosphors which includes CRT, PDP, FED, VFD, and EL.

### 1.3.1.1 CATHODE RAY TUBE (CRT)

The maturest technology within the emissive display is the 100 years old CRT[4]. It is still the vital display used in homes throughout the world as the television receiver and computer monitor despite the ever increasing demand of LCDs, plasma display and projection TV for it's replacement. The sustainability of the CRT is mainly due to it's inherent advantages such as high response speed suitable for high frame rate, high resolution video, wide viewing angle, saturated colours, high peak luminance and high contrast and cost.

The CRT is a catholuminescent[5] device, light is generated by the impact of high energy electrons on the phosphor. Illustrated in figure 1.5[6] is the basic operation of the CRT, the electron beam is generated by the electron gun and directed by the yoke. The electrons are then allowed to travel freely in vacuum and finally hit the phosphor layer and hence generates light. The colour of the light being generated depends on the phosphor material.

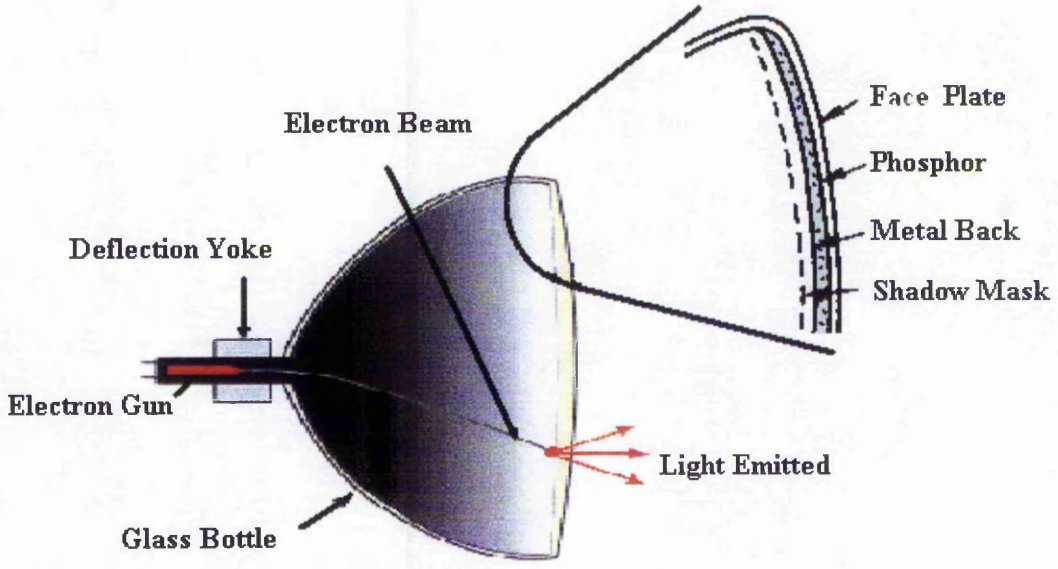


Figure 1.5: Principles of CRT

Despite its superior characteristic, serious disadvantages such as heat dissipation, colour and image vibration, large size and weight have limited its competitiveness compared to other modern FPDs.

### 1.3.1.2 PLASMA DISPLAY PANEL (PDP)

The plasma display panels (PDP) are also referred to as gas discharge displays due to their operating principles. PDP can also be viewed as a matrix of tiny fluorescent tubes which are controlled in a sophisticated fashion. There are two main types of PDP, Direct Current (DC) and Alternating Current (AC) of which the latter has become mainstream because of its simpler structure and longer lifetime. Figure 1.6 illustrates the structure and the principles of an AC- PDP[3]. By passing a high voltage through a low pressure neon gas, the result is a temporary charging of the gas; ultraviolet (UV) light is generated when a spontaneous discharge of the gas occurs. The generated light then strikes and excites red, green or blue phosphor along the face of each pixel, causing them to glow in their respective colour. This form of light generation is known as photoluminescence. Barrier ribs are used to confined the gas discharge from interaction with other pixels.

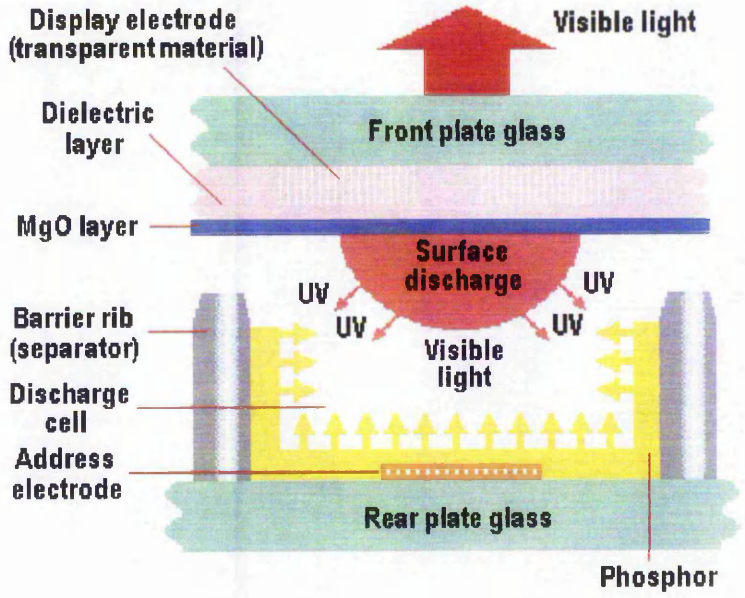


Figure 1.6: Structure of PDP

The advantage of PDP over other display devices is the feasibility for large panel displays, with diagonal sizes up to 61 inches readily available in the market. The overall thickness of less than 4 inches plus the ability of full colour and high information content, makes it the ideal technology for wall mounted display applications. The main obstacle for the PDP is the pixel size, which limits its application for the mainstream desktop PCs.

#### 1.3.1.3 FIELD EMITTING DISPLAY (FED)

The Field Emitting Display is another device based on the cathodoluminescent principle. The general principle of the FED is similar to that of a CRT, electrons are created, excited and impact on phosphors for the generation of light. Due to its closeness with CRT, the FED has sometimes been referred to as ThinCRT[7]. The main difference between FED and CRT is that rather than electrons being created from a single electron gun as in the CRT, the electron emission is from thousands of sharp cold cathodes or nanocones[8,9].

Figure 1.7 illustrates the cross section of a typical FED device[3]. When an electric field exists between the electrodes, electrons are emitted from the tips. These electrons are then used to excite the phosphor for the generation of visible light. The conductive grid layer (Niobium gate metal) is used for controlling the cathode emission.

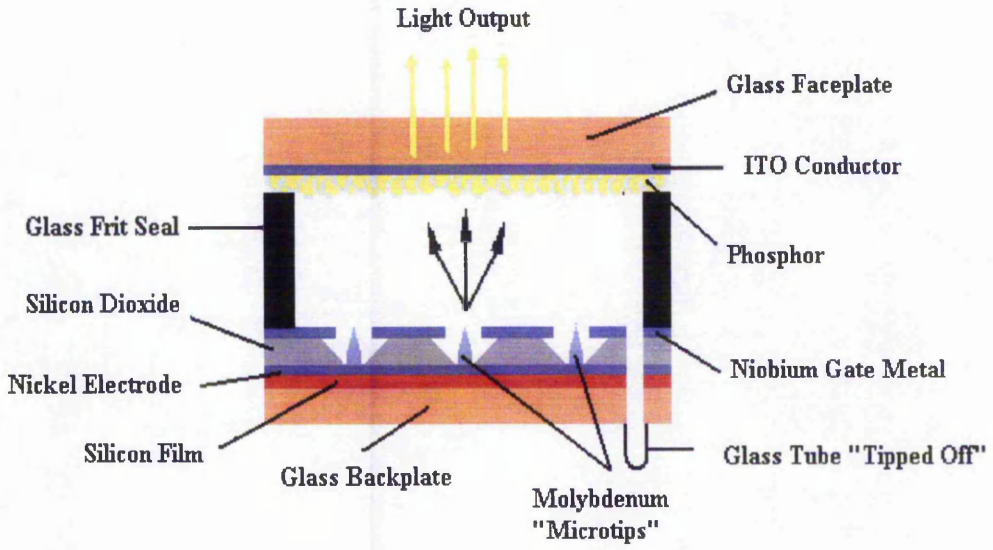


Figure 1.7: Cross Section of a Field Emission Display

In addition, as electrons are generated by field emission rather than thermal emission the device consumes much less power and can be turned on instantly. Due to its similarity to CRTs, it also inherited some of the superiority of the CRTs, such as wide viewing angle and high luminance. However, the main problem with the FED is the difficulty in large scale production due to complication in achieving good yield for the fabrication of the nanocones. In addition, as the FED is a vacuum device, atmospheric pressure becomes a severe problem for large-area panels. In particular, internal support posts which prevent the device from imploding, must be thin enough to fit into spaces between pixels. This together with lifetime issues[10,11] and reducing the driving voltage[12] are the main challenges ahead for FED developers[13]

### 1.3.1.4 VACUUM FLUORESCENT DISPLAY (VFD)

The Vaccum fluorescent display is another type of display that utilises thermal emission of electrons for phosphor excitation to generate colour. Figure 1.8 shows a cross section of a VFD[14]. VFD consists of three electrodes; the cathode (Filament), Anode (Phosphor) and Grid under the high vacuum condition in a glass envelope as shown in figure 1.8. In essence, the VFD is a display tube whose origins lie with the long abandoned triode valve – once the work horse of electronics. Electrons are emitted from the cathode by heating the filament. These electrons are then accelerated by the positive potential of the Grid and the anode. Pixel on-off is determined by the charge applied to each individual pixel. The 'ON' pixel is charged positively to attract the electron for phosphor excitation from electron bombardment while the 'OFF' pixel is negatively biased to repel electrons.

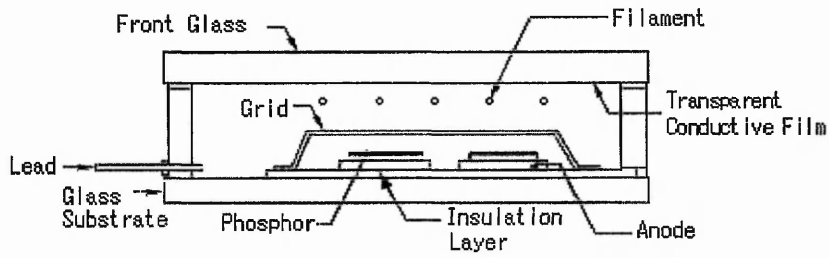


Figure 1.8: Cross Section of VFD

An advantage of VFDs against the FEDs is that no spacers are needed between pixels. As the phosphor can be patterned into any shape, VFDs are widely used for icon displays in consumer electronics and are becoming popular with the automotive industry. Although in principle, VFDs could be used in large scale displays, apart from complication due to its vacuum component, it is still very difficult and expensive for the manufacturing of high pixel count VFDs typically for their application as monitors.

### 1.3.1.5 LIGHT EMITTING DIODE

Nearly everyone is familiar with LEDs (Light Emitting Diodes) from their use as indicator lights and numeric displays on consumer electronic devices. The basic LED is a junction which gives off light when an electric current passes through it. It consists of a semiconductor diode mounted in the reflector cup of a lead frame that is connected to electrical wires. The whole device is then encased in a solid epoxy lens. When sufficient forward bias voltage is applied to the LEDs, the p-n junction will breakdown allowing electrons to flow in one direction within the device in opposite direction to the flow of holes. Light is generated when recombination of minority carriers occurs within the p-n junction. This process is also known as Electroluminescence. Figure 1.9 shows a typical LED structure.

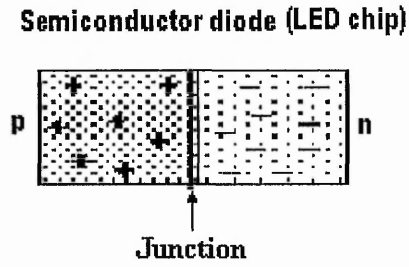


Figure 1.9: LED structure

LED devices are now starting to replace the incandescent lamp typically those of status indicators. They exhibit high luminous intensity, capable of fast switching speed, full colour and low power requirement making them suitable for large open air display. The negative side of the LED is the minimum size requirement per pixel and its heat generation, preventing their use as high resolution display devices.

### 1.3.1.6 ORGANIC ELECTROLUMINESCENT

Organic Electroluminescence (OEL) or better known as Organic Light Emitting Diode (OLED) is probably the 'youngest' among all the FPDs. The first light emission from an organic display based on small molecule organic system was in 1987 by Tang and van Slyke of Eastman Kodak[15]. Ever since, there has been a rapid increase in the discovery of other organic electroluminescent displays, such as the polymer based OLED by Cambridge Display Technology (CDT) in 1990[16]. With this, many abbreviation have been introduced such as PLED for polymer LED, SMLED for small molecule LED, etc. Figure 1.10 shows a schematic of a basic OLED device. OLED operates solely in a diode mode. Upon the application of voltage, electrons are injected from the cathode through to the electron transport layer (ETL) while simultaneously, holes are injected from the anode to the hole transport layer (HTL). As holes are able to tunnel into the ETL while on the other hand, electrons are unable to penetrate the HTL, naturally the recombination occurs in the ETL. Light is then emitted from a thin region within the ETL. This region is also known as the emissive layer.

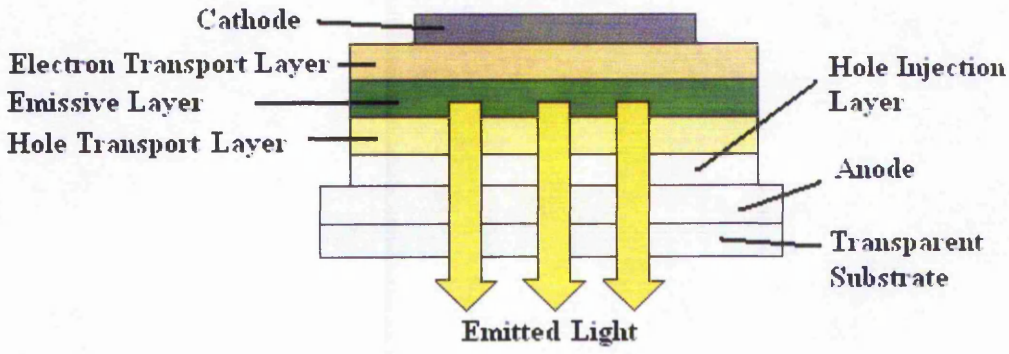


Figure 1.10: The Fundament OLED device

OLED displays offer many important advantages over other FPDs. As an emissive display, it offers a superior viewing angle, contrast ratios, low drive voltage and fast response time. However, being the youngest technology, there are many major obstacles being faced by OLEDs such as the absent of standardized processing and

testing equipment, poor material stability mainly due to the sensitivity of organic material towards oxygen, water vapour and temperature, which subsequently leads to lifetime issues.

### 1.3.1.7 HIGH FIELD ELECTROLUMINESCENT

High Field Electroluminescent (HF-EL) device can be divided into two main categories; DC EL and AC EL. Both categories are further separated in either powder or thin film. The only technology among all HF-EL devices capable of use for high information content displays is the AC thin film electroluminescence device (ACTFEL) technology. ACTFEL displays are composed of stacked layer of metal electrode, insulator, phosphor layer, insulator and conductor as illustrated in figure 1.11. Application of a field above the threshold voltage will result in emission of light from the phosphor. A detail operation of the mechanism will be explained in a later section.

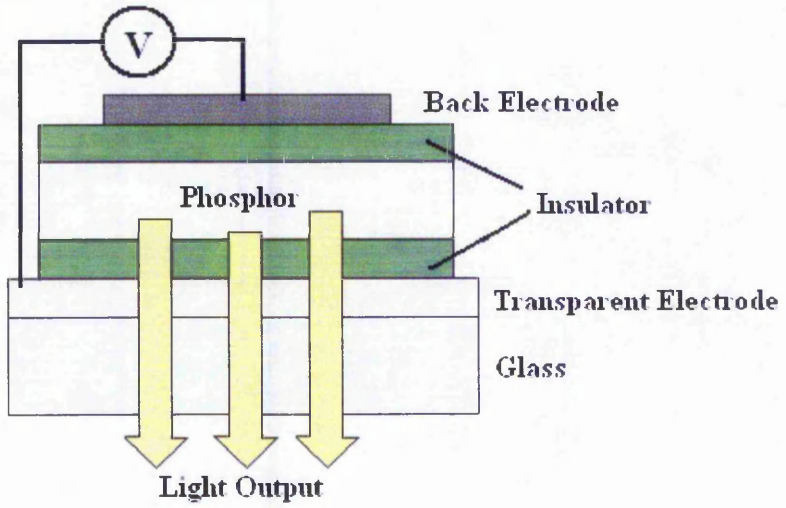


Figure 1.11: Schematic drawing of ACTFEL

ACTFEL is one of the few displays devices that are readable under all light conditions, ranging from total darkness to full sunshine. Contributed by its all solid state structure, it is relatively easy to manufacture and exhibits high ruggedness, apart from other emissive display advantages. The disadvantages of ACTFEL is the lack of

an efficient blue emitting phosphor and its relatively higher drive voltage when compared to OLEDs.

### 1.3.2 NON EMISSIVE DISPLAY

Despite all the advantages inherited by emissive displays, non emissive displays which only exhibit some of their advantages occupy the majority of all the FPD markets. The two strongest players for non emissive displays are the Liquid Crystal Display (LCD) and the Digital Mirror Device (DMD).

#### 1.3.2.1 LIQUID CRYSTAL DISPLAY

LCD is generally a transmissive technology. The display works by letting various amounts of a fixed-intensity white backlight through an active filter. The red, green and blue elements of a pixel are achieved through simple filtering of the white light. All liquid crystal are organic compounds and almost transparent. Liquid crystals utilise the ability of such organic compounds to align in the presence of electric fields. As illustrated in figure 1.12[17], light is allowed to pass through the liquid crystal when no electric field is applied to the electrode but are blocked when such a field is applied.

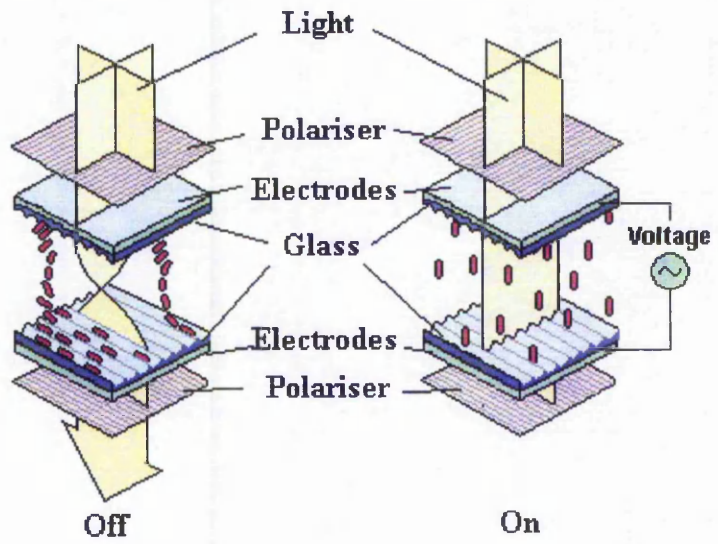


Figure 1.12: Pixel construction of a Twisted Nematic LCD

Development of LCDs have greatly benefited from the advancement in the IT industry. Being light weight and capable of full colour, it has been the technology of choice for the display device of notebook computers and is also a preferred alternative for desktop computers. The disadvantage of LCDs compared to other technologies has always been its limited viewing angle. Power consumptions of the LCD, although low compared to CRTs, is still moderately higher then those of OLEDs.

### 1.3.2.2 DIGITAL MIRROR DEVICE

Digital Mirror Device (DMD)[18] which is also called Digital Light Processing (DLP) was first demonstrated by its sole producer, Texas Instrument (TI) in 1993[19]. The device operates by reflecting lights from an external source towards the pupil of an imaging lens. It is probably the only display device that operates 100% digitally. The 'on' pixel is when the mirror directs the light into the pupil while the 'off' pixel is when the mirrors reflect light away from the imaging lens. The colour of the pixels is determined by the colour of the incidence light while the gray scale is determined by the duration of the on period. Figure 1.13[18] illustrates the schematics of a typical DMD.

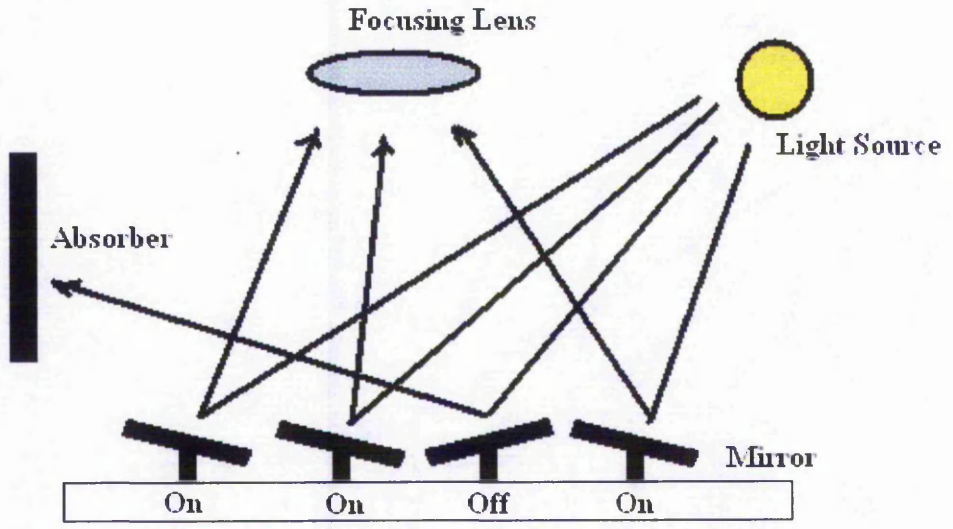


Figure 1.13: Schematic of a Digital Mirror Device

DMD devices are very popular components in many light valve projectors due to its excellent resolution and brightness, high contrast and colour fidelity, and fast response times. However, projectors suffer from a high contrast issues at high ambient light typically critical for consumer High Definition Television (HDTV).

## 1.4 CURRENT AND FUTURE TREND OF FLAT PANEL DISPLAY

It is very difficult to determine the future of flat panel display technology. Market forecast for FPDs has to be reviewed quarterly if not monthly. There are many factors contributing to this uncertainty such as consumer spending confidence, investor confidence, and not least innovative technology breakthroughs. Many analyses had forecasted that LCD would have replaced all CRT for desktop monitors by the year 2000, but two years later, CRT desktop monitors can still be found in abundance all around us.

The author would like to take the opportunity to forecast the future technology of FDPs with relation to display size, based on current status in research and development.

| Display Size | Technology of Choice | | Competing Technology | Comment |
|---|---|---|---|---|
| | Present | Future | | |
| Billboard Size | Incadescent, LED | LED, DLP | LCOS, Si LCD | DLP projection should replacing conventional cinema projector and will have many new applications with the advancement the technology |
| Very Large Area (>40") | | | | |
| Projection | CRT | DLP | LCOS, Si LCD | DLP will replace CRT due its light weight, all digital addressing |
| Direct View | PDP | PDP | LCD | 60" PDP although available nowadays unfortunately carries a heavy price tag |
| Large Area (30"~40") | CRT | LCD | EL | LCD price of 40" and below should be affordable by then, while CRT shoud still dominant the lowend market. |
| Normal Size (14"~30") | CRT, LCD | LCD | EL | CRT will slowly be replaced by LCD typically with the introduction of LCDTV |
| Small Area (<14") | LCD | EL | FED, VFD | EL, most likely be organic based should be the choice due to its emissive nature |
| Microdisplay | EL | EL | DLP, LCD | Inorganic EL will still dominant within micro display for rough enviroment, while the organic EL will be utilised for others |

*EL includes Organic and Inorganic

Table 1: Current and Future Trend of Flat Panel Display

**REFERENCES**

[1] "Market Watch", http://www.stanfordresources.com. [Accessed 3 January 2002].

[2] Mark Fihn, "Global Display Market", http://www.displaysearch.com. [Accessed 1 July 2002].

[3] Flat Panel Display Handbook, Stanford Resources, Inc., Third Edition, 2001.

[4] F Braun, Wied.Ann., Vol. 60, 552, 1897.

[5] L Oxawa, "Cathodoluminescence, Theory and Applications", VCH, Weinheim, 1990.

[6] "Multimedia/Panel Display", http://www.pctechguide.com/07pan2.htm#ThinCRTs. [Accessed 6 May 2002].

[7] "ThinCRT Concept", www.candescent.com. [Accessed 9 May 2002].

[8] I. Shah, Field Emission Display, Physics World, June, pp. 44-48, 1997.

[9] B.R. Chalamala, Y. Wei, B.E. Gnade, 'FED up withnthe flat tube', IEEE Spectrum, Aprils pp. 42-51, 1998.

[10] R A Tuck et al., "Printable Field Emitting Materials for Large-Area, Low-Cost Field Emission Displays", Proceedings of the EID, 1997.

[11] G Hopple and C Curtin, "FED Life and Reliability", Information Display, Official Monthly Publication of the SID, July, 1999, Vol.16, No. 45.

[12] G. Hopple and C. Curtin, Information Display 16, No. 4/5, 34, Apr/May 2000.

[13] R.H. Reuss and B.R. Chalamala, 'How Do FEDs Really Fail?' Information Display, Vol17, No. 7, July 2002.

[14] "Vacuum Florescent Display", http://hem.passagen.se/communication/vfd.html. [Accessed 11 May 2002].

[15] C.W. Tang and S.A. VanSlyke, Appl. Phys. Lett., Vo. 51, pp. 913, 1987.

[16] J.H. Burroughes, D.D.C. Bradley, A.R. Brown, R.N. Marks, R.H. Friend, P.L. Burn and A.H. Holmes, Nature 347, 539, 1990.

[17] "Multimedia/Panel Display", http://www.pctechguide.com/07panels.htm#Liquid_crystal_displays. [Accessed 6 May 2002].

[18] L.J. Hornbeck, Deformable Mirror Spatial Light Modulators, Proc. SPIE, Vol. 1150, Spatial Light Modulators and Application III, 1989.

[19] "Texas Instruments Demonstrates a Digital Projection Display System Using New Imaging Technology Digital Micromirror Device Pivotal to Future High-Definition Displays", http://www.ti.com/corp/docs/company/history/digitaldisplay.shtml. [Accessed 31 May 2002].

# CHAPTER 2

# TFEL TECHNOLOGY, NOVEL DEVICES & PROCESSING

## 2.1 REVIEW OF TFEL TECHNOLOGY

### 2.1.1 INTRODUCTION

Generally there are two main ways of producing light; incandescence and luminescence. For incandescence, heat is produced when electrical current is passed through a conductor or filament. The greater the temperature of the filament, more light is being produced. In contrast, luminescence is the name given to all forms of visible radiant energy due to causes other than temperature. Luminescence is further categorised in term of excitation, such as photoluminescence[1], chemiluminescence[2], cathodoluminescence[3], electroluminescence[4], and others. Most 'glow in the dark' devices are based on the photoluminescence phenomena. Light is produced after a photoluminescent material is exposed to intense light. Light generation due to chemical reaction such as those occurring in the body of the firefly are known as chemiluminescence. Cathodoluminescence is given to phenomena whereby light is generated due to electron bombardment, a typical example is the CRT. Electroluminescence on the other hand, is the non thermal light generation process resulting from the energy conversion of an applied electrical energy in a solid material.

Electroluminescence (EL) devices can be separated into two different classes. One is the familiar LED devices, where light is generated by electron hole recombination near a p-n junction. TFEL devices however, belongs to the other class of EL devices, in which the generation of light is due to impact excitation of a light emitting center or luminescence center by high energy electrons.

### 2.1.2 BRIEF HISTORY

The electroluminescence (EL) phenomenon was first observed by Captain Henry Joseph Round in 1907[5]. He reported that yellow light was generated when current was being passed through a silicon carbide detector. This observation was later demonstrated by Georges Destriau in 1936[6] whereby light was being produced when an alternating current was applied to a copper doped zinc sulphide powder dispersed in castor oil. Although very poor luminance was achieved, the Destriau cell triggered great interest in EL, particularly powder based EL during the early years after the Second World War. The 50s and 60s investigation in powder EL ended without much success owing to poor performance, poor reliability, and lack of scientific understanding of the process. Although powder EL had improved throughout time, there is not much commercial interest nowadays.

Although thin film EL structures were first introduced as early as the late 1950s by Vlasenko and Popkov[7], and the double insulating layer ac thin film EL structure in 1967[8], it was not until Inoguchi et al[9] introduced the first high luminance, long lifetime, double insulating layered yellow emitting ZnS:Mn ACTFEL at the 1974 SID International Symposium that really generated industrial interest in thin film EL displays. Even so, the first commercial thin films products were only introduced in 1983 by Sharp[10]. Since then, many companies such as Sharp, Planar system, Finlux (Planar International) and Lite Array have started manufacturing displays based on TFEL technology. TFEL displays now exhibit high brightness and contrast, wide viewing angle, ruggedness to shock and temperature, fast response time and long lifetime.

### 2.1.3 BLUE TFEL PHOSPHORS

Prior to Okamoto reporting on rare-earth doped ZnS in 1981 [11], EL displays were only capable of displaying one colour. In order to tackle this handicap, a lot of work had been carried out typically in finding suitable combination of new host materials and luminescent centers, in order to obtain a suitable blue phosphor.

The first discovery was done by W. Barrow et al in 1984 [12]. They reported a blue-green emission from cerium (Ce) doped strontium sulphide (SrS) which was also the first alkaline-earth TFEL phosphor. Although the brightness, efficiency and chromaticity have been improved through out the years, SrS:Ce still suffers heavy luminous loss due to heavy filtering in order for it to be utilised in TFEL display as blue emitters. The best blue chromaticity for SrS:Ce was achieved by Westaim Cooparation with CIE coordinate of $x = 0.19$ and $y = 0.36$ [13].

Nine years after the discovery of the first blue emitting phosphor, the same group announced the discovery of two new blue phosphor, namely $SrGa_2S_4$:Ce and $Ca_2GaS_4$:Ce in 1993 [14]. The following year, after a total of 10 years of research, the first commercial full colour TFEL was introduced [15]. Despite good blue chromaticity of these phosphors, these thiogallate materials unfortunately exhibits extremely low efficiency (0.02 ~ 0.03 lm/w) [16].

It was not until 1997 with the introduction of SrS:Cu[17] by Sey Shin Sun et al or more specifically SrS:Cu,Ag in 1998[18] that finally ended the search for a true efficient blue phosphor. The new phosphor exhibits good EL performance ( $L_{40} \approx 34$ cd/m$^2$ , $\eta \approx$ 0.24 lm/W , 60 Hz) [19]. A true white monochrome TFEL display of high luminance and stability was later made available using this blue phosphor in a SrS:Cu,Ag/ZnS:Mn multi-layer structure [20]. SrS:Cu remains as the only sputterable high efficient blue phosphor at the time of writing.

Recently lead doped calcium sulphide (CaS:Pb) has been listed as a promising blue TFEL phosphor by S.J. Yun el al[21]. Although CaS:Pb exhibits good luminance and close match to the colour coordinates of the cathode ray tube, a demonstrator has yet to be shown.

The latest addition for a candidate of blue TFEL phosphor is the europium activated barium thioaluminate ($BaAl_2S_4$:Eu) developed by N Miura el al of Meiji University[22]. Recently, iFire Technology Inc announced of a colour performance of $L_{60}$ > 200 cd/m$^2$ with CIE coordinate x = 0.135 and y = 0.105 with 120 Hz ac excitation at 60 volts above threshold at the SID 2002 in Boston[23]. Unfortunately, $BaAl_2S_4$:Eu films currently can only be produced by dual e-beam evaporation which may not be suitable for this phosphor for mass production.

Table 2 shows a summary of performance for the major blue TFEL phosphor and its relative CIE colour coordinates.

| Phosphor Material | CIE Colour Coordinate | | Luminance |
|---|---|---|---|
| | x | y | cd/m$^2$ |
| SrS:Ce | 0.19 | 0.36 | 100 |
| $SrGa_2S_4$:Ce | 0.15 | 0.10 | 5 |
| $Ca_2GaS_4$:Ce | 0.15 | 0.19 | 10 |
| SrS:Cu | 0.169 | 0.273 | 34 |
| SrS:Cu,Ag | 0.17 | 0.13 | 28 |
| CaS:Pb | 0.15 | 0.10 | 80 |
| $BaAl_2S_4$:Eu | 0.135 | 0.105 | 200 |

Table 2: Summary of Major Blue Emitting TFEL Phosphor

## 2.1.4 TFEL DEVICE STRUCTURE & ELECTRICAL CHARACTERISTIC

### 2.1.4.1 DEVICE STRUCTURE

Since the report of high luminance and long lifetime EL devices by Inoguchi et al[9], ac TFEL with double insulating layer[8] as in figure 2.1 has been the basic structure for the studies on ac TFEL devices. The structure is relatively simple, comprising a phosphor layer situated between two insulting layers which is sandwiched by two electrodes. One of the electrodes is usually constructed from a transparent material. This is to enable the penetration of light being generated within the phosphor layer, hence allowing the viewing of such emission.

### 2.1.4.2 EMISSION MECHANISM

The electroluminescent (EL) mechanism for ac thin films consists of four individual processes. This mechanism is indicated in figure 2.1. The EL emission occurs in the following way.

1) When the applied voltage exceeds the threshold voltage of the device, electrons are injected by field-assisted tunnelling into the bulk phosphor layer from the interface states, between the phosphor and insulating layers.
2) These injected electrons are accelerated by the applied field hence gaining kinetic energy.
3) Electrons with sufficient kinetic energy, referred to as 'hot electrons', excite luminescence centers. Energy is exchanged between the electron and the ion causing excitation. The radiative transition of the manganese or other luminescent from the excited state to the ground state results in EL emission.
4) The 'hot electron' will continue to travel within the phosphor layer towards the anode exciting any luminescent ion within its path. When the electron is finally trapped at the interface states at the anode side, polarisation occurs.
5) If the applied voltage remains unchanged, the EL emission will gradually reduce and finally stop when the system reaches equilibrium.

6) When the polarity of the ac voltage is reversed, the same process takes place but in the opposite direction.

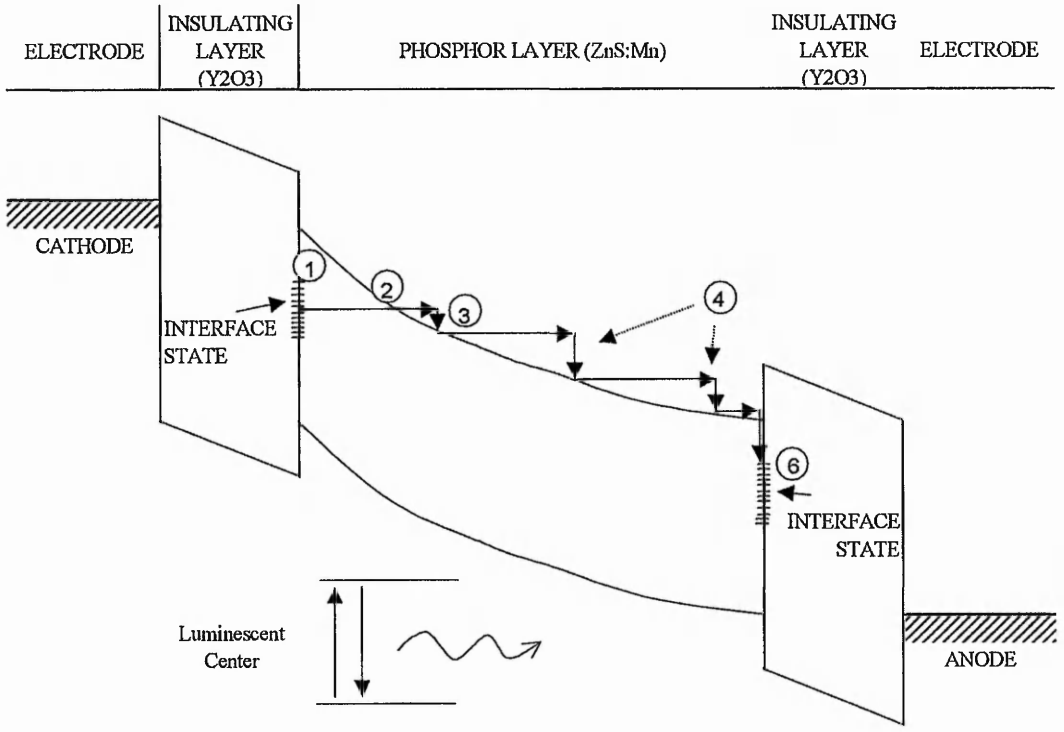


Figure 2.1: Energy band diagram of the double insulating ac thin film and the El emission mechanism

Energy exchange between 'hot electrons' and the lattice, usually in the form of impact excitation is observed in all wide-band gap semiconductors. This form of emission mechanism is also generally accepted for any EL devices. The quantitative understanding behaviour of SrS based material however, has not yet been concluded. This confusion is mainly attributed by the omnipresent of trailing edge emission (TEE) from SrS based ACTFEL devices. TEE refers to light generation after the applied voltages switches to low state. Several mechanism for the TEE have been put forward[24,25,26,27] as well as the role of space charge in this process[28,29,30,31]. Apart from TEE, there have been reports of light emission when the applied voltage was zeroed, namely premature emission (PM) for Cu doped SrS devices[32,33,34].

## 2.2 NOVEL DEVICES & PROCESSING

### 2.2.1 INTRODUCTION

Over the past two decades, electroluminescene devices had enjoyed a slow but steady progress, advancing from single colour devices to full colour, and full motion display devices. It had also generated great commercial interests mainly attributed to its simple display structure in addition to its inherent ruggedness. Since the first introduction of high luminance, long lifetime double insulator ACTFEL device, there has been various studies in order to improve ACTFEL device performance and consequently expanding ACTFEL applications. Among such novel improvements are the utilisations of ACTFEL as the light emitter for the exposure system for electrophotography printing, the introduction of active matrix electroluminescene (AMEL)[35] devices, barrier layer (BL)[36] devices, lateral emitting thin film electroluminescene (LETFEL)[37] devices and thick dielectric electroluminescene (TDEL)[38] devices.

### 2.2.2 TFEL EDGE EMITTER

For a copier or printer, the exposure system forms the heart of the engine. The exposure system in the machine is the dominant factor determining the overall performance, particularly the resolution and often the print speed. Before the arrival of lasers, cathode ray tubes (CRT) were the common light source for a copier. The CRT however was not suitable for use as a printer exposure system due to its nature. It is only suitable for flash exposure directly onto chemically coated paper plus limitation of black and white output.

The introduction of the laser polygon system by IBM in 1975 was a major break through in electrophotographic printing. Modern electrophotographic printers or laser printers which utilised semiconductor lasers have significantly reduced the size of the original IBM machine. However, the use of the laser polygon system involves complicated optics making such system relatively more expensive compared with ink

jet printers. To overcome this limitation, image bars constructed by arrays of LEDs were introduced in 1986 by OKI. These removed the complexity of manufacturing complicated optics and hence reduced the manufacturing cost. Due to the fact that minimum size requirement for the individual LED which limits the prints quality, ACTFEL were introduced by Westinghouse[39] as an alternate light source for electrophotographic exposure system to tackle the limiting size for individual pixels.

D.H. Smith[40] in 1983 observed that the luminous efficiency of TFEL devices is an order of magnitude higher when the light emitted from the edge of the thin films is included. Utilising this finding, Kun et al of Westinghouse proposed edge emitting TFEL devices as in figure 2.2 as a mean of producing a high intensity image bar array for the use in electrophotography printers.

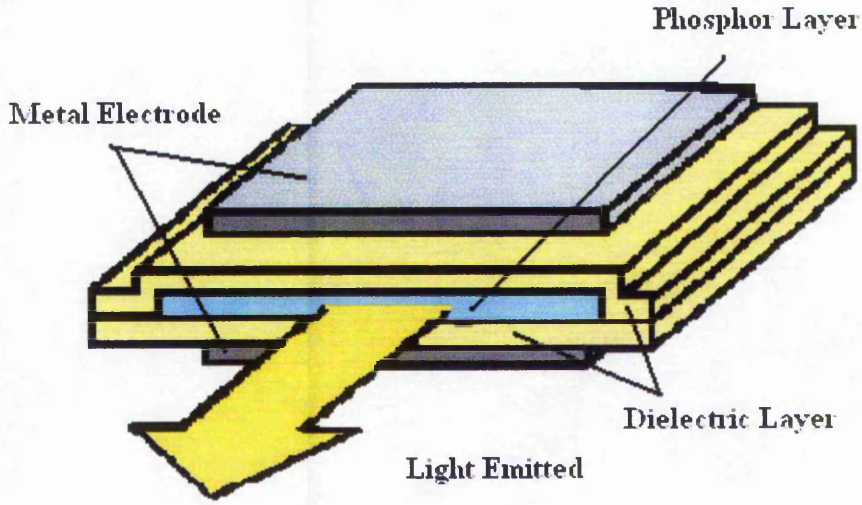


Figure 2.2 Schematic of a pixel of Westinghouse edge emitter

The image bar was constructed by fabricating an array of the edge emitting TFELs. Although print quality of 400 dpi were demonstrated, due to edge blur of the printer quality plus the inability to provide uniform illumination of the photoconductors of the electrophotography, the work to utilises TFEL devices for printing devices was halted. Never the less, the work had clearly demonstrated the potential of obtaining brighter TFEL devices if the internal confined light was to be out coupled.

### 2.2.3 LATERAL EMITTING THIN FILM ELECTROLUMINESCENCE DEVICE (LETFEL)

Following the foot steps of Kun et al, the Optoelectronics Group of The Nottingham Trent University (NTU) came out with an innovation to incorporate micro mirrors within the TFEL devises to redirect light from the edge emission of a TFEL device for surface emission utilisation[37]. The cross section of the NTU Lateral Emitting TFEL (LETFEL) is shown in figure 2.3

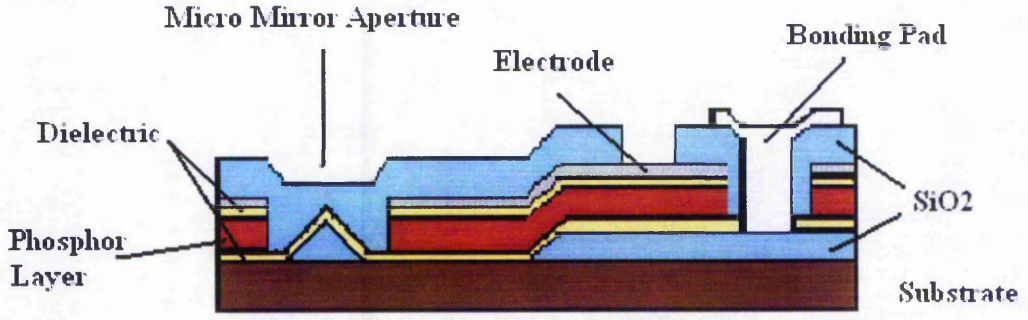


Figure 2.3 Schematic cross section of a LETFEL

The advantages of this structure are two fold: namely a Lambertion distribution of light from each source and secondly being a pure semiconductor based device, lenses can be integrated with the LETFEL devices. The device although first intended to be uses as a light source for electrophotography printing similar to those of the Westinghouse application had also been demonstrated for HMD application[41,42]. Recently, it has also been shown that the complex electronics required for addressing and driving such linear arrays for electrophotographic printing exposure can also be integrated into the substrate[43].

### 2.2.4 ACTIVE MATRIX ELECTROLUMINESCENCE DEVICE

With the advancement of technology, there is a growing demand for small and high resolution displays for head mounted display (HMD) applications, display devices for projection system and many others. Interconnects play the role in determining the pixel density of a display. Interconnect density for chip on glass technology is no way near that of the Silicon based technology. This is mainly due to the benefit enjoyed by silicon technology from the advancement in information technology. Driven by the need for extremely high resolution of future display, there is a need to replace the conventional glass substrate of TFEL devices with those of the silicon substrate. Sarnoff Corporation was the first to apply active matrix technology to TFEL devices[44]. Figure 2.4 shows the comparison between the typical TFEL and an AMEL display.

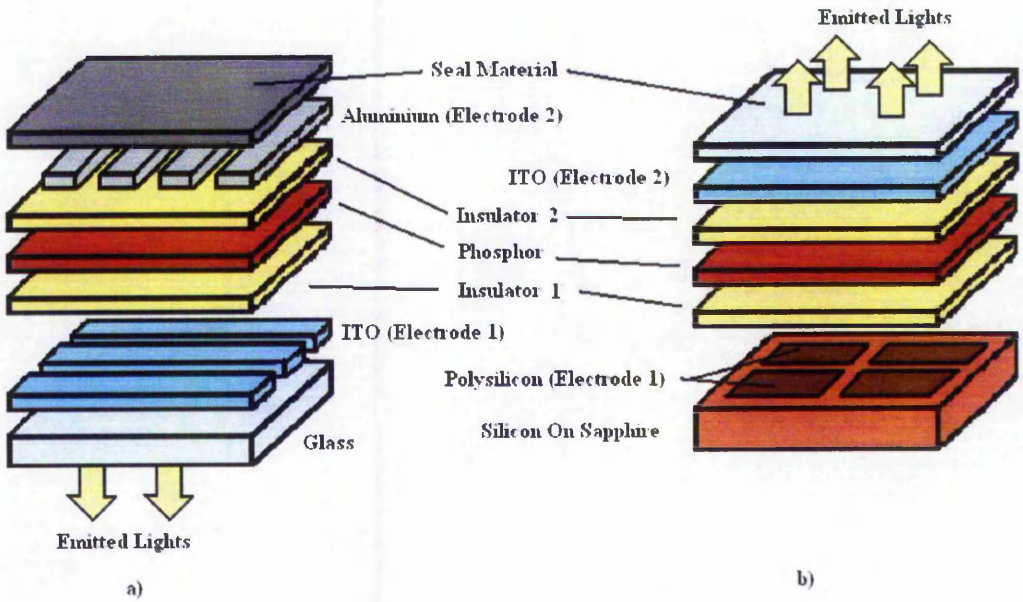


Figure 2.4 Comparison of the typical TFEL (a) and AMEL (b)

The main differences between the standard TFEL and the AMEL are the utilisation of silicon on sapphire wafers instead of the conventional glass substrate and the use of an inverted structure with a top transparent layer. The advantage of utilising silicon

wafers is that all the drive electronics may be incorporated into the device. This not only simplifies wiring for the overall display but also allow easy integration of optics, creating a high resolution, small size, light weight, full semiconductor based technology display. Currently Planar America uses Sarnoff AMEL technology to manufacture government and commercial HMD display devices.

### 2.2.5 BARRIER LAYER PHOSPHOR

The excitation mechanism for ZnS:Mn devices is accredited to the impact excitation of luminous center by hot electrons with energy around 2.4 eV. In order to generate hot electrons with such energy, an operating field of 1.5 ~ 2 MV/cm needs to be applied. Work by W.M. Cranton had shown that it is possible to increase the amount of hot electrons by re-engineering the TFEL structure by introducing a thin dielectric layer/layers within the phosphor layer[36,42]. It is believed that electrons gains energy when travel through this thin dielectric layer/layers, hence creating more hot electrons and evidently increase the probability of impact excitation for light generation. Such devices are usually referred to as barrier layer TFEL devices.

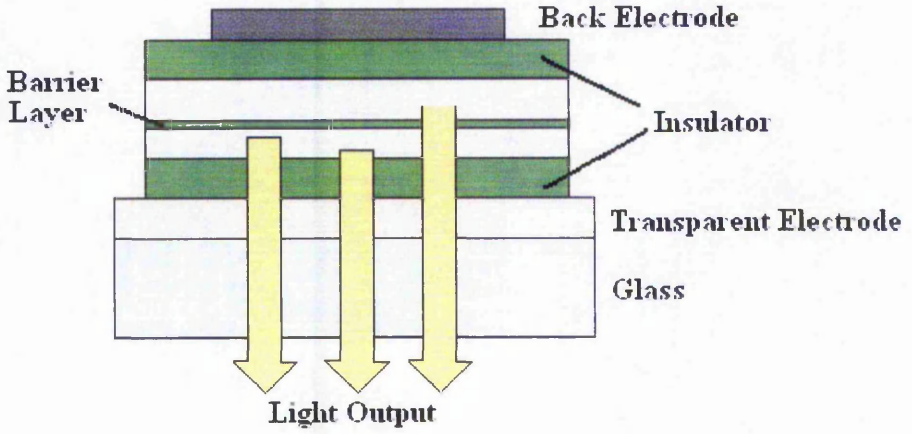


Figure 2.5: Barrier Layer Device

Figure 2.5 shows a single barrier layer device. The thickness of the barrier layer is normally in the order of 100 Å. Multi-barrier layers may be fabricated within the phosphor layer in order to further improve the luminous efficiency.

### 2.2.6 HYBRID INORGANIC ELECTROLUMINESCENT DEVICES

Hybrid Inorganic Electroluminescent device[38] or better known as thick film dielectric electroluminescent devices (TDEL) is a new type of electroluminescent devices developed by iFire Technology Inc. , a wholly owned subsidiary of The Westaim Corporation. The basic concept of this device is to combine the simple thick film processing with high brightness thin film phosphors for the realisation of a pure solid state display. Figure 2.6 shows a basic structure of a hybrid Inorganic EL device.

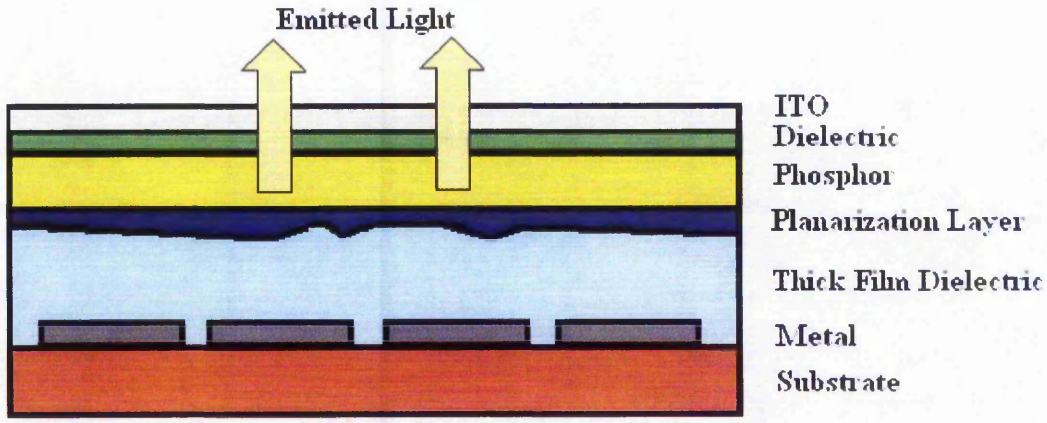


Figure 2.6: Basic Structure of Hybrid Inorganic EL Device

Unlike all previously mentioned devices, apart from the vacuum deposition techniques for thin films, the fabrication of TDEL also involves a combination of screen printing technology for the fabrication of the metal rows and thick film dielectric layer, and the sol-gel coating process for the forming of the planarisation layer. The planarisation layer is needed to provide a smooth surface for the following thin film process due to the rough surfaces of the finished thick film dielectric layer.

According to iFire, the utilisation of thick films improves the brightness and the efficiency of EL phosphors by a magnitude over 300% over conventional thin film dielectric EL displays[38]. Remarkably, progress has been made over the years in the development of TDEL including the demonstration of full colour video display with CRT like performance in SID Boston 2002.

**REFERENCES**

[1] J. Wilson and J.F.B. Hawkes, "Optoelectronics, An Introduction", Prentice Hall, 1989.

[2] Givens, R. S.; Schowen, R. L., "The Peroxyoxalate Chemiluminescence Reaction In Chemiluminescence and Photochemical Reaction Detection in Chromatography", J. W. Birks, Ed., VCH: New York, pp. 125-147, 1989.

[3] L Oxawa, "Cathodoluminescence, Theory and Applications", VCH, Weinheim, 1990.

[4] P.J. Dean et al., "Electroluminescence", Springer-Verlag, New York, 1977.

[5] Henry J. Round, "A Note on Carborundum", Electrical world, Vol. 19, pp. 309, 9 February 1907.

[6] G.Destriau, "Recherches sur les scintillations des sulfures de zinc aux rayons", Journal de Chemie Physique, vol 34, pp. 587-625, 1936.

[7] N.A. Vlasenko and Iuri A. Popkov, "Study of the Electroluminescence of a Sublimed ZnS-Mn Phosphor", Optics & Spectroscopy, Vol. 8, pp. 39-42, 1960.

[8] M.J. Russ and D.I. Kennedy, Journal of the Electrochemical Society, vol. 114, pp. 1066-1071. 1967.

[9] T. Inoguchi, M. Takeda, Y. Kakahara, Y. Nakata and M. Yoshida, SID 1974 Digest, pp. 84, 1974.

[10] M. Takeda, Y. Kanatani, H. Kishishita and H. Uede, Proc. SPIE 386, Advances in display Teechnology III (1983) 34.

[11] K. Okamoto, Ph.D. Thesis, Osaka University, 1981.

[12] W.A. Barrow, R.E. Coovert and C.N. King, Digest of 1984 SID International symposium, pp. 249, 1984.

[13] X. Wu, Proceeding of 1997 International Display Workshop, pp. 593, 1997.

[14] W.A. Barrow R.C. Coovert, E. Dickey, C.N. King, C. Lasskso, S.S. Sun, R.T. Tuenge, R. Wentross and J. Kane, Digest of 1993 SID Interanational Symposium, pp. 761, 1993.

[15] W. Barrow, R. Coovert, E. Dickey, T. Flegal, M. Fullman, C. King and C. Laakso, Conference Record of the 1994 International Display Research Conference, pp. 448, 1994..

[16] S.S. Sun, E. Dickey, R.T. Teunge, R. Wentross and J. Kane, J. SID, 4(4), pp. 305, 1996.

[17] S.S. Sun, E. Dickey, J. Kane and Y.N. Yocom, Conf. Rec. 1997 Inter. Display Res. Con., Toronto, pp.301, 1997.

[18] S.S. Sun. 4th Inter. Conf. Sci. Tech. display Phosphor, Extended Abstracts, Bend, OR, pp. 183, 1998.

[19] S.S. Sun, 18th Inter. Display Res. Con, Seoul, 1998.

[20] S.S. Sun, M.S. Browen, J.L. Daniel, S. Moehnke, A. Hodge, R.T. Tuenge, S. Pearson, J. Phillips, L. Simonsen and C.N. King, SID Symposium Digest of Technical Papers, pp. 1146-1149, 1999.

[21] S.J. Yun, Y.S. Kim, J.-S. Kang, S.H. Ko Park, K.L. Cho and D.S. Ma, Proc. Of 17th IDRC/'98 Asia Display, pp. 933, 1998.

[22] M. Kawanishi, N. Miura, H. Matsumoto and R. Nakano, 6th International Display Workshops, pp. 821, 1999.

[23] D. Cheong, A. Nakua and P. Del Bel Belluz, SID 2002 International symposium Digest of Technical Papers, Boston, pp. 105-107, 2002.

[24] S. Tanaka, H. Yoshiyama, Y. Mikami, J. Nishiura, S. Ohsio and H. Kobayashi, Jpn. Display Proc. Pp. 242, 1986.

[25] H. Yoshiyama, S.H. Sohn, S.Tanaka and H. Kobayashi, in Electroluminescence, Proc. 4th Int. Workshop for Electroluminescene, pp. 11, 1988.

[26] R.S. Crandall, Appl. Phys. Lett, 50, pp. 551, 1987

[27] V.P. Singh and D.C. Morton, IEEE Trans. Electron Device, Vo. 39, pp. 1331, 1992.

[28] K.A. Neyts and E. Soininen, IEEE Trans. Electron Device, Vol. 42, pp. 1086, 1995

[29] K.A. Neyts, IEEE Trans. Electron Device, Vol. 43, pp. 1343, 1996.

[30] M. Peter, S. Nishimura, M. Murayama, K. Ohmi, S. Tanaka and H.K. Kobayashi, J. Appl. Phys. Vol. 86, pp. 7071, 1999.

[31] K. Ohmi, K. Yamabe, H. Fukada, T. Fujiwara, S. Tanaka and H. Kobayashi, J. Appl. Phys. Vol. 73, pp. 1889, 1998.

[32] G. Stuyven, K. Nyets, P. De Visschere and Y. Meuret, Proceedings of the 19th International Display Research Conference, Berlin, Germany, pp. 151, 1999.

[33] K. Nyets and G. Stuyven, Appl. Phys. Lett. Vol. 75, pp. 2593, 1999.

[34] K. Nyets, Y. Meuret, G.Stuyen, P. De Visschere and S. Moehnke, J. Appl. Phys. Vol. 88, pp. 2906, 2000.

[35] R. Khormaei, K. Ping, M. Rhoads, B. Aitchison, C.N. King, G. Dolny, A. Ipri, F-L. Hsueh, R.G. Steward, T. Keyser, G. Becker, D. Kagey and M. Spitzer, SID 95 Digest, pp. 891, 1995.

[36] CB Thomas, WM Cranton, Applied Physics Letter, vol. 63, no.6, (1993).

[37] R. Steven, CB. Thomas, and WM. Cranton, IEEE Electron Device Letter, vol. 15, no.3 pp. 97-99, 1994

[38] X Wu, P. Bailey, D. Carkner, D. Doxsee, K. Foo, S. Sladen. W. Smy, and R. Williamson, Proc. 1994 International Workshop on Electroluminescene, pp. 232, 1994.

[39] ZK Kun, D Leksell, PR Malmberg, J Asars, and GB Brandt, International Symposium Of The Society For Information Display 1986, Digest of Technical Papers, SID86, pp270, (1986).

[40] D.H. Smith, J. Lum, Vol. 23, pp. 209, 1983.

[41] R. Steven, Ph D Thesis, University of Bradford, 1995.

[42] W.M. Cranton, Ph D Thesis, University of Bradford, 1995.

[43] PS Theng, PhD Thesis, The Nottingham Trent University (2000).

[44] "Active Matrix Electroluminescent Displays", http://www.sarnoff.com/products_services/displays/amel.asp [ Accessed 9 October 2002].

# CHAPTER 3

# EXPERIMENTAL DETAIL

## 3.1 INTRODUCTION

For the investigation of SrS based thin films, it is necessary to establish a path to fabricate TFEL devices. Various fabrication techniques have been used for the investigation of SrS:Ce thin films ranging from electron beam evaporation[1] to atomic layer epitaxy (ALE)[2]. For the case of SrS:Cu,Ag, ALE has not yet been realised due to the absence of suitable Ag precursors for ALE[3]. For this work, the rf magnetron sputtering technique[4] was chosen as the preferred fabrication technique mainly due to the fact that the first successful attempts on fabricating such devices were based on this technique[5]. Apart from that, sputtering is also the most frequently used thin film deposition technique not only for display industry but also generally for the fabrication of microcircuits.

Owing to the intrinsic characteristic of the sputtering process, the crystallinity of the as deposited films is usually relatively poor. Post deposition annealing is generally employed to improve the overall film quality. SrS based films are generally annealed at relatively high temperature, above 500°C typically for SrS:Cu,Ag films prior to the deposition of the top insulator[5,6,7]. In order for the investigation of post deposition annealing effect on such films, both conventional thermal annealing techniques and rapid thermal annealing techniques were employed. In addition, following the successful laser annealing on ZnS:Mn by the optoelectronics group of the Nottingham Trent University[8], a similar technique was also employed for the same studies.

Both photoluminescence (PL) and electroluminescence (EL) measurement are the major method employed for the studies of the post deposition annealing effects on SrS based thin films. X-ray diffraction (XRD) examinations were also carried out.

This chapter will provide a general background on thin film fabrication technology involved in this study. In addition to that, the experimental arrangement for post deposition annealing, PL, EL and XRD will also be elucidated.

## 3.2 THIN FILM FABRICATION

Deposited films are widely used in the fabrication of modern day integration circuits. Benefiting from the advancement of microelectronics, a range of film deposition techniques were developed alongside the need for faster, more sophisticated microelectronics. Thin film fabrication is also a major part of the fabrication of modern day display technology typically flat panel technology as no FPDs may be fabricated without the utilisation of at least one thin film deposition technique. There are numerous ways to deposit thin films[9]. They are generally categorised into Chemical Vapor Deposition (CVD) or Physical Vapour Deposition (PVD). CVD is a process whereby the creation of solid material is the result of chemical reaction in gas and/or chemical composition near or on the substrate material. PVD on the other hand, relies on the physical reaction of source material on the substrate.

The common techniques utilised for the fabrication of TFEL devices are sputtering, evaporation, molecule beam epitaxy (MBE) and atomic layer epitaxy (ALE). While sputtering is most favoured by manufacturers, due to the simplicity of the process and easy scalability. For this study rf magnetron sputtering was used for the fabrication of the transparent electrodes, the insulators and the phosphor layers. The transparent electrodes are of indium tin oxide (ITO), the insulator is yttrium oxide ($Y_2O_3$), while the phosphor layer is either Strontium Sulphide doped with cerium (SrS:Ce) or Strontium Sulphide doped copper and silver (SrS:Cu,Ag). The top electrodes are usually made from evaporated aluminium (Al).

### 3.2.1 RF MAGNETRON SPUTTERING

Sputter deposition, first reported by Grove in 1852[10], has now developed into an essential tool in the semiconductor manufacturing industry. It utilise the momentum transfer from an incident particle to an atom in the solid target[11] in order for it to leave the surface of the target and redeposit onto the substrate. As there is no chemical reaction involved, sputtering is categorised under PVD. Today, there are a number of sputtering system that can be used for film deposition. The difference among all the available sputter deposition system is only their means of delivering ions to the sputtering source or target. Among them, rf magnetron sputtering is the most widely used due to its cheap, simple and easy adaptation to high volume manufacturing.

For the studies of blue emitting TFEL devices, SrS based phosphor had been chosen as the choice phosphor not only due to its emission colour but also its fabrication technique ie, rf magnetron sputtering. For aid in this study, the author commissioned a custom made multi cluster rf magnetron sputtering system. A schematic diagram and a photograph of the sputtering system is shown in figure 3.1.

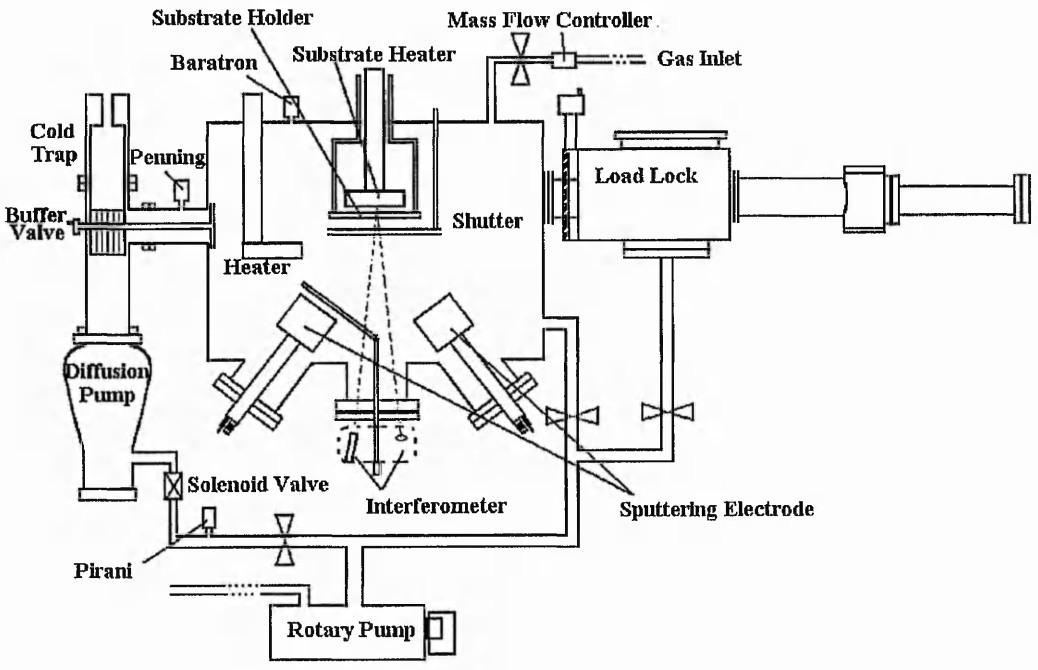


Figure 3.1 a: Schematic diagram of the RF Magnetron Sputter system

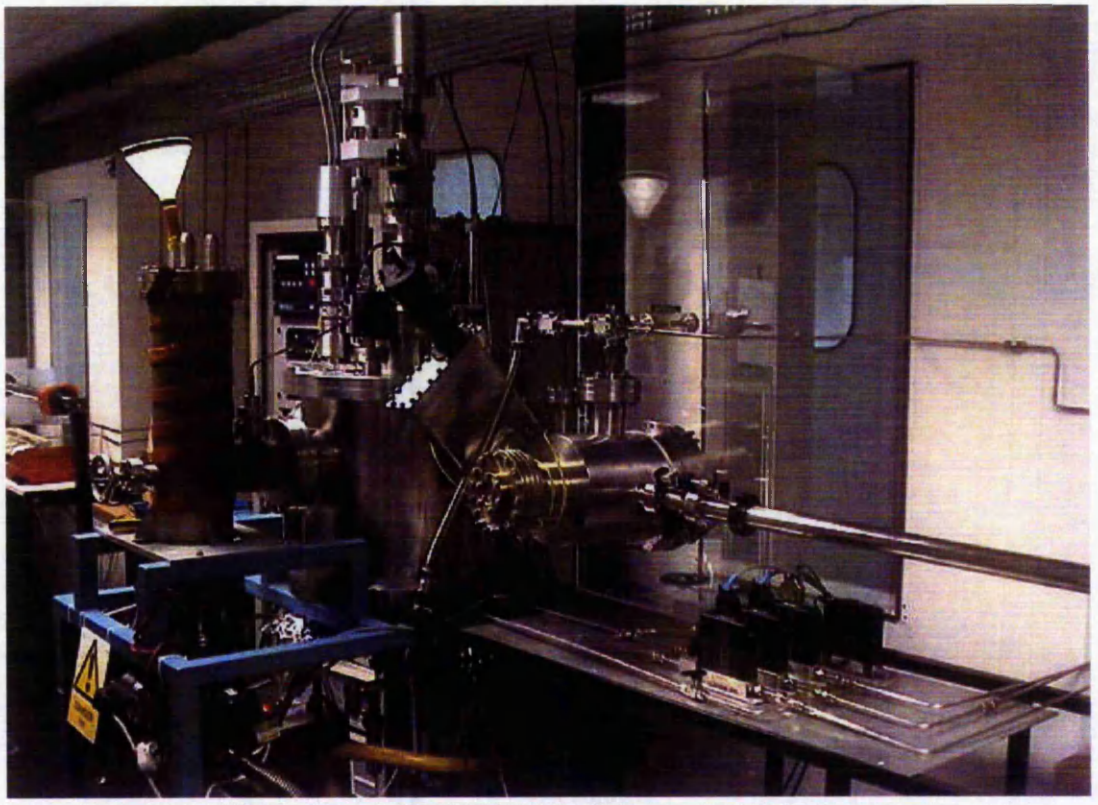

Figure 3.1b: Photograph of the RF Magnetron Sputtering System

The required clean vacuum for the above sputtering system is provided by a combination of nitrogen cold trap and a diffusion pump backed by a rotary pump. A pressure of lower then $1x10^{-6}$ mbar can be achieved within the deposition chamber with this arrangement. The pumping system is monitored by a Penning gauge within the cold trap and a Pirani gauge situated between the outlet of the diffusion pump and the rotary pump. The Pirani gauge is interconnected to a solenoid valve. In the event whereby the pressure at the outlet of the diffusion pump rises above $1.2 \times 10^{-1}$ mbar, the solenoid valve will trip preventing a back draft from the rotary pump towards the diffusion pump due to pressure difference. At the same time, the power to the heater of the diffusion pump will also be automatically cut off preventing over heating of the diffusion pump oil (Santovac 5). Apart from this automated valve, manual valves were also fitted to enable the loading and unloading of substrates.

The deposition chamber is separated from the atmosphere by a load lock. The introduction of the load lock is to ensure that the substrate can be introduced or removed from the deposition chamber via the aid of a magnetically coupled loading arm without exposing the deposition chamber to air. The reason for this is to prevent or to minimise the outgassing of water vapour from the deposition chamber walls during deposition as the residue pressure for a leak free stainless steel chamber when pumped down to 10-4 Pa is determined by the outgassing of water vapour. For the case whereby the deposition chamber was exposed to air, usually after target changes, heating tape wrapped around the outside of the chamber is used to assist in the baking out of the chamber prior to any deposition. This is to accelerate the outgassing process.

Two heaters have been introduced into the deposition chamber. One is used as the substrate heater during sputtering while the other is used for post deposition annealing. The distance between the heaters and the heating elements are adjustable mainly to enable the use of different substrates but also to allow finer adjustment to heating parameters. Due to this, the substrate shutter height is also made adjustable. The substrate is held by a rotating substrate holder so as to provide even heating during deposition and annealing, hence leads to an even thickness of film deposited. The use of the post deposition annealing heater will be discussed in a later section.

As it is essential to maintain the pressure during deposition a buffer valve is fitted in between the deposition chamber and the cold trap to act as a flow controller during deposition. The pressure of the applied gas is monitored by a Baratron pressure transducer located within the deposition chamber.

Three electrodes are situated within the deposition chamber as the initial idea for the fabrication of SrS:Cu,Ag films was to utilise the duo-sputtering technique. This however was later abandoned as reasonable films could be produced without the need for such complicated techniques. The third electrode was intended for the insulating material. The growth parameters for the SrS based thin films will be discuss in Chapter 4.

This deposition system is only used for the deposition of insulator and phosphor material while a similar deposition system is used for the deposition of transparent coatings to provide electrodes (ITO).

### 3.2.2 EVAPORATOR

Deposition of films via thermal evaporation is the simplest techniques among all film fabrication processes. Unlike sputtering, evaporation[12] is the result of energy delivered to a solid to raise its temperature to the point where atoms obtain enough energy to leave the surface of the solid.

For this study, aluminium is evaporated using the thermal evaporator shown in figure 3.2. The energy transfer source for this system is based on resistive heating of aluminium wire within a tungsten basket, heated by passing a high current of approximately 30A. When sufficient temperature is achieved by the tungsten basket, the aluminium wire within the basket starts to melt and the metal is evaporated. The evaporated aluminium is deposited on the substrate at the rate of 50 Å/s.

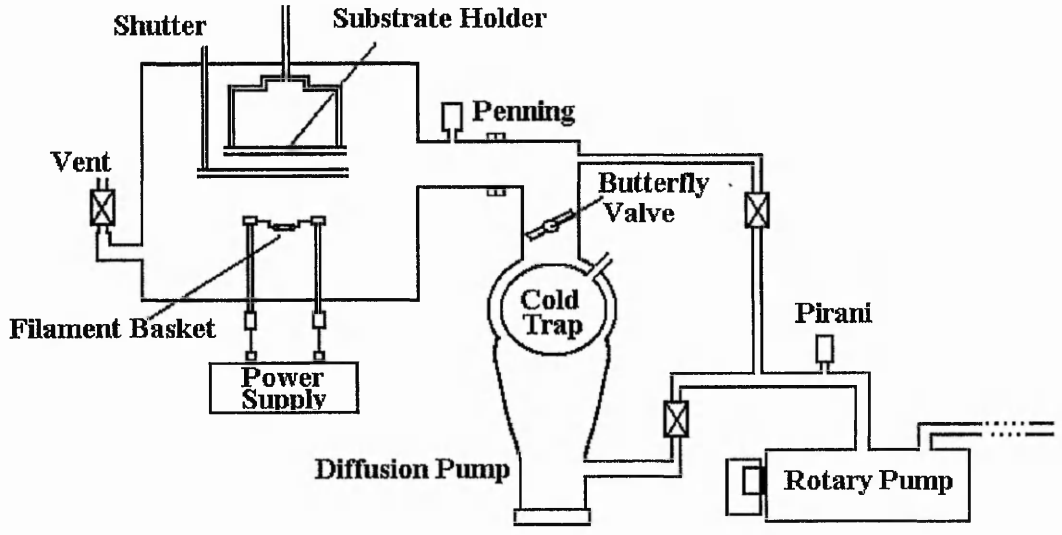


Figure 3.2 a: Schematic Diagram of the Thermal Evaporator

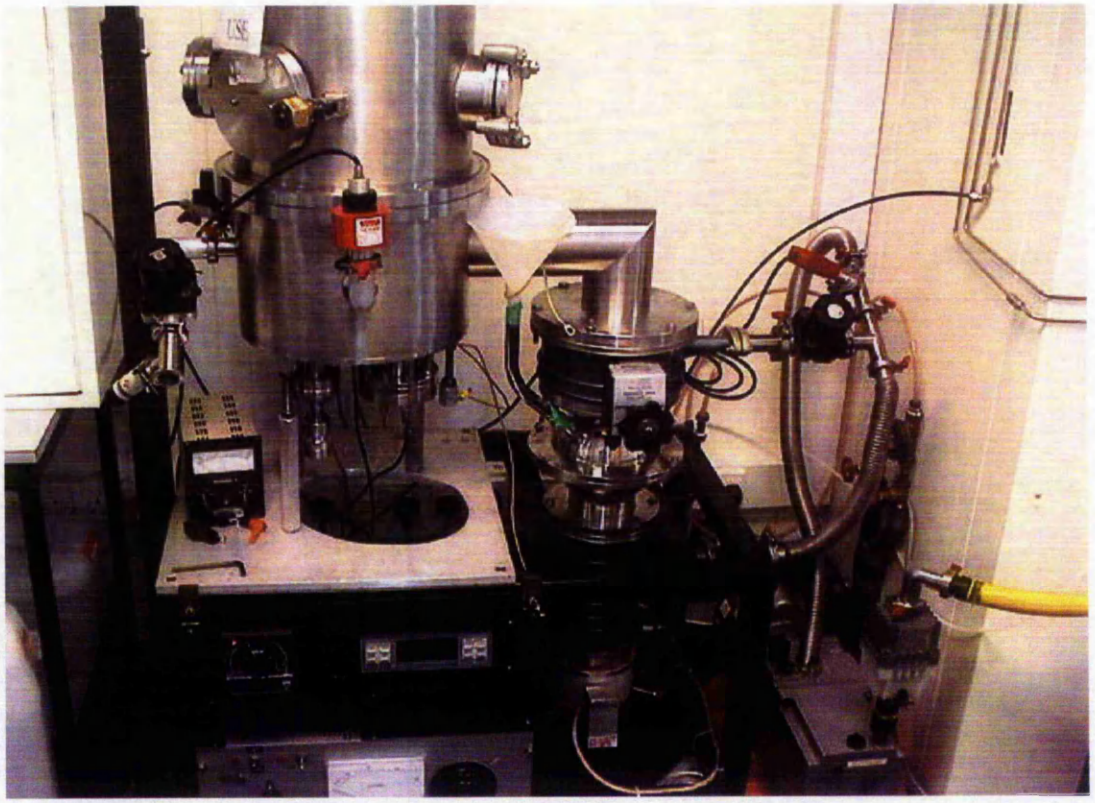

Figure 3.2 b: Photograph of the Thermal Evaporation System

## 3.3 SAMPLE PREPARATION

For the experiments, SrS based thin films of different structure and on different substrates were prepared by RF magnetron sputter deposition. Typically, SrS phosphor thin films having a thickness of 5000 Å sandwiched between two $Y_2O_3$ layers of 2000 Å deposited on either silicon or glass substrates. For samples on silicon substrates, the polished silicon was used as the bottom electrodes while sputtered ITO forms the top transparent electrode to allow EL measurement of these samples. Some samples also had gold (Au) sputtered electrodes instead of ITO as the top electrode. In the case of glass substrates, the glass substrate is first coated with ITO prior to the fabrication of the TFEL stacks. Aluminium is later evaporated to form the top electrodes. These top electrodes (Al and ITO) are made out of 5 mm spots instead of conventional strips (rows and columns). Figure 3.3.1 illustrates the difference between conventional rows and columns test devices with the spots devices. The utilisation of spot electrodes was to allow the use of non patterned bottom electrodes and also to facilitate the fabrication of different test devices for each electrode, typically for the studies of laser annealing.

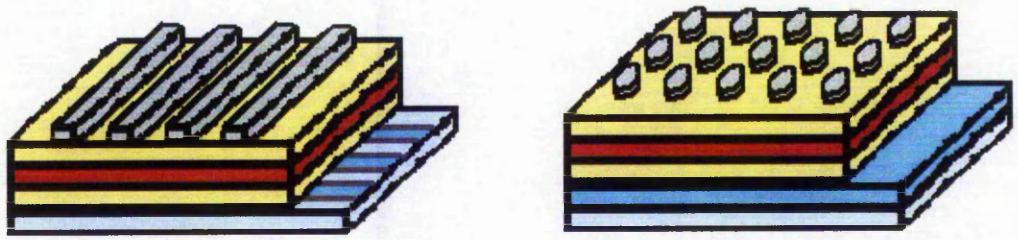


Figure 3.3.1: a) Conventional Row and Column Devices and b) Spots Electrodes Devices

As for the studies of barrier layer devices, an additional layer of insulating material; $Y_2O_3$ with typical thickness of about 100Å was introduced within the SrS based phosphor layer. Some devices were fabricated with various barrier layer thicknesses to allow studies of the possible tunnelling effect. Here again, both silicon and glass substrates were used. Figure 3.3.2 illustrates the two main non barrier layer TFEL device structure utilised in this work. The two main architectures used for barrier layer devices were exactly the same as those illustrated in figure 3.3.2 except for the additional layer within the phosphor film.

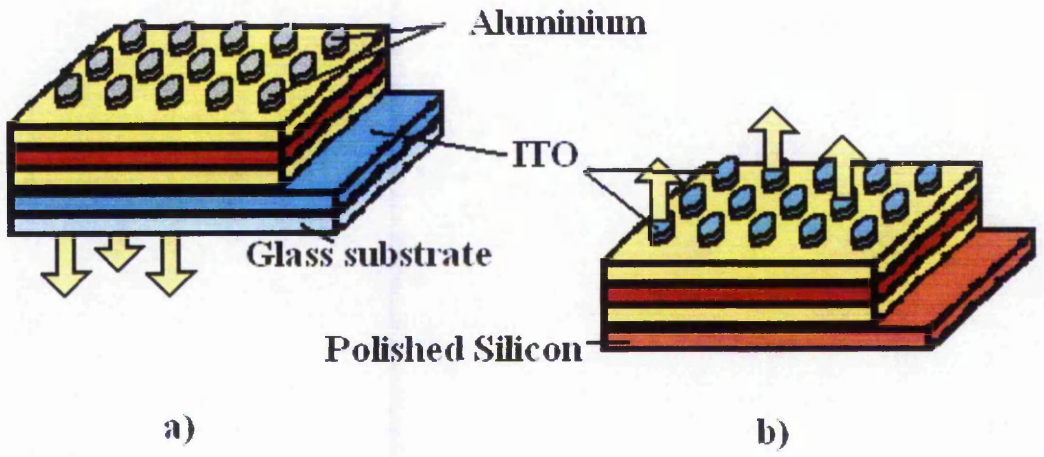


Figure 3.3.2: Test Device Architecture on a) Glass Substrate b) Silicon Substrate

For all cases, PL measurements were performed prior to the formation of the top electrodes. Also, to allow XRD measurement of the test devices, some devices were fabricated on silicon without the top electrodes.

## 3.4 POST DEPOSITION ANNEALING

Ion implantation is a key material processing technology for doping semiconductors in the integrated circuit industry[13,14,15]. Annealing was first introduced as a post treatment process after ion implantation because ion implantation generates crystal damage caused by bombardment of ions with the atoms of the host crystal. In addition, a significant amount of the implanted ions are located in the non-electrically active sites in the lattice. Annealing results in the crystallisation of the amorphous region, reduces the density defects in the regrown single crystal region and activation of dopant atoms by causing them to occupy substitutional sites in the lattice[16].

For the case of TFEL fabrication, typically for this work, as the films were prepared by rf magnetron sputtering, annealing is essential to improve the poor crystallinity of the as deposited films. It is also essential for the activation of the phosphor i.e. ensuring that the luminescent centre occupies the appropriate lattice site. In fact this is more important that any recrystallisation; which is likely to be negligible for heat treatment above 700 °C. Annealing of the phosphor layers removes strain in the films, enhances crystallinity of the grains and accelerates dopant diffusion[17]. Although post deposition annealing is commonly not a favoured process in commercial production[18], appropriate annealing normally results in luminescent enhancement for TFEL devices regardless of the deposition technique employed. Hence the challenge is to find an annealing technique of appropriate parameters for maximum luminous improvement.

There are generally two forms of annealing namely furnace annealing and rapid thermal annealing[19]. For this work, both furnace annealing and RTA were investigated in order to determine which annealing process is able to provide the best device improvement typically in terms of luminescent properties. Annealing was performed on samples with and without the top insulator.

### 3.4.1 FURNACE ANNEALING

Furnace annealing, better known as thermal annealing, is the most basic form of annealing. This is also the most common post deposition technique utilised in commercial TFEL production. For this work, the sputter deposition chamber was used as the furnace. The experimental set up to perform furnace annealing is shown in figure 3.4. (lable substrate holder india)

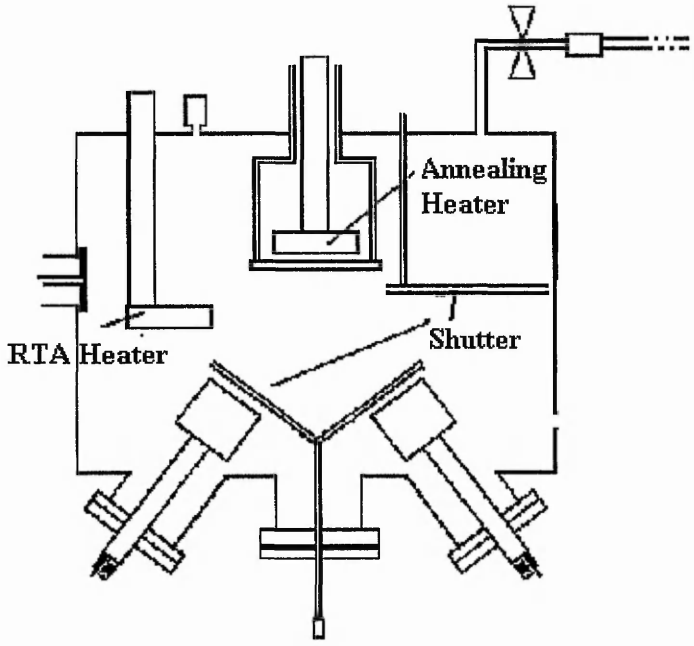


Figure 3.4.1: Furnace Annealing Set up

Generally for furnace annealing, the duration of annealing is about 1 hour. The shutter for the electrode remained closed in order to protect the target from over heating, while the wafer shutter is usually opened to prevent contamination as some material tends to become a residue on the upper side of the shutter. However, studies have been done showing that annealing with the wafer shutter closed doesn't effect the overall result of the annealing process, provided the temperature on the sample remains the same. All annealing has been performed in vacuum although literature[20,21,22] suggested that with suitable gases, for this case Hydrogen Sulphide ($H_2S$) or Nitrogen ($N_2$) , may further enhance the benefit of annealing. The constant rotation of the substrate holder ensures an even heating throughout the whole surface of the wafer.

### 3.4.2 RAPID THERMAL ANNEALING

The goal of annealing for phosphor materials is to activate luminescent centres and improve lattice structure. However, prolonged annealing at high temperature will result in significant redistribution of dopant atoms. Rapid thermal annealing is a term given to various methods of annealing whereby the heating period is between 100 seconds down to nanoseconds in order to minimise the redistribution of dopant. RTA can be divided into three classes: isothermal, thermal flux and adiabatic annealing[23].

Isothermal annealing[19] is an annealing process whereby the heating process lasts in excess of 1second. Rapid isothermal annealing (RIA) utilises tungsten halogen lamps[24] or a graphite heater[25] to heat the samples. Thermal flux[19] annealing covers an annealing process that lasts between $10^{-7}$ to 1 second. The heating for such annealing is provided by a laser, electron beam or flash lamps. For adiabatic annealing[19], the heating time is extremely short; less then $10^{-7}$ seconds. High energy laser pulses[26] are often used for this process. Adiabatic annealing is sometimes also referred as laser annealing.

For the production of TFEL blue emitting devices, RTA and in particular rapid isothermal annealing at high temperature is an essential part in the fabrication path of these devices. This is especially true for SrS based TFEL devices, particularly devices prepared by sputtering due to intrinsic characteristics of the sputtering technique. SrS:Ce are generally subjected to RIA at about 500°C while SrS:Cu is annealed at much higher temperature of about 800°C. Prior to this work, laser annealing is only a potential annealing method for non blue emitting TFEL devices whereas ZnS based material have been widely investigated.

### 3.4.2.1 RAPID ISOTHERMAL ANNEALING

For these studies, the rapid isothermal annealing (RIA) was carried out in the deposition chamber of the rf magnetron sputtering system. Instead of utilising the substrate heater as a heat source for annealing, an additional heater namely the RTA heater was utilised. The introduction of this additional heater within the deposition chamber is to facilitate the possibility of annealing the TFEL devices without having to expose the TFEL devices to air. Figure 3.4.2.1 illustrates the position of the heaters and shutters during the isothermal annealing process. The heating time is determined by the total duration whereby the RTA heater is situated at the bottom of the substrate holder. For a typical annealing process, the RTA heater is first allowed to heat up on the side of the deposition chamber. When the required temperature is achieved, the RTA heater is swung under the bottom of the substrate holder and remains at the bottom of the substrate holder for the whole annealing duration. The RTA heater is then swung away after the required amount of time. The substrates were allowed to cool down normally.

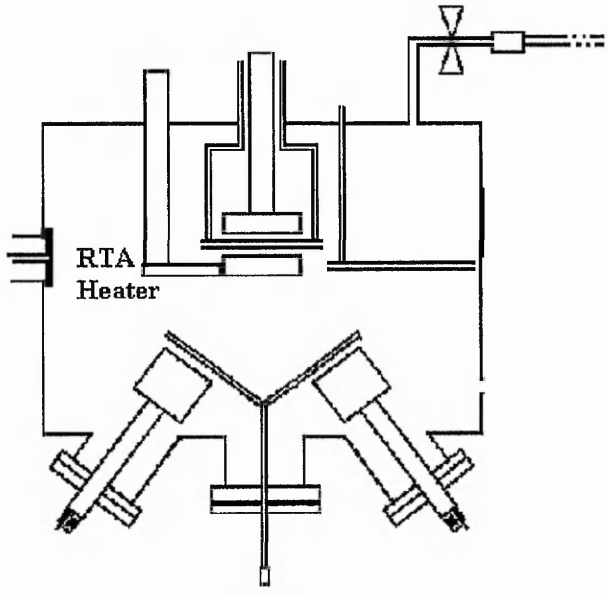


Figure 3.4.2.1: Isothermal Annealing Set up

### 3.4.2.2 LASER ANNEALING

Ever since the first use of lasers for material processing in 1982[26], lasers have been extensively developed in order to satisfy the demands for the development and enhancement of various microfabrication technique to support device fabrication of micro and nano technologies. Together with this, the application of laser continue to expand. Today, lasers are not only used for micromachining, and structural modification of different materials, but also employed in medical application such as the use of intense excimer pulsed laser at 193nm to reshape human corneas for correction of short or long sightedness[27].

The use of lasers for annealing systems in production has been implemented since 1998[28]. The system is now extensively utilised in the manufacturing of active matrix LCD monitors. Laser annealing of phosphor material although also first investigated as early as 1982[29], has yet to be realised in production. This is mainly attributed to the lack of understanding of the effect of laser annealing on phosphor material.

The true advantages of utilising laser annealing technique TFEL phosphor material over other conventional annealing method in terms of EL improvement were only demonstrated recently by E.A. Mastio el al of Nottingham Trent University Optoelectronics Group in addition to a detail investigation into the effect of laser annealing on phosphor material[30,31,32,33,34,35]. All work prior to this investigation has concentrated on ZnS:Mn.

The investigation of laser annealing for SrS based TFEL phosphor material is a part of a parallel PhD program with Mr D. Koutsogeorgis. An experimental arrangement similar to those made by E.A. Mastio was utilised. The main difference between Mastio's experimental arrangement compared to this work is the addition of an Exitech homogeniser EX-HS-700D. The use of the beam homogeniser not only enhances the output of the laser from 700m J/cm$^2$ to 1.6 J/cm$^2$ but also improves the uniformity of the laser spots. The laser annealing arrangement utilised for this work is illustrated in figure 3.4.2.2.

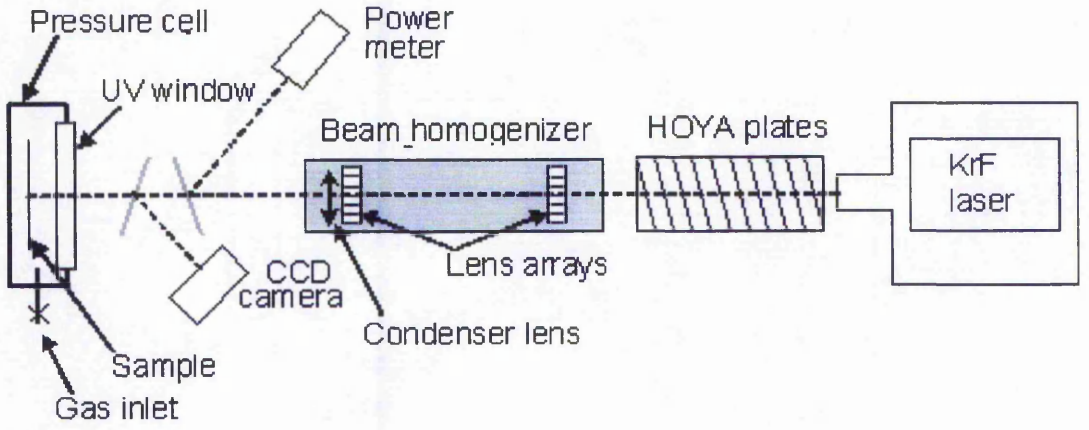


Figure 3.4.2.2 a) Schematic of the laser annealing set up

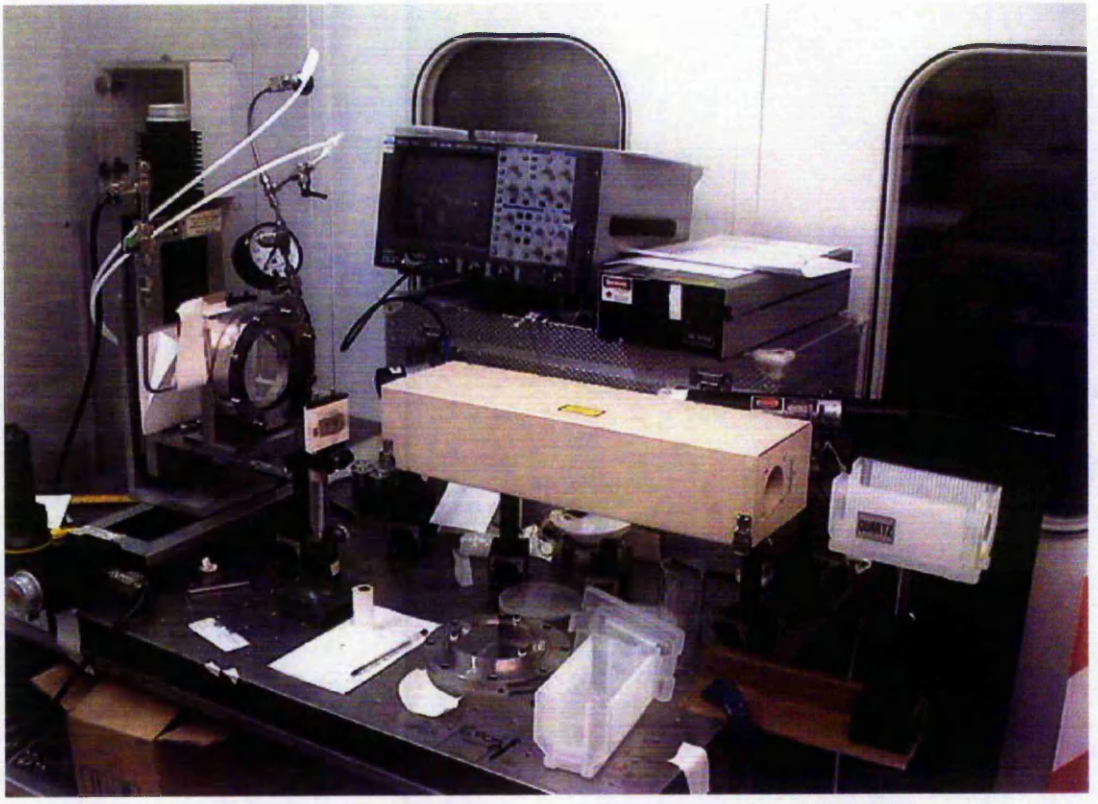

Figure 3.4.2.2 b) Photograph of the laser annealing set up excluding the laser

The laser utilised here is the Lambda Physik LPX 220i excimer laser charged with KrF, emitting pulses of 20 ns at 248nm. The laser beam is first directed through a variable number of Hoya plates, then through the beam homogeniser before being incident onto the samples. The Hoya plates are made out of uncoated quartz plates and are utilised for the attenuation of the laser fluence. The greater of the number of Hoya plates used in the line of the laser beam path, the lower the irradiation energy on the sample. The sample is situated in a pressure cell mounted on two translation stages. The pressure cell is basically a stainless steel chamber with an inch thick quartz window that can house a 4'' wafer.The use of the pressure cell is to minimize ablation, which resulted in material loss. The need of a pressure cell for laser annealing of phosphor material has been determined since the very first work of laser annealing on ZnS:Mn[29]. The translation stages are used to move the in x and y coordinates perpendicular to the incident laser beams. Typically, for laser annealing, the pressure cell is filled with 150 psi of argon gas.

There are many factors that affect laser annealing which include laser wavelength, polarization, energy and fluence of the incident light, pulse length, number of pulses, environmental pressure, environmental composition and environmental temperature. For this study, main concentration is on the affect of laser fluence and the number of pulses. This study covers both the non barrier layer and barrier layer SrS:Cu,Ag TFEL devices. In addition, some work has been carried into the investigation of pulse length, environmental composition and environmental pressure effect on laser annealing of SrS:Cu,Ag TFEL devices. For laser annealing, no SrS:Ce films were studied as SrS:Cu,Ag material exhibits better potential as an efficient blue emitting phosphor for TFEL devices.

## 3.5 CHARACTERISATION SYSTEM

For the evaluation into the effect of post deposition annealing on SrS:Cu,Ag films, the photoluminescence (PL) and electroluminescence (EL) characteristic of the films were studied. PL measurement is one of the major methods employed for the study of the luminescence properties of SrS based blue phosphor. The reason is that the PL emission of SrS based films closely resembles the EL emissions. Ultimately, EL characterisation is needed for the studies of luminance and efficiency of the device. XRD examinations were performed on some of the laser annealed SrS:Cu,Ag films for analysis of the crystallinity.

### 3.5.1 PHOTOLUMINESCENCE MEASUREMENT

The photoluminescence measurement was performed in a dark room in order to improve the signal to noise ratio. The PL measurements were performed via excitation with a Omnichrome 30mW Helium Cadmium Ultraviolet (UV) laser at 326nm, using an Ocean Optics Spec 2000 detector. The laser beam first passes through a band pass UV filter (UG5) before being incident on the sample at an angle to allow the mounting of a quartz fibre perpendicular to the samples. The fibre is fitted with a visible cut out filter (GG385) to filter any UV scattering from the samples. The light collected by the fibre is then directed in to the spectrometer prism and analysed by the CCD array. A photograph of the PL arrangement is shown in figure 3.5.1. All PL measurements were performed prior to the deposition of the top electrodes, at which stage annealing was performed.

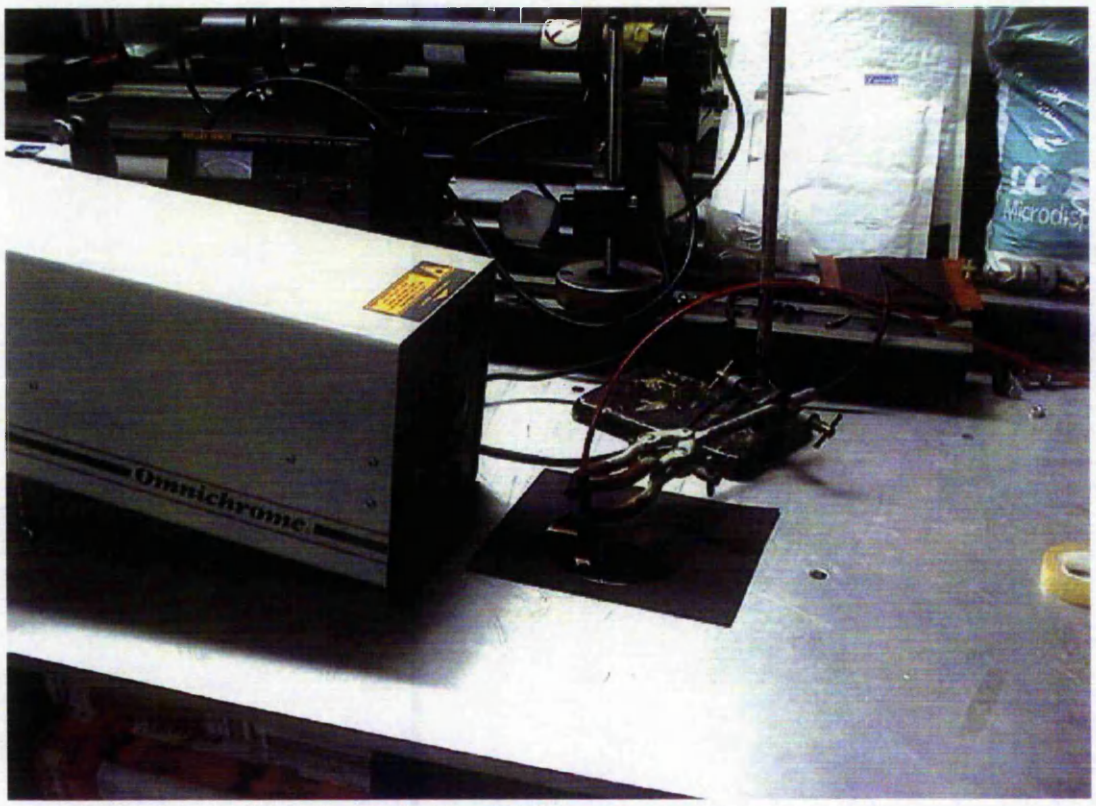


Figure 3.5.1: PL Measurement Arrangement

### 3.5.2 ELECTROLUMINESCENCE MEASUREMENTS

For the study of electroluminescence of SrS films, two different arrangements have been used in order to facilitate the studies of EL characteristic of two different substrates. The study of EL characteristics for devices on silicon were performed in probe station one (photographed in figure 3.5.2.1) while devices on glass substrates were carried out in a custom built probe station as illustrated in figure 3.5.2.2.

For devices on silicon substrates, the sample is placed on the metal vacuum chuck. The device is probed from the top while the polished silicon is the ground for the device. The light emitted from the device is measured in foot lambert (fL) by a luminance meter (MINOLTA LS110) positioned 20cm away from the device. The luminance meter provides an acceptance angle of 1/3° and only measures a small circular area of 1.1mm$^2$.

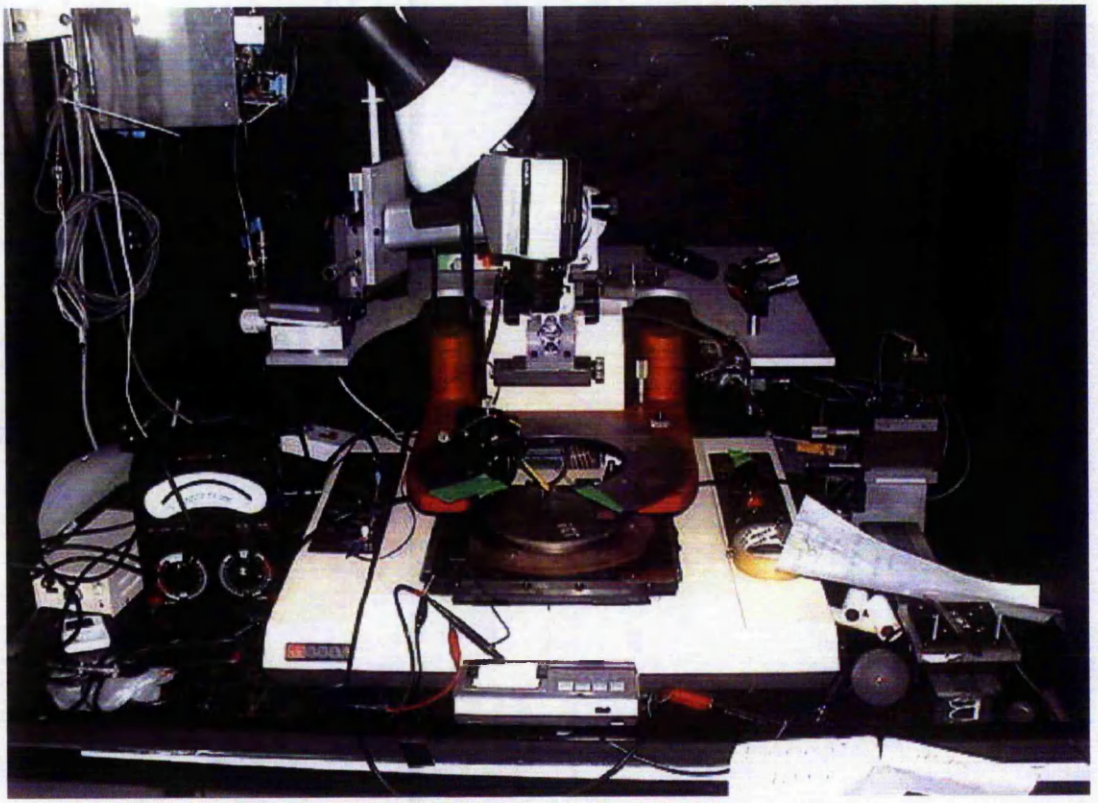

Figure 3.5.2.1: Photograph of Probe Station One

For transparent devices; devices are fabricated on glass substrates, as the emission was supposed to be measure from the glass area and not the top electrodes. It has proven to be very difficult to use probe station one as the measurement equipment. A custom made arrangement is utilised mainly to assist in the probing of the device. A schematic of the test station is shown in figure 3.5.2.2.

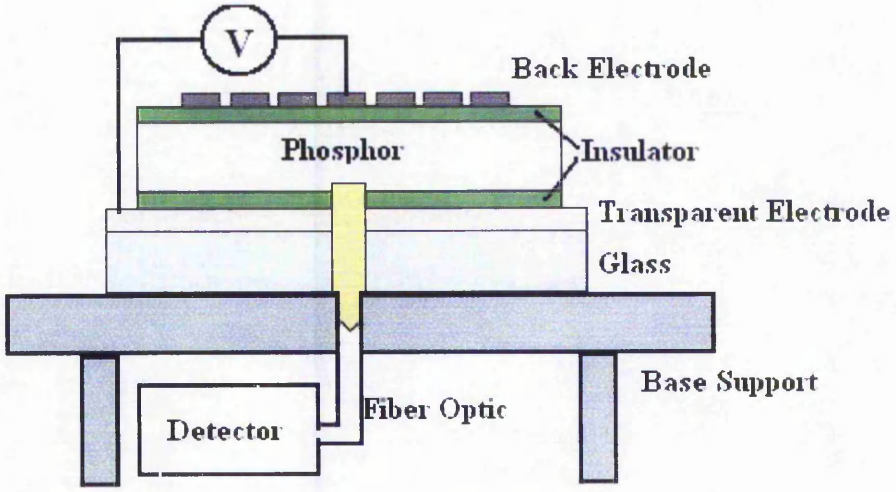


Figure 3.5.2.2 a: Schematic Diagram of the Custom Made Test station

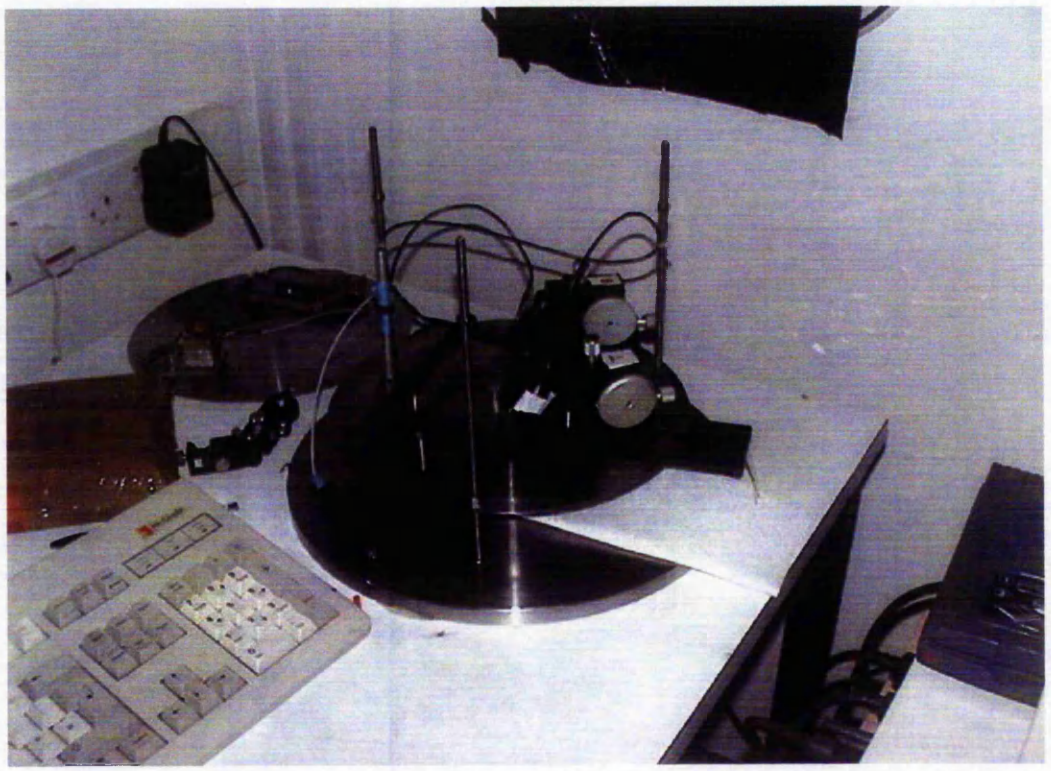

Figure 3.5.2.2 b: Photograph of the Custom Made Test station

The sample to be tested is placed on the top of the base support. The device to be tested is then aligned to the tip of the fibre optic connected to the base support. The opening of the fibre is much smaller then the overall size of the device making this task a simple one. The fibre is connected to either a photo-multiplier or a photo diode which acts as the detector for the emitted lights. With this arrangement the probing of the device can be done from the top of the device making it much easier an arrangement compared to probe station one.

For both cases, the AC amplifier supplies a constant 5 kHz sine wave. The voltage is ramped from 50 Volt peak to peak ($V_{p-p}$) to 700 $V_{p-p}$ in 8 volts steps. The intensity values are taken for each step increment starting from 250 $V_{p-p}$ up to 700 $V_{p-p}$ . All measurements were performed in a dark ambient environment and at room temperature.

**REFERENCES**

[1] X. Wu, P. Bailey, K. Foo and J. Stiles, SID 94 Digest, pp. 558, 1994.

[2] T. Suntola. Handbook of Crystal Growth 3, (ed. D.T.J. Hurle), Elsevier, pp. 605, 1994.

[3] Private conversation with W.M. Li, University of Helsinki, Finland.

[4] H. Ohnishi, K. Yamamoto and Y. Katayama, Conference Record of the 1985 International Display Research Conference, pp. 159, 1985.

[5] S.S. Sun. E. Dickey, J. Kane and P.N. Yocom, Conference Record of the 1997 International Display Research Conference, Toronto, pp. 301, 1997.

[6] S.S. Sun. 4th Inter. Conf. Sci. Tech. display Phosphor, Extended Abstracts, Bend, OR, pp. 183, 1998.

[7] S.S. Sun, Conf. Rec. 1998 Inter. Display Research Conf., Asia Display '98, Souel, Korea.

[8] E.A. Mastio, W.M. Cranton, C.B. Thomas, E. Fogarassy and S. Unamuno, Applied Surface Sciences, 139, pp. 35, 1999.

[9] D.A. Glocker and S.I. Shan: Handbook of thin film process technology, Institute of Physics Publishing Bristol and Philadelfia, October 1995.

[10] W.R. Grove, Philos. Trans. R. Soc London, A 142, pp. 87, 1852.

[11] G.K. Wehner and G.S. Anderson, Handbook of Thin Film Technology, L.I. Maissel and R. Glang, Eds, McGraw Hill, Chapter 3, New York, 1970.

[12] J.M.Hurd and C.N. King, J. Electronic Material, Vol. 8, pp. 879, 1979.

[13] H. Ryssel and H. Glawischnig, Ion Implantation Techniques, Spinger-Verlag, Berlin, 1982.

[14] H. Ryssel and I. Ruge, Ion Implantation, John Wiley & Son, New York, 1986.

[15] J.F. Ziegler, Ion Implantation: Science and Technology, Academic Press, Orlando, Florida, 1984.

[16] R.A. Levy, Microelectronic Materials and Processes, Kluwer Academic Publishers, Dordrecht, The Netherlands, 1989.

[17] Y.A. Ono,Electroluminescent Displays, World Scientific, Singapore, 1995.

[18] M.R. Davidson, B. Pathangey, P.H. Holloway, P.D. Rack, S-S. Sun, and C.N. King. Journal of Electronics Materials, Vol. 26, No. 11, pp. 1355-1360, Nov 1997.

[19] S.M. Sze, VLSI Technology, McGraw-Hill Book Company, 1988.

[20] D. Poelman, D. Wauters, R.L. Van Meirhaeghe and F. Cardon, Solid State Communications, Vol. 113, pp. 405-410, 2000.

[21] C.J. Summers, B.K. Wagner, W. Tong, W. Park, M. Chaichimansour and Y.B. Xin, Journal of Crystal Growth, 214-215, pp. 918-925, 2000.

[22] D. Poelman, D. Wauters. J. Versluys and R.L. Van Meirhaeghe, Journal of Applied Physics, Vo. 90, No. 1, pp. 248-251, 2001.

[23] C. Hill, Beam Processing in Silicon Device Technology, Laser and Electron Beam Solid Interaction and Material Processing, J.F. Gibbons, L.D. Hess and T.W. Sigmon, Eds., North-Holland, New York, 1981.

[24] A. Gat, IEEE Electron Device Lett, Vol. 2, pp. 85, 1981.

[25] R.T. Fulks, C.J. Russo, P.R. Hanley and T.I. Karmins, Appl. Phys. Lett, Vol. 39, pp. 604, 1981.

[26] G. Foti and E. Rimini, Laser Annealing of Semiconductor, J.W. Mayer and J.M. Poate, Eds., Academic Press, New York, pp. 203, 1982.

[27] Ming Wang , "LASIK Vision Correction: The Exciting New Eye Surgery." Med World Publishing, 2000.

[28] V. Pfeufer, F. Voß, B. Becker-de Mos, U. Stamm, H. Endertand D. Basting, Proc. SPIE 2992-05, 35, 1997.

[29] H.S. Reehal, J.M. Gallego and C.B. Edwards, Appl. Phys. Lett. Vol 40, No 3, pp. 258-260, 1982.

[30] E.A. Mastio, W.M. Cranton, C.B. Thomas, E. Fogarassy and S. de Unamuno, Applied Surface Science, Vol. 138-139, pp. 35-39, 1999.

[31] E.A. Mastio, M.R. Craven, W.M. Cranton, C.B. Thomas, M. Robino and E. Fogarassy, Journal of Applied Physics, Vol.86, No. 5, pp. 2562-2570, 1999.

[32] E.A. Mastio, E. Fogarassy, W.M. Cranton and C.B. Thomas, Applied Surface Science, Vol. 154-155, pp. 35-39, 2000.

[33] E.A. Mastio, C.B. Thomas, W.M. Cranton and E. Fogarassy, Applied Surface Science, Vol. 157, pp. 74-80, 2000.

[34] W.M. Cranton, E.A. Mastio, C.B. Thomas, C. Tsakonas and R. Stevens, Electronics Letters, Vol. 36, No. 8, pp. 754-756, 2000.

[35] E.A. Mastio, W.M. Cranton and C.B. Thomas, Journal of Applied Physics, Vol. 89, No. 3, pp. 1605-1611, 2001.

# CHAPTER 4

# GROWTH & CHARACTERISATION OF SrS THIN FILMS

## 4.1 INTRODUCTION

For over four decades now, Thin Film Electroluminescence (TFEL) has been of commercial and scientific interest in the field of emissive flat panel display technology. However, the lack of an efficient blue emitting phosphor has hampered the advancement of TFEL technology, particularly in the realisation of full colour devices. The two best known blue phosphors, (SrCa)$Ga_2S_4$:Ce[1] and SrS:Ce[2] both have distinctive limitation that require significant enhancements before they can be utilised for true blue or full colour TFEL displays. (SrCa)$Ga_2S_4$:Ce offers a much more saturated blue colour than SrS:Ce but has a very poor luminous efficiency and is very difficult to grow thin films with good crystallinity at low substrate temperature[3]. SrS:Ce on the other hand, provides very good efficiency but unfortunately suffers from a bluish green emission[4,5]. Hence requires heavy filtering which evidently reduces its efficiency. For the case of true blue emitting SrS:Cu,Ag[6] developed after the discovery of the efficient blue emitting SrS:Cu[7] phosphor, although it exhibits an efficient and highly saturated blue emission, it requires very high temperature post deposition annealing to obtain excellent EL performance.

For this study therefore, the use of SrS:Cu,Ag as the active phosphor layer for blue emitting TFEL seemed pertinent, considering the requirement for high luminance and efficiency. However, the initial goal was to demonstrate blue emitting Lateral Emitting Thin Film Electroluminescence (LETFEL) devices, the project was also directed towards the improvement of luminance by various post deposition annealing techniques. Under such circumstances, the reproducibility of the phosphor layer deposition is equally important. The following describes the growth of SrS:Ce and SrS:Cu,Ag thin films.

### 4.1.1 POWDER TARGET

As an alternative to commercial sputtering targets, the source material consisted of phosphor powder to form the sputtering targets for this work. These powders are manufactured by Phosphor Tech Ltd. In order to utilise these phosphor powder for sputter deposition, it is necessary to transform these phosphor powder into solid targets. This was achieved by compressing the powder in a stainless steel tray matching the dimension of an equivalent solid target size: 3 inch diameter by ¼ inch thickness. These targets were fabricated in a custom made hydraulic press shown in figure 4.1.

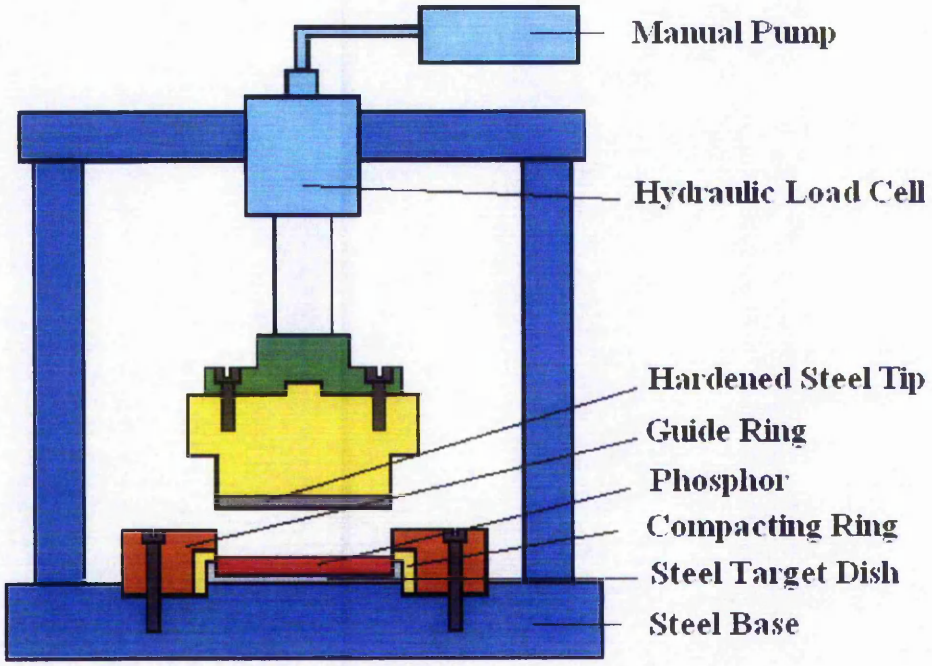


Figure 4.1: Schematic Diagram of the Hydraulic Press

The phosphor powder is first added to the target tray. The excess powder is later removed by a steel ruler, leaving a smooth surface. The target tray with the powder is later put into the press and compressed up to a pressure of 4000 lb/in$^2$ for about 3 minutes. The pressure remains constant for the whole duration of the process. The pressure is then released and the punch is disconnected from the hydraulic load cell and removed away from the pressed powder. Finally, the guide and compress ring is disconnected from the target tray, forming a target suitable for sputter deposition.

## 4.2 THIN FILMS OF SrS:Ce

### 4.2.1 INTRODUCTION

Ce activated SrS (SrS:Ce) has been one of the promising blue-green emitting phosphor materials for EL devices[2,8,9]. Ever since it first discovery by W.A. Barrow et al in 1984[2], work has been carried out to improve its luminance efficiency and colour coordinate. Throughout these times, SrS:Ce TFEL devices have been fabricated using several deposition methods, such as electron beam (EB) evaporation[10,11], reactive evaporation[12,13], sputtering[14,15,16], multisource deposition (MSD)[17] and atomic layer epitaxy (ALE)[18]. There are striking differences between the performance of SrS:Ce TFEL samples deposited by these various methods which may be the result of thin films properties relating to the deposition technique itself[19]. However, regardless of which ever type of technique is utilised for the fabrication of these thin films, post deposition annealing at temperature of at least 500 °C is usually employed, in order to improve the quality of the TFEL not only in term of luminance and efficiency but also to recrystallize the phosphor layer and also activate the dopant[20,21].

For this work, the SrS:Ce phosphor was used primarily to familiarise the procedures necessary to fabricate targets and deposit films based on this compound. The utilisation of sputtering process for the fabrication of SrS:Ce thin films is advantageous in the sense that sputtering generally result in stoichiometric films at low substrate temperature[22] and also enables the deposition of high crystalline quality films at a significant lower substrate temperature, particularly when compared with those utilising evaporation[16].

### 4.2.2 EXPERIMENTAL DETAIL

Depositions of the films were performed using the cluster electrode rf magnetron sputtering system with three magnetron electrodes as described in section 3.2.1. The phosphor films were deposited on polished silicon wafer of 4" diameter in an argon environment. The silicon wafer substrates are used since it is the established fabrication path for LETFEL devices[23]. The effect of chamber pressure, substrate temperature and post deposition annealing technique and temperature were investigated. The chamber sputtering pressures during sputtering in an argon atmosphere were varied from 3 mTorr to 15 mTorr while the substrate temperatures were varied from room temperature up to 450 °C. The post deposition annealing techniques employed were furnace annealing and rapid isothermal annealing (RIA) with varying annealing temperature ranging from 500 °C to 900 °C. Barrier layer devices of 100 Å thick $Y_2O_3$ were also examined. Table 3 lists the ranges over which these parameters were studied.

| Parameter | Range | |
|---|---|---|
| Chamber Sputtering Pressure | 3 - 15 m Torr | |
| Substrate Temperature | Room Temperature - 450 °C | |
| Furnace Annealing | 15 min - 1 hour | 500 -900 °C |
| Rapid Isothermal Annealing | 100 sec - 15 min | 500 -900 °C |

Table 3: Deposition and Annealing Parameters and their ranges for SrS:Ce phosphor films fabrication.

Generally, two type of test device depositions were fabricated; initially, SrS:Ce films of 5000 Å – 8000 Å thickness were grown directly on the polished silicon to evaluate the luminescent properties exhibited by PL excitation. For EL excitation testing, the conventional double insulting dielectric structure was fabricated by growing films of various SrS:Ce thicknesses sandwiched between successive deposition of 3000 Å thick $Y_2O_3$ films. The majority of these devices were annealed prior to the deposition of the top insulating material with a small number of devices annealed with a thin layer of top insulator. The electrodes consisted of thermal evaporated aluminium of 500 Å thick as the top electrode with the silicon substrate forming the bottom electrode.

### 4.2.3 RESULT

The first series of samples were deposited at room temperature in a 3m Torr argon environment and subsequently annealed utilising both furnace annealing and rapid isothermal annealing at temperature ranging from 500 °C to 900 °C. All samples did not exhibit any PL emission prior to annealing while only samples annealed by RIA with a thin top insulator were able to show some very weak PL emission. All films annealed at temperature above 600 °C show signs of crazing with films facing the annealing heater being the worse.

In order to tackle the crazing effect, the substrate temperature was raised to 200 °C for the second series of samples. These films exhibits less crazing compared to those grown in room temperature but still do not demonstrate sufficient PL emission. Unfortunately, no EL emission can be observed from these films. For films grown at substrate temperature of 450 °C, RIA at 850 °C although exhibit the best PL emission among all the above mentioned devices, its emission was unfortunately still too weak for any detection by the Ocean Optics Spec 2000 detector. In addition, no EL emission can be observed from all these films.

As EL emission can be improved by the addition of a thin dielectric within the phosphor layer for ZnS:Mn; namely barrier layer devices[24], similar devices have been fabricated utilising SrS:Ce instead. These devices were fabricated with substrate temperature fixed at 200 °C but with sputtering pressure of 5m Torr and 15m Torr. This is because films grown at higher gas pressure exhibit better film uniformity over the whole 4" wafer. Unfortunately, there was still no EL emission from these films.

A Summary of these disappointing results obtained from thin film sputtering of SrS:Ce is given in table 4.

| Substrate Temperature | Sputtering Pressure | Post Deposition Annealing | | Remarks |
|---|---|---|---|---|
| | | Furnace Annealing | Rapid Isothermal Annealing | |
| Room Temperature | 3 m Torr | 500, 600, 800, 850, 900 °C | 500, 800, 850, 900 °C | Uneven films, films crazes when annealed at temperature above 600 °C, weak PL for RIA devices with thin top insulator, No EL Emission. |
| 200 °C | 3 m Torr | 500, 550, 700, 800 °C | 750, 850, 900 °C | Less crazing of films post annealed at high temperature, No EL emission detected. Weak PL for RIA films. |
| 200 °C | 5 m Torr | 600, 800, 900 °C | | No PL and EL detected |
| 200 °C | 15 m Torr | 500, 600, 800 °C | 600, 800, 900 °C | Even film deposition, weak PL emission from RIA films, No EL emission. |
| 450 °C | 3 m Torr | | 600, 750, 850 °C | Weak PL emission, but no EL emission. No evident of film crazing |

Table 4: Summary of the result obtained from SrS:Ce films deposited from different deposition and post deposition annealing parameters.

## 4.3 THIN FILMS OF SrS:Cu,Ag

### 4.3.1 INTRODUCTION

One of the most exciting development in electroluminescent phosphors in recent years was the development of SrS:Cu,Ag two component phosphors[6]. The development was mainly attributed to the discovery of good blue chromaticity and efficient EL emission SrS:Cu[7]. Prior to this discovery, reports on copper doped alkaline earth sulphide (AES) were scarce. Vecht et al reported that DCEL devices fabricated with SrS:Cu powder gave a green emission in 1981[25]. In 1985, the first blue emitting SrS:Cu TFEL device was reported by Kane et al[26]. Next comes CaS:Cu,F thin films by Nakanishi et al in 1987[27]. Unfortunately, all these devices exhibited very poor luminance performance attracting little interest for further improvement. The success of SrS:Cu in 1997, resulted in the development of SrS:Ag which although exhibiting poor EL performance has a highly saturated blue emission. The new SrS:Cu,Ag was later designed by Sun[6] to take advantage of both the efficiency of Cu and the chromaticity of Ag.

Originally, the efficient SrS:Cu was prepared by rf magnetron sputtering. Since then, other deposition techniques have been adopted to fabricate such films; such as ALE[28], molecular beam epitaxy (MBE)[29], and EB deposition[30]. This situation is also true for SrS:Cu,Ag, except that at the time of writing, there is not yet a suitable Ag precursors for ALE preventing the use of ALE technique for the fabrication of SrS:Cu,Ag films. Similarly to SrS:Ce, regardless of deposition techniques, post deposition annealing at high temperature is essential for crystallinity and luminance improvement of SrS:Cu,Ag films. For this work, only sputter deposition techniques are considered due to the fact that the first successful SrS:Cu,Ag devices were fabricated utilising this technique.

### 4.3.2 CHARACTERISATION PROCESS

The SrS:Cu,Ag (0.4 $^{m}$/o Cu, 0.6 $^{m}$/o Ag) powder used here was also prepared by Phosphor Tech Ltd. Similarly, SrS:Cu,Ag films was deposited utilising the same cluster electrode rf magnetron sputtering system with three magnetron electrodes as described in section 3.2.1. The characterisation for various sputtering parameters for SrS:Cu,Ag films was carried out on polished silicon wafers. This is mainly to enable the investigation of a wide range of substrate temperature both during sputtering and also post deposition annealing. Initially, the samples were sputter deposited at different substrate temperature ranging from room temperature up to 600 °C in 3mTorr Argon gas environment. Sputtering pressure of 3m Torr was chosen as it is the typically sputtering pressure for the in house fabrication of $Y_2O_3$ and ZnS:Mn films. A series of depositions at room temperature for the investigation into the post deposition annealing effect on these films was later carried out as deposition at all other substrate temperature fail to form thin films on the silicon wafer. It was later discovered that the reason for the inability of film to be deposited on substrate with temperature above room temperature previously was due to insufficient pre sputtering time. It was determined that following a change in the sputtering target, pre sputtering time of 8 hours is required prior to any films deposition.

Additional series of films were deposited with similar substrate temperature range as previous. These films were used mainly to establish an acceptable sputter growth condition. In addition, in order to tackle the film uniformity issue resulting from the first series of films, several measurements were taken including substrate biasing, changing angle of electrode, distance between substrate and electrode and not the least, argon pressure during sputtering.

The optimum growth parameters for sputtering in argon atmosphere was later determined to be sputtering in a pressure of 15 m Torr at 200 °C substrate temperature with the distance 5 cm between the substrate and the sputtering electrode.

### 4.3.2.1 EFFECT OF SUBSTRATE BIASING

It is known that substrates can have DC or RF bias potential applied during sputtering to modify film properties and to alter surface chemical reactivity or net deposition rates. In addition, substrate biasing can affects film morphology dramatically and be used to control film stoichiometry. For this work, the substrate is biased from -20 V to +20 V only with all other parameters being fixed; sputtering at room temperature with 3 mTorr argon pressure. Unfortunately, there is no clear visible difference in term of PL emission prior to post deposition annealing between films deposited in this condition. In addition, the application of substrate biasing between this ranges does not seems to alter the growth rate. The result of this study is shown in figure 4.2. As the main interest at time of investigation was to establish acceptable growth condition for SrS:Cu,Ag thin films, no further efforts have been concentrated in this area.

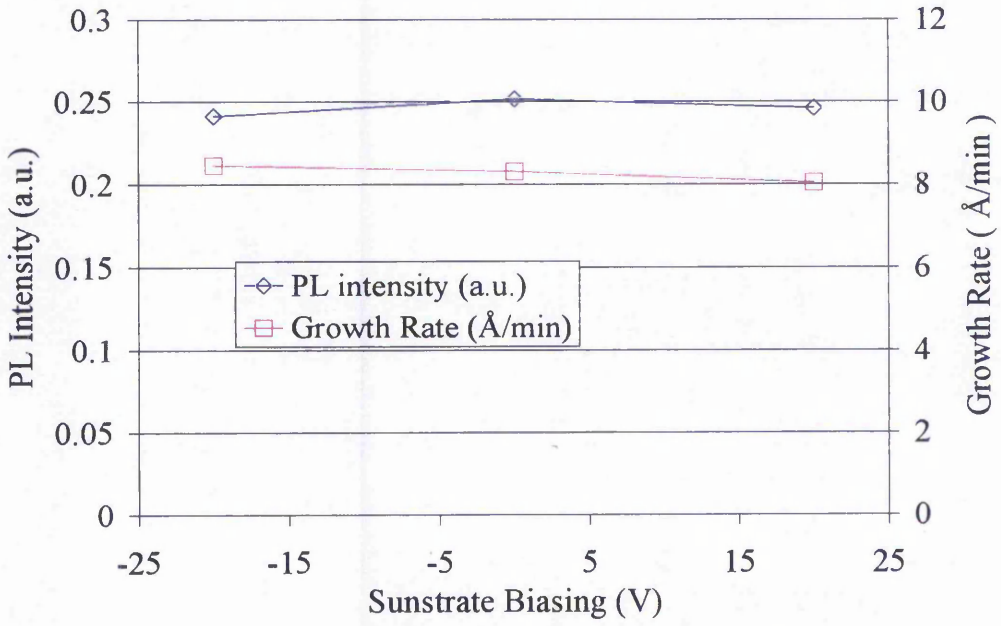


Figure 4.2: Effect of Substrate Biasing on Growth Rate and PL Emission Prior Annealing

### 4.3.2.2 EFFECT OF DEPOSITION TEMPERATURE

Control of the substrate temperature during sputter deposition is crucial as it is directly related to film uniformity in terms of thickness and luminance[31]. Substrate temperature generally used for sputtering of SrS:Cu,Ag is in the region of 150 – 350 °C[6,7]. As the group has no past experience in sputtering of SrS:Cu,Ag films, a decision was made to investigate the effect of deposition temperature on SrS:Cu,Ag films. The parameter for this investigation was in the range of room temperature up to 600 °C. Figure 4.3 shows the performances of films sputtered in 3m Torr argon environment with various substrate temperatures. The behaviour can be separated into three different regions; below 200 °C the emission is low, the emission is strong in the region of 200 – 350 °C, while no emission can be observed for films above 600 °C.

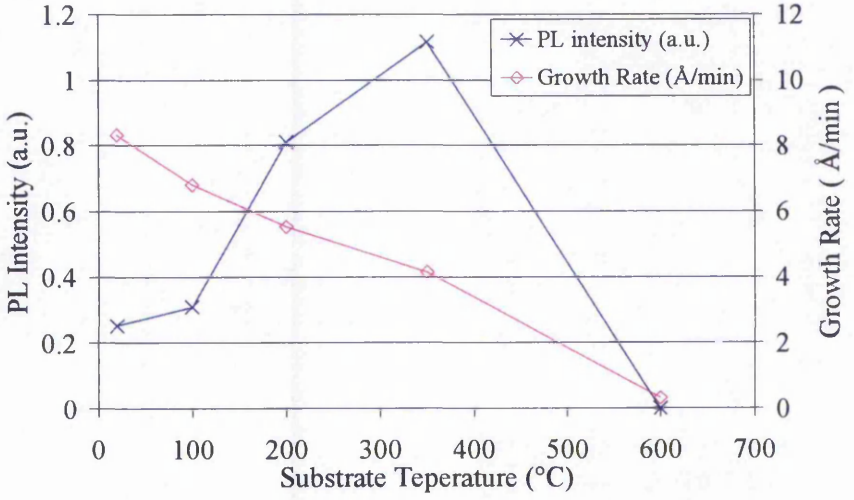


Figure 4.3: PL intensity of as deposited films and growth rate versus substrate temperature for 5000 Å thick SrS:Cu,Ag thin films.

Figure 4.3 also show the affect of substrate temperature on the deposition rate of SrS:Cu,Ag films grown in 3m Torr argon environment with 80W rf power. The figure clearly indicated that the growth rate even at room temperature is not acceptable for a production system. Despite inadequate growth rate, approximately 50% of films grown in room temperature show signs of hazing upon removal from the load lock. A clear evidence of hydrophilic attack possibly due to moisture within the atmosphere.

### 4.3.2.3 EFFECT OF SPUTTERING PRESSURE

Films grown in argon pressure of 3m Torr shows signs of uneven deposition regardless of substrate temperature. Rings of different colours were noticeable through out the whole wafer suggesting difference in film thickness. Several steps were taken in order to improve uniformity, including varying the sputtering electrode angle and sputtering pressure. All these experiment were carried out in argon environment with the substrate temperature fixed at 200 °C.

The uniformity issue was solved by increasing the sputtering pressure from 3m Torr up to 15m Torr. The increase of sputtering pressure however, further reduces the growth rate from 5.55 Å/min to 4.29 Å/min for films deposited at 200 °C substrate temperature. The relationship between sputtering pressure versus growth rate is illustrated in figure 4.4. The figure also shows the PL intensity of these films prior to any post deposition annealing. There are no clear difference for PL intensity for films grown in sputtering pressure in the range of 3 mTorr and 15 m Torr.

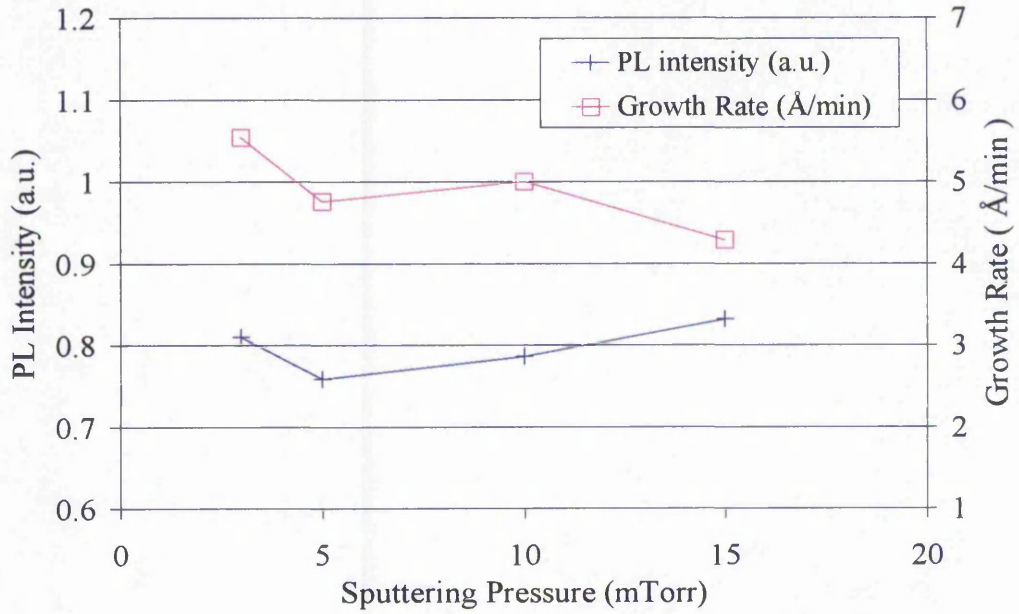


Figure 4.4: PL intensity of as deposited SrS:Cu,Ag films and growth rate versus sputtering pressure.

### 4.3.2.4 EFFECT OF DISTANCE BETWEEN SUBSTRATE AND ELECTRODE

Although films of acceptable quality can be produced by sputtering in a 15m Torr argon environment at a substrate temperature of 200 °C, the deposition rate was regretfully too slow to be realised for any production purposes. In order to tackle this difficulty, the distance between the substrate holder and the electrode during sputtering was reduced. The effect of this study is shown in figure 4.5.

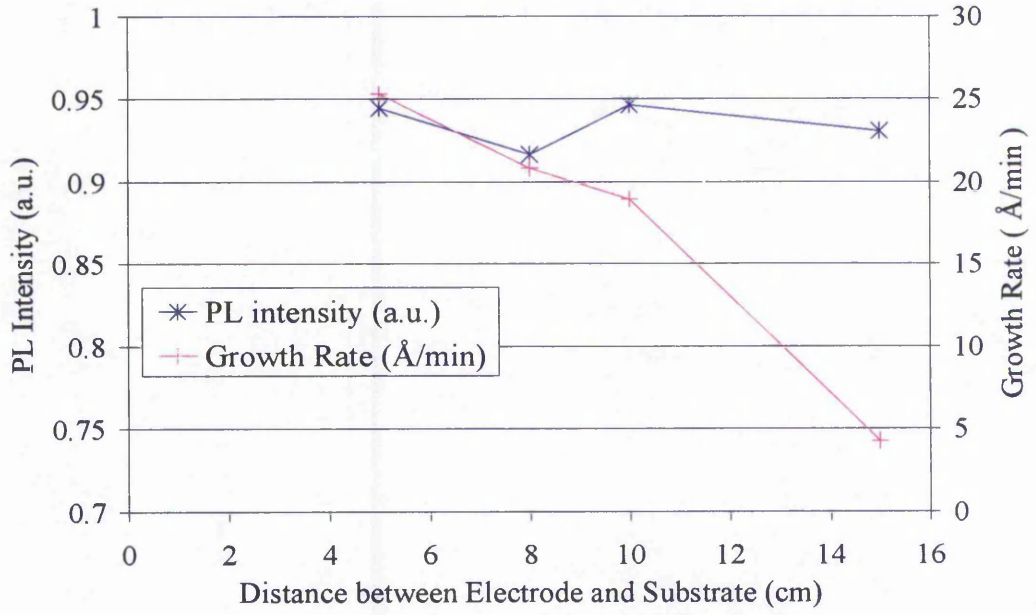


Figure 4.5: PL intensity of 5000 Å thick as deposited films and growth rate versus distance of between substrate holder and electrode.

The growth rate drastically improved by a factor of 5 when the distance between the electrode and the substrate is reduced from 15 cm to 5 cm. Film quality in term of luminance from PL excitation of non annealed films did not seem to show any great difference between the two. This is believed to be a valuable result in defining the parameters of a production system.

## 4.4 POST DEPOSITION ANNEALING OF SrS:Cu,Ag FILMS

It is the nature of the sputtering process that the as deposited films are of relatively poor quality, hence the utilisation of post deposition annealing is necessary for the studies of PL and EL excitation properties of SrS:Cu,Ag films. Initially only thermal based annealing was considered as this was the proven technique as well as rapid thermal annealing (RTA). All SrS:Cu,Ag devices from literature search suggested RTA at temperature around 850 °C [6,32,33] as the post deposition annealed method to improve the luminescence properties of these films. There is however, no publication on SrS:Cu,Ag devices annealed by furnace annealing.

For this work, both furnace annealing and rapid thermal annealing in the form of rapid isothermal annealing were investigated. The studied annealing temperature ranged from 400 °C up to 900 °C, with annealing times varied from as short as 100 seconds up to 1 hour. The main concentration on the improvement of these films was on its PL performance with some work on investigation of the EL performance of annealed films as Toppenz et al[34] reported that there is only marginal differences between EL and PL emission characteristic of SrS:Cu,Ag TFEL devices.

### 4.4.1 EFFECT OF FURNACE ANNEALING TEMPERATURE

The effect of furnace annealing on SrS:Cu,Ag films is least known as there is no literature covering SrS:Cu,Ag devices post deposition annealed by this method. For this study, the samples were annealed in vacuum in the sputtering chamber for a duration of ~ 1 hour. The SrS:Cu,Ag film studied were grown at substrate temperature fixed at 200 °C in 15 mTorr argon atmosphere with a thickness of 5000 Å. Figure 4.6 illustrates the effect of furnace annealing temperature on the luminance from PL excitation of these films.

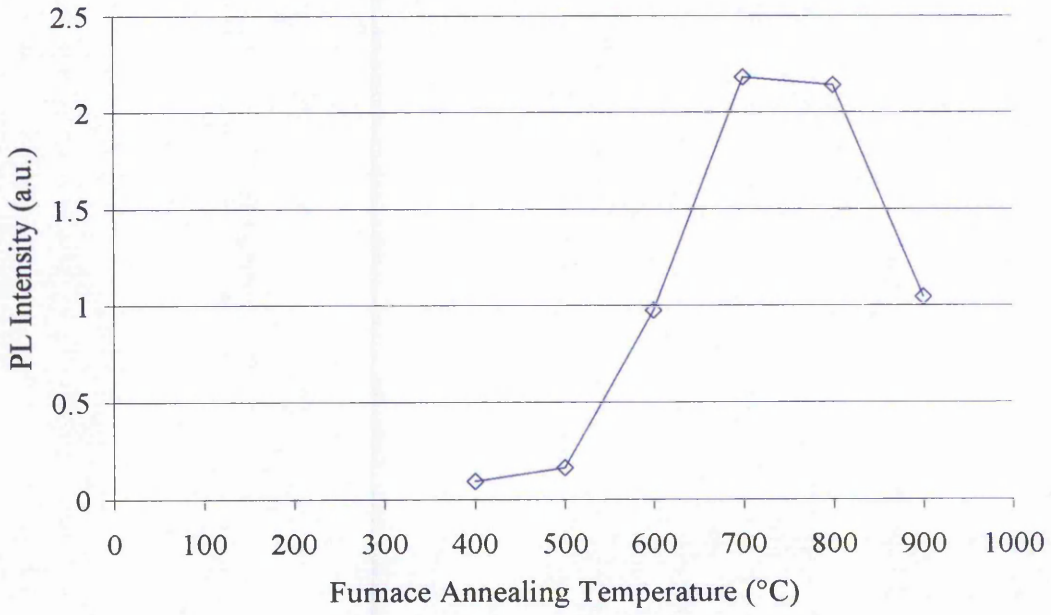


Figure 4.6: PL Intensity versus Furnace Annealing Temperature.

From figure 4.6, the best annealing temperature for furnace annealing is around 700 – 800 °C. The PL intensity which dropped when annealed at 900 °C was mainly attributed to the heavy damage to the films due to crazing. No or little annealing effects are noticeable for devices annealed below 500 °C.

### 4.4.2 EFFECT OF SUBSTRATE TEMPERATURE

As films annealed at temperature above 800 °C suffer the effect of crazing, a solution to this was to increase the substrate temperature during sputter deposition. From previous growth experiment, it is known that films grown at temperature below 200°C were very hydrophilic. The increase of substrate temperature improves the durability of the films and also improves luminance of PL excitation for non annealed devices. For this work, devices were grown at room temperature, 200, 350 and 600 °C similar to those in previous experiments sputtered in 15mTorr argon atmosphere. The annealing temperature investigated ranged between 600 and 900 °C. The result of this investigation is illustrated in figure 4.7 below.

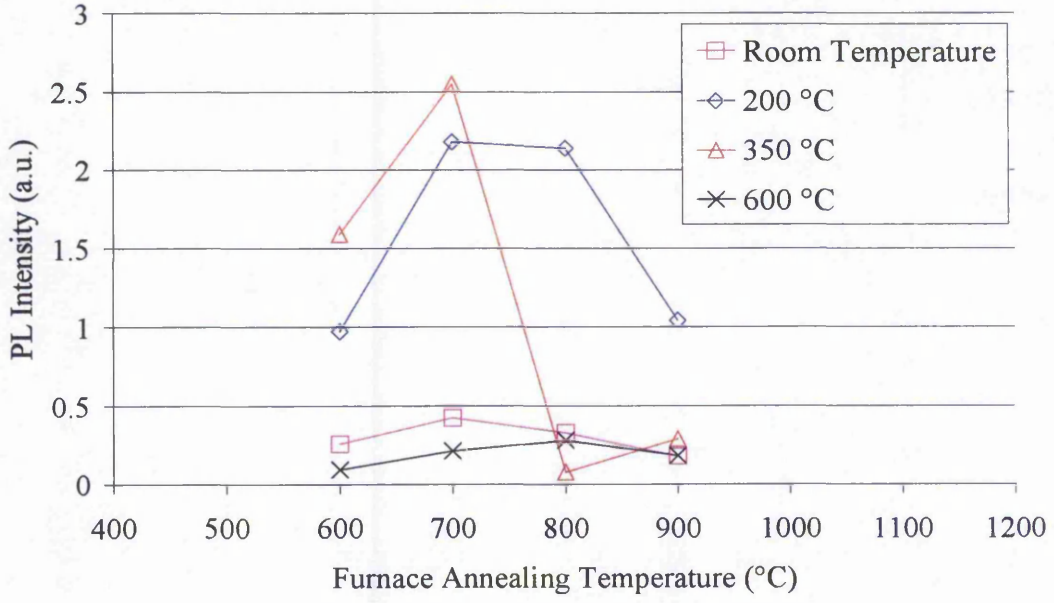


Figure 4.7: Furnace Annealing Temperature effect on PL Intensity of devices grown at different substrate temperature.

Devices grown at 350 °C substrate temperature although showing best PL improvement after annealing at 700 °C, unfortunately do not luminesce when annealed at temperature above 800 °C. This is despite the reduction in crazing effects hence hinting the possibility of over annealing or lost of luminescence centers. Not much improvement can be observed for films fabricated at 600 °C substrate temperature.

### 4.4.3 EFFECT OF RAPID ISOTHERMAL ANNEALING

It is known from literature search that RTA is an essential path of fabricating SrS based devices not only for the improvement of quality of films but also for the enhancement of EL performance of such TFEL device. All published work recommended an RTA temperature of ~850 °C. However, no detail publication can be found on the effect of different RTA temperature on the improvement of SrS:Cu,Ag films.

For this study, the RTA was carried out in an experimental configuration discussed previously in Chapter 3. This is however, not a commercial RTA equipment but only a simulated RTA tool. The heating calibration can be found in appendix B. Figure 4.8 shows the relationship of PL intensity versus RIA temperature.

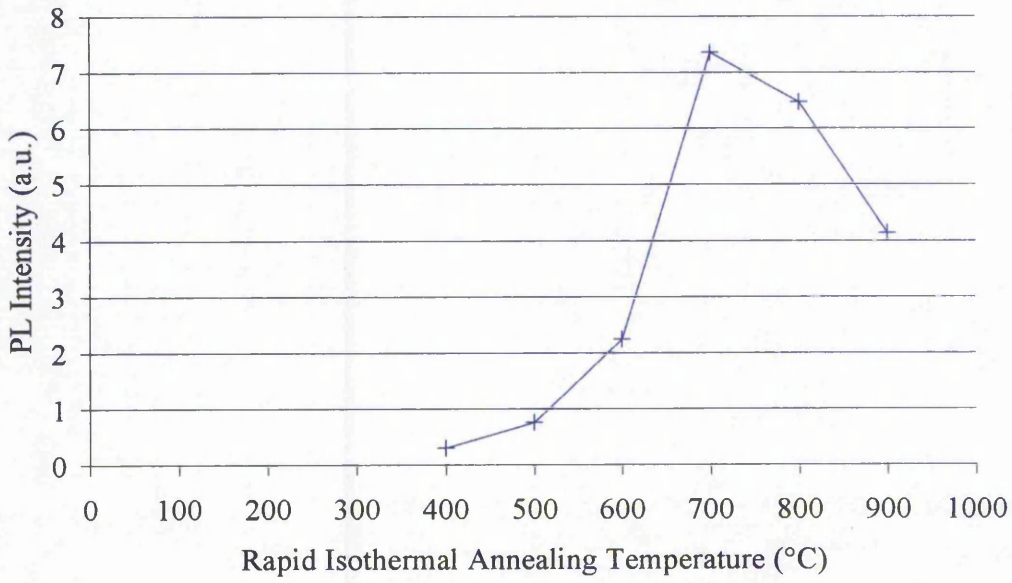


Figure 4.8: PL Intensity versus Rapid Isothermal Annealing Temperature

When utilising RIA, similar to furnace annealing, the best annealing temperature is in the region around 700 °C. PL intensity decreases when annealed at temperature above 700 °C was probably due to crazing of the films. This crazing however, was less than those furnace annealed.

### 4.4.4 EFFECT OF THERMAL ANNEALING TIME

The main difference between furnace annealing and RTA is the heating duration. With the establishment of suitable annealing temperature for both annealing methods, a direct study into the effect of different annealing method i.e. annealing time or more precisely heating time can be performed.

All annealing was performed in a vacuum environment within the sputtering chamber with the annealing temperature fixed at 700 °C. The annealing time was however, varied from 100 seconds up to a total of 1 hour. To enable direct comparison, all annealing was performed utilising the RTA heater as described n Chapter 3. The relationship between annealing time and PL performance is shown in figure 4.9.

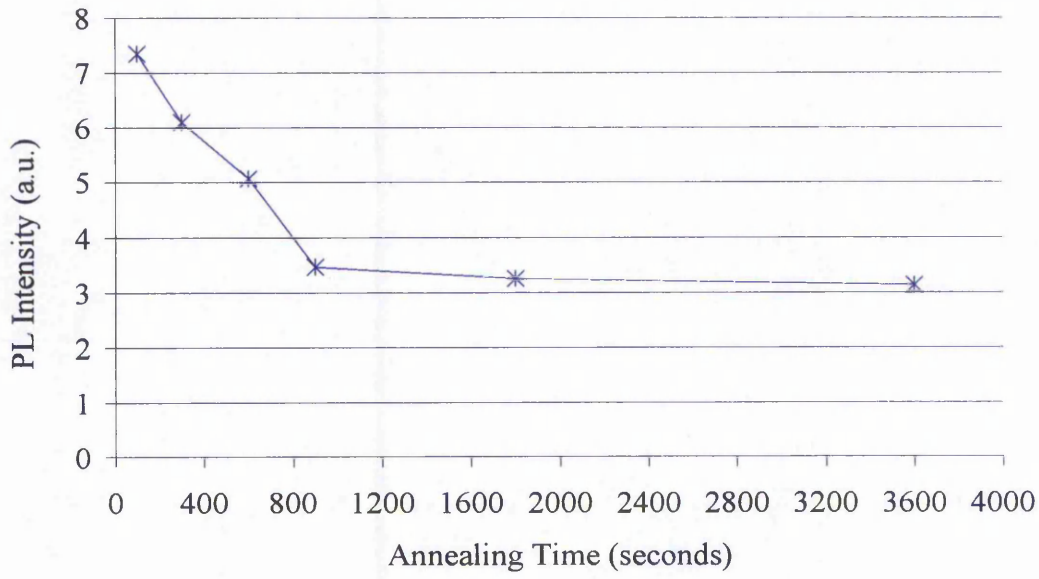


Figure 4.9: PL Intensity versus Annealing Time for films sputtered in 15m Torr argon atmosphere at 200 °C substrate temperature.

With the increase of annealing time, the luminance from PL excitation decreases. There are only marginal differences for samples annealed for 15 minutes or more, while the highest improvement was achieved by samples being annealed for a total of 100 seconds.

### 4.4.5 ANNEALING WITH TOP INSULATOR

SrS based films are known to be substoichiometric. As annealing was performed in vacuum instead of sulphur environment, in order to prevent further loss of sulphur during annealing, work has been done to examine the effect of annealing device with top insulator. Samples were annealed at different temperature and later compared to those annealed in the conventional way, i.e. prior to the deposition of top insulator.

Generally, the trend for the annealing effect is similar to those annealed without the top insulator. The main difference was the improvement in total luminance, with luminance of sample annealed with top insulator was reduced by a factor of 3.3 as shown in figure 4.10.

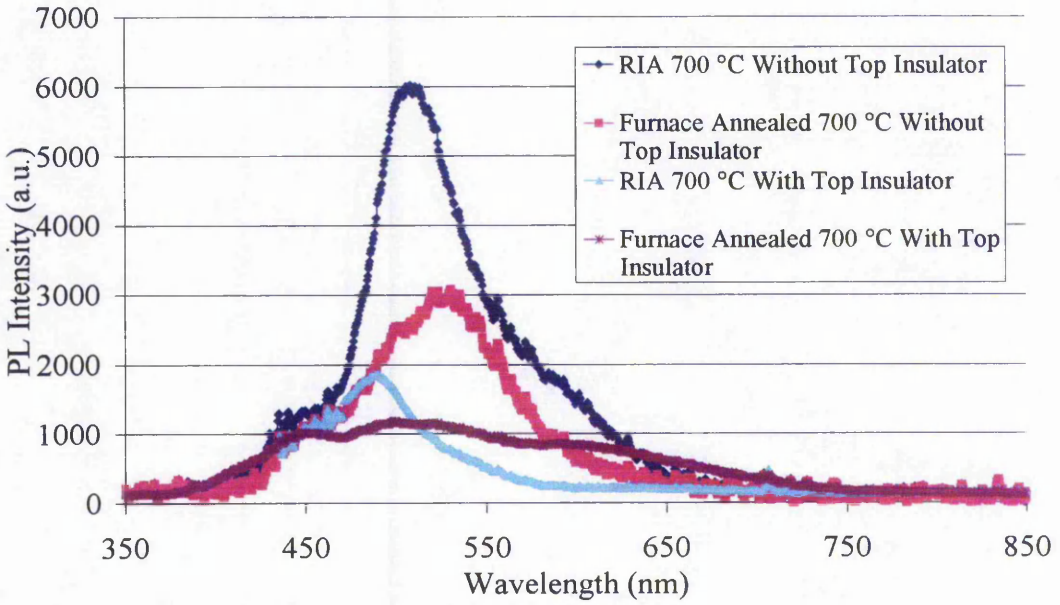


Figure 4.10: Comparison between Annealing With and Without Top Insulator.

### 4.4.6 ELECTROLUMINESCENCE CHARACTERISTIC OF THERMAL ANNEALED FILMS

As the aim for this work is to produce blue emitting LETFEL devices for either head mounted application or light source for electrophotographic printers, it is therefore necessary to electrically characterise SrS:Cu,Ag devices.

The EL characterisation was carried out utilising the probe station shown in figure 3.5.2.1. Although some emission was noticeable for RIA devices at 700 °C, the emission was too weak to be detected by the MINOLTA LS110 luminance meter, hence prohibiting any brightness voltage characterisation. In addition, most devices cannot be measured mainly due to the serious crazing of the films after post deposition annealing typically those furnace annealed at high temperature.

Hence it must be concluded that SrS:Cu,Ag deposited by magnetron sputtering of powder pressed target followed by conventional annealing is unsuitable for the fabrication of reliable EL devices. Probably due to a need for very short annealing times which cannot be achieved with existing RTA system or the lack of a true RTA system. Therefore, decision was made to explore annealing with nano seconds laser pulses i.e. laser annealing.

## 4.5 CONCLUSION

Deposition of SrS:Cu,Ag films from powder pressed target by rf magnetron sputtering followed by conventional post deposition annealing has been demonstrated to be a non possible mean of producing blue emitting TFEL devices, despite the establishment of a suitable deposition parameters i.e. sputtering in 15m Torr argon atmosphere at 200 °C substrate temperature with the distance between electrode and substrate to be 5 cm or less. In order for the fabrication of SrS:Cu,Ag EL devices, a path to anneal the deposited film without damaging the surface of the films must first be established. It has also been shown that to further enhance the luminescence properties of these films; a shorter annealing time is beneficial. This has resulted in the investigation into an alternative form of annealing, namely laser annealing, a parallel program carried out within the optoelectronics group of the Nottingham Trent University. The effect of laser annealing on SrS:Cu,Ag films will be discussed in the next chapter.

In addition, as SrS based films are found to show signs of substoichiometry, sputtering and annealing in a hydrogen sulphide ($H_2S$) environment may be favourable to produce a true blue emitting TFEL device.

The failure of the sputtered SrS:Ce films to produce any emission may due to the fact that the sputtering was from a SrS:Ce (0.3 $^{m}$/o Ce). Most literature suggest the use of SrS:$CeF_3$ in a $H_2S$ environment.

**REFERENCES**

[1] W.A. Barrow R.C. Coovert, E. Dickey, C.N. King, C. Lasskso, S.S. Sun, R.T. Tuenge, R. Wentross and J. Kane, Digest of 1993 SID Interanational Symposium, pp. 761, 1993.

[2] W.A. Barrow, R.E. Coovert and C.N. King, Digest of 1984 SID International symposium, pp. 249, 1984.

[3] S.S. Sun, E. Dickey, R.T. Teunge, R. Wentross and J. Kane, J. SID, 4(4), pp. 305, 1996.

[4] S.S. Sun, T. Nguyen, M. Bowen, J. Kane, P.N. Yocom, A. Naman, K. Jones, P.H. Holloway, D.R. Evans and W.M. Dennis, extended abstracts od 2nd Intl. Conf. On the Sci. Tech. of Display Phosphors, pp. 61, 1996.

[5] K.O. Velthous, B. Huttle, U. Troppenz, R. R. Herrman and R.H. Mauch, SID '97 Digest, pp. 411, 1997.

[6] S.S. Sun. 4th International Conf. Sci. Tech. Display Phosphors, Extended Abstratcts, Bend, Oregon, pp. 183, 1998.

[7] S.S. Sun, E. Dickey, J. Kane and P.N. Yocom, SID 97 Conference Record, SID, Santa Ana, pp. 301, 1997.

[8] E. Soininen, M. Leppanen and A. Pakkala, Proceeding of the 13th International Display Research Conference, Strasbourg, France, pp. 233, 1993.

[9] B. Huttl, U. Troppenz, K.O. Velthaus, C.R. Ronda and R.H. Mauch, J. Appl. Phys. Vol. 78, pp. 7282, 1995.

[10] S. Tanaka, H. Yoshiyama, Y. Mikami, J. Nishiura, S. Ohshio and H. Kobayashi, Proc. 6th Int. Display research Conf, pp. 242, 1986.

[11] S. Tanaka, H. Morita, K. Yamada and H. Kobayashi, Conf. Record 1991 Int. Display research Conf., San diego, pp. 137, 1991.

[12] R.H. Mauch, K.O. Velthaus, G. Bilger and H.W. Schock, Journal of crystal growth, **117**, pp. 964, 1992.

[13] K.O. velthaus, U. Troppenz, B. Huttl, R. Herrmann and R.H. Mauch, Conference Record of the 1991 International display Research conference, San Diego, pp. 137, 1991.

[14] H. Ohnishi, R. Iwase and Y. Yamasaki, SID 88 Digest, pp. 289, 1988.

[15] G.O. Mueller, R. Mach, B. Selle, H. Ohnishi, J. Cryst. Growth, 101, pp. 999, 1990.

[16] H. Ohnishi and T. Okuda, SID 90 Digest, pp. 31, 1990.

[17] Y. Chubachi and K. Aoyama, J. Electrochem Soc., **139**, pp. 2677, 1992.

[18] P. Soininen, E. Nykanen, M. Leskela and L. Niinisto, Proc. 19th Int. Display Research Conf., Strasbourg, pp. 511, 1993.

[19] R. Mach, G.O. Mueller, R.U. Reinsperger, SID 92 Digest, pp. 367, 1992.

[20] K. Ohmi, K. Fujimoto, S. Tanaka and H. Kobayashi, J. Appl. Phys. **78**, pp. 428, 1995.

[21] S. Okamoto, T. Kuki and T. Suzuki, Jpn. J. Appl. Phys., Part 1 **32**, pp. 1672, 1993.

[22] G.O. Mueller, R. Mach and H. Ohnishi, 10th Intl. Display Research Conf. Amsterdam, pp. 88, 1990.

[23] R. Steven, PhD Thesis, University of Bradford, 1994.

[24] C.B. Thomas and W.M. cranton, Applied Physics Letter, Vol. 63, no. 6, 1993.

[25] A. Vecht, M. Waite, M. Higton, R. Ellis and J. Lumin, J. Lumin, 24/25, pp. 917, 1981.

[26] J. Kane, W. Harty, M. Ling and P.N. Yocom, SID 85 Digest, pp. 163, 1985.

[27] Y. Nakanishi, G. Shimoka, Extended Abstract #1224, 172nd Electrochem. Soc. Meeting, 1987.

[28] K. Nyets and G. Stuyven, Applied Physics Letter, Vol. 75, No. 17, pp. 2593, 1999.

[29] C.J. Summers, B.K. Wagner, W. Tong, W. Park, M. Chaichimansour and Y.B. Xin, Journal of Crystal Growth, 214-215, pp. 918, 2000.

[30] S.S. Lee, S. Lim and G.K. Chang, . 4th International Conf. Sci. Tech. Display Phosphors, Extended Abstratcts, Bend, Oregon, pp. 251, 1998.

[31] C. Frey, Society of Information Display International Symposium 88 Digest, pp. 16, 1988.

[32] H.M. Menkara, W. Park, M. Chaichimansour, T.C. Jones, B.K. Wagner, C.J. Summers and S.S. Sun, . 4th International Conf. Sci. Tech. Display Phosphors, Extended Abstratcts, Bend, Oregon, pp. 191, 1998.

[33] D. Poelman, D. Wauters. J. Versluys and R.L. Van Meirhaeghe, Journal of Applied Physics, Vo. 90, No. 1, pp. 248-251, 2001.

[34] U. Troppenz, B. Huttl, U. Storz, P. Kratzert, K.-O. Velthaus, S.S. Sun and D. Tuenge, 4th International Conf. Sci. Tech. Display Phosphors, Extended Abstratcts, Bend, Oregon, pp. 187, 1998.

# CHAPTER 5

# LASER ANNEALING OF SrS:Cu,Ag

## 5.1 INTRODUCTION

In the field of material processing, lasers have been utilised in many application such as welding, bonding, cutting, and drilling. In the semiconductor industry, the use of lasers in various aspects of the device fabrication process is found to have vast advantages over other conventional tools. For conventional laser processing, it is principally a non reactive process involving mainly a thermal mechanism and usually performed in vacuum or in a non reactive atmosphere. The use of laser radiation for lattice improvement namely laser annealing can be classified into two categories, solid phase annealing and liquid phase annealing[1]. Solid phase annealing is similar to the conventional furnace annealing process while liquid phase annealing involved localised melting on the surface of the material induced by the laser radiation.

All previous attempt on laser annealing of SrS based thin films utilising a Xenon Chloride (XeCl) laser have ended with disappointing results[2]. We believe this is due to the lack of photon energy from the laser as XeCl can only deliver 4.13 eV while the band gap of strontium sulphide is ~4.4 eV. In addition, the laser annealing was performed with the absence of a pressure cell, where as successful laser annealing reported by Reehal[3,4,5,6] and Mastio[7,8,9,10,11,12,13] was carried out in an over pressure environment. For this work, laser annealing was performed in a pressurised argon environment utilising a KrF laser capable of delivering 5.13 eV photon energy.

As stated earlier, laser annealing was a parallel PhD programme undertaken by D. Koutsogeorgis. Koutsogeorgis work concentrated mainly on ZnS:Mn with a limited feasibility study of laser annealing of electron beam deposited SrS:Cu,Ag thin films on both silicon and glass substrates. He demonstrated that laser annealed SrS:Cu,Ag thin films exhibit greater PL improvement compared with conventional thermally annealed films and suggested that similar EL improvements could benefit for laser annealed SrS:Cu,Ag devices. Due to this, plus the inability to fabricate sputter deposited SrS:Cu,Ag TFEL devices utilising conventional thermal annealing techniques, an interest arose in investigating the laser annealing of sputtered SrS:Cu,Ag thin films.

The aim of this work was to investigate the effect of laser annealing on sputter deposited SrS:Cu,Ag thin films. In addition, an optimisation of the laser annealing process was also carried out. The parameters examined were laser fluences, number of radiation pulses and environmental pressure. This work also represented the first successful attempt on laser annealing of sputter deposited SrS:Cu,Ag thin films for EL devices.

All work on investigating the effect of laser annealing and process optimisation of sputter deposited SrS:Cu,Ag thin films was carried out at the Central Laser Facility of Rutherford Appleton Laboratory (CLF-RAL) utilising the experimental configuration as described in section 3.4.2.2.

## 5.2 LASER ANNEALING OF SrS:Cu,Ag THIN FILM ON SILICON SUBSTRATE

### 5.2.1 EFFECT OF LASER FLUENCE AND NUMBER OF PULSES

Initially, SrS:Cu,Ag thin films were sputtered on silicon substrates utilising the system described in Chapter 3 with the optimum sputtering conditions established in chapter 4. Due to the great interest in EL, the majority of the phosphor thin films were grown on silicon substrates coated with an insulating layer of $Y_2O_3$. This allows the fabrication of ACTFEL devices after the laser annealing process by depositing the top insulating layer followed by the top electrodes. Some samples of SrS:Cu,Ag were fabricated directly on polished n-type silicon substrates for comparative studies.

The laser annealing process was performed under an pressurised argon environment at 150 psi. Laser pulses of 5x5 mm with fluences in the range of 300 $mJcm^{-2}$ up to 1.6 $Jcm^{-2}$ were irradiated on the samples. The number of laser pulses irradiated on the same device with the same laser fluence was varied from a single pulse up to a maximum of 8 pulses. The combination of various laser fluences and number of laser pulses creates a matrix of laser annealed spots on the sample as shown in Figure 5.1. Usually each row represented a particular laser fluence while the columns

represented a fixed number of laser irradiations. The coloured square shows evident of laser ablation of a maximum of 300 Å of films being ablated measured using a DEKTAK profilometer.

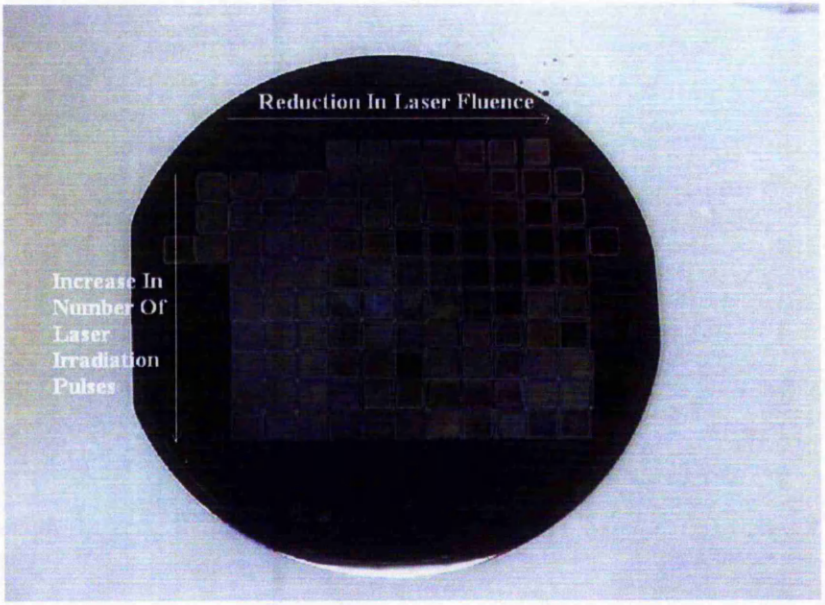


Figure 5.1: Photograph of a typical Laser Annealing Test Sample

### 5.2.1.1 PHOTOLUMINESCENE OF LASER ANNEALED SrS:Cu,Ag THIN FILM ON SILICON

The following 8 graphs show the PL emission for all the laser fluences investigated. Each graph represented PL improvement for specific number of laser pulses. All emission was acquired utilising system described in Chapter 3. In addition, all the emissions shown are after subtractions of background noise.

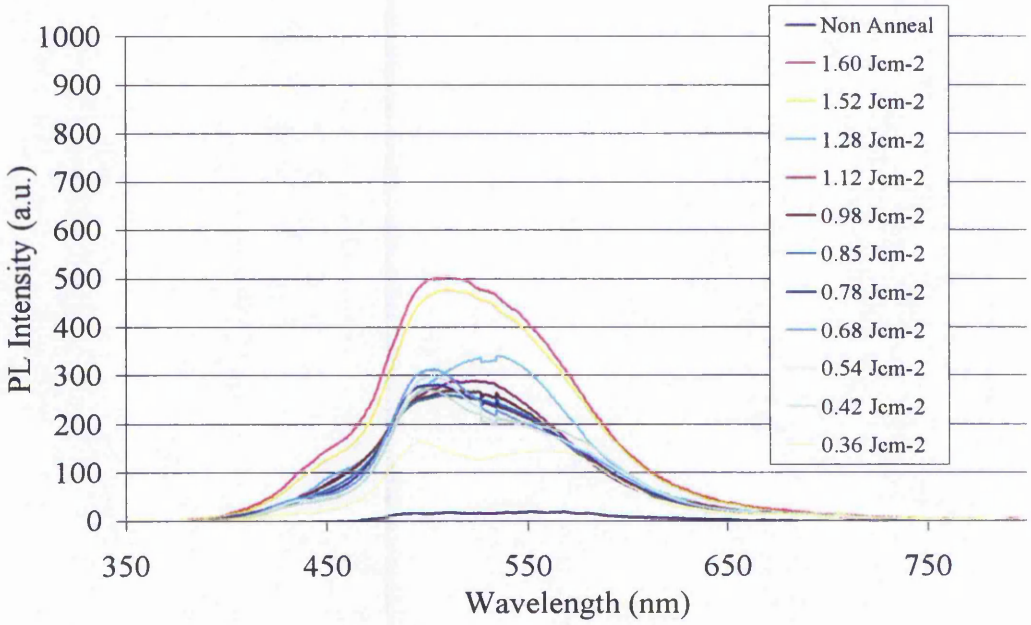


Figure 5.2: PL Intensity acquired by single laser irradiation at various laser fluences for a 500nm thick SrS:Cu,Ag thin film on $Y_2O_3$ coated silicon substrate.

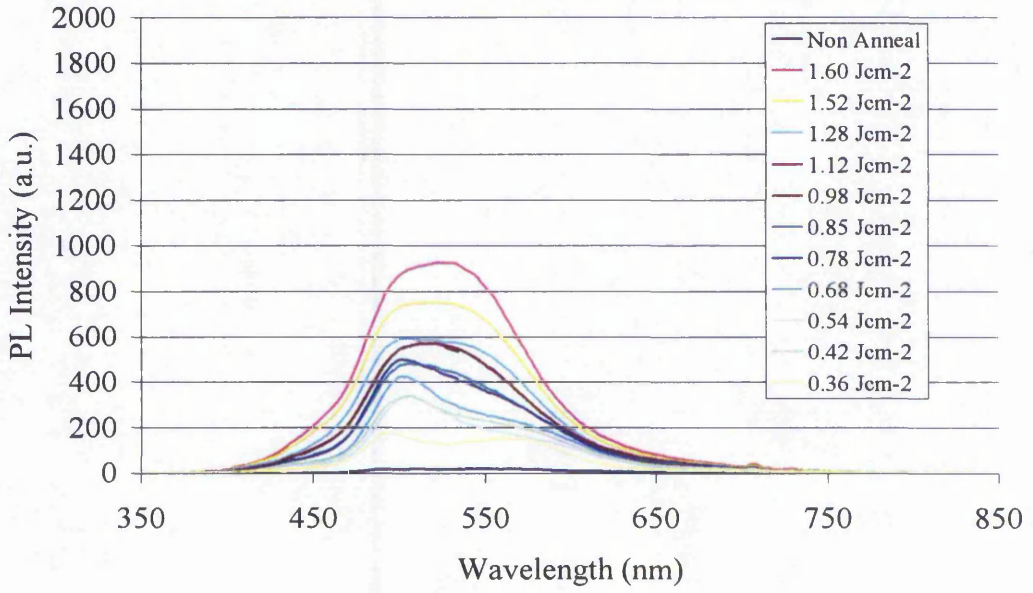


Figure 5.3: PL Intensity acquired by 2 laser irradiations at various laser fluences for a 500nm thick SrS:Cu,Ag thin film on $Y_2O_3$ coated silicon substrate.

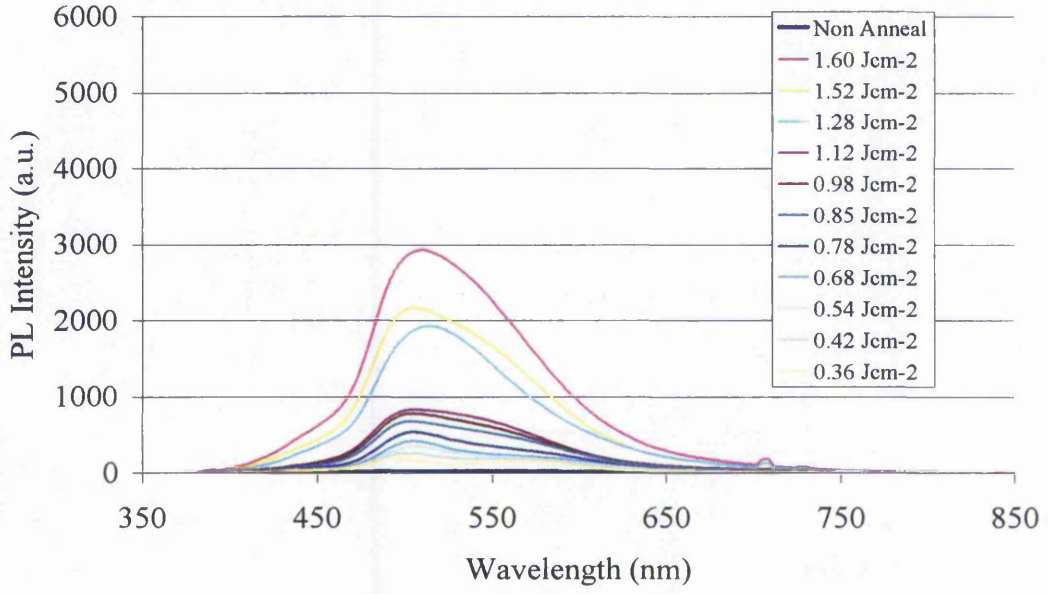


Figure 5.4: PL Intensity acquired by 3 laser irradiations at various laser fluences for a 500nm thick SrS:Cu,Ag thin film on $Y_2O_3$ coated silicon substrate.

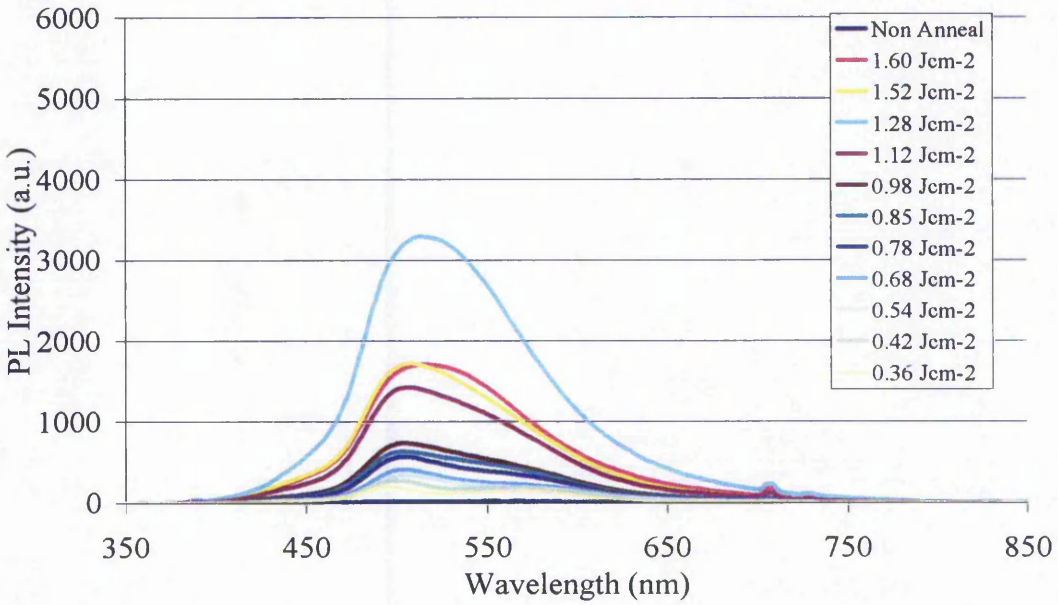


Figure 5.5: PL Intensity acquired by 4 laser irradiations at various laser fluences for a 500nm thick SrS:Cu,Ag thin film on $Y_2O_3$ coated silicon substrate

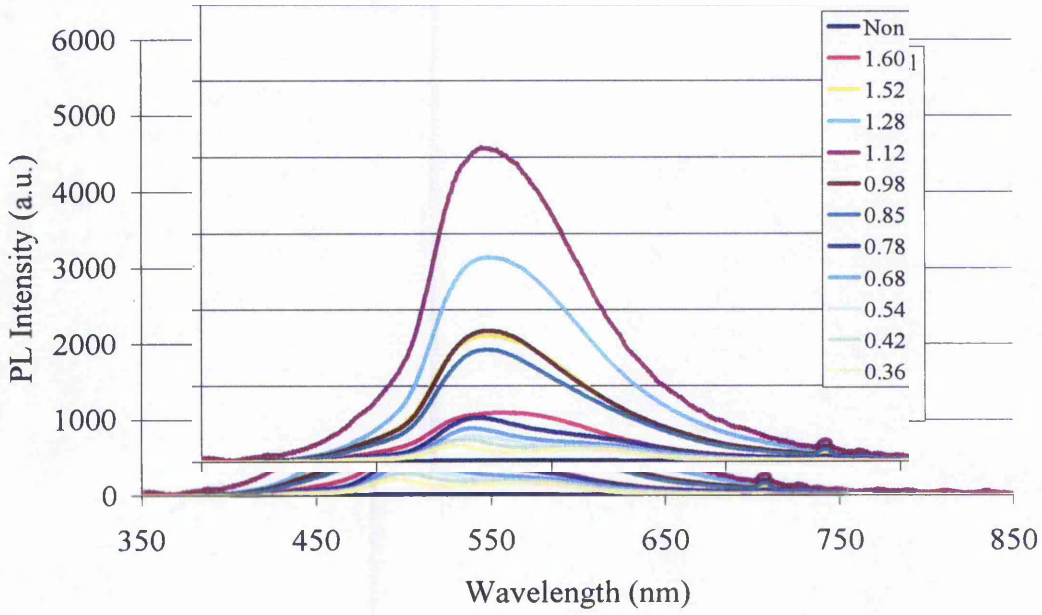


Figure 5.6: PL Intensity acquired by 5 laser irradiations at various laser fluences for a 500nm thick SrS:Cu,Ag thin film on $Y_2O_3$ coated silicon substrate

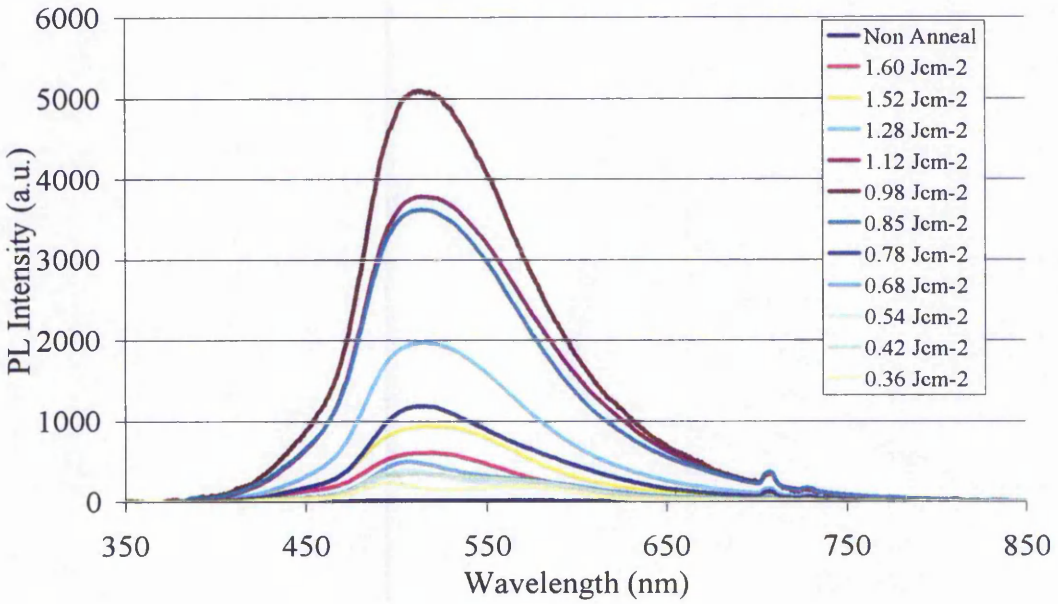


Figure 5.7: PL Intensity acquired by 6 laser irradiations at various laser fluences for a 500nm thick SrS:Cu,Ag thin film on $Y_2O_3$ coated silicon substrate

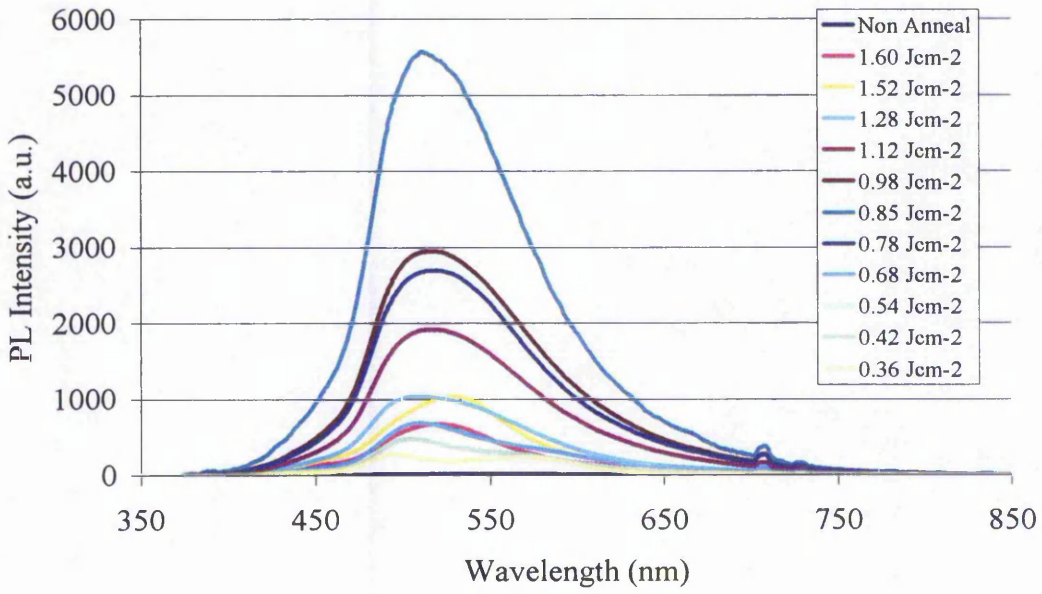


Figure 5.8: PL Intensity acquired by 7 laser irradiations at various laser fluences for a 500nm thick SrS:Cu,Ag thin film on $Y_2O_3$ coated silicon substrate

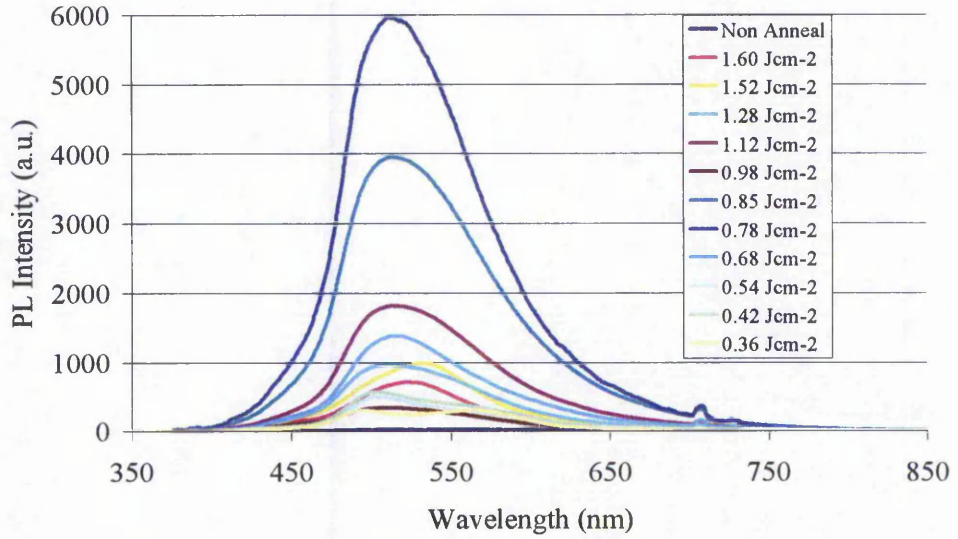


Figure 5.9: PL Intensity acquired by 8 laser irradiations at various laser fluences for a 500nm thick SrS:Cu,Ag thin film on $Y_2O_3$ coated silicon substrate

It is clear that by increasing the number of laser irradiation pulses, there is an increase in the total PL intensity. It is however extremely difficult to determine the best laser annealing parameter by PL emission spectra only. The observed spectra shift for different laser annealing parameter is believed to be caused by activating specific luminescent center which are dependent on specific laser annealing parameter.

Integration of the spectra was carried out for all the above PL emission in order to calculate the total emission. These values were then normalised to compare their improvement over non annealed films. The result of these improvements is shown in figure 5.10.

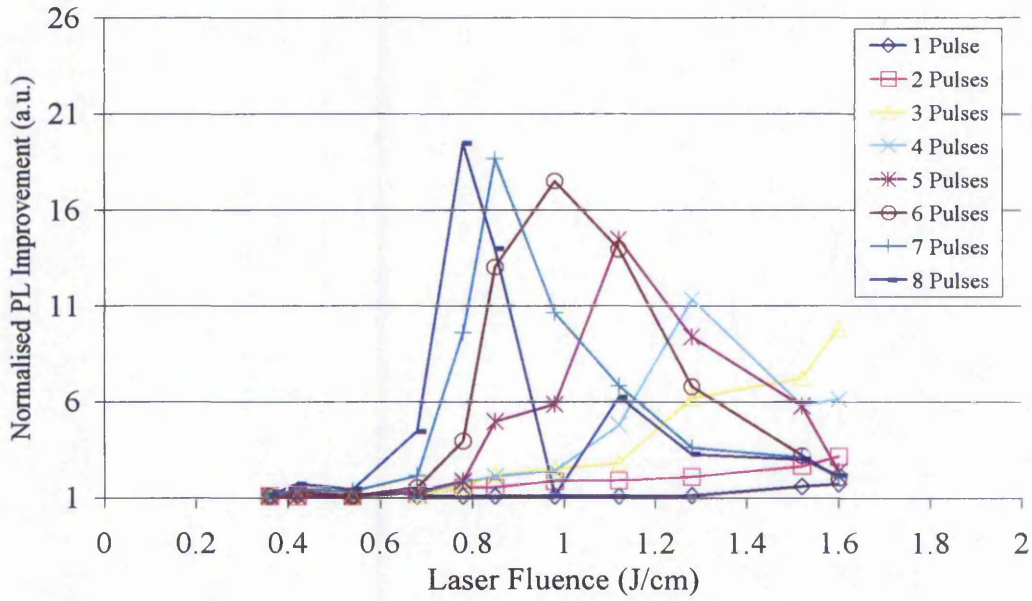


Figure 5.10: Normalised PL Improvement of laser annealed SrS:Cu,Ag films grown on $Y_2O_3$ coated silicon substrate, based on total PL emissions.

From figure 5.10, the best improvement was achieved at 0.78 $Jcm^{-2}$ with 8 laser pulses. In fact there is an optimum number of pulses for each particular laser fluence. For example, the optimum number of pulses for laser annealing at 1.28 $Jcm^{-2}$ is 4 while 6 pulses best suits laser annealing with laser fluence of 0.98 $Jcm^{-2}$. There is little to no noticeable improvement from devices laser annealed with laser fluence lower then 0.78 $Jcm^{-2}$. Also, as seen in figure 5.10, at low number of laser irradiation ( 1 – 3 pulses), the laser fluence seems to play a major part in improving PL emissions of SrS:Cu,Ag thin films. This improvement is more visible for 3 pulses laser irradiation as there is little improvement for 2 or less laser irradiation pulses. The trend of 3 pulse laser irradiation suggested a better improvement can be achieved by increasing the number of laser fluence. However, the ability to improve film quality at lower laser fluences such as those achieved by 5 pulses and above is beneficial typically in term of cost of laser annealing.

Figure 5.10 also shows a trend whereby reducing the fluence while increasing the number of irradiated pulses, the improvement is far superior then those annealed at high fluence but with a lower number of pulses. This effect is better illustrated by re-plotting figure 5.10 using only the best improvement for each individual laser fluence except for laser fluence less then 0.78 Jcm-2 as shown in figure 5.11.

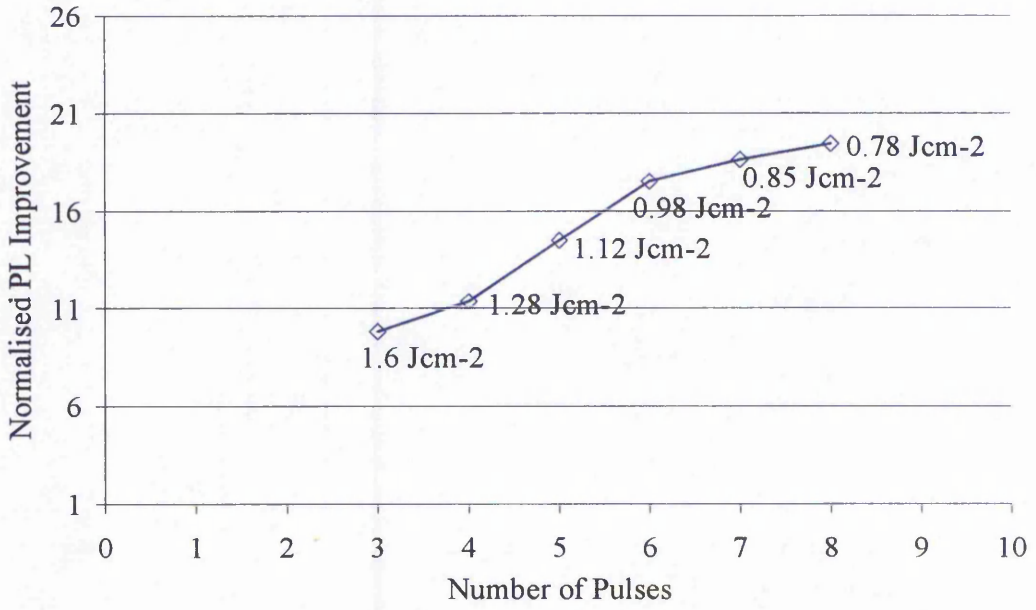


Figure 5.11: Plot of Best PL Improvement Parameter for Each Laser Fluence for laser annealed SrS:Cu,Ag films grown on $Y_2O_3$ coated silicon substrate.

As seen in figure 5.11, the trend suggested that, further improvement on the PL intensity may be achieved by increasing the number of laser irradiation while at the same time reduces the laser fluence. This is probably achievable by a high number of laser irradiation pulses at 0.68 $Jcm^{-2}$. In addition, from figure 5.10, annealing with laser fluence 0.68 $Jcm^{-2}$ after 8 consecutive pulse irradiation, the PL improvement only starts to improve hinting a possible further improvement by increasing the number of irradiated pulses.

The total energy of each laser annealing spot was calculated and the best devices for each number of laser pulses is plotted in figure 5.12. This shows the improvement of PL intensity is directly related to the total laser energy irradiated on the SrS:Cu,Ag thin films. With the present experimental data, the figure suggested best laser annealing may be achieved when the total energy irradiated on the samples is in the region of 6 $Jcm^{-2}$. This also complies with previous result as laser annealing at 0.68 $Jcm^{-2}$ with 9 irradiation pulses will have a total energy of 6.12 $Jcm^{-2}$, hence, potential for even better improvement over laser annealing at 0.78 $Jcm^{-2}$ with 9 irradiation pulses

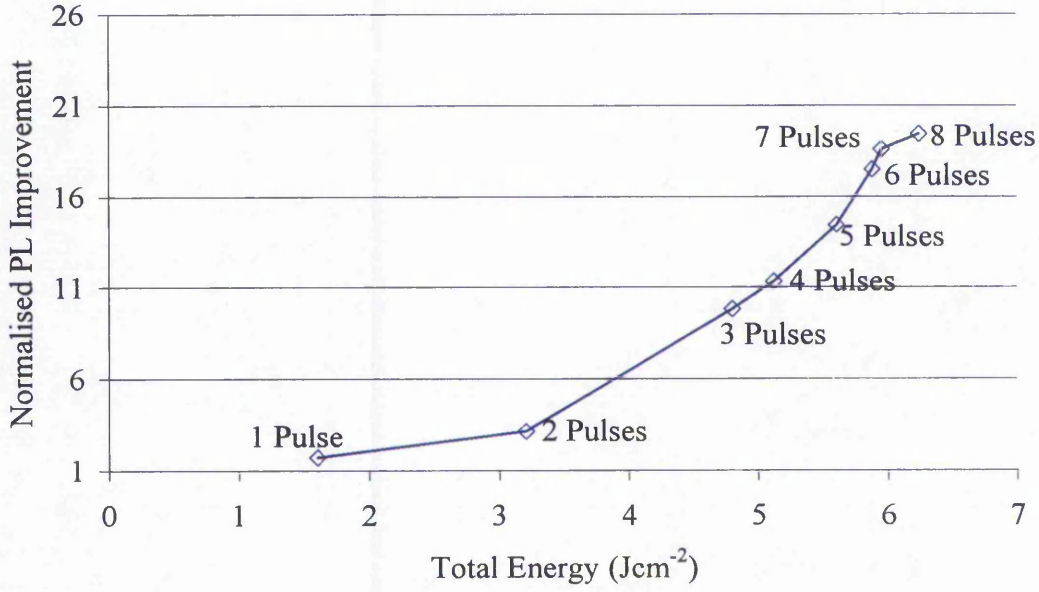


Figure 5.12: Improvement of PL Intensity Over Total Energy Irradiated for laser annealed SrS:Cu,Ag films grown on $Y_2O_3$ coated silicon substrate.

### 5.2.2.2 ELECTROLUMINESCENCE OF LASER ANNEALED SrS:Cu,Ag ON SILICON SUBSTRATE

For EL characterisation, evaporated aluminium of 3x3mm was used as the top electrode in the beginning. However, no emission can be measured from these devices as most light was confined within the aluminium electrode. Alternative top electrodes in the form of in-house sputtered ITO and gold were utilised in order to facilitate EL measurements. The in-house sputtered ITO failed as top electrodes due to the fact that this ITO tends to crack and eventually burned off when a high voltage is applied. This cracking of ITO is believed to be caused by diffusion of tin into the insulating layer ($Y_2O_3$) during sputtering. Although the cracking affect can be minimised by applying passivation in the form of silicone oil over the ITO surfaces, it still not able to withstand high enough voltages for obtaining any EL measurement. The thin gold electrodes though able to withstand higher voltages compared to ITO, the emission was however too weak to be detected by the MINOLTA LS110 luminance meter. In addition, the emitted spectrum was however somewhat altered as the yellowish colour of gold electrode, playing the role of a yellow filter. This evidently leads to the need to investigates laser annealing of SrS:Cu,Ag devices sputter deposited on glass substrates.

This is very unfortunate as some SrS:Cu,Ag thin films were also deposited on silicon wafers with micro mirror for the study of blue emitting LETFEL devices. Similar difficulty was faced with these devices prohibiting any electrical measurement. Disappointingly, due to the inability to measure the light emission from devices on silicon substrates, no characterisation of laser annealed LETFEL devices can be done.

### 5.2.2 LASER ANNEALING WITH THIN TOP INSULATOR

As laser annealing was perform at CLF-RAL in Oxford, in order to prevent degradation of SrS:Cu,Ag caused by humidity and oxidation, a thin layer of 100 Å thick $Y_2O_3$ was deposited on to the SrS:Cu,Ag thin film layer. The use of a thin insulator instead of a full thickness top insulator is because, it is known from previous experiments on ZnS:Mn that laser annealing will not work when the annealing was performed with a full top insulator. Figure 5.13 shows a schematic of different stage at which laser annealing can be performed.

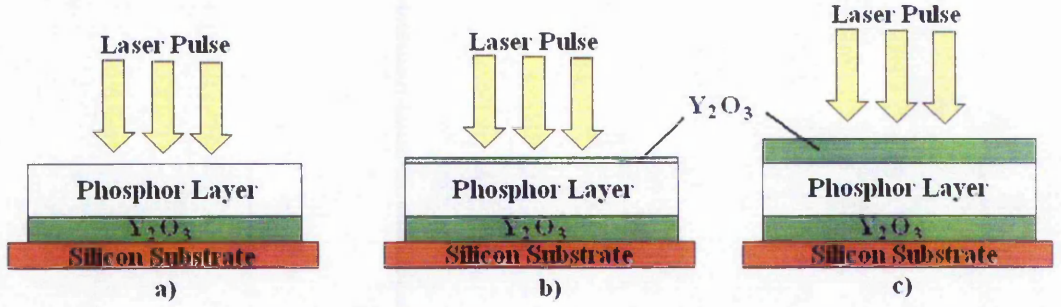


Figure 5.13: a) Typical Laser Annealing Without Any Top Insulator, b) Annealing With Thin Top Insulator, c) Annealing With Full Top Insulator

This experiment was basically identical to the previous experiment carried out on the studies of laser annealing effect on SrS:Cu,Ag thin films. Samples were laser annealed with fluences in the range of 0.36 $Jcm^{-2}$ to 1.6 $Jcm^{-2}$. The number of laser pulses varied from 1 up to a maximum of 8. Figure 5.14 shows the best performing device for each number of laser annealing pulses. The best performing devices for laser annealing without the thin top insulator is also included for comparison purposes.

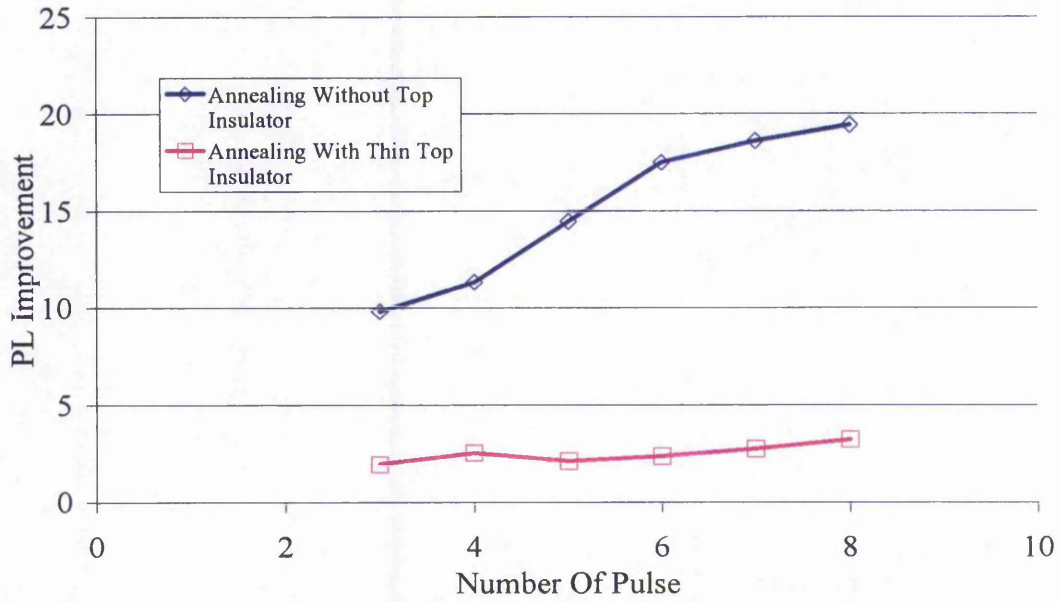


Figure 5.14: Comparison Between Laser Annealing With And Without Thin Top Insulator Layer For SrS:Cu,Ag Thin Films On $Y_2O_3$ Coated Silicon Substrate.

The improvement for laser annealing with thin top insulator basically matches the trend of improvement for devices annealed without the top insulator except the fact that the overall improvement was a fifth reduction in intensity. The limited phosphor ablation due to laser annealing completely removed the thin top insulator. The removal of the thin top insulating layer above the SrS:Cu,Ag thin films is believed to decrease the actual laser energy that reaches the phosphor layer hence reducing the improvement.

### 5.2.3 EFFECT OF ENVIRONMENTAL PRESSURE

The reason for the use of a pressure cell for laser annealing is to provide a pressurised environment during annealing. This is to minimise any ablation caused by the irradiation of laser pulses which is easily visible as seen in figure 5.1. This experiment was to study the effect of environmental pressure on the effect of laser annealing on SrS:Cu,Ag thin films, at which the argon pressure was varied from 14.4 psi to 150 psi. The laser fluence used in this experiment was in the range of 0.5 – 1.3 $Jcm^{-2}$ with the number of laser pulses varied from a single irradiation up to a maximum of 4 pulses. The result of this experiment is shown in the following graph.

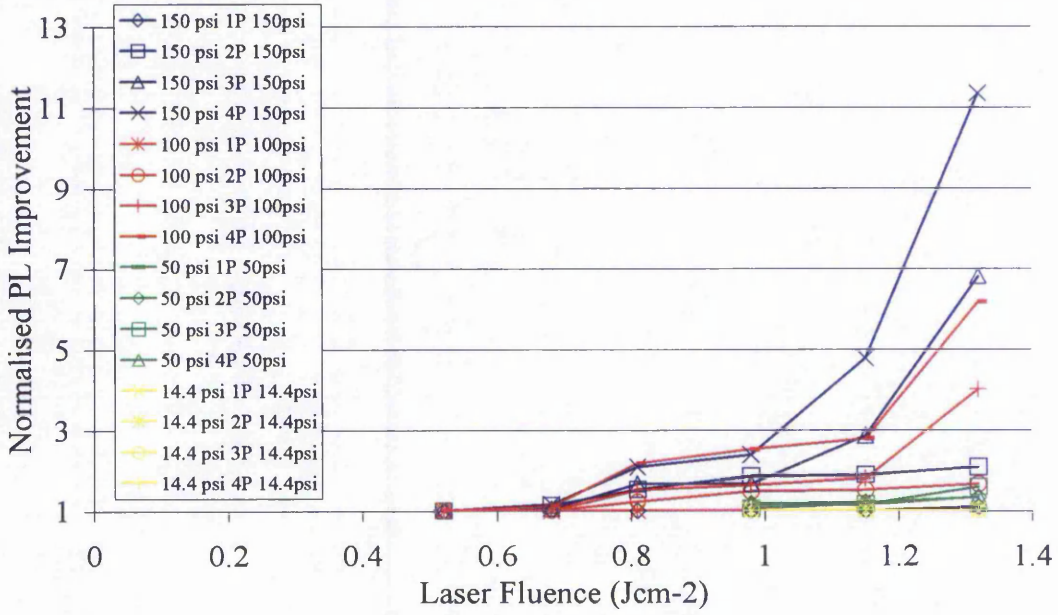


Figure 5.15: Normalised PL Improvement for Laser Annealed SrS:Cu,Ag thin film in Argon Pressure of 14.4psi, 50 psi, 100psi and 150 psi.

There is little or no improvement for devices annealed in a pressurised argon environment at 50 psi and below. The improvement for device annealing at 100 psi is about half of those annealed at 150 psi. Therefore, the optimum over pressure of argon environment obtained is 150 psi. The further increase in argon pressure during annealing may be beneficial but the pressure cell was built to withstand an over pressure of up to 160 psi, hence to allow further investigation, a new pressure cell would have to be made.

## 5.3 LASER ANNEALING OF SrS:Cu,Ag THIN FILM ON GLASS SUBSTRATE

Devices on silicon failed to yield any EL either due to device failure caused mainly by electrode failure or the emitted light was too weak for the detection of the luminance meter, an additional series of films was sputtered on ITO coated glass substrates. These were used to study the effect of laser fluence and number of laser irradiation on electrical behaviour of SrS:Cu,Ag thin films. Since laser annealing do not involve any high temperature process, this enable the use of normal glass substrates.

For this study, all laser annealing was performed prior to the deposition of any form of top insulator since the result on silicon suggested better annealing effect when laser annealing was performed directly on the phosphor layer to be studied. On some samples, the maximum number of laser irradiations per device was also increased from 8 to 12 as the PL trend obtained from silicon devices suggested better improvement can be achieved with lower laser fluence at a higher number of pulses. Unfortunately, due to a break down of the central air conditioning system in CLF-RAL, samples laser annealed with pulses up 12 were damaged by moisture from the portable air conditioning system, hence only devices annealed up to 8 laser pulses were examined.

Similar to devices on silicon, both PL and EL characterisation was carried out. The PL characterisation was performed on the same characterisation tools as devices on silicon substrate. The EL characterisation however, was performed utilising the custom made probe station which utilises a spectrometer instead of the Minolta luminance meter.

### 5.3.1 PHOTOLUMINESCENT STUDY OF LASER ANNEALED SrS:Cu,Ag THIN FILM ON GLASS SUBSTRATE

Figure 5.16 shows the summary for the PL study on rf magnetron sputter deposited SrS:Cu,Ag on glass substrates coated with ITO and $Y_2O_3$. The samples were laser annealed with laser fluence up to 1.6 $Jcm^{-2}$ with 1 to 8 laser irradiation pulses in an argon over pressured environment of 150 psi. The PL improvements represented by the vertical axis was obtained from the total emission of the SrS:Cu,Ag thin films normalised to the non annealed SrS:Cu,Ag thin film.

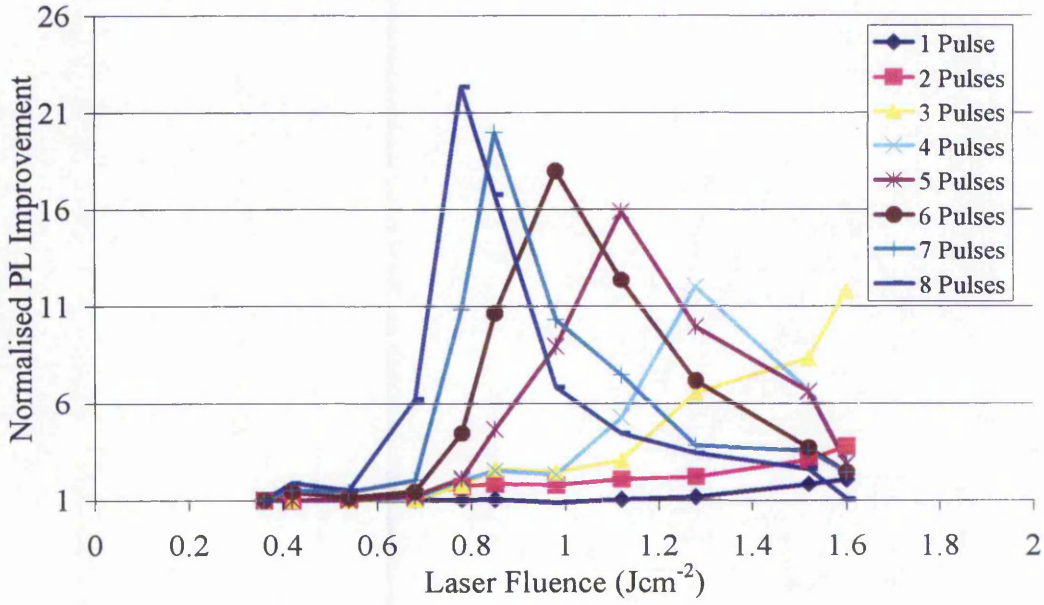


Figure 5.16: Normalised PL Improvement of laser annealed SrS:Cu,Ag films grown on $Y_2O_3$ for ITO coated glass substrate.

The general trend of improvement matches those of laser annealed SrS:Cu,Ag thin films on silicon substrates as shown in figure 5.17. Similarly, for each laser fluence investigated, there is a optimum number of laser irradiation pulses for the best PL improvement. The PL improved by 22 times over non annealed films when the film is laser annealed at 0.78 $Jcm^{-2}$ for a total of 8 laser pulses.

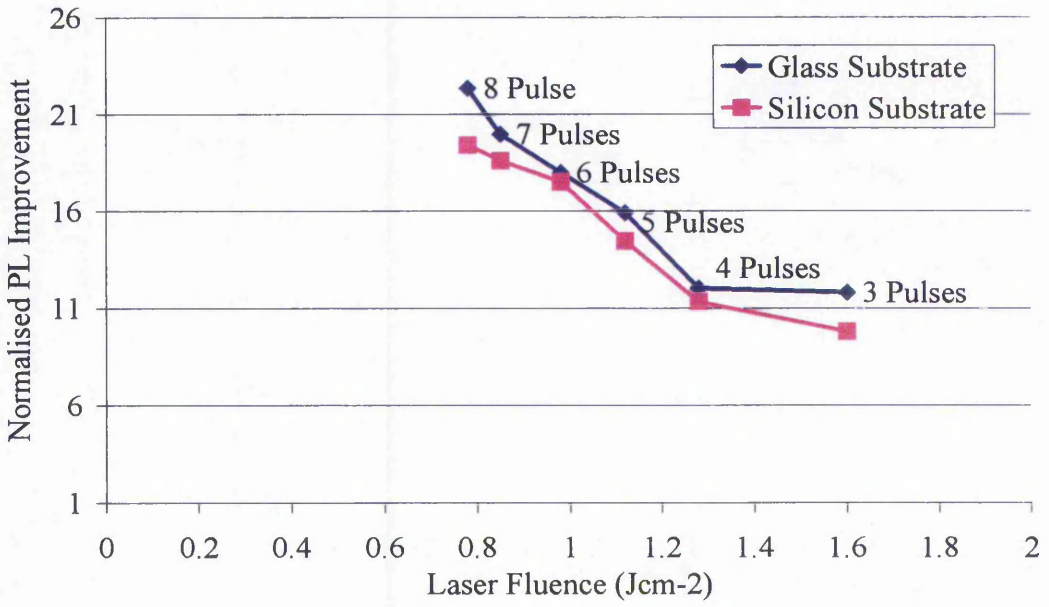


Figure 5.17: Comparison between PL Improvement of laser annealed SrS:Cu,Ag films grown on $Y_2O_3$ for ITO coated glass substrate and films on $Y_2O_3$ coated silicon substrate.

### 5.3.2 ELECTROLUMINESCENT STUDY OF LASER ANNEALED SrS:Cu,Ag DEVICES ON GLASS SUBSTRATE.

In order to fabricate laser annealed ACTFEL devices, each sample was re-introduced into the sputtering chamber for the deposition of the top insulator for completing the double insulating structure, and later followed by evaporation of aluminium utilising the evaporation system.

Figure 5.18 to 5.23 shows the brightness versus voltage (BV) for laser annealed devices with 3 to 8 laser irradiation pulses and laser fluences varied in the range of 0.36 – 1.60 $Jcm^{-2}$. Each graph represented the effect of laser fluence over the luminance improvement for a specific number of laser irradiation pulse.

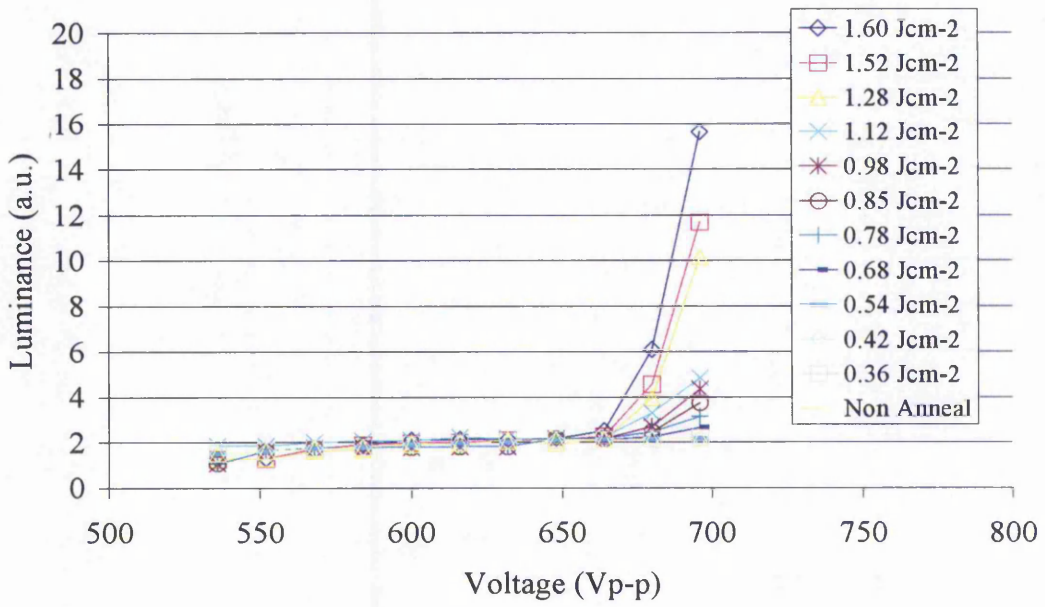


Figure 5.18: BV Characteristic of TFEL devices laser annealed with 3 laser irradiation pulses at laser fluence ranging from 0.36 – 1.60 $Jcm^{-2}$.

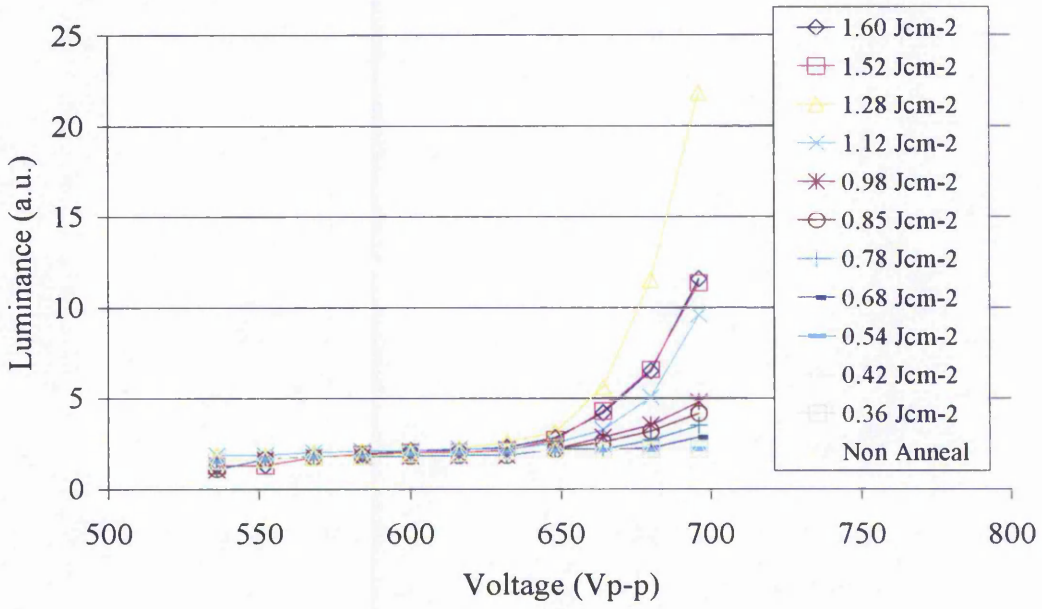


Figure 5.19: BV Characteristic of TFEL devices laser annealed with 4 laser irradiation pulses at laser fluence ranging from 0.36 – 1.60 $Jcm^{-2}$.

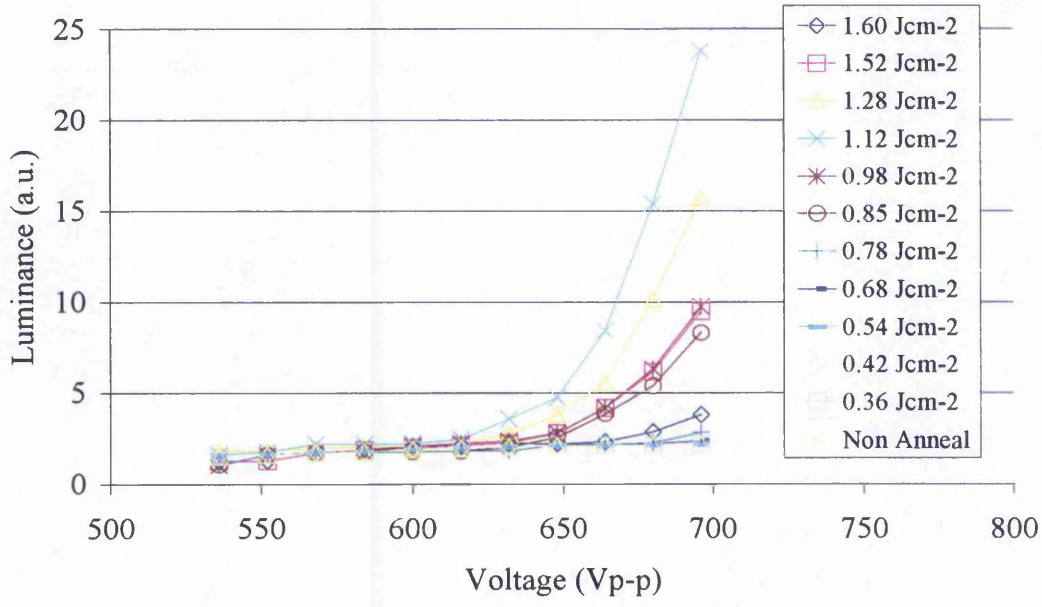


Figure 5.20: BV Characteristic of TFEL devices laser annealed with 5 laser irradiation pulses at laser fluence ranging from 0.36 – 1.60 $Jcm^{-2}$.

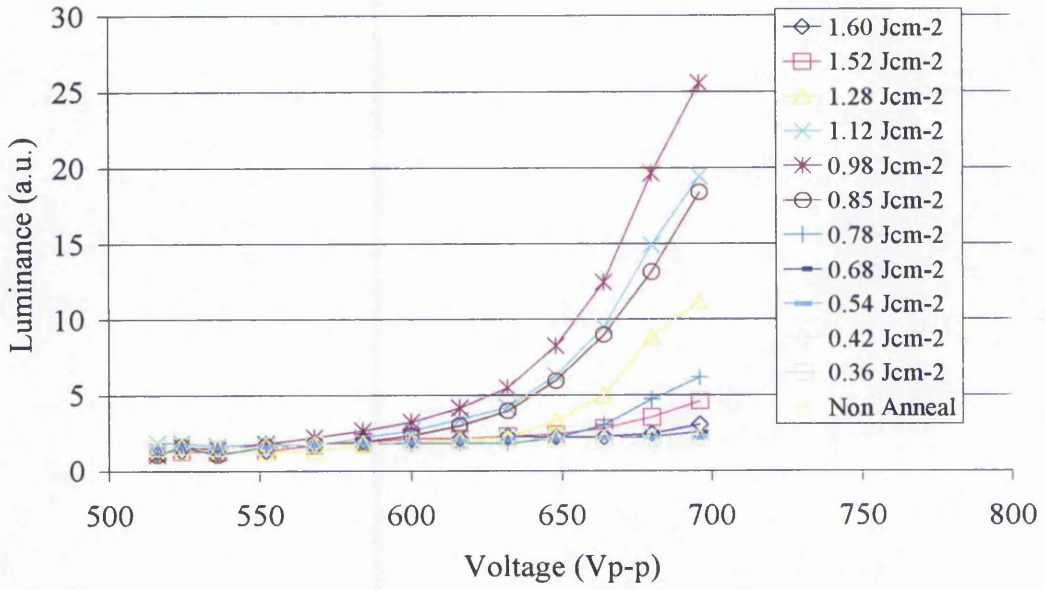


Figure 5.21: BV Characteristic of TFEL devices laser annealed with 6 laser irradiation pulses at laser fluence ranging from 0.36 – 1.60 $Jcm^{-2}$.

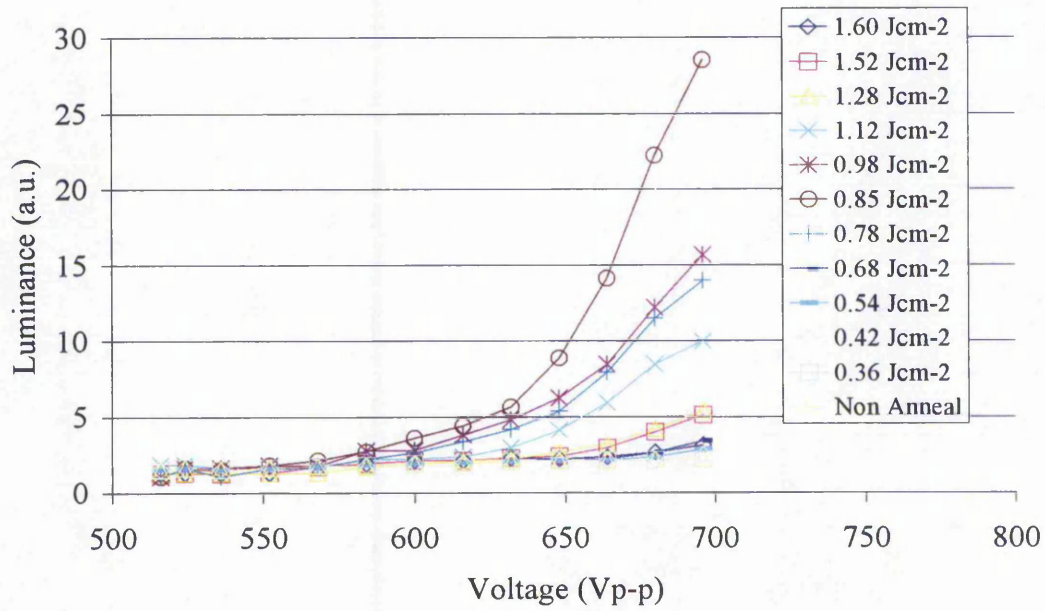


Figure 5.22: BV Characteristic of TFEL devices laser annealed with 7 laser irradiation pulses at laser fluence ranging from 0.36 – 1.60 $Jcm^{-2}$.

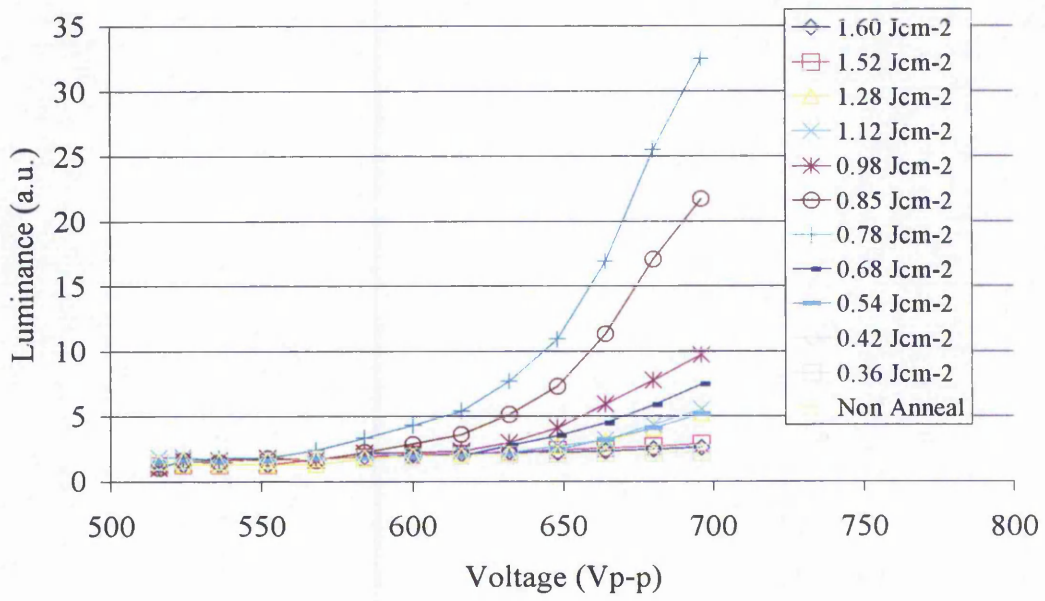


Figure 5.23: BV Characteristic of TFEL devices laser annealed with 8 laser irradiation pulses at laser fluence ranging from 0.36 – 1.60 $Jcm^{-2}$.

To summarise the BV characteristic of laser annealed SrS:Cu,Ag TFEL on ITO coated glass substrate, the BV for the best performing device for each laser fluence is shown in figure 5.24.

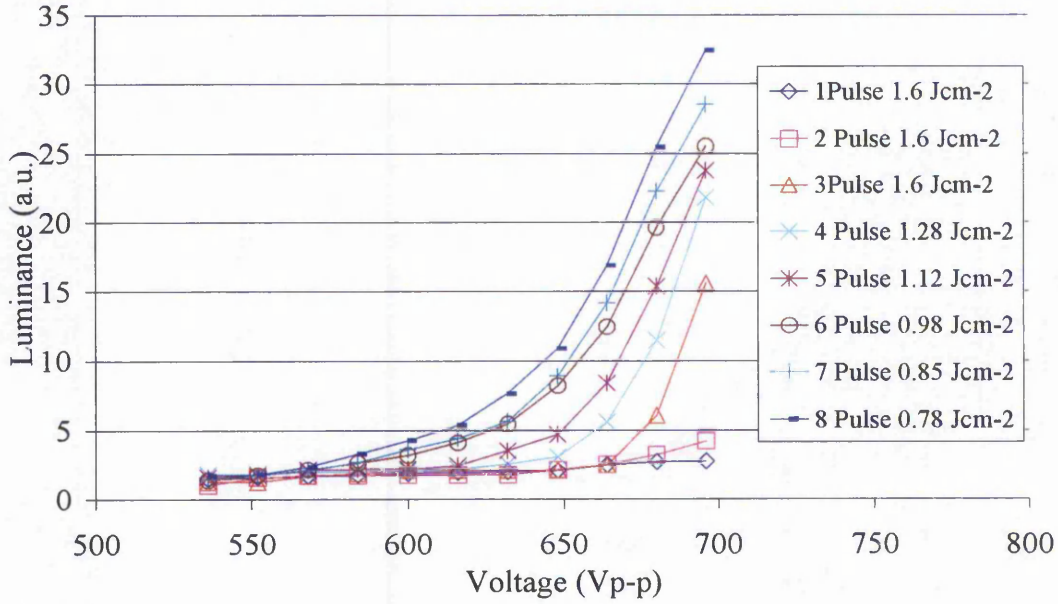


Figure 5.24: BV Characteristic of Best Performing SrS:Cu,Ag TFEL devices On Glass For Each Laser Fluence Investigated.

There is no distinct difference in the sharpness of the BV curve between devices, however, with the increase of number of laser irradiation pulses, there is a reduction in the turn on voltage. The turn on voltage difference between 1 pulse laser annealing and 8 pulse laser annealing is approximately 50 $V_{p-p}$. This reduction is believed to be the result of ablation. With the increase of number of laser pulses, there is an increase in the amount of material being removed caused by laser ablation. This reduction in the thickness of the phosphor layer of the TFEL subsequently reduces the overall thickness whole device allowing a lower turn on voltage.

This experiment also suggested that for laser annealing of SrS:Cu,Ag thin films, the minimum number of laser irradiation pulses is 3 as no significant improvement can be observed from devices laser annealed with 2 laser pulses or lower regardless of laser fluences. The optimum laser annealing parameter for laser annealing of SrS:Cu,Ag in 150 psi argon atmospheric environment obtained from these experiment is 0.78 $Jcm^{-2}$ with 8 irradiation pulses.

## 5.4 PL VERSUS EL

Figure 5.25 shows the PL and EL emission of the best performing laser annealed SrS:Cu,Ag on glass substrate for each number of laser irradiation pulse investigated. The PL emission was taken after the deposition of the top insulator but prior to the deposition of top electrodes while all EL emission was taken at 648 $V_{p-p}$.

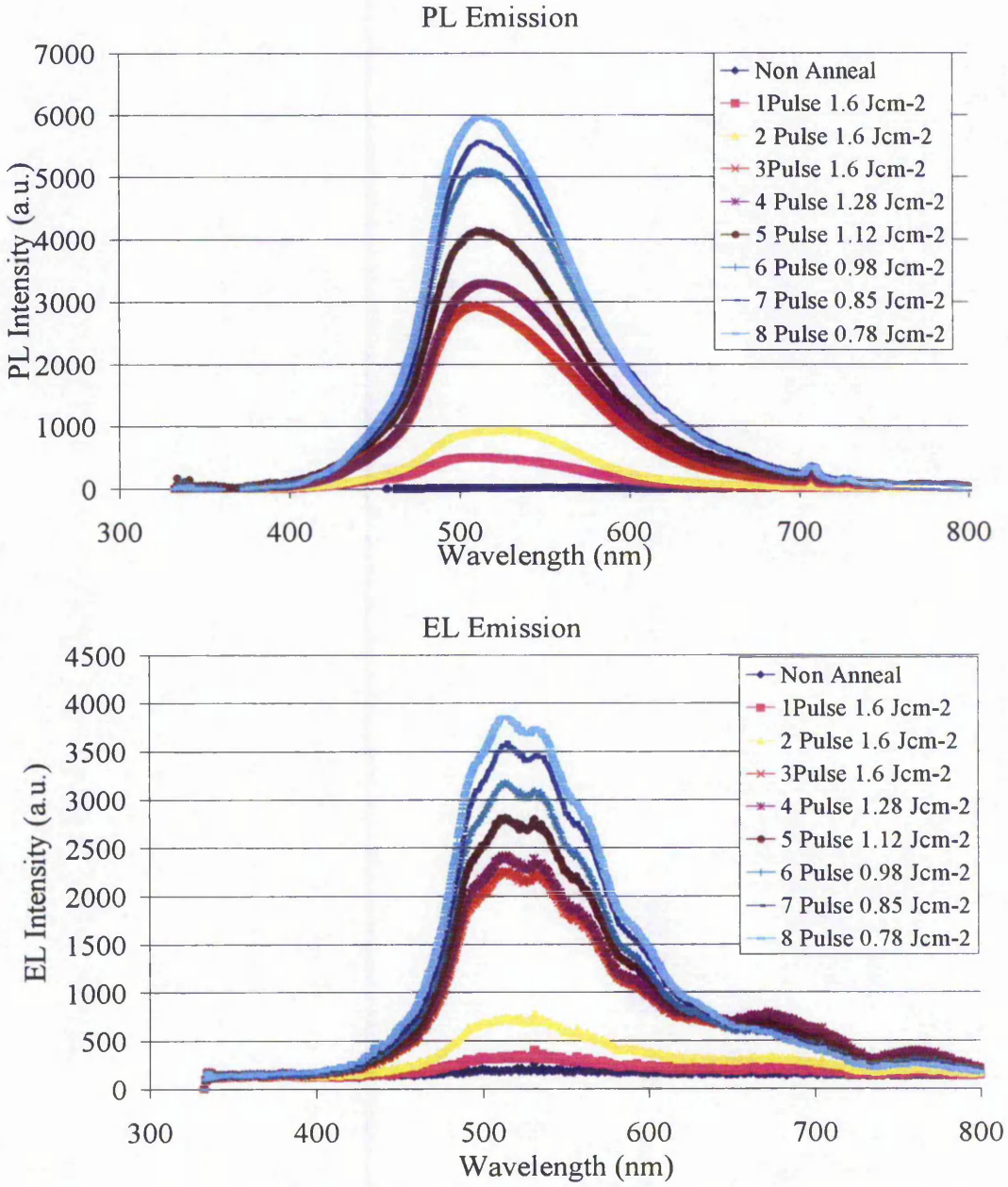


Figure 5.25: PL and EL Emission of Laser Annealed SrS:Cu,Ag Thin Films On ITO Coated Glass Substrate.

Although the structure of devices for the studies of EL and PL was slightly different, there is little difference between the peak emission for these devices. The small vibration in the EL spectra is due to interference based on the stacked layers of the device.

From the brightness voltage characterisation studies on laser annealed SrS:Cu,Ag thin film, it is evident that the best PL performing device is also the best EL performing device (refer to figure 5.17 & 5.23). This study was to investigate the relationship between photoluminescent and electroluminescent for SrS:Cu,Ag thin films. Figure 5.26 shows the ratio of improvement of laser annealed devices over non annealed devices for both the PL and EL excitation. Each point represented the average value of 3 identical devices.

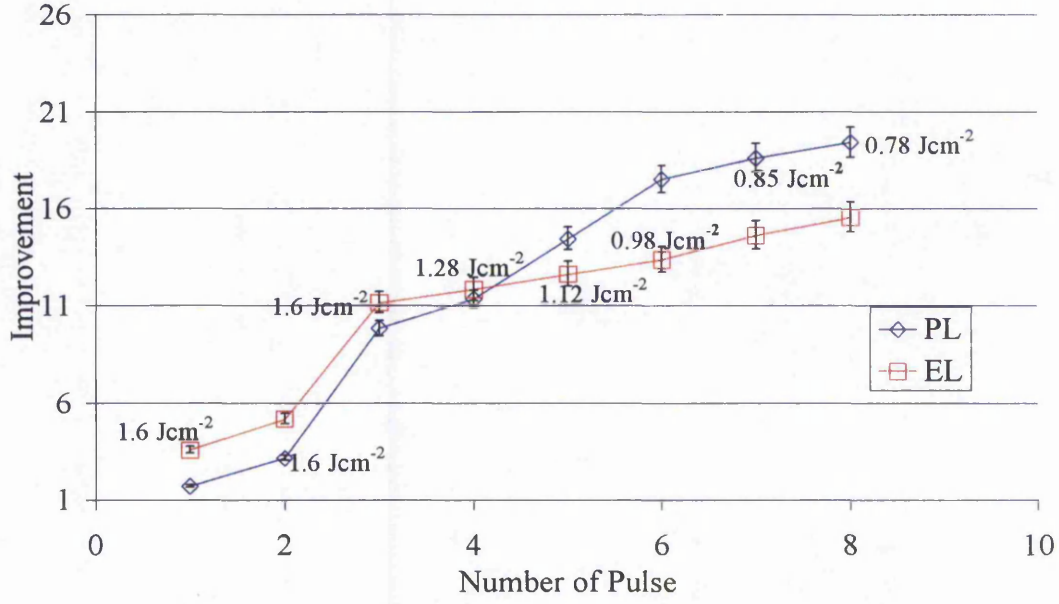


Figure 5.26: Ratio of Improvement For Total Emission OF Laser Annealed SrS:Cu,Ag Device over Non anneal SrS:Cu,Ag device

With 3 pulses at 1.6 $Jcm^{-2}$, a factor of 10x improvement over non anneal devices was achieved. This factor was increased to 16x when the laser fluence was reduced to 0.78 $Jcm^{-2}$ while increasing the number of laser pulses to 8 pulses. It is also shown that there is little difference in the ratio of improvement between devices on their PL and EL performance. This allows the use of PL measurement as a valid indication of the EL improvement over non annealed devices. This finding greatly reduces the

time required to investigates EL performance of laser annealed devices, evidently allowing the investigation and quality control of more laser annealing parameters.

## 5.5 X-RAY DIFFRACTION

Figure 5.27 shows the XRD pattern for non annealed and laser annealed SrS:Cu,Ag TFEL devices at 0.52, 0.98 and 1.6 $Jcm^{-2}$ laser fluence for single pulse irradiation. The devices investigated were fabricated on $Y_2O_3$ coated silicon substrates, hence, peak intensity between 28.5 and 29 degree should be ignored as this represented $Y_2O_3$ XRD lines.

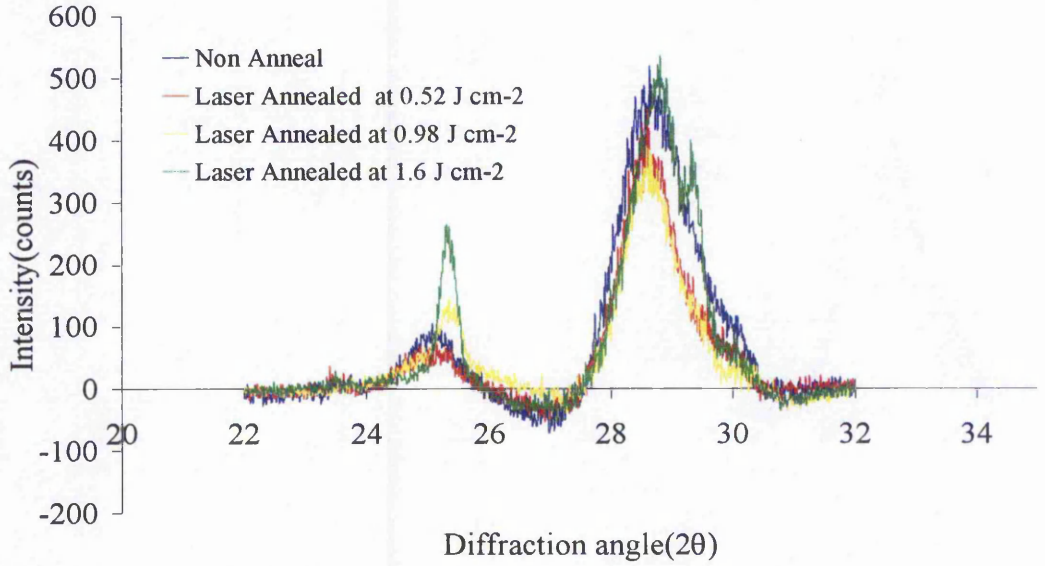


Figure 5.27: XRD pattern for non anneal and laser annealed SrS:Cu,Ag TFEL at 0.52, 0.98 and 1.6 $Jcm^{-2}$ for single pulse irradiation.

From figure 5.27, it is clear that with crystallinity of the SrS:Cu,Ag thin film improved with laser annealing. This is especially true for high energy laser annealing as indicated by green plot in figure 5.27.

## 5.6 SCANNING ELECTRON MICROSCOPY

To get an idea of the morphology and structure of the SrS:Cu,Ag layers, scanning electron microscopy pictures (SEM) were taken. Figure 5.28 shows the comparison between non anneal SrS:Cu,Ag thin films and thermal annealed SrS:Cu,Ag thin films. Figure 5.29 and 5.30 shows SEM picture for laser annealed SrS:Cu,Ag thin film laser annealed at various fluences with 2 laser irradiation pulse at 1250 X and 5000 X magnification respectively.

It can be seen that with increasing laser fluence the number of cracks increases. Similarly, works by Poelman et al have observed that severe film cracking occurs for rapid thermally annealed films[14]. In addition, they also shown that emission of SrS:Cu,Ag thin films originates from the bulk of the grain. The combination of these cracks associated with the improvement in crystallinity is beneficial as this leads to more efficient optical outcoupling of the internal emitted light, and therefore to a higher light output from the device surface.

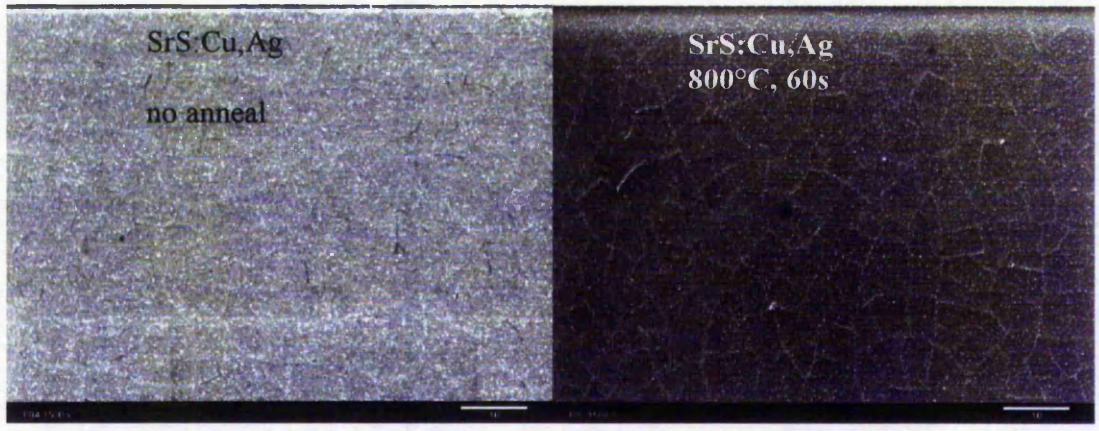


Figure 5.28: SEM Picture Of Non Anneal And RTA SrS:Cu,Ag Thin Films At 1250x Magnification.

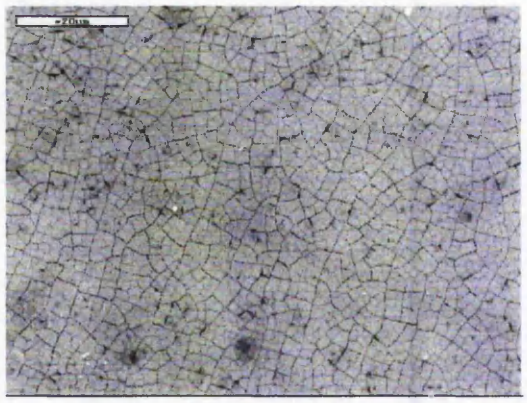

laser anneal 2 x 1300 μJ/cm2

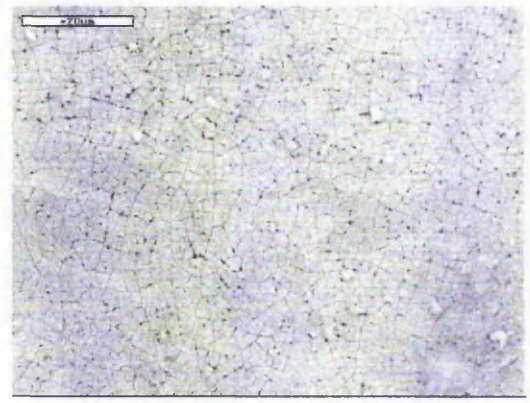

laser anneal 2 x 1100 μJ/cm2

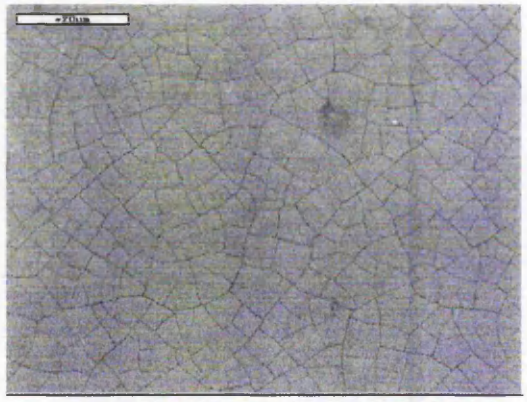

laser anneal 2 x 820 μJ/cm2

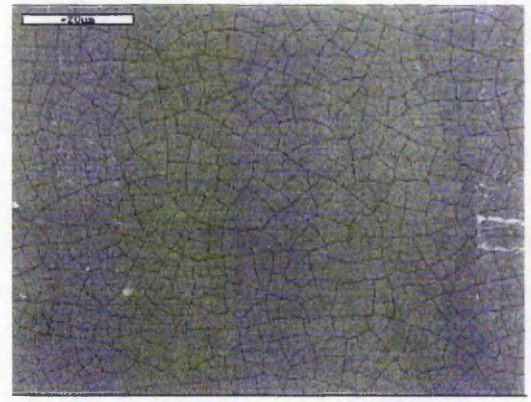

laser anneal 2 x 500 μJ/cm2

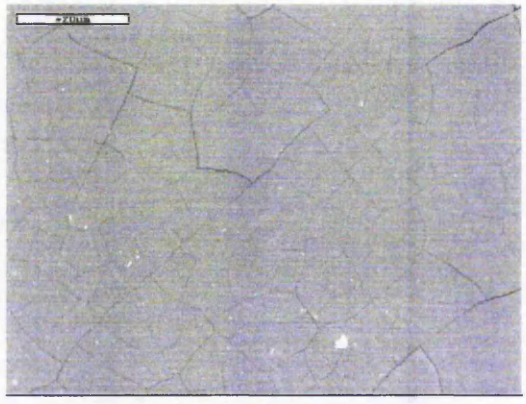

laser anneal 2 x 320 μJ/cm2

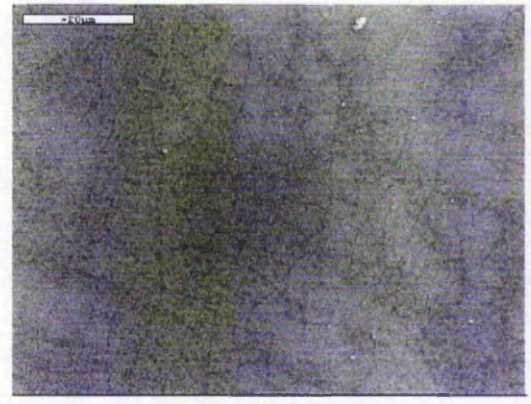

no laser anneal

Figure 5.29: SEM Picture At 1250x Magnification for SrS:Cu,Ag Thin Film Laser Annealed At Various Fluences With 2 Laser Irradiation Pulse.

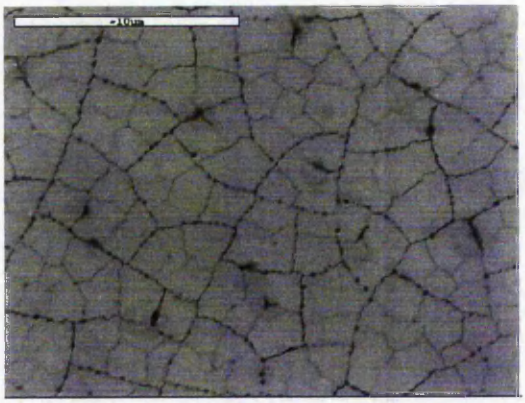

laser anneal 2 x 1300 μJ/cm2

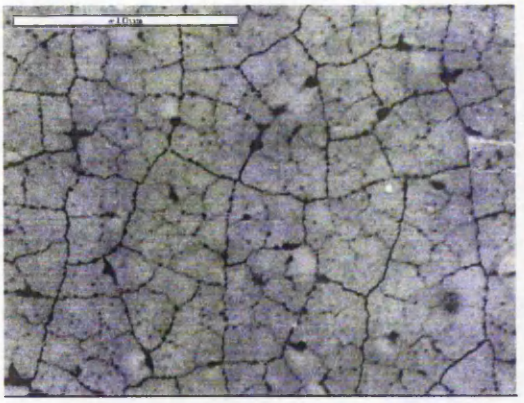

laser anneal 2 x 1100 μJ/cm2

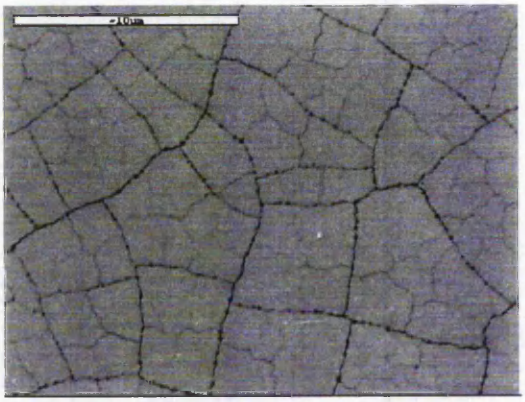

laser anneal 2 x 820 μJ/cm2

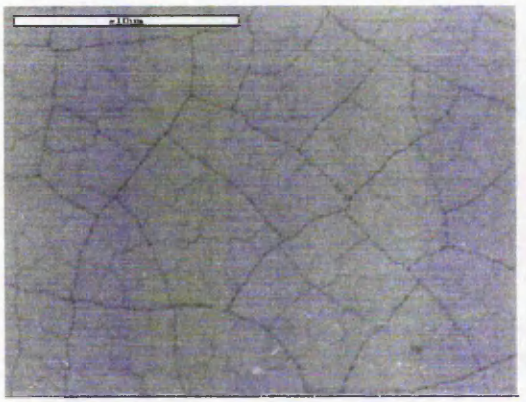

laser anneal 2 x 500 μJ/cm2

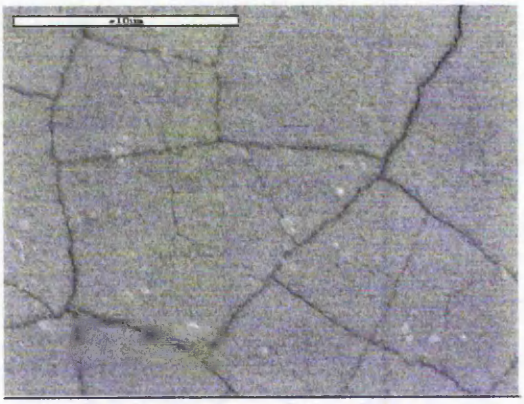

laser anneal 2 x 320 μJ/cm2

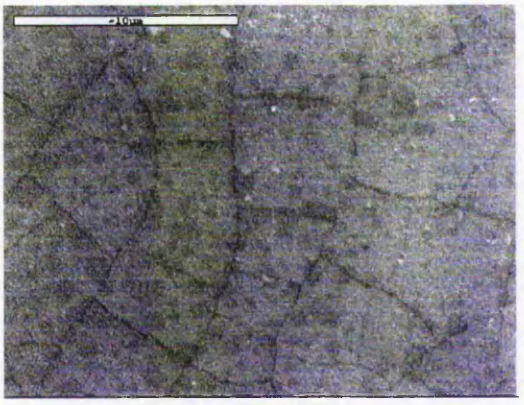

no laser anneal

Figure 5.30: SEM Picture At 5000x Magnification for SrS:Cu,Ag Thin Film Laser Annealed At Various Fluences With 2 Laser Irradiation Pulse.

## 5.7 CONCLUSION

The study on laser annealing of SrS:Cu,Ag thin films and devices grown on either polished silicon or glass substrates has demonstrated a strong improvement on both photoluminescent and electroluminescent performance. The laser annealed samples generally outperform conventional thermally based annealing by a factor of 5x. Figure 5.31 shows PL comparison of this result. The PL and EL improvement was similar allowing the use of PL for identifying efficient devices without the need for electrical investigation. Laser annealing was also found to be improving the crystallinity of the thin films while at the same time creating sub micron cracks which benefited the device as a whole typically in improving the outcoupling efficiency.

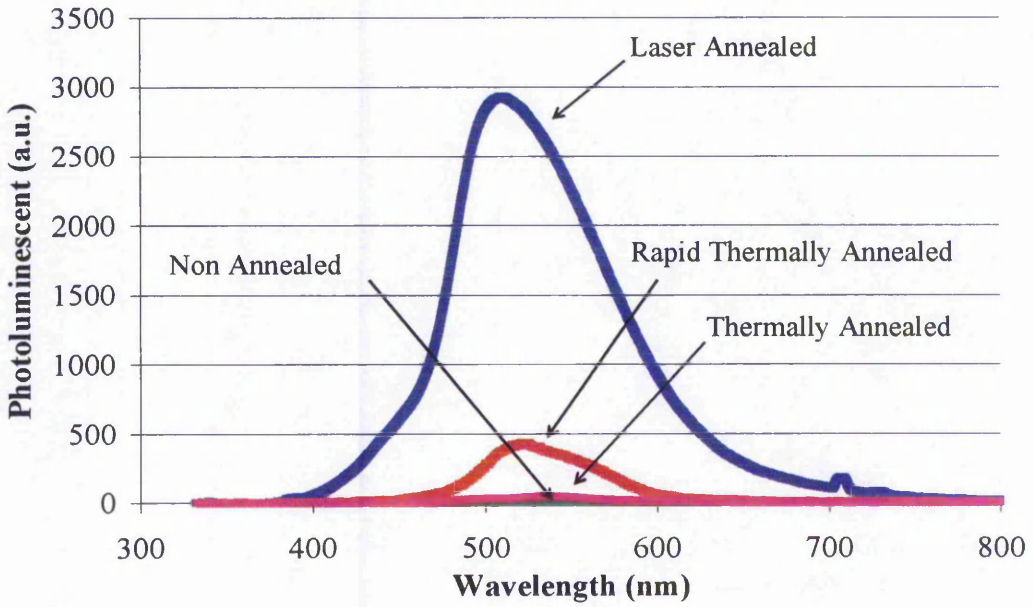


Figure 5.31: Photoluminescent of Non Anneal, Thermally Annealed, Rapid Thermally Annealed and Laser Annealed of SrS:Cu,Ag Thin Films on Silicon Substrate.

**REFERENCES**

[1] Ian W. Boyd, Laser Processing of Thin Films and Microstructures, Springer-Verlag, 1987.

[2] Private Conversation with W.M. Cranton, The Nottingham Trent University.

[3] H.S. Reehal, J.M. Gallego and C.B. Edwards, Appl. Phys. Lett. Vol 40, No 3, pp. 258-260, 1982.

[4] H.S. Reehal, C.B. Edwards, J.M. Gallego and C.B. Thomas, Proc 5th National Quantum Electronics Conf. Hull 1981, Quantum Electronics and Electro-Optics, pp. 97-101, Jonh Wiley & Sons 1983.

[5] H.S. Reehal and C.B. Edwards, Ann. Rep. Laser Facility Committee, SERC Rutherford and Appleton Labs, 2.17-2.18, 1981.

[6] H.S. Reehal, C.B. Thomas, J.M. Gallego, G. Hawkins and C.B. Edwards, Mat. Res. Soc. Symp. Proc., Vol. 13, 1983.

[7] E.A. Mastio, W.M. Cranton, C.B. Thomas, E. Fogarassy and S. de Unamuno, Applied Surface Science, Vol. 138-139, pp. 35-39, 1999.

[8] E.A. Mastio, M.R. Craven, W.M. Cranton, C.B. Thomas, M. Robino and E. Fogarassy, Journal of Applied Physics, Vol.86, No. 5, pp. 2562-2570, 1999.

[9] E.A. Mastio, E. Fogarassy, W.M. Cranton and C.B. Thomas, Applied Surface Science, Vol. 154-155, pp. 35-39, 2000.

[10] E.A. Mastio, C.B. Thomas, W.M. Cranton and E. Fogarassy, Applied Surface Science, Vol. 157, pp. 74-80, 2000.

[11] W.M. Cranton, E.A. Mastio, C.B. Thomas, C. Tsakonas and R. Stevens, Electronics Letters, Vol. 36, No. 8, pp. 754-756, 2000.

[12] E.A. Mastio, W.M. Cranton and C.B. Thomas, Journal of Applied Physics, Vol. 88, No. 3, pp. 1606-1611, 2000.

[13] E.A. Mastio, W.M. Cranton and C.B. Thomas, Journal of Applied Physics, Vol. 89, No. 3, pp. 1605-1611, 2001.

[14] D. Poelman, D. Wauters, J. Versluys and R.L. Meirhaeghe, Journal of Applied Physics, Vol 90, No. 1, pp. 248-251, 2001.

# CHAPTER 6

# BARRIER LAYER SrS:Cu,Ag DEVICES

## 6.1 INTRODUCTION

The barrier layer device is basically a variation from the standard double insulator TFEL devices. The only difference of barrier layer devices when compared to these standard TFEL devices is the incorporation of an extra insulating layer within the middle of the phosphor layer. The effect of this barrier layer together with its architecture has been extensively studied by W.M. Cranton in 1995[1]. That study was concentrated solely on the luminous enhancement of ZnS:Mn TFEL devices. He demonstrated that a 8000 Å thick ZnS:Mn phosphor thin film sandwiched between a 3000 Å thick $Y_2O_3$ insulating layer, incorporating a 100 Å insulating layer within the middle of the phosphor layer fabricated by sputtering $Y_2O_3$ provided 35% improvement in luminance over devices without this thin insulating layer.

The fabrication steps for barrier layer devices are fairly similar to the fabrication of double insulating TFEL devices, except the sputtering deposition of the phosphor layer was interrupted when the thickness reaches half the required overall thickness. This is to allow the fabrication of the thin insulating layer. Following the deposition of this thin insulating layer, sputtering of the phosphor material is resumed for the deposition of the remaining half thickness phosphor layer.

Due to the success of the barrier layer on ZnS:Mn TFEL devices, a similar study was carried out to investigates the effect of a barrier layer on SrS:Cu,Ag TFEL devices. In addition, as the post deposition annealing technique utilised for this studies was laser annealing, together with the required stoppage during the fabrication of the phosphor layer, it was decided to investigate the effect of laser annealing either the top phosphor layer or the bottom phosphor layer or both layers. The effect of varying the barrier layer thickness on the luminous improvement was also performed.

## 6.2 EFFECT OF BARRIER LAYER

For this study, the barrier layer devices were grown on glass substrate as the main interest for this type of this devices is its EL emission improvement. In order to have direct comparison between barrier and non barrier layer devices, both types of device were fabricated on the same substrate and laser annealed utilising the same set of parameters. To allow the fabrication of such samples, half the sample was covered by a contact mask during the sputter deposition of the thin insulating layer. The covered area designates the region of the non barrier layer devices or the standard devices while the exposed area was used for the barrier layer devices. Figure 6.1 shows the step for the fabrication of the barrier layer for a test device and schematic of a finished test structure.

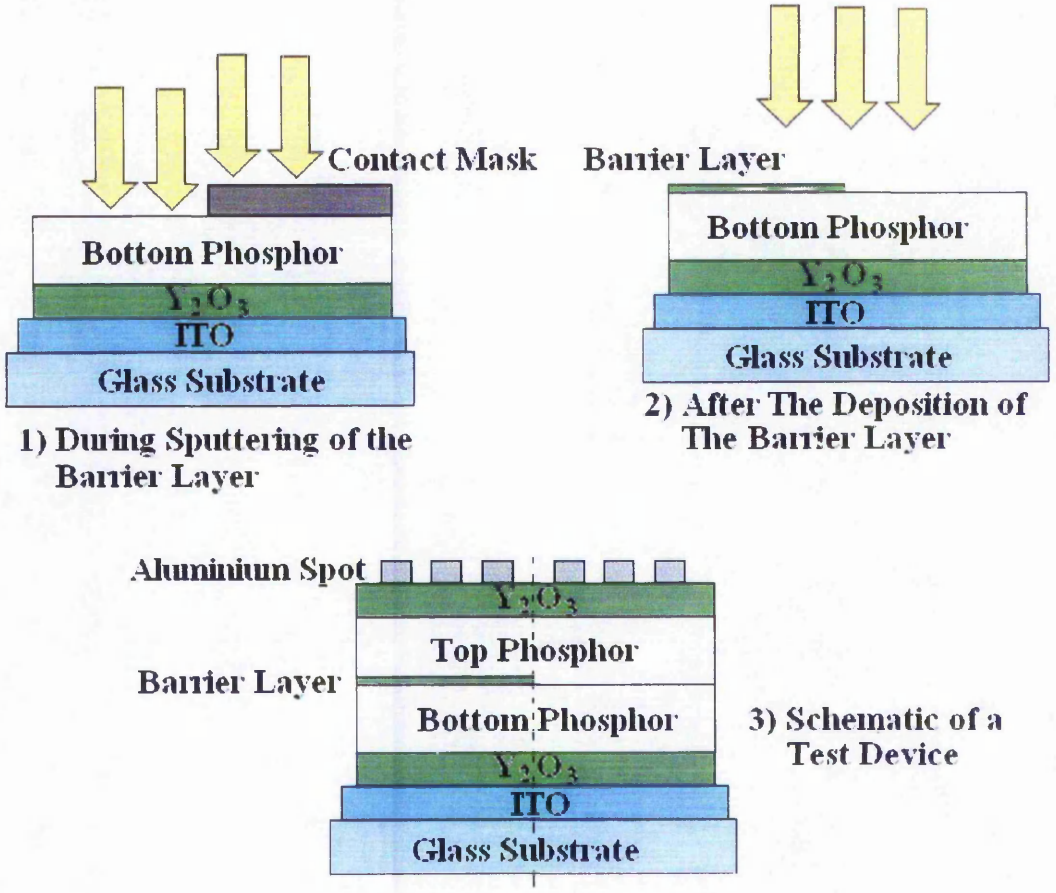


Figure 6.1: Fabrication Step Of The Barrier Layer Of The Test Device And The Schematic Of A Typical Barrier Layer Test Device.

The device was laser annealed prior to the deposition of the top insulator similar to the previous experiment on the examination of laser annealing effect on SrS:Cu,Ag thin films described in chapter 5. Here, only 4 different fluences were examined; 0.96, 1.20, 1.32 and 1.58 $Jcm^{-2}$, while the number of irradiation was varied from 1 up to a total of 8 pulses. All the following results were obtained from barrier layer devices with the barrier layer thickness fixed at 100 Å as this was found to be optimum for ZnS:Mn devices[1,2]. The thickness of the barrier layer was predicted by the known deposition rate of $Y_2O_3$. The following 6 graphs show the comparison between barrier and non barrier devices for different laser annealing parameter. Each graph represents a fixed number of laser irradiation pulses of variable laser fluence. No B-V measurement can be obtained from laser annealing with single and 2 laser irradiation pulses.

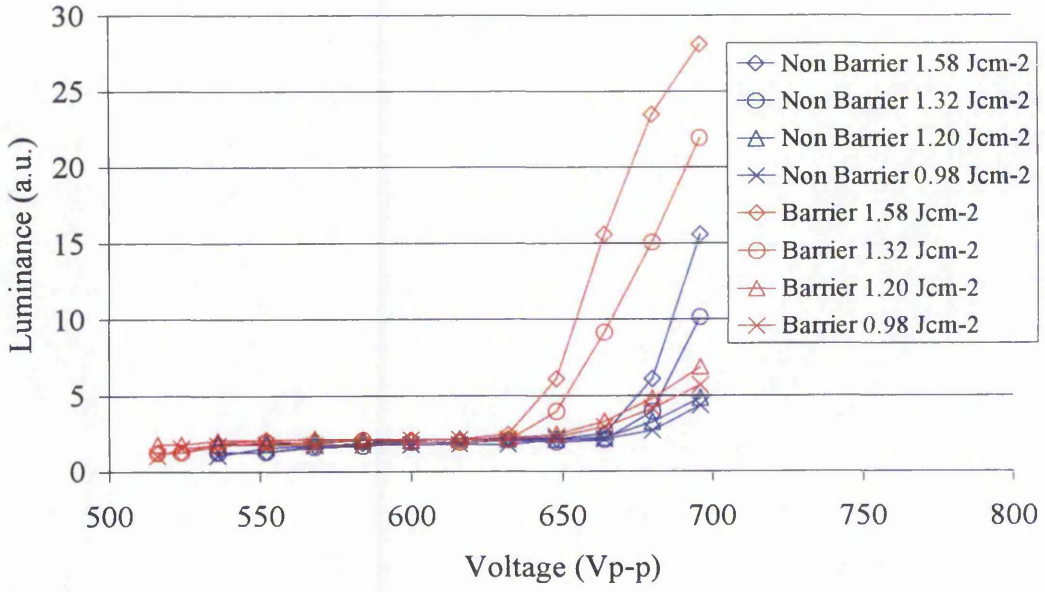


Figure 6.2: BV Of Barrier And Non Barrier Layer SrS:Cu,Ag Devices On Glass Substrate Laser Annealed With 3 Laser Irradiation Pulses Of Various Laser Fluence.

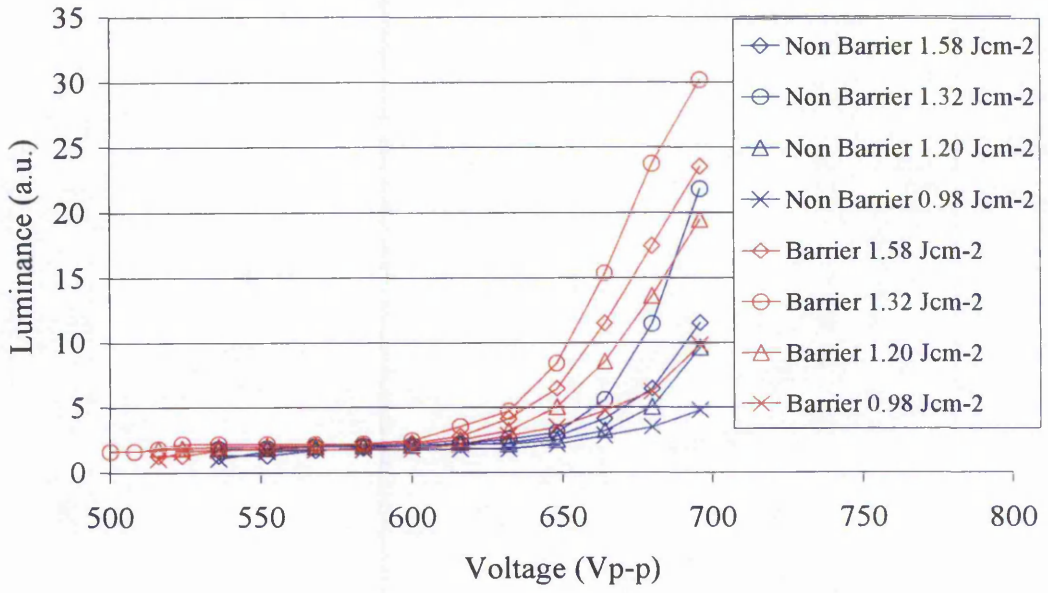


Figure 6.3: BV Of Barrier And Non Barrier Layer SrS:Cu,Ag Devices On Glass Substrate Laser Annealed With 4 Laser Irradiation Pulses Of Various Laser Fluence.

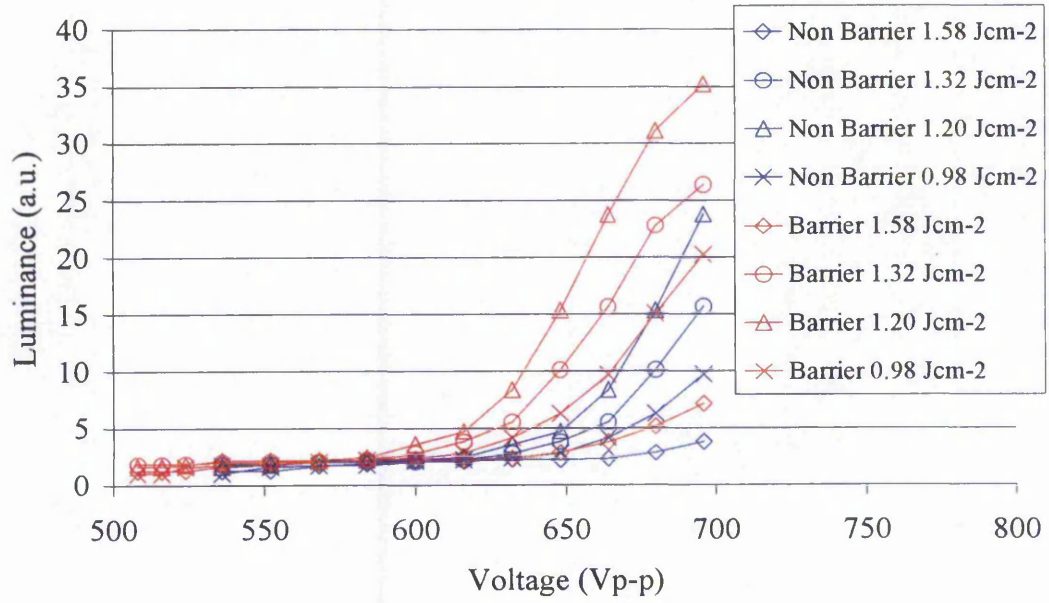


Figure 6.4: BV Of Barrier And Non Barrier Layer SrS:Cu,Ag Devices On Glass Substrate Laser Annealed With 5 Laser Irradiation Pulses Of Various Laser Fluence.

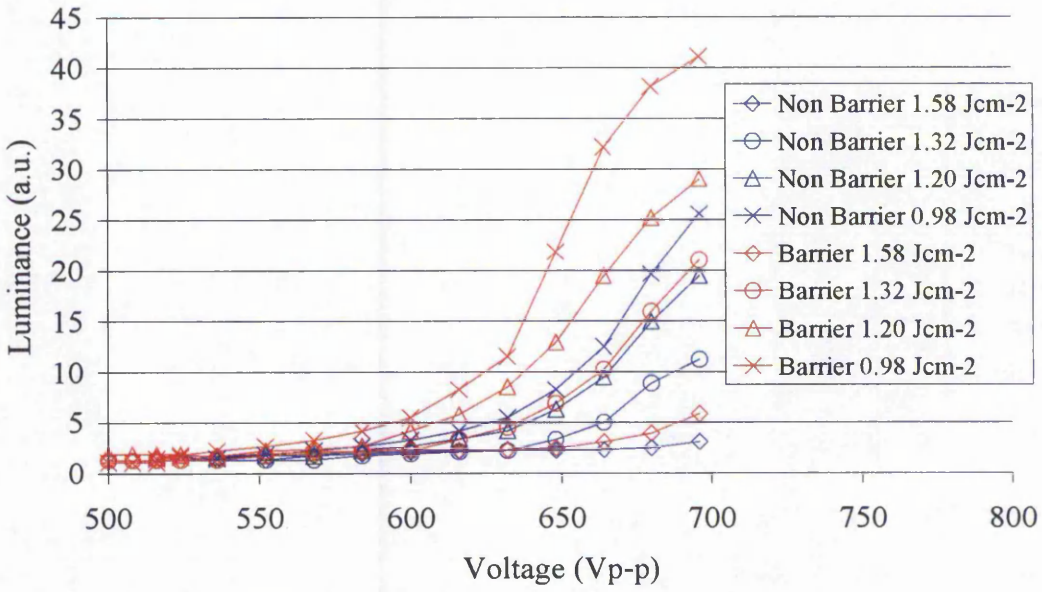


Figure 6.5: BV Of Barrier And Non Barrier Layer SrS:Cu,Ag Devices On Glass Substrate Laser Annealed With 6 Laser Irradiation Pulses Of Various Laser Fluence.

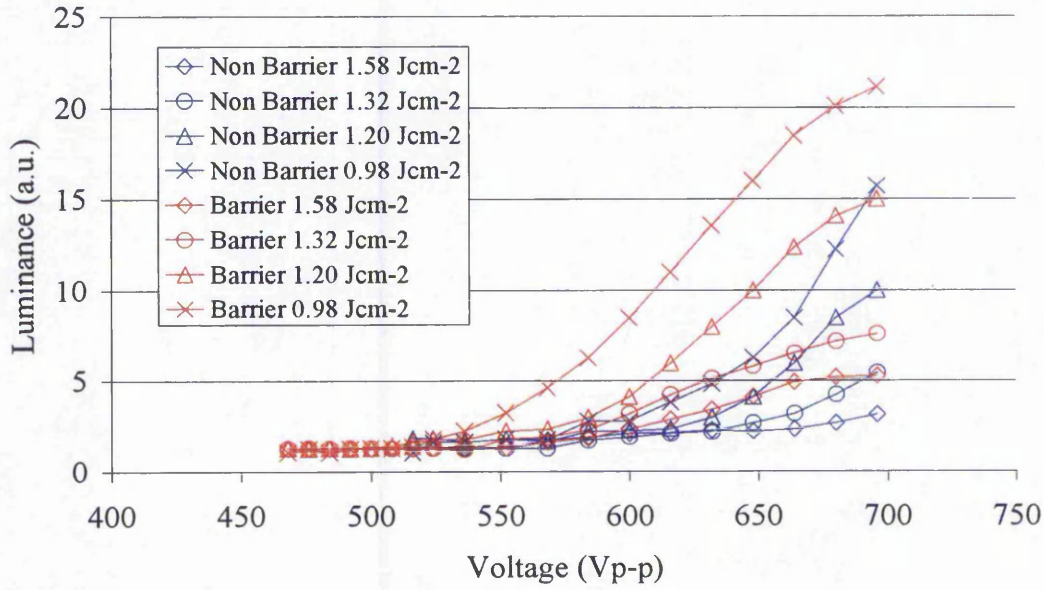


Figure 6.6: BV Of Barrier And Non Barrier Layer SrS:Cu,Ag Devices On Glass Substrate Laser Annealed With 7 Laser Irradiation Pulses Of Various Laser Fluence.

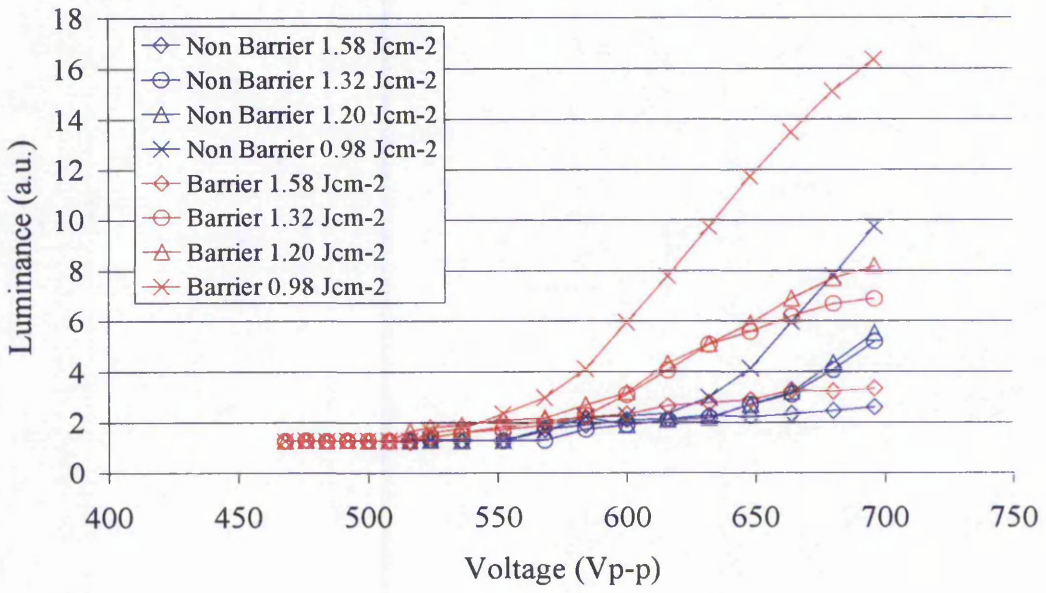


Figure 6.7: BV Of Barrier And Non Barrier Layer SrS:Cu,Ag Devices On Glass Substrate Laser Annealed With 8 Laser Irradiation Pulses Of Various Laser Fluence.

For case of ZnS:Mn TFEL devices, the effect of the barrier layer is to provide a sharper BV curve and higher luminance. For SrS:Cu,Ag devices, although the barrier layer improved the overall brightness of the devices over non barrier layer devices operated at a similar voltages. There was however, little sharpening of the BV curves. The optimum laser annealing parameter for barrier layer SrS:Cu,Ag TFEL devices matches the finding from studies of laser annealing for standard SrS:Cu,Ag as described in chapter 5, whereby at laser fluence of 0.98 $Jcm^{-2}$ with 6 laser irradiation pulses resulted in the best performing device.

## 6.3 EFFECT OF LASER ANNEALING AT DIFFERENT STAGES OF FABRICATION OF BARRIER LAYER SrS:Cu,Ag TFEL DEVICE

Laser Annealing was believed to cause the increase of temperature on the surface of the thin film irradiated by the laser pulse. This heat will then propagates into the thin film creating a temperature gradient between the surface and the depth of the thin film as shown by thermal model developed by Mastio at al[3]. The existence of this thermal gradient and the necessary stoppage during the fabrication of barrier layer devices, led to the idea of laser annealing at different stages or thickness of the phosphor layer.

Figure 6.8 illustrates the different types of laser annealed devices resulting from investigation on the effect of laser annealing at different stages of the fabrication step of a barrier layer SrS:Cu,Ag devices. In order to laser anneal the bottom phosphor, laser annealing was performed after depositing half the required thickness of the phosphor layer but before the deposition of the thin barrier layer.

The effect of laser annealing only the bottom phosphor for non barrier layer devices is shown in figure 6.9 while figure 6.10 shows the effect of laser annealing the bottom phosphor on barrier layer SrS:Cu,Ag devices. These devices are laser annealed with 3 laser irradiation pulses.

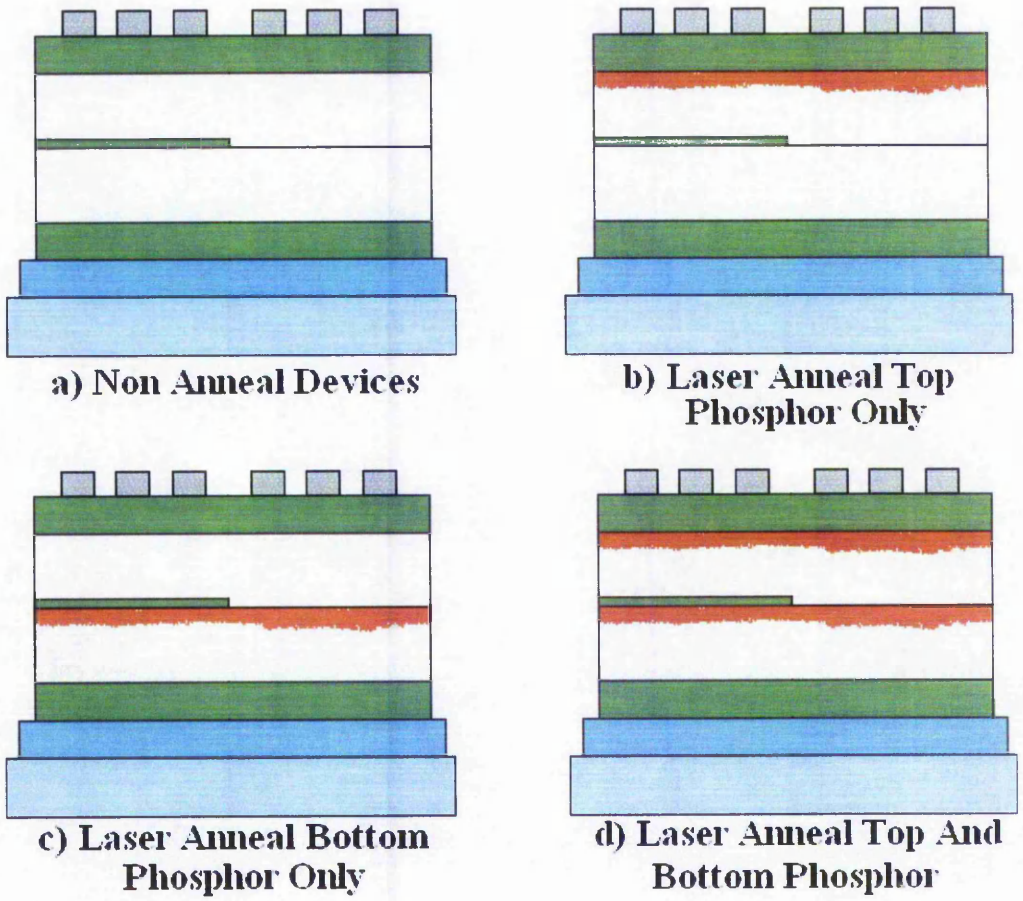


Figure 6.8: Illustration Of Different Laser Annealing Stages

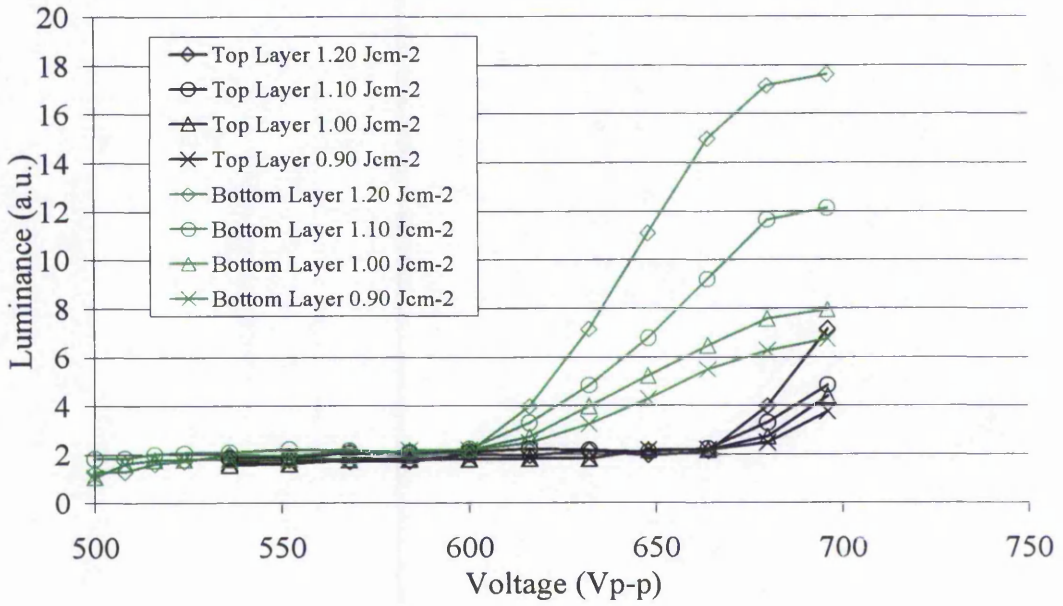


Figure 6.9: Comparison Of BV Curve For Non Barrier Layer SrS:Cu,Ag Devices Laser Annealed Bottom Phosphor Only & Laser Annealed Top Phosphor Only With 3 Laser Irradiation Pulses Of Various Laser Fluence.

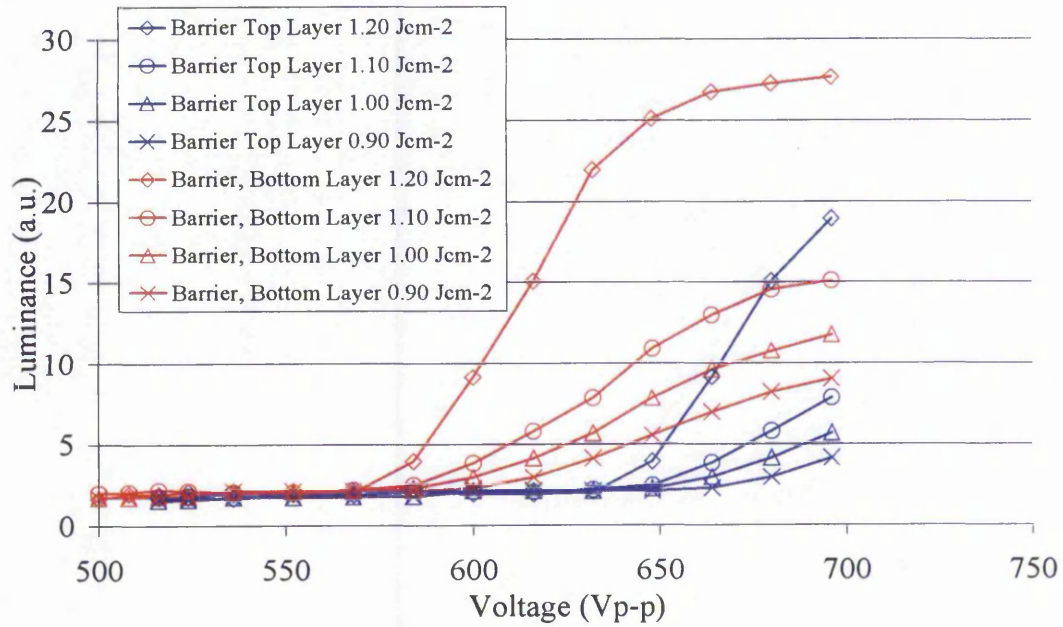


Figure 6.10: Comparison Of BV Curve For Barrier Layer SrS:Cu,Ag Devices Laser Annealed Bottom Phosphor Only & Laser Annealed Top Phosphor Only With 3 Laser Irradiation Pulses Of Various Laser Fluence.

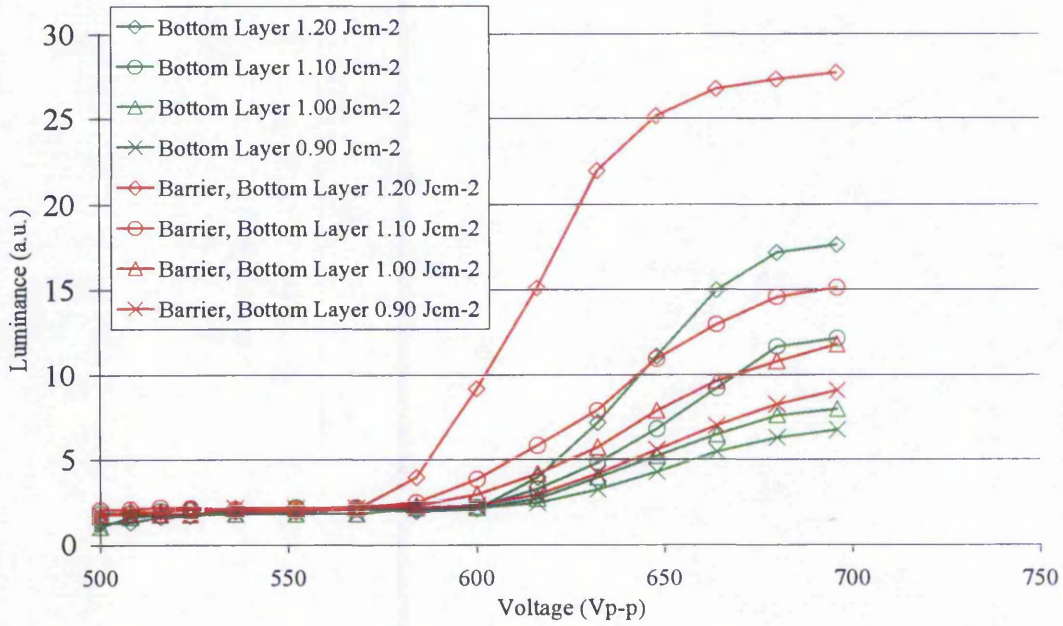


Figure 6.11: BV Of Barrier And Non Barrier Layer SrS:Cu,Ag Devices On Glass Substrate With The Bottom Phosphor Layer Laser Annealed With 3 Laser Irradiation Pulses Of Various Laser Fluence.

For laser annealing of bottom phosphor layer only, the best parameters for laser annealing is 1.20 $Jcm^{-2}$ with 3 laser irradiation pulses followed by 1.10 $Jcm^{-2}$, 1.00 $Jcm^{-2}$ and finally 0.90 $Jcm^{-2}$. This is similar to the effect of laser annealing top phosphor layer only for SrS:Cu,Ag devices as in chapter 5 and also the barrier layer SrS:Cu,Ag in previous section.

Because the devices were only driven by a maximum voltage of 700 $V_{p-p}$, it is not known from this experiment whether the laser annealing of the bottom phosphor layer instead of the top phosphor layer will result in a brighter device. This is due to the limits of the power supply together with the high turn on voltage of devices when only the top phosphor layer is laser annealed, limiting the measurement up to 700 $V_{p-p}$. However, when the bottom phosphor layer of the SrS:Cu,Ag devices is laser annealed, the turn on voltages is reduced, hence increasing the overall efficiency of the device.

It is known from SEM of laser annealed samples that laser annealing creates sub-micron cracks as described in Chapter 5. From Otero-Barros work[4] shows that for a TFEL, the internally generated light couples principally into the fundamental mode and propagates as such along the TFEL stacked structure. When laser annealing was performed on the bottom phosphor layer, the sub-micron cracks which situated roughly in the middle of the TFEL stacks is believed to disturb the light propagation resulting in higher probability for the generated lights to be emitted from the device. This consequently leads to a reduction of turn on voltage as seen in figure 6.9 and 6.10.

Interestingly, for non barrier layer devices, laser annealing of the bottom phosphor seems to simulate the deposition of the barrier layer as shown in figure 6.12. It is believed that films deposited after laser annealing is more amorphous than films deposited on phosphor layer without laser annealing. This amorphous layer acts as a barrier layer resulting in a characteristic similar to a barrier layer device.

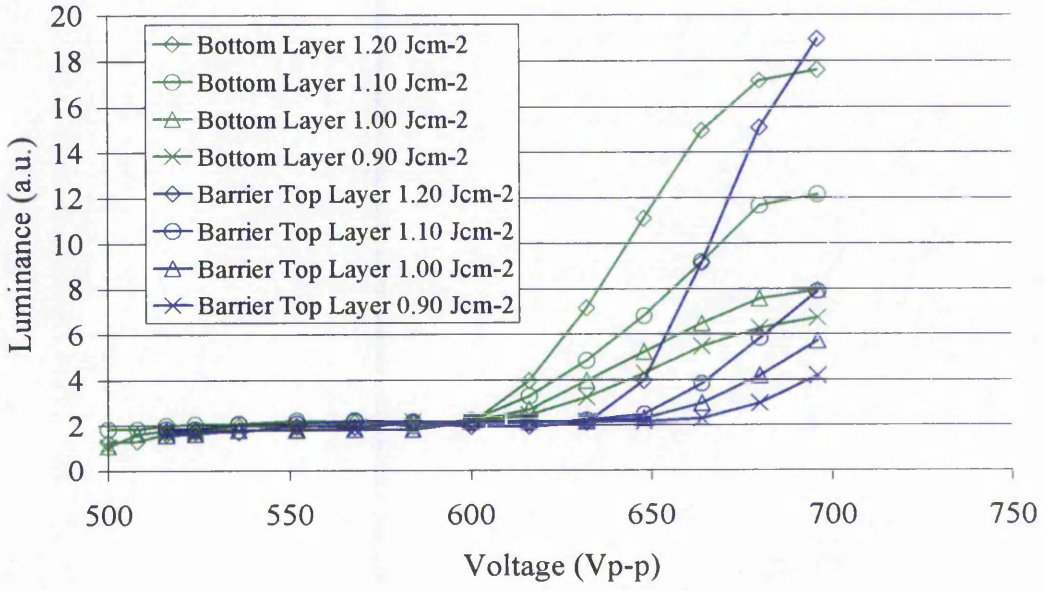


Figure 6.12: BV Of Barrier Layer SrS:Cu,Ag Devices With The Top Phosphor Layer and Non Barrier Layer SrS:Cu,Ag Laser Annealed With The Bottom Phosphor Layer Laser Annealed Utilising 3 Laser Irradiation Pulses Of Various Laser Fluence.

In addition, by laser annealing the bottom phosphor layer instead of the top phosphor, the effect of the introduction of thin barrier layer within the phosphor layer can be better illustrated. From figure 6.11, it is clear that with the incorporation of a thin insulating layer within the phosphor layer resulted in a device capable of providing higher luminance over conventional double insulating TFEL device. Barrier layer devices also show a slightly sharper BV characteristic.

Figure 6.13 shows the summary of laser annealing effect at various fabrication stage of the phosphor layer including devices with both top and bottom phosphor layers annealed with the same parameter. It is clear that when both top and bottom phosphor layer of the SrS:Cu,Ag devices is laser annealed, the overall brightness of the device is twice that of those with only the bottom phosphor layer laser annealed.

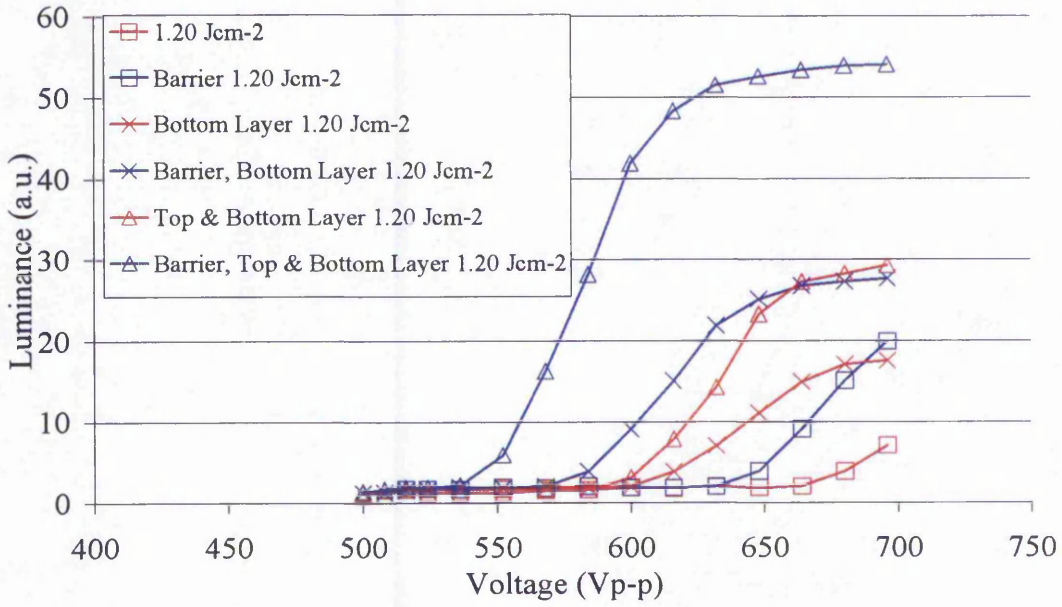


Figure 6.13: BV Of SrS:Cu,Ag TFEL laser annealed at 1.20 Jcm$^{-2}$ with 3 laser irradiation pulses before deposition of the barrier layer and completing the deposition of the phosphor layer.

The EL emission of SrS:Cu,Ag TFEL devices laser annealed at 1.20 Jcm$^{-2}$ with 3 laser irradiation pulses before deposition of the barrier layer and a commercially available full colour LCD display for a mobile phone is shown in figure 6.14. Note, the slight fluctuation of the EL spectrum is caused by interference due to the TFEL stacks while the spectrum of the commercial device which contain a white backlight source was taken through the protective glass of the LCD display.

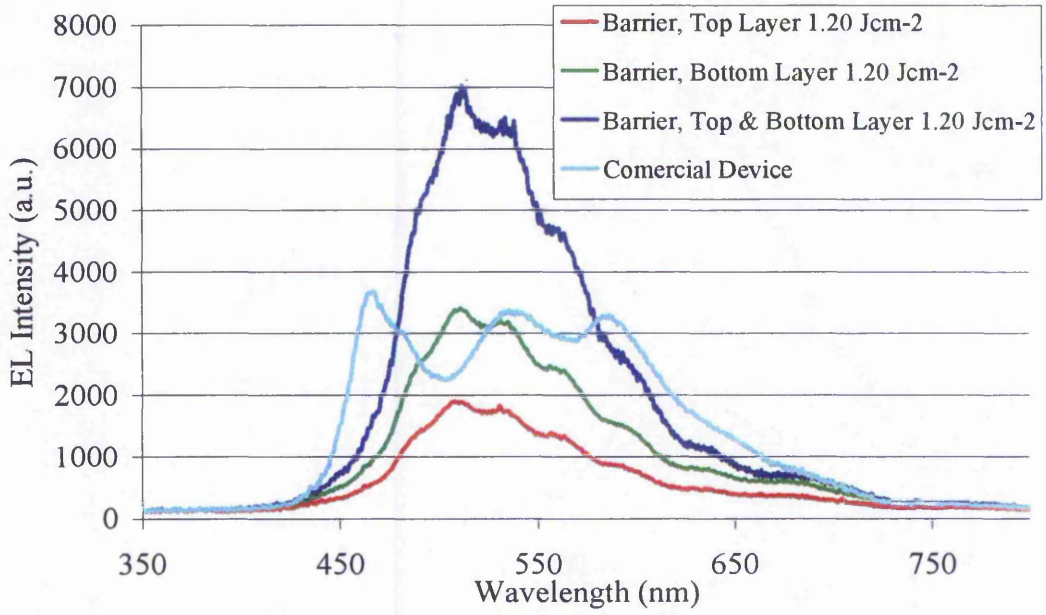


Figure 6.14: EL Emission Of SrS:Cu,Ag TFEL laser annealed at 1.20 Jcm$^{-2}$ with 3 laser irradiation pulses before deposition of the barrier layer and a commercial mobile phone display

Clearly the barrier layer SrS:Cu,Ag device with both the top and bottom phosphor layer laser annealed exhibited highest EL intensity, out performing the commercial device. The improvement of the double annealed devices is believed to be caused by a more efficient way of annealing. As it is believed that laser annealing only affects a thin layer of the phosphor layer, by laser annealing at different thickness of the phosphor layer, the overall enhancement of the phosphor layer is improved. Unfortunately, devices with both the phosphor layer laser annealed generally less stable than devices with only the bottom phosphor layer laser annealed. Laser ablation is believed to be the cause of this instability.

## 6.4 EFFECT OF THE BARRIER LAYER THICKNESS

As non barrier layer SrS:Cu,Ag device with the bottom phosphor layer laser annealed behaved similarly to a laser annealed barrier layer SrS:Cu,Ag devices, plus the good EL characteristic of barrier layer devices with its bottom phosphor layer laser annealed, a further experiment was carried out to examine the effect of the thickness of this thin insulating layer on the electrical performance of barrier layer SrS:Cu,Ag TFEL devices.

For this study, the thickness of the barrier layer was varied from 100 Å up to 300 Å. In order to facilitate direct comparison between all these devices, the different thickness barrier layer devices were fabricated on the same sample as shown by the wafer quarter mapping in figure 6.15. For these experiment, only the bottom phosphor layer was laser annealed.

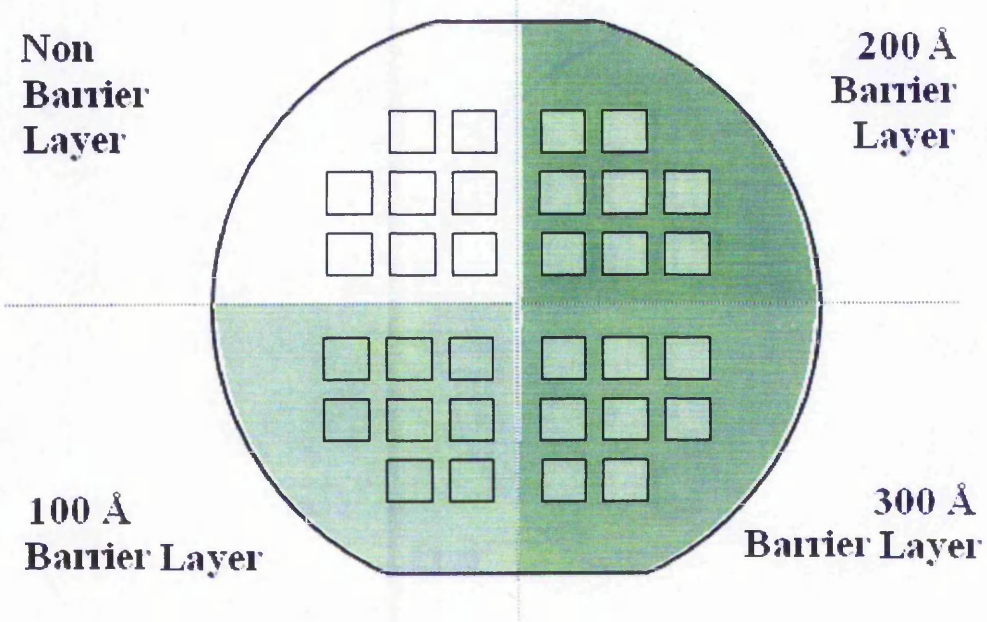


Figure 6.15: Device Mapping For Different Thickness Barrier Layer Test Wafer

The effect of barrier layer thickness on SrS:Cu,Ag TFEL devices performance are shown in figure 6.16 and 6.17. Each device has a BV characteristic response that is highly dependent on the thickness of the incorporated barrier layer.

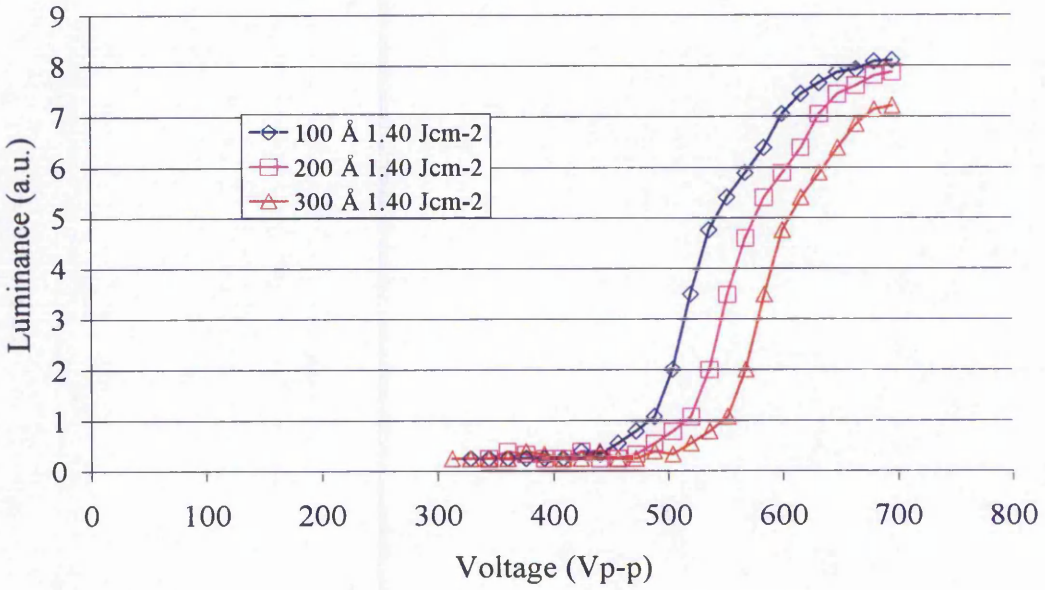


Figure 6.16: BV of different thickness barrier layer SrS:Cu,Ag TFEL devices laser annealed at 1.40 Jcm$^{-2}$ for 3 laser irradiation pulses.

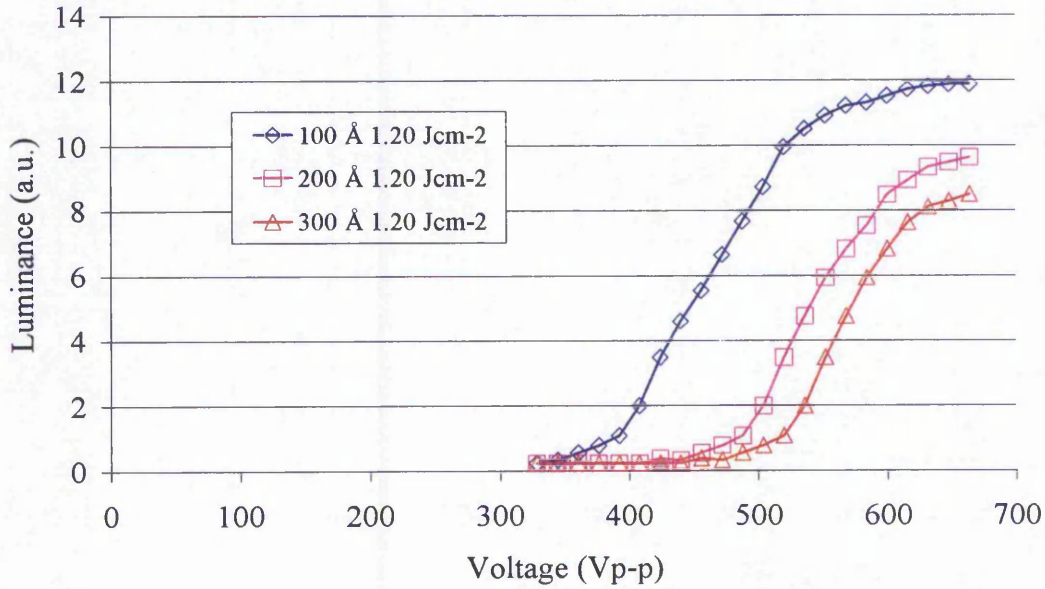


Figure 6.17: BV of different thickness barrier layer SrS:Cu,Ag TFEL devices laser annealed at 1.20 Jcm$^{-2}$ for 5 laser irradiation pulses.

For both parameters of laser annealing, the 100Å barrier layer device exhibited the highest luminance. With the increase in the thickness of the barrier layer, the overall brightness of the device is reduced. The turn on voltages of the thicker barrier layer devices were also higher compared to thinner barrier layer devices.

Although copper doped alkaline earth sulphide phosphors have been known for a long time[5], the emission mechanism is still poorly understood. It has been suggested that SrS:Cu emission mechanism may due to the donor-acceptor recombination process similar to the well known ZnS:Cu mechanism[5,6,7]. However, a more recent proposed model suggested that the luminescence is due to a $3d^{10} - 4d^9 4s$ transition of $Cu^+$ ion[8,,9,10]. The luminescence of SrS:Cu,Ag is even less understood. The energy transfer from $Cu^+$ ion to $Ag^+$ center was proposed for electroluminescene of this phosphor[11]. When the applied voltage exceeds the threshold voltages, electrons are injected via tunnelling into the bulk of the phosphor layer from the interface states between the phosphor and insulating layers. The injected electrons are accelerated by the applied field gaining enough kinetic energy for impact ionisation. Light is produced when electrons created by tunnelling or impact ionisation recombine with ionised $Cu^+$ centers, subsequently energy transfer to non symmetric $Ag^+$ centers occur. The study of barrier layer effect on SrS:Cu,Ag TFEL devices agrees with this model.

From barrier layer works on ZnS:Mn[1,2], it is agreed that electrons tunnel through the barrier layer gain energy. This consequently increases the probability for impact ionisation for the later half of the SrS:Cu,Ag films. As the thickness of the barrier layer increases, the thin insulating layer acts more as a true barrier to the tunnelling electrons as the mean path of the electrons increases plus higher probability of collisions, consequently reduces the total density of electrons capable for tunnelling. This evidently resulted in a reduction in the total light output.

## 6.5 CONCLUSION

The study of laser annealed barrier layer SrS:Cu,Ag TFEL devices have concluded that these devices exhibit higher luminance under EL excitation compared with the standard non barrier layer devices laser annealed under the same laser annealing condition. This improvement is believed to be the result of electrons tunnelling and gaining energy when travelling through the thin insulating barrier layer similar to those of the ZnS:Mn devices. However, the main mechanism here is impact ionisation rather than impact excitation for the case of ZnS:Mn devices.

It is also found that laser annealing of the bottom phosphor layer of a non barrier layer device resulted in a device with similar characteristic as those incorporating a thin insulating barrier layer. This is believed to be caused by the creation of a discontinuity of film situated in the middle of the phosphor layer.

In the present form, the optimum SrS:Cu,Ag TFEL devices configuration consisted of a single 100 Å thick barrier layer device laser annealed at 1.2 $Jcm^{-2}$ with 5 laser irradiation on the bottom phosphor layer, as devices with both bottom and top phosphor layer laser annealed are generally less stable.

**REFERENCES**

[1] W.M. Cranton, PhD Thesis, University of Bradford, 1995.

[2] Thomas, C.B., and Cranton, W.M.: 'High Efficiency ZnS:Mn ac Thin Film electroluminescent Device Structure', Appl. Phys. Lett., 63 (23), 1993, 3119

[3] E.A. Mastio, W.M. Cranton, C.B. Thomas, E. Fogarassy and S. de Unamuno, Applied Surface Science, Vol. 138-139, pp. 35-39, 1999

[4] S.Otero-Barros, PhD Thesis, The Nottingham Trent University, 2000.

[5] W. Lehmann, J. Electrochem. Soc. **117,** pp. 1389, 1970.

[6] Y. Nakanishi, K. Natsume, Y. Fukuda, G. Shimaoka, H. Tatsuoka, H. Kuwabara and E. Nakazawa, J. Cryst. Growth, **101,** pp. 462, 1990.

[7] R. Pandey and S. Sivaraman, J. Phys. Chem. Solids, **52,** pp. 81, 1991.

[8] N. Yamashita, Jpn. J. Appl. Phys., Part 1, **30**, pp. 3335, 1991.

[9] D.S. McClure and S.C. Weaver, J. Phys. Chem. Solids, **52,** pp. 211, 1991.

[10] W. Park, T.C. Jones, W. Tong, B.K. Wagner, C.J. Summers and S.S. Sun, 3th International Conference on the Science and Technology of Display Phosphor, Extended Abstract, Huntington Beach, CA, pp. 57, 1997.

[11] W. Park, T.C. Jones, E. Mohammed, C.J. Summers and S.S. Sun, 4th International Conference on the Science and Technology of Display Phosphor, Extended Abstract, Bend, OR, pp. 215, 1998.

# CHAPTER 7

# CONCLUSION AND FUTURE WORK

## 7.1 INTRODUCTION

The main aim of this PhD work was to investigate a means for enhancing the luminescent efficiency of SrS:Cu,Ag thin film for the application of an efficient blue emitting electroluminescence phosphor to be utilised in TFEL display devices. In order to facilitate this study, a suitable fabrication path for SrS:Cu,Ag thin films was first established utilising the rf magnetron sputter deposition technique. This was followed by work on enhancing the luminescent efficiency of SrS:Cu,Ag thin films at which, conventional thermal post deposition annealing and novel laser pulses irradiation annealing was performed. In addition, the effect of the incorporation of thin insulating layer within the phosphor layer of the ACTFEL stack was also investigated.

### 7.1.1 FABRICATION OF SrS:Cu,Ag THIN FILMS

For the fabrication of SrS:Cu,Ag thin films, rf magnetron sputter deposition was utilised. In order to establish a suitable sputtering condition for the deposition of quality SrS:Cu,Ag thin films, the effect of various parameters concerning the sputter deposition techniques on the quality of the deposited films was investigated. They include substrate biasing, deposition temperature, sputtering environmental pressure and distance of source and substrate.

The substrate biasing study was not conclusive due to the limits of the power supply used for the substrate bias while the optimum deposition temperature for SrS:Cu,Ag was found to be comparable to those of in-house fabricated ZnS:Mn and $Y_2O_3$. The sputtering environmental pressure for SrS:Cu,Ag thin films on the other hand, required a much higher pressure that the sputtering environmental pressure optimum for the ZnS:Mn and $Y_2O_3$. In addition,the deposition rate for SrS:Cu,Ag thin film was found to be too slow when the electrode is situated at the designed distance from the substrate.

From the results obtained from various thermal based post deposition annealing, it was concluded that although reasonable success was achievable for PL improvement of SrS:Cu,Ag thin films, thermal based annealing was not suitable as the post deposition technique for the fabrication of SrS:Cu,Ag ACTFEL as these films required high temperature post deposition annealing resulting in crazing of films. The crazing causes the device to short out when high field is applied across the device, subsequently leading to device failure.

### 7.1.2 LASER ANNEALING

SrS:Cu,Ag devices when post deposition annealed, utilising conventional thermal based annealing, failed to produce any reliable ACTFEL devices. The effect of utilising an alternative novel technique of pulsed laser irradiation, namely laser annealing was investigated and optimised. Among the many parameters affecting the effect of laser annealing, only laser fluences, number of irradiation pulses and pressure of the inert environment was investigated.

It was found that for laser annealing, it is essential to have a pressurised environment emphasising the importance of the pressure cell. In addition, there is also a close relation between the laser fluences and number of irradiation pulses. The result suggested better laser annealing effect when laser annealing was performing in a high over pressure argon environment with low laser fluence but high number of laser irradiation pulses. Laser annealed SrS:Cu,Ag devices was also found to outperform conventional thermally annealing devices.

XRD results along with SEM pictures suggested that laser annealing not only shown as improvement of the crystallinity of the SrS:Cu,Ag thin films but also creation of sub-micron cracks the on surface of the laser irradiated films. These cracks are believed to be beneficial for the enhancement of the luminescent efficient of SrS:Cu,Ag thin films as it provided a rougher surface resulting in a more efficient optical outcoupling of the internally emitted light. Therefore creating a higher light output from the layer surface.

### 7.1.3 BARRIER LAYER DEVICES

The method previously employed for improving the luminous efficiency of ZnS:Mn ACTFEL devices by structure modification to include a thin insulating layer within the phosphor layer was also studied here for SrS:Cu,Ag ACTFEL. The post deposition utilised here was laser annealing instead of thermal based annealing due the inability to produce reliable SrS:Cu,Ag device from thermally based annealing caused by the crazing affect of thermally annealed SrS:Cu,Ag thin films. In addition, due to the nature of fabrication path of barrier layer devices, laser annealing was also performed prior to the deposition of the thin insulating barrier layer.

The incorporation of barrier layers on SrS:Cu,Ag ACTFEL devices although exhibits higher luminance over non barrier layer devices, it however only slightly sharpens the BV characteristic curve whereas for ZnS:Mn there was a noticeable sharpening of the BV response curve. The close relationship of laser fluence and number of irradiation pulses found in non barrier layer devices also applies to barrier layer devices, whereby it was found that devices laser annealed at low fluence with high number of laser irradiation pulses generally exhibit much higher luminance then devices laser annealed at high laser fluence with low number of laser irradiation pulses. The improvement caused by barrier layer devices on SrS:Cu,Ag devices is believed to be accredited to energy gain by electron tunnelling through the layer similar to ZnS:Mn devices, but instead of having more hot electrons for impact ionisation as for ZnS:Mn, it is believed that for SrS:Cu,Ag devices, it resulted in a more efficient impact ionisation of the $Cu^{+}$ activator with resonant energy transfer to the $Ag^{+}$ ion.

Laser annealing prior to the deposition of the thin insulating barrier layer is found to be even more beneficial than laser annealing prior to the deposition of the top insulating layer. This is believed to be the benefit of the sub-micron cracks created by laser annealing. The cracks when situated within the phosphor layer disrupted the propagation of light towards the edge of the ACTFEL device, resulting in a higher light emission from the surface of the ACTFEL device. In addition, devices laser annealed prior to the deposition of barrier layer but without a barrier layer,

performed similar to devices with barrier layer but laser annealed prior to the deposition of the top insulating layer.

## 7.2 ACHIEVEMENT

The achievement for this work can be summarised below;

a) Benefit of laser annealing over conventional thermal based post deposition annealing.

b) Possibility of fabricating SrS:Cu,Ag TFEL devices without the need for high temperature processes.

c) Advantage of barrier layer on the performance of SrS:Cu,Ag ACTFEL devices.

d) Commercial production of SrS:Cu,Ag ACTFEL devices with barrier layer effect but without the need for barrier layer deposition.

Generally, laser annealed devices outperform conventional thermally annealed devices by a factor of 5. This is especially true for devices laser annealed at low laser fluence but with high number of laser irradiation pulses in a pressurised argon environment.

As laser annealing does not require any high temperature process, for a typical laser annealed SrS:Cu,Ag TFEL device, the only process involving any form of a heater is during the sputter deposition. This not only allows the use of cheaper substrates such as normal glass or even plastic substrate for the fabrication of flexible substrate, it also reduces the potential contamination from particles emitted from the heater due to the heating process. It is also believed that by utilising laser annealing as the post deposition technique instead of conventional thermal based annealing, the output of commercial production can be increased as laser annealing not only avoided the need

for uniform high temperature heater but also drastically reduces the post annealing time from tens of minutes to mere seconds.

The incorporation of a thin insulating layer within the phosphor layer of SrS:Cu,Ag devices also further enhances the luminance of the SrS:Cu,Ag devices. With the incorporation of a barrier layer, the performance of the SrS:Cu,Ag is also double that of non barrier layer devices. The fabrication of barrier layers however, is not a feasible path for a fully automated commercial production unit which is typically an inline system. As found, the thickness of the barrier layer greatly influences the overall performance of the device. It is therefore very uneconomic to introduce a system to control the deposition of the barrier layer.

In order to fabricate non barrier layer SrS:Cu,Ag devices with the similar characteristic of a barrier layered device in an automated production line, the deposition of the phosphor layer need to be broken into two separated section. This is to allow the laser annealing process to be carried out at half thickness of the phosphor layer. The proposed system is as follows; the deposition of the phosphor layer is stopped when it reaches half thickness. The samples are then transferred to a pressure cell for laser annealing. Following laser annealing, the samples are again transferred to a vacuum chamber for the deposition of the remaining half of the TFEL device structure.

## 7.3 FUTURE WORK

As mentioned previously, there are many parameters affecting the effect of laser annealing. Although an optimum laser annealing parameter was obtained from this work, the true optimisation of laser annealing has yet to be carried out. Among many other parameters affecting laser annealing, the author believed with the current parameters, at least two additional parameters should be investigated and may result in a better performing device. They are environment temperature and environmental gas composition.

The nature of the SrS:Cu,Ag films is know to be substoichiometric, therefore annealing in sulphide environment such as $H_2S$ should be beneficial typically in reducing any sulphur vacancies possibly created by laser annealing. The environmental temperature should greatly influence the result of laser annealing as this would affect the temperature gradient created during laser annealing process. The higher the environmental temperature during laser annealing should result in a better improvement of the quality of films in term of crystallinity. In addition, in order to minimise laser ablation, laser annealing with samples immersed in some form of inactive liquid could be beneficial.

It is shown that laser annealing performed within the phosphor layer is beneficial. By laser annealing more of the phosphor layer, a further enhancement of the overall performance of the ACTFEL device can be achieved, as this should not only drastically improve the crystallinity of the overall phosphor layer but also improve the overall outcoupling of the internal generated light to be emitted to the surface of the device.

Nevertheless, the experiments carried out in this work should be repeated for a phosphor with different concentration of Cu and Ag, or different blue emitting phosphor such as the recent CaS:Pb or $BaAl_2S_4$:Eu. The author believes that the use of laser annealing as a post deposition technique should provide the ultimate dream of fabricating an efficient blue emitting ACTFEL.

# CHAPTER 8

# APPENDIXES

# APPENDIX A: Argon Etching

## INTRODUCTION

Although the following equipment and procedure were not used in the main portion of the thesis, these systems were investigated and commissioned to facilitate the production of 'blue emitting' LETFEL devices. This ambitious goal could not be achieved, but for completeness sake, the technology is included in the thesis.

The established fabrication path of LETFEL devices prior to this work was to utilise ion-milling technique as the primary tool for etching of the top insulators[1]. For the examination of a alternate fabrication path for LETFEL devices, a custom designed system to investigate the etching of LETFEL materials has been commissioned and calibrated to examine the etch rates and profiles for the following thin film materials: ZnS:Mn, $Y_2O_3$, and SiON; currently, the primary materials for ZnS:Mn based LETFEL devices.

Also, prior to the commissioning of the etching system, lithography process equipment has also been commissioned. This includes commissioning a photoresist spinner, mask aligner and oxygen asher for the removal of photoresist.

# LITHOGRAPHY EQUIPMENT

## PHOTORESIST SPINNER

The very first process for microfabrication is to coat the material to be patterned/etched with a masking layer. The most common masking layer used is a coat of optical photoresist. The layer is usually applied centrifugally on to the high speed rotating surface of a silicon wafer; a process referred to generally as 'spin coating'.

The 'Solitec 5100' spinner has been commissioned in the new HEFCE funded Clean Room of the NTU optoelectronics group. The spinner is driven by a brushless dc motor which can provide a spin speed of between 250 and 8000 rpm with a spin acceleration of 1000 – 40000 rpm/sec. The wafer is held on the chuck by vacuum provided by an Edwards rotary pump. Photoresist is manually dropped on to the wafer by the aid of pipette.

## MASK ALIGNER

The Canon - Parallel light mask aligner (PLA-500F) has been set up and commissioned in order to form the desired pattern on to the photoresist. The exposure for the photoresist is a g-line mercury lamp (436nm). The vacuum is again provided by an Edwards rotary pump while the clean air is provided by a portable compressor. In order to avoid contamination of the wafers by the compressor, a combination of filters is being used. This combination consists of 3 individual filters which are a general purpose filter for removal of water vapour and particles, an oil removal filter and finally an oil vapour filter.

The photoresist is sensitive to ultraviolet (UV) light in the sense that when it is exposed to UV light, the property of the photoresist changes. For positive photoresist, the photoresist loses its' resistance against the developer when it is exposed to UV light while the negative photoresist has the opposite properties. Hence, by exposing the photoresist with UV light through a mask, an image of this mask can be formed after washing with the appropriate developer.

**ASHER**

The Tegal Plasmaline 415 oxygen asher has been commissioned to remove the photoresist used during etching. Both the oxygen and the nitrogen are supplied from gas bottles with clean air being provided by a filtered compressor, while vacuum is provided by a rotary pump. For plasma removal, the oxygen is blended into a high vacuum reaction chamber, at a rate of several hundred cubic centimetres per minutes. The radio frequency (r.f.) energy then excites the oxygen, creating active species that reduce the photoresist polymeric chains to a simpler and lower molecular groups. These then volatilise and are pulled out of the system by the rotary pump.

Plasma removal of photoresist offers several advantages compared to wet chemical stripping, namely:

- Safer operating condition for operators.
- No metal ion contamination
- Fewer process steps
- No attack on underlying surfaces

# ARGON SPUTTER ETCHER

Reactive Ion etching (RIE) of silicon and other surfaces is an important material processing technique that is widely employed by the semiconductor industry [2,3] for the fabrication of integrated circuits. No known gases exist for the reactive ion etching of the insulator material, $Y_2O_3$ used in LETFELs plus the problem identified by ion milling of LETFELs[1] forms the main reason for the need to investigate etching of LETFELs material by pure physical sputtering. The term ' reactive ion etching' (RIE) is used to distinguish the chemical nature of the process from purely physical sputtering, e.g., etching by $Ar^+$ bombardment only. Due to the absence of suitable gases, only etching by $Ar^+$ bombardment can occur.

An existing Magnetron Reactive Ion Etching (MRIE) system formally used for other TFEL devices was modified to form an argon sputter etch system. This etching system is used to investigate the etching of LETFELs materials utilising argon gas. Figure I shows the schematic outline of the initial configuration of the whole etching system including the transfer mechanism. As the flow rate of this system was found to be insufficient plus the difficulty in controlling the flow with the butterfly valve, the pumping system of this system was reconstructed to incorporate the use of a buffer valve and a more efficient diffusion pump as shown in figure II. In addition, a Penning gauge was introduced to better monitor the vacuum of the chamber while a Pirani gauge was placed between the outlet of the diffusion pump and the inlet of the rotary pump for monitoring of the suction of the rotary pump.

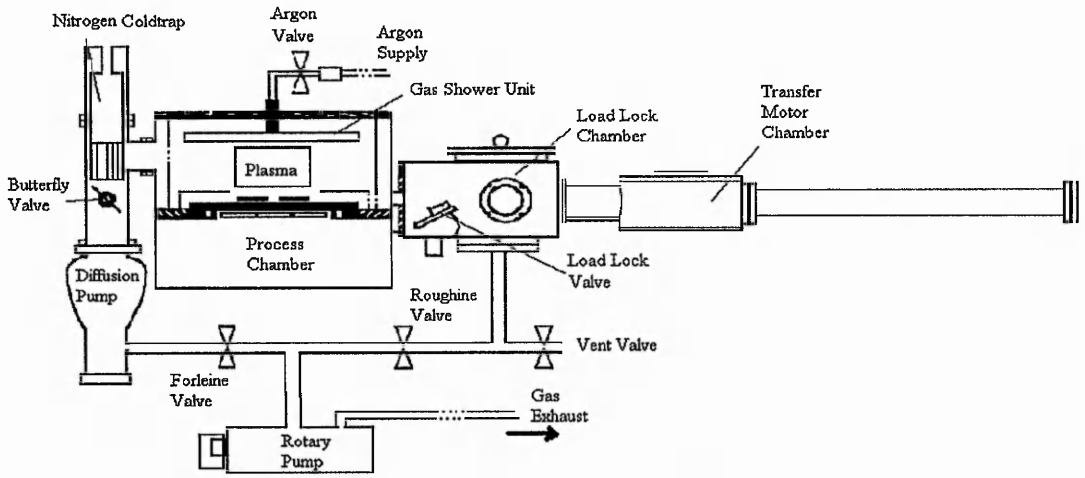


Figure I: Initial Configuration OF The Argon Etcher

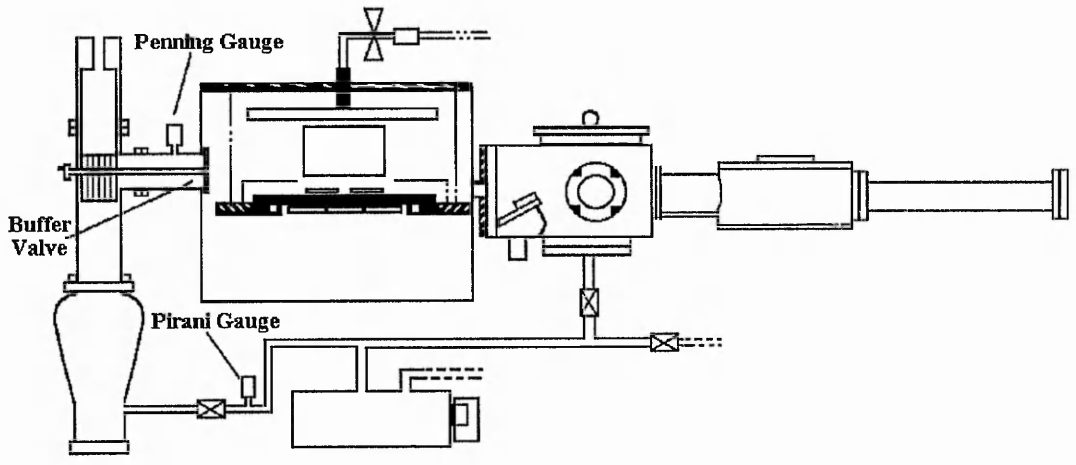


Figure II: Final Configuration OF The Argon Etcher

The distinct difference between this system compared with the other vacuum systems of the NTU optoelectronics group is the automated loading system. With this, potential mistakes during manual loading are minimised, especially errors in wafer alignment during the wafers transfers from the loading arm to the electrode within the process chamber. Apart from that, the employment of the custom made gas shower unit, ensures an even flow of gas into the process chamber. Finally, this system has the ability to process two 4" size wafers simultaneously while the previous systems were designed for holding and processing only one wafer.

## ETCHING CALIBRATION FOR LETFELS MATERIAL

Prior to the calibration of the photoresist, an initial investigation into the etch rates and the etch profiles of several different LETFEL material was performed utilising the shadow mask technique. The calibration was carried out mainly to investigate the functionality of the system. The materials being investigated were silicon dioxide ($SiO_2$) and yttrium oxide ($Y_2O_3$). Etching of these materials have been carried out at 10mTorr of argon gas with a variation in RF power from 100W to 250W. A summary of the etch rates is shown in table I.

| Material | Power (W) | Etch Rate (Å/min) |
|---|---|---|
| SiO2 | 250 | 36 |
| | 200 | 24 |
| | 150 | 20 |
| | 100 | 13 |
| Y2O3 | 250 | 30 |
| | 200 | 25 |
| | 150 | 19 |
| | 100 | 11 |

Table I: Etch Rates Obtained From Etching System Prior to Modification

Based on these finding and results, the new gas extraction system was designed and fitted on the Argon Etcher as shown in figure II. The new design removed the troublesome butterfly valve nitrogen cold trap and replaced both with a baffle valved nitrogen cold trap. A larger diffusion pump (E06K) also replaced the E04K. This configuration provides not only better extraction of gases but also enables better control of the process gas pressure during sputter etching.

With the commissioning of the redesigned Argon Etcher, the etching conditions can be calibrated not only based on variance of power but also with a variance of vacuum suction and process gas flow. With these capabilities, photoresist masks on plain silicon were used during initial testing of the machine. Shown was that by having a constant inlet flow of process gas, the higher the gas pressure within the process chamber then the lower the etch rate during the etching process. Similar behaviour is observed for the converse situation, namely a constant pumping speed and variability of inlet gas flow. Although relatively high etch rates can be achieved at low process pressure, the photoresist however, becomes unreliable. 'Burning' or polymerisation of photoresist occurs for process pressures lower then 18mTorr. A compromise between durability of the photoresist and the etch rate restrict the process pressure to 20mTorr.

As mentioned above, with the absence of hard baking in the photolithography process, the durability of the photoresist was extended during etching. Polymerisation only occurs after long hours of operation (up to 3 hour). The reason for this is the fact that

Argon Sputter etching is not chemically based as in the case of Reactive Ion Etching (RIE). The argon sputter etching process acts to provide hard baking during the initial period, but when the chemical compound within the photoresist changes state due to heat of ion bombardment it will slowly polymerise and create a 'burned' effect. This 'burn effect' is a highly undesirable effect, since this 'burned' photoresist tends to stick to the surface causing great difficult later during removal.

Apart from the removal of the hard baked photoresist, an intermediate ashing process was also included into the argon etching process. Etching with Argon gas with 10% oxygen was introduced for long etching processes in order to prolong the durability of the photoresist. This process results in the removal of a small proportion of the photoresist during etching. It is believed that removing this surface layer of the photoresist surface provides the continuing argon etching process with a continuously upgraded photoresist chemical compound.

With the establishment of the above procedures, the recalibration of etch rates for the two primary material of LETFELs; ZnS:Mn and $Y_2O_3$ were carried out. The etching results are shown in table II.

| Material | Process Pressure (mTorr) | Power (W) | Etch Rate (Å/min) | | Gas | Photoresist Status | Note |
|---|---|---|---|---|---|---|---|
| | | | Center | Edge | | | |
| ZnS:Mn | 20 | 250 | - | - | Ar | Burned | Not able to remove the burned photoresist |
| | | 200 | 95 | 115 | Ar | Clean | Removed by Asher |
| | | 150 | 62 | 72 | Ar | Clean | Removed by Asher |
| | | 100 | 48 | 55 | Ar | Clean | Removed by Asher |
| ZnS:Mn | 40 | 200 | 13 | 15 | Ar | Clean | Removed by Asher |
| | | 150 | 10 | 11 | Ar | Clean | Removed by Asher |
| | | 100 | 8 | 10 | Ar | Clean | Removed by Asher |
| ZnS:Mn | 18 | 200 | 300 | 380 | Ar | Burned | Photoresist is removal by scrapping the surface with hard object |
| | | 150 | 220 | 240 | Ar | Burned | |
| | | 100 | 100 | 110 | Ar | Burned | |
| Y2O3 | 20 | 200 | 13 | 15 | Ar | Clean | Removed by Asher |
| | | 150 | 10 | 11 | Ar | Clean | Removed by Asher |
| | | 100 | 8 | 10 | Ar | Clean | Removed by Asher |

Table II: Etch Rate for ZnS:Mn and $Y_2O_3$ of the Custom Made Argon Etcher

The etch rates of Table I represent the etch rates at the centre and edges of 4 inch diameter wafers, coated with films of $Y_2O_3$ and ZnS:Mn. A picture of a typical ZnS:Mn sample is shown in figure III. A clear change of colour can be seen starting from yellowish green in the middle, followed by a bluish ring with finally a clear green at the edge. The colour change is directly related to the variation of the etch rate. For the sample shown, the etch rate in the middle is 62 Å/min while at the adge the rate is 72 Å/min. Hence the Ar-ion etcher – although designed to provide uniform etching rates, has non uniform etch rates. Indeed uniformity exists only in the central portion of the wafer i.e. within a circle of 2 inch diameter

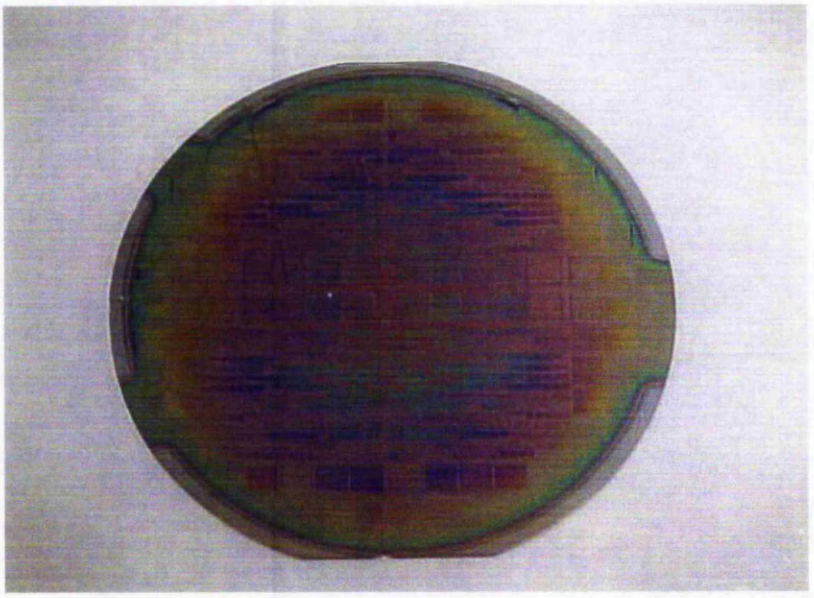

Figure III: Photograph Of A Etched ZnS:Mn Sample

This non uniformity is mainly due to the shape of the earth shield as illustrated in figure IV. The plasma is more intense in the region nearer to the earth shield, hence producing a higher etch rate. The middle of the sample though lacking in etch rate nevertheless gains in uniformity. Notice that the wafer is slightly larger then the earth shield which has a rectangular shape. This rectangular shape causes the non-uniformity etch rate to be rectangular as can be observed in figure III.

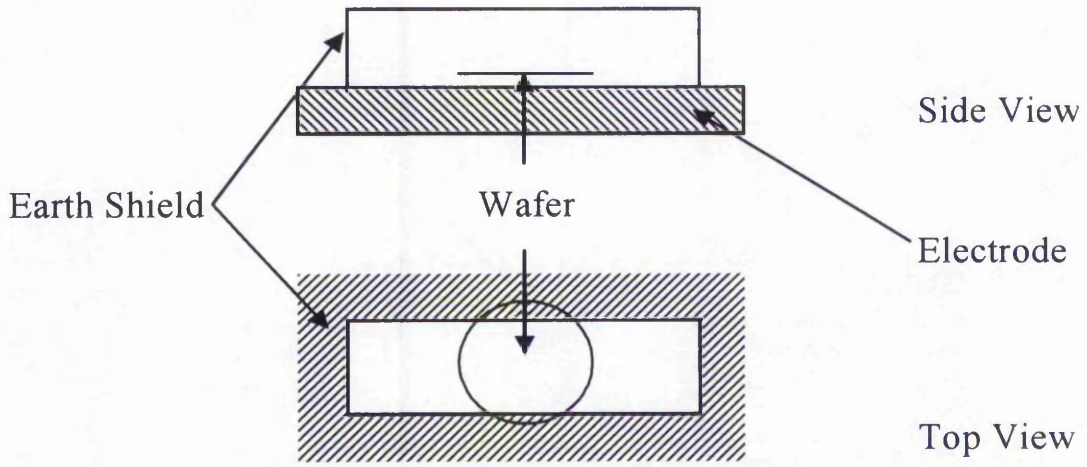


Figure IV: Earth Shield of the Etching System

This non-uniformity however, was not noticeable for the case of $Y_2O_3$. Figure V shows a typical sample of etched $Y_2O_3$. Notice that there is no coloured ring as observed . The hardness of the material is the main contributor to this different observation.

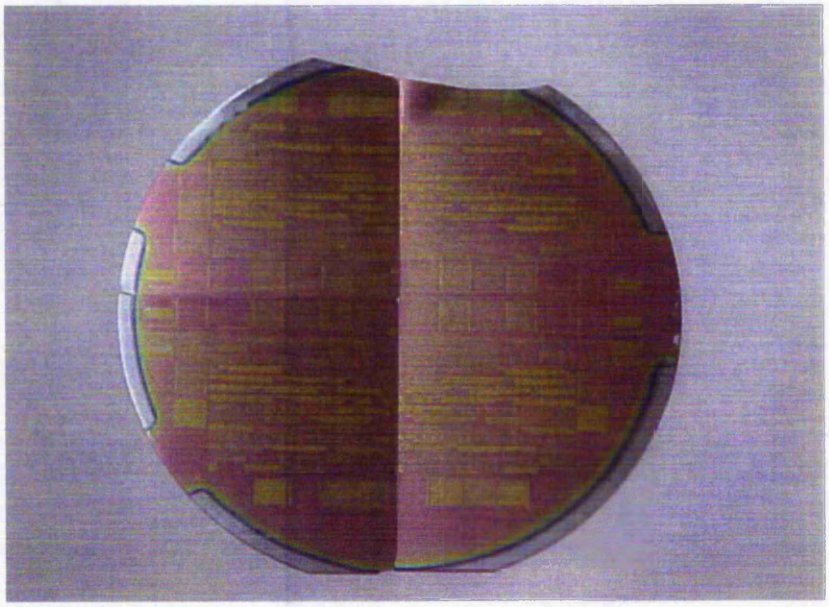

Figure V: Photograph Of A Etched $Y_2O_3$ Sample

## CONCLUSION

From the results obtained, it is concluded that utilisation of argon sputtering etching for the machining of $Y_2O_3$ film for LETFELs devices has inherited some of the difficulties faced during fabrication of devices by ion-milling. The reason is due to the chemical and physical inertness iof $Y_2O_3$ to plasma etching. As shown in table I, etch rates of only 10Å per minute are achieved. Additionally, the amount of $Y_2O_3$ which can be removed is between 300 to 500 Å before the durability of the photoresist comes into question. Hence, it is not possible to fabricate LETFELs based on the procedure suggested previously[1] and which are shown schematically in figure VI.

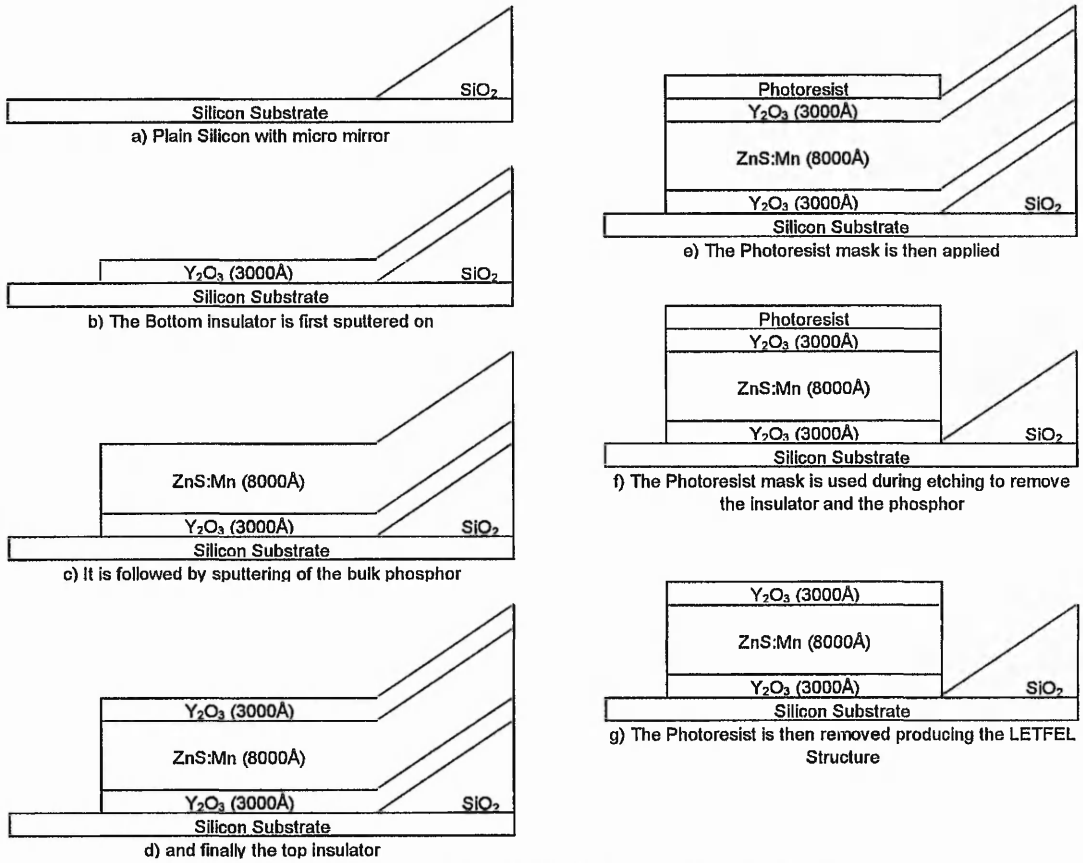


Figure VI: An Ideal LETFEL Fabrication Path

Based on the findings from these experiments, two alternative fabrication paths have been suggested by the author. The major alteration is avoidance of the etching of 3000Å of $Y_2O_3$ deposited above the ZnS:Mn film. First Proposed is that a thin layer of $Y_2O_3$ (~300 Å ) will be deposited instead, which will act as a protective layer for the interface state between the insulator and the phosphor. A photoresist mask will then be used to identify the structure of LETFELs, followed by etching of this thin film of $Y_2O_3$ and ZnS:Mn. Only after this etching will the upper layer of $Y_2O_3$ of 3000Å be deposited. The suggested fabrication path is shown in figure VII. In addition to being a protective layer for the interface state, this thin layer of $Y_2O_3$ can also be utilised as a sacrificial mask.

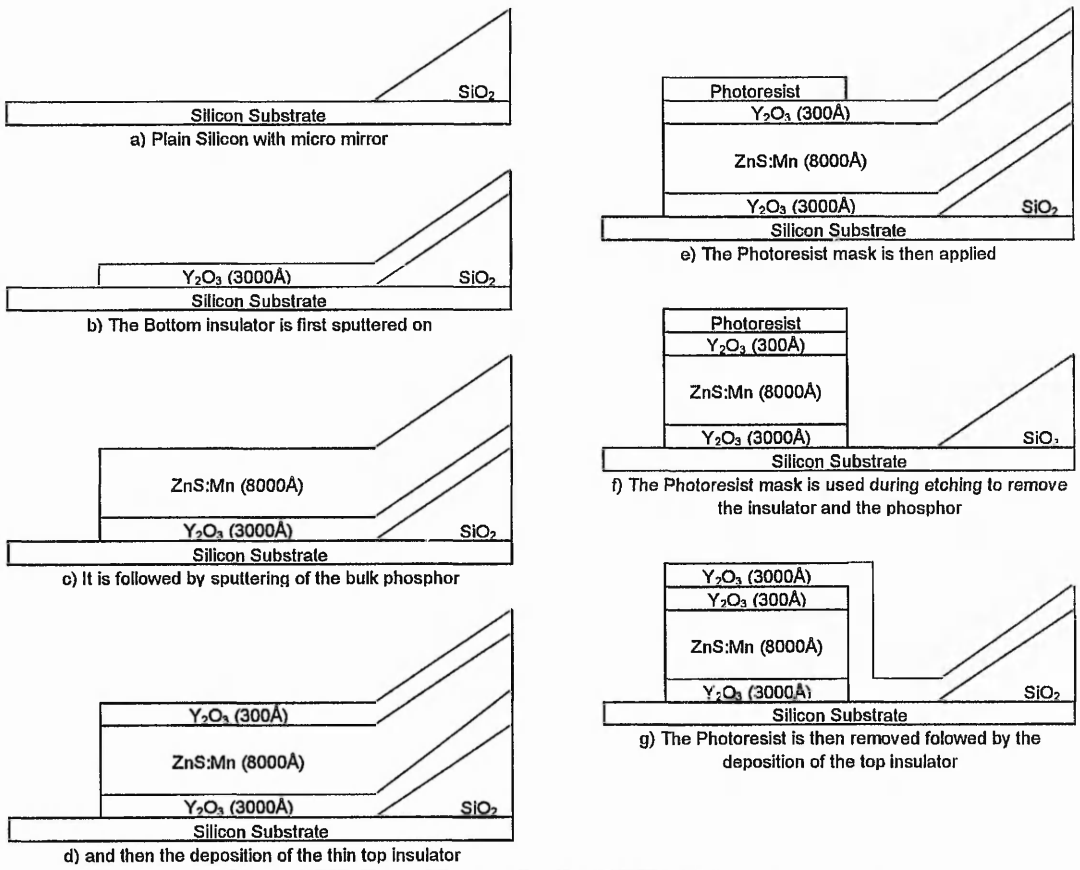


Figure VII: The Alternative LETFEL Fabrication Path

The second proposal is the introduction of a technique called self aligned patterning technique[4,5]. The main advantage of this technique is that no etching need to be performed. Device patterning is carried out after the deposition of the bottom insulator as shown in figure VIII. This is followed by the deposition of the Phosphor layer and the top insulating layer. Finally, the photoresist is removed revealing the typical LETFEL structure. The photoresist patterning can be carrier out twice if the durability of the photoresist is in question. This maybe essential when thermal based annealing is involved. For this case, the photoresist is first removed after the deposition of the phosphor layer to facilitate thermal based annealing. This may not be necessary for laser annealing as laser annealing is a more controlled technique. After

post deposition annealing, the photoresist is again re-patterned on sample allowing the forming of patterned top insulator.

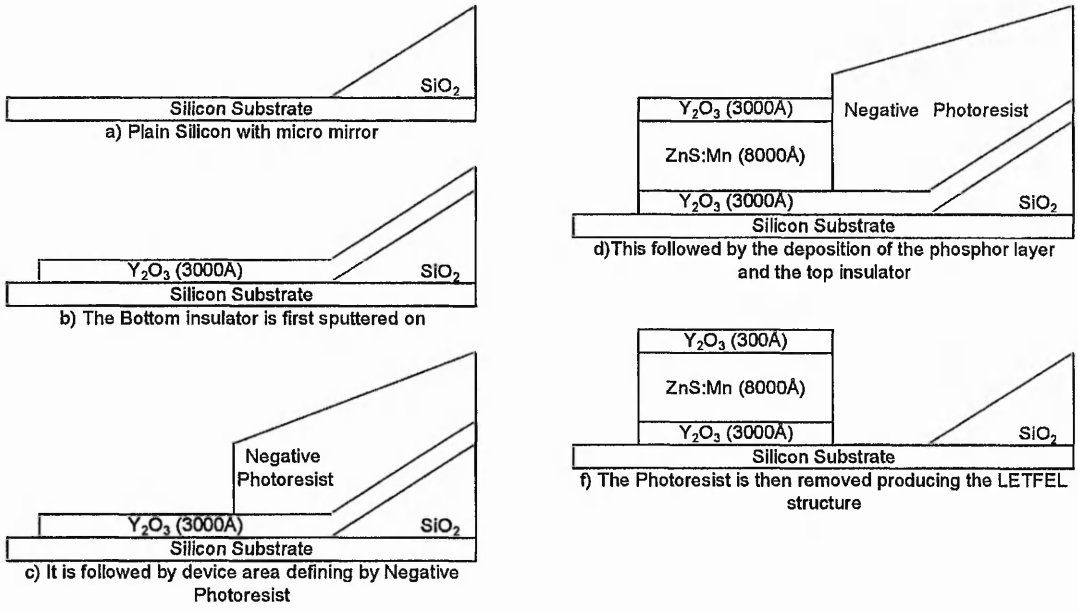


Figure VIII : Self Aligned Patterning Technique

## References

[1] S. O-Barros, PhD Thesis, The Nottingham Trent Univerisity, 2000.

[2] DB Graves, IEEE Trans. Plasma Sci. 22, 31, 1994.

[3] H Winters and J Coburn, Surf. Sci. Rep. 14, 163, 1992.

[4] D. Seale and X. Wu, Proc. 6th International Display Workshop, pp. 861, 1999.

[5] D. Cheong, A. Nakua and P. Del Bel Belluz, SID 2002 Digest, pp.105, 2002.

# APPENDIX B: Heater Calibration Charts

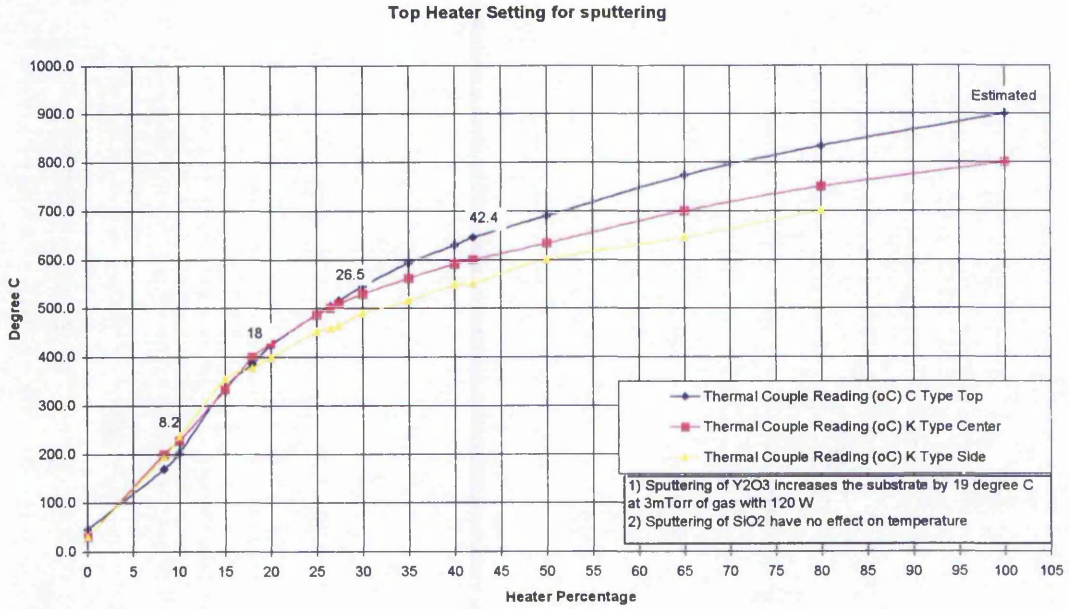


Figure IX: Heater Calibration Chart for Sputtering

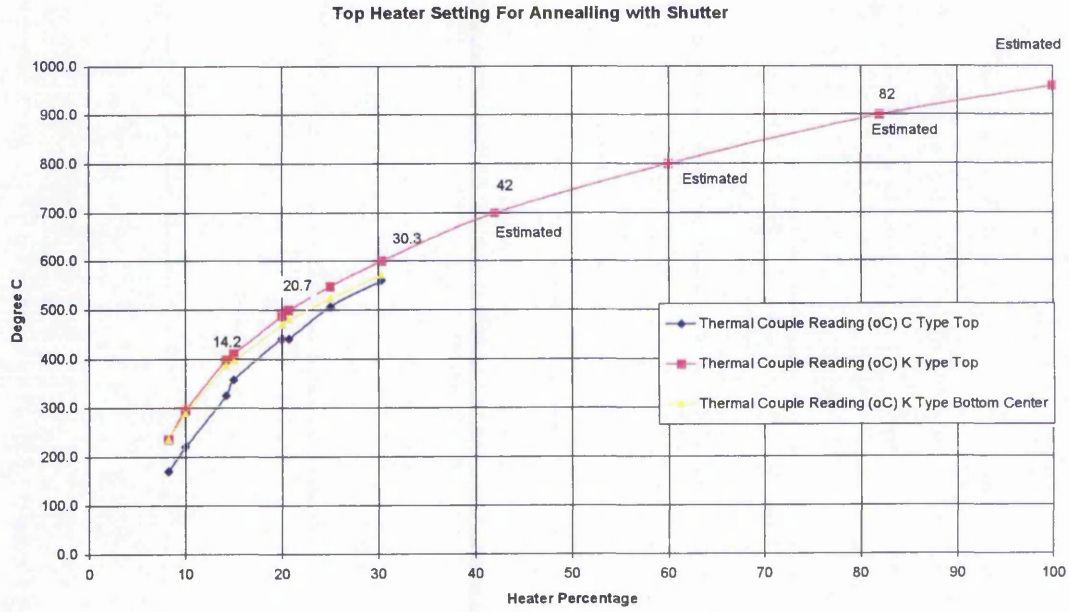


Figure X: Heater Calibration for Thermal Annealing

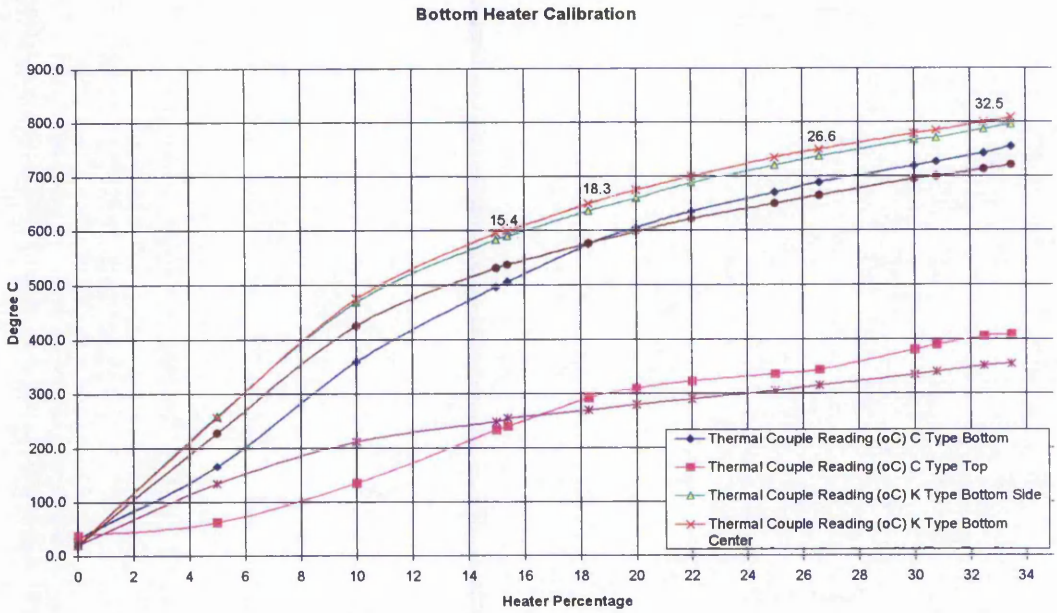


Figure XI: Heater Calibration for Rapid Isothermal Annealing

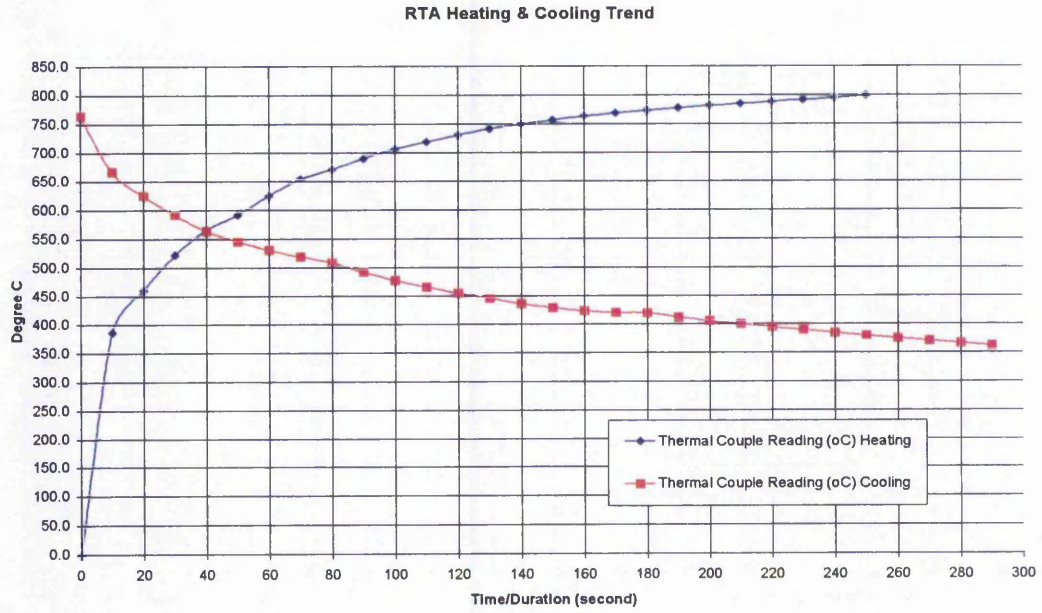


Figure XII: Heating and Cooling Trend for Rapid Isothermal Annealing

# APPENDIX C: Publication Copies

optical components used in Fig. 1 are fibre pigtailed, and no alignment of optical paths is necessary.

An optical pulse under test is incident on a Mach-Zehnder interferometer. Acousto-optic intensity modulators, AOM 1 and AOM 2, are placed in paths 1 and 2 of the interferometer, and are driven at modulation frequencies of $f_1 = 2.19$ MHz and $f_2 = 2.10$ MHz, respectively. The time delay $\tau$ in the path 1 is mechanically swept at the speed of 16 ps/s.

The output from the interferometer is launched on a Si APD. The electrical signal from the Si APD is detected by a lock-in amplifier, where the reference frequency is the difference frequency between the two modulation frequencies, $f_1 - f_2 = 90$ kHz. An oscilloscope monitors the output of the lock-in amplifier, and the background-free intensity autocorrelation trace is displayed.

The intensity autocorrelation $S_2(\tau)$ measured in the conventional colinear configuration is given as

$$S_2(\tau) = \langle I_1^2 \rangle + \langle I_2^2 \rangle + 4\langle I_1(\tau) I_2(0) \rangle \quad (1)$$

where $I_1$ and $I_2$ stand for intensities from the two paths. The background level is given as $I_B = \langle I_1^2 \rangle + \langle I_2^2 \rangle$, and the cross term $G_2(\tau) = \langle I_1(\tau) I_2(0) \rangle$ is the background-free correlation we need.

When we use the double chopping scheme with AOMs, the background term $I_B$ appears at the frequencies of 0, $f_1$, and $f_2$, whereas $G_2(\tau)$ appears at the frequencies of 0, $|f_1 - f_2|$, and $f_1 + f_2$. By using lock-in detection of the TPA signal with the reference frequency of $|f_1 - f_2|$, we can extract $G_2(\tau)$. Note that $f_1, f_2 \gg |f_1 - f_2| \gg 0$ in our case in order to filter out only the difference-frequency component.

*Pulse measurement results:* Using a regenerative modelocked fibre ring laser (MLFL), with repetition frequency and centre wavelength of 10 GHz and 1554.0 nm, we demonstrate the background-free intensity autocorrelation measurement. The optical average power launched on the Si APD is 1.5 dBm.

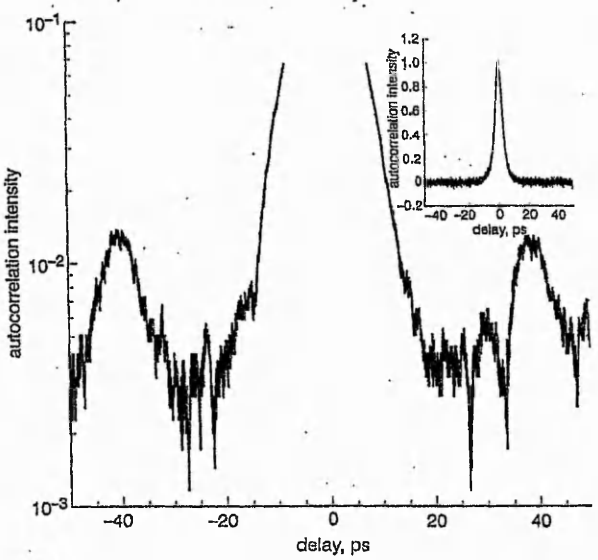


**Fig. 3** *Intensity autocorrelation trace in log scale*
Inset: Intensity autocorrelation trace in linear scale

Fig. 2*a* shows the intensity autocorrelation trace $S_2(\tau)$ with the background measured by the conventional configuration without AOMs [4]. In Fig. 2*a* the ratio of background level to the peak value of the autocorrelation is 0.4. This value agrees with that derived from (1), because $\langle I_2 \rangle / \langle I_1 \rangle = 0.45$ in our experiment. In contrast, Fig. 2*b* shows the autocorrelation trace measured by the newly developed background-free autocorrelator. We find that the background level is eliminated completely. When we assume that the pulse has a $\text{sech}^2$ intensity distribution, the estimated pulse width is 3.29 ps.

Since the autocorrelation does not include the DC level, we can display the trace in the log scale, which enables us to diagnose the pedestal wing of the pulse in a precise manner. Fig. 3 represents the pulse edge part of the intensity autocorrelation trace in the log scale, and the inset is the trace shown in the linear scale. The satellite pulse, which is 40 ps apart from the main pulse, is clearly shown in the log scale. The intensity of the satellite pulse is about 20 dB lower than that of the main pulse. The satellite pulse comes from insufficient adjustment of the modelocking condition of the MLFL. The dynamic range of the background-free autocorrelator is as high as 30 dB.

*Conclusion:* We have developed the background-free Si-APD autocorrelator, which has a dynamic range as high as 30 dB. Using the autocorrelator, we diagnosed the pulse waveform of the modelocked fibre laser under an insufficient modelocking condition, and could find a satellite pulse, with an intensity 20 dB lower than that of the main pulse. The background-free Si-APD autocorrelator we have developed is very suitable for pulse measurement in OTDM systems.


*23 August 2002*
*Electronics Letters Online No: 20020979*
*DOI: 10.1049/el:20020979*

K. Taira, Y. Fukuchi, R. Ohta, K. Katoh and K. Kikuchi (*Research Center for Advanced Science and Technology, University of Tokyo, 4-6-1 Komaba, Meguro-Ku, Tokyo 153-8904, Japan*)

E-mail: tir@ginjo.rcast.u-tokyo.ac.jp

**References**

1 NAKAZAWA, M., YAMAMOTO, T., and TAMURA, K.R.: '1.28 Tbit/s-70 km OTDM transmission using third- and fourth-order simultaneous dispersion compensation with a phase modulator', *Electron. Lett.*, 2000, **36**, (24), pp. 2027–2029
2 BARRY, L.P., BOLLOND, P.G., DUDLEY, J.M., HARVEY, J.D., and LEONHARDT, R.: 'Autocorrelation of ultrashort pulses at 1.5 μm based on nonlinear response of silicon photodiodes', *Electron. Lett.*, 1996, **32**, (20), pp. 1922–1923
3 BARRY, L.P., THOMSEN, B.C., DUDLEY, J.M., and HARVEY, J.D.: 'Autocorrelation and ultrafast optical thresholding at 1.5 μm using a commercial InGaAsP 1.3 μm laser diode', *Electron. Lett.*, 1998, **34**, (4), pp. 358–360
4 KIKUCHI, K.: 'Highly sensitive interferometric autocorrelator using Si avalanche photodiode as two-photon absorber', *Electron. Lett.*, 1998, **34**, (1), pp. 123–125
5 XU, C., ROTH, J.M., KNOX, W.H., and BERGMAN, K.: 'Ultra-sensitive autocorrelation of 1.5 μm light with single photon counting silicon avalanche photodiode', *Electron. Lett.*, 2002, **38**, (2), pp. 86–88
6 KIKUCHI, K., FUTAMI, F., and KATOH, K.: 'Highly sensitive and compact cross-correlator for measurement of picosecond pulse transmission characteristics at 1550 nm using two-photon absorption in Si avalanche photodiode', *Electron. Lett.*, 1998, **34**, (22), pp. 2161–2162

## Pulsed KrF laser annealing of blue emitting SrS:Cu,Ag thin films

S.C. Liew, D.C. Koutsogeorgis, W.M. Cranton and C.B. Thomas

The first successful attempt at utilising pulsed KrF (248 nm) laser annealing as a post-deposition process for RF sputtered SrS:Cu,Ag phosphor films used for thin film electroluminescent (TFEL) devices is presented. Using this novel annealing method, the luminance of the TFEL devices is observed to improve as laser fluence increases. Hence, the potential for luminance improvement of SrS:Cu,Ag TFEL devices without the need for a high temperature annealing process is demonstrated.

*Introduction:* Historically, the lack of an efficient blue emitting phosphor has hampered the advancement of thin film electroluminescent (TFEL) technology in the realisation of full colour TFEL devices. Until recently, SrS:Ce, a blue green electroluminescene (EL) emitter in combination with the yellow emission of ZnS:Mn had shown the best potential in fulfilling this demand [1]. SrS:Ce is consequently one of the most widely investigated blue emitting inorganic TFEL phosphors. However, SrS:Ce emission must be heavily filtered in order to have colour comparable to that of the cathode ray tube (CRT), hence causing a reduction in brightness of up to 90% [2]. More recently, work on phosphor materials based on SrS:Cu has generated

renewed interest in blue emitting TFEL devices [3]. This is because the emission spectrum from this material is more blue saturated than SrS:Ce. Furthermore, an efficiency of 0.25 lm $w^{-1}$ can be achieved for blue at CIE colour co-ordinate (0.17, 0.28) without the need for a colour filter [4]. In addition, the discovery of SrS:Cu,Ag which exhibits the advantages of the good chromaticity of Ag and the high efficiency of Cu provides a more saturated blue than SrS:Cu with a peak intensity at 440 nm [5, 6] matching that of the CRT. Unfortunately, the reported SrS:Cu-based films have required post-deposition annealing at high temperature (~800°C), which prohibits the use of normal glass substrates (Corning 1056 or 1737). In this Letter, utilising the laser annealing technique previously demonstrated successfully on ZnS:Mn [7], we report the results of the first laser annealing of SrS:Cu,Ag films and the probability of fabricating such devices at low temperature.

*TFEL device fabrication:* SrS:Cu,Ag films were prepared at The Nottingham Trent University by RF magnetron sputtering of a powder pressed target with the substrate temperature fixed at 200°C. The phosphor layer, 500 nm thick, is sandwiched between two $Y_2O_3$ insulating films with a thickness of 200 nm. The bottom electrode is either a polished silicon surface or a layer of RF magnetron sputtered ITO deposited on a glass substrate. The top electrode is deposited by evaporation of aluminium with the aid of a patterned shadow mask to create test devices of 3 mm diameter. Laser annealing of the phosphor thin film using pulsed laser irradiation with a beam spot of 5 × 5 mm was performed prior to the deposition of the second insulating layer.

*KrF laser annealing:* For the purpose of laser annealing, the experimental arrangement was equivalent to that used for ZnS:Mn films reported previously [7, 8]. The laser utilised was a KrF laser delivering 248 nm pulses of 20 ns duration. The output of the laser was first directed through a beam homogeniser (Exitech Ltd., type EX-HS 700D) before being delivered to the sample. By varying an in-line attenuator, the irradiation of the laser fluences can be varied in the range 0.4–1.8 J $cm^{-1}$.

*Device testing:* The SrS:Cu,Ag TFEL devices were characterised for both the photoluminescent (PL) and electroluminescent behaviour. The PL measurements were performed via excitation with a 12 mW helium cadmium ultraviolet (UV) laser at 325 nm, using an Ocean Optics Spec 2000 detector. EL characterisation was carried out in a custom-made probe station.

*Results:* Fig. 1 shows the characteristic of photoluminescent intensity against laser fluence. An increase in PL intensity as laser pulse fluence increases can be observed. At maximum fluence of 1.8 J $cm^{-1}$, the PL intensity exhibits the best response in terms of peak intensity.

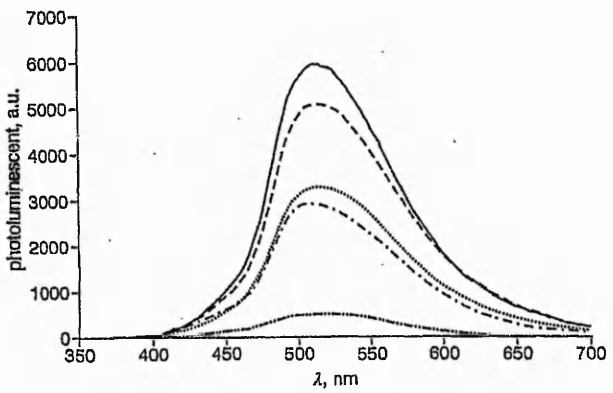


**Fig. 1** *Characteristic of photoluminescent intensity against laser fluence*
- 1.0 J $cm^{-1}$
- 1.2 J $cm^{-1}$
- 1.4 J $cm^{-1}$
- 1.6 J $cm^{-1}$
- 1.8 J $cm^{-1}$

A comparison of PL intensity between laser annealed devices, rapid thermally annealed devices and thermally annealed devices is shown in Fig. 2. These results show that the laser annealed samples consistently produce the highest gain in photoluminescence against annealing.

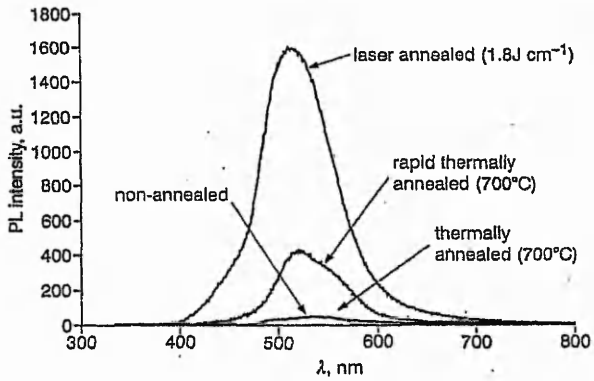


**Fig. 2** *Effect on photoluminescent by different annealing method*

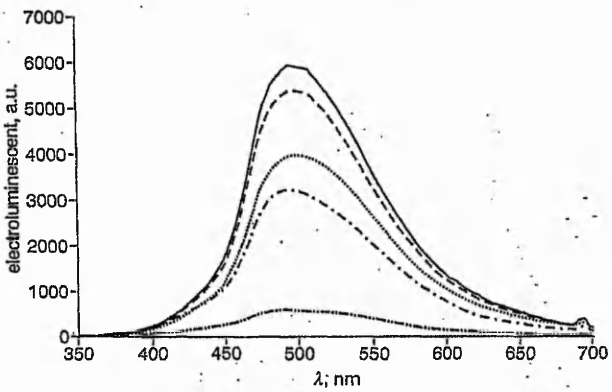


**Fig. 3** *Characteristic of electroluminescent intensity against laser fluence*
- 1.0 J $cm^{-1}$
- 1.2 J $cm^{-1}$
- 1.4 J $cm^{-1}$
- 1.6 J $cm^{-1}$
- 1.8 J $cm^{-1}$

The spectrum of the laser annealed devices, both of EL and PL, are very similar. This had been previously reported by Troppenz *et al.* [9], which indicates that PL is a valid technique for assessing the quality of EL for SrS:Cu,Ag phosphors. Fig. 3 shows the EL luminance with respect to laser fluence. What is interesting is that the improvement in PL between two different fluences is similar to the improvement which is observed for EL. Unfortunately, EL measurements could not be taken from the thermally annealed devices as the film was crazed or there was insufficient luminance for characterisation.

In addition to the luminance improvement, the voltage threshold is found to decrease with the increase of fluence of the laser annealing pulse. This factor is believed to be due to enhancement of the film crystallinity by the high laser fluence, which would be consistent with previous work on laser annealing on ZnS:Mn [10].

*Conclusion:* For the first time, TFEL devices based on SrS:Cu material have been successfully laser annealed for enhanced performance. Using a single 20 ns pulse from a KrF laser with high fluence, the luminance of the devices is at least two times greater than that of rapid thermal annealing (RTA) at high temperature (~700°C) and also significantly better than that of normal thermal annealing at high temperature (600–800°C) for 1 h. The effect is believed to be associated with improvement in the film crystallinity, this being currently under investigation. The advantage of the laser processing provides the possibility of fabricating SrS:Cu,Ag TFEL devices on substrates of non-high-temperature tolerance. In addition, laser annealed devices were found to be more stable then those thermally annealed.

*Acknowledgment:* S.C. Liew wishes to thank The Nottingham Trent University for the award of a research bursary.


*12 August 2002*
*Electronics Letters Online No: 20020878*
*DOI: 10.1049/el:20020878*

S.C. Liew, D.C. Koutsogeorgis, W.M. Cranton and C.B. Thomas (*Centre For Creative Technologies, The Nottingham Trent University, Burton Street, Nottingham NG1 4BU, United Kingdom*)

## References

1 ONO, Y.: 'Electroluminescene display' (World Scientific, 1995), p. 90
2 SOININEN, P.J., NYKANEN, E., NIINISTO, L., and LESKELA, M.: 'Improved luminance from electroluminescent SrS:Ce thin films deposited by the atomic layer epitaxy process' *in* MAUCH, R.H., GUMLICH, W., and GUMLICH, T. (Eds.): 'Proc. Inorganic and Organic Electroluminescene/EL 96,' Berlin, Germany, 1996), pp. 149–152
3 SUN, S.S., DICKEY, E., KANE, J., and YOCOM, P.: 'A bright and efficient new blue TFEL phosphor' *in* MORREDLE, J. (Ed.): Conf. Record of the 1997 IDRC, Santa Ana, CA, USA, 1997, Sponsored by SID, p. 301
4 NEYTS, L., and STUYVEN, G.: 'Low field recombination in SrS:Cu,Ag thin-film electroluminescent devices', *Appl. Phys. Lett.*, 1999, 75, (17), pp. 2593–2595
5 SUN, S.S.: 'Blue emitting SrS:Cu,Ag TFEL devices'. 4th Int. Conf. on the Science and Technology of Display Phosphor, Bend, OR, USA, September 1998, pp. 183–186
6 PARK, W., JONES, T.C., and SUMMERS, C.J.: 'Optical properties of SrS:Cu, Ag two-component phosphor for electroluminescent devices', *Appl. Phys. Lett.*, 1999, 74, (13), pp. 1785–1787
7 MASTIO, E.A., CRANTON, W.M., THOMAS, C.B., FOGARASSY, E., and UNAMUNO, S.: 'Pulsed KrF laser annealing of RF sputtered ZnS:Mn thin films', *Appl. Surf. Sci.*, 1999, 139, p. 35
8 KOUTSOGEORGIS, D.C., MASTIO, E.A., CRANTON, W.M., and THOMAS, C.B.: 'Pulsed KrF laser annealing of ZnS:Mn laterally emitting thin film electroluminescent displays', *Thin Solid Films*, 2001, 383, pp. 31–33
9 TROPPENZ, U., HÜTTL, B., STORZ, U., KRATZERT, P., and VELTHAUS, K.-O.: 'Photoluminescene and electroluminescence studies on Cu and Ag doped SrS ACTFEL devices'. 4th Int. Conf. on Electroluminescent, Bend, OR, USA, September 1998, pp. 187–190.
10 MASTIO, E.A., CRAVEN, M.R., CRANTON, W.M., THOMAS, C.B., ROBINO, M., and FOGARASSY, E.: 'The effects of KrF pulsed laser and thermal annealing on the crystallinity and surface morphology of radio frequency magnetron sputtered ZnS:Mn thin films deposited on Si', *J. Appl. Phys.*, 1999, 86, (5), pp. 2563–2570

# Quantum efficiency evaluation method for gated-mode single-photon detector

A. Yoshizawa, R. Kaji and H. Tsuchida

A novel method based on time-interval analysis of single-photon detection times is presented, which makes it possible to evaluate the quantum efficiency of a gated-mode single-photon detector operating at gate frequencies such that after-pulses are involved in detection. The after-pulse probability per gate is also evaluated from the same data.

*Introduction:* Single-photon detectors (SPDs) are a key device in high-resolution spectroscopy, fluorescence measurement, optical time-domain reflectometry [1, 2], eye-safe lidar [3] and quantum cryptography (QC) [4–6]. Recently, QC has attracted much research interest because its security is based on the laws of quantum mechanics rather than the complexity of computational tasks. Silicon avalanche photodiodes (APDs) well work as SPDs in the range 600–900 nm [7]. However, since the most attractive wavelength is 1550 nm from the viewpoint of fibre transmission, indium-gallium-arsenide APDs are adopted for detection [8–10]. A commonly used method for detecting a photon at 1550 nm is referred to as the gate mode. In this operating mode, the APD is pulse-biased above its breakdown for a very short period of time (typically, a few nanoseconds), during which photon-induced avalanche grows into a macroscopic pulse. For evaluating the quantum efficiency, we send weak light pulses to the APD and count the number of avalanches [11]. However, carriers are trapped every avalanche, and if one emits during a subsequent gate-on time, it can trigger a new avalanche (after-pulse). As the gate frequency increases, we encounter after-pulses more frequently in detection, thereby overestimating the quantum efficiency by counting after-pulses as photons.

This Letter we propose a novel method based on time-interval analysis of single-photon detection times, which makes it possible to evaluate the quantum efficiency for gate frequencies such that non-negligible after-pulses are involved in detection. The after-pulse probability per gate is also estimated from the same data. In the demonstration, the proposed method is applied to the characterisation of a 1550 nm SPD gating at 5 MHz.

*Evaluation method:* Let $\Delta t$ be the interval between sequential detection times and $P_{interval}(\Delta t)$ the probability of finding $\Delta t$ among the recorded intervals. Also, let $P_{after\text{-}pulse}(\Delta t)$ be the probability of finding an after-pulse that is counted after $\Delta t$ from the previous count. Furthermore, the avalanche probability per gate including photons, after-pulses and dark counts is denoted by $P_{avalanche}$. If the photon number per pulse follows Poisson statistics and also if $P_{after\text{-}pulse}(\Delta t) = 0$ for all $\Delta t$s, one finds [12] that

$$P_{avalanche} = 1 - (1 - P_{dark\text{-}count})e^{-\eta\mu} \tag{1}$$

where $\eta$ and $\mu$ represent the quantum efficiency and the mean photon number per pulse, respectively, and $P_{dark\text{-}count}$ is the dark-count probability per gate. In our previous experiment and others [11–12], the relationship between $P_{avalanche}$ and $\mu$ was investigated, and $\eta$ was determined by curve-fitting the data to (1). However, if after-pulses are involved in detection and counted as photons, we overestimate the value of $\eta$. In the proposed method, if $P_{dark\text{-}count} \ll 1$, we have:

$$P_{interval}(\Delta t_n) = c(\Delta t_n)e^{-(n-1)\eta\mu}[(1 - e^{-\eta\mu}) + P_{after\text{-}pulse}(\Delta t_n)] \tag{2}$$

where $\nu$ is the gate frequency and $\Delta t_n = n/\nu$ $(n = 1,2,3,\ldots)$. In this equation, we use $c(\Delta t_n) = \prod_{k=1}^{n-1}[1 - P_{after\text{-}pulse}(\Delta t_k)]$ as the probability of finding no after-pulses within $\Delta t_n$. For sufficiently long $\Delta t_n$s, $P_{after\text{-}pulse}(\Delta t_n) \sim 0$, thereby the natural logarithm (ln) of $P_{interval}$ becomes

$$\ln P_{interval}(\Delta t_n) = -\eta\mu n + \eta\mu + \ln(1 - e^{-\eta\mu}) + \ln c(\Delta t_n) \tag{3}$$

Since $c(\Delta t_n)$ becomes $n$-independent in this region, curve-fitting the measured data of $\ln P_{interval}(\Delta t_n)$ to $-an + b$ determines $\eta$ from $a$, where $a$ and $b$ are constants. Furthermore, noticing that $c(\Delta t_1) = 1$, we can calculate $P_{after\text{-}pulse}(\Delta t_n)$ with $n = 1,2,3,\ldots$ by substituting the estimated value of $\eta$ into (2).

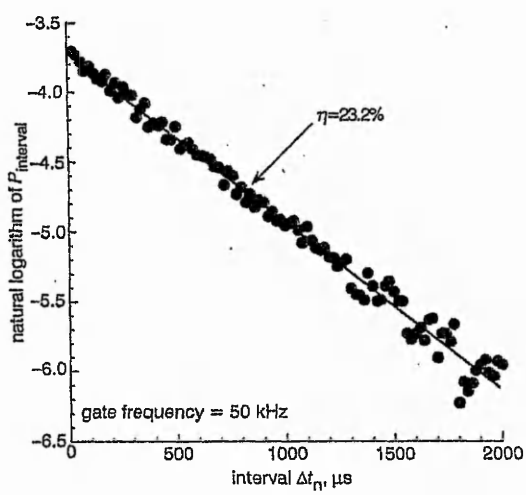


**Fig. 1** *Natural logarithm of $P_{interval}$ measured at 50 kHz74*

*Results:* The proposed method is applied to the characterisation of a 1550 nm gated-mode SPD [11]. First, we chose $\nu = 50$ kHz, then 5 MHz. The former ensures that $P_{after\text{-}pulse}(\Delta t_n) = 0$ for all $\Delta t_n$s while the latter includes after-pulses in detection. Fig. 1 shows the data measured at 50 kHz for $\mu = 0.11$. The data acquisition time was adjusted such that $10^6$ light pulses were involved for the

# Thin film electroluminescent devices based on SrS:Cu,Ag

**S.C. Liew,* D.C. Koutsogeorgis, W.M. Cranton and C.B. Thomas**

The Nottingham Trent University, Center For Creative Technology, Burton Street, Newton Building,

Nottingham NG1 4BU, United Kingdom

## ABSTRACT

For decades, the search for a bright blue thin film electroluminescent device has been the object of many research groups around the world. Since the rediscovery of SrS:Cu by Sun et al, SrS:Cu,Ag had gained much interest due to it's ability for true blue emission. In this paper, we introduced a novel annealing technique of pulsed laser irradiation to improve the brightness of SrS:Cu,Ag thin film devices. By utilising this annealing technique, the need of high temperature post deposition annealing can be avoided. Moreover, the addition of a thin dielectric layer named a 'barrier layer' within the phosphor layer together with the utilisation of laser annealing were investigated, resulting in a further enhancement in the luminance of SrS:Cu,Ag devices.

## INTRODUCTION

The major obstacle for the realisation of full colour thin film electroluminescence (TFEL) displays has been the lack of an efficient blue emitting phosphor. By utilising 'colour by white' approach [1], significant progress has been achieved in the performance and commercialisation of colour TFEL devices in recent years. This technique utilises filters for filtering the primary emission from a broadband emitting phosphor. This is also widely recognised to be the most effective way of producing full colour electroluminescent (EL) display, mainly due to the simplicity of the fabrication process.

A reported broadband phosphor consisted of a ZnS:Mn/SrS:Ce stack where ZnS:Mn provides red and green emission while SrS:Ce provides blue and green emission through colour filters [2]. Although SrS:Ce has been demonstrated to have very good efficiency, it's emission however is of a bluish green colour [3]. Hence, to achieve a true blue colour, the use of heavy filter over SrS:Ce becomes unavoidable. This greatly reduces the original luminance typically when true blue filtering is utilised and consequently also limits its commercial application

* Corresponding author. Tel: +44 7900995666.
Electronic Mail: shan.liew@ntu.ac.uk

More recently, phosphor material based on SrS:Cu, is becoming a more promising phosphor for blue emitting TFEL devices [4]. This is mainly because the spectrum from this material is more saturated then SrS:Ce, and also an efficiency of 0.25 lm $w^{-1}$ can be achieved for blue at CIE colour co-ordinate (0.17, 0.28) without the presence and need of a colour filter [5]. More excitingly, the SrS:Cu,Ag which takes advantage of both the good chromatically of Ag and the high efficiency of Cu, provides an even more saturated blue then SrS:Cu with a peak intensity at 440 nm matching those of the CRT [6].

Unfortunately, all previously reported SrS:Cu based films needed subsequent post annealing at high temperature (~800°C), this prohibits the use of normal glass substrate. To overcome this problem, we demonstrated that by utilising the laser annealing technique, SrS:Cu,Ag devices can be fabricated at low temperature. In addition, the incorporation of the use of barrier layer was also investigated. This resulted in a further enhancement to the luminance efficiency of the blue emitting thin film electroluminescent phosphor.

## EXPERIMENTAL DETAIL

In the present work, the phosphor and the insulating layers of SrS:Cu,Ag devices were deposited utilising rf magnetron sputtering technique. The deposition temperature for all the layers was fixed at approximately 200°C. The phosphor layer was sputtered from a powder pressed target. The insulating layer used in the double insulating thin film EL devices was yttrium oxide deposited from sputtering of a solid target. The films were sputter on to ITO coated glass while the top electrodes were made out of evaporated aluminium.

For the barrier layer devices, sputtering of the phosphor layers was temporarily interrupted when the thickness of the required phosphor layer reaches half of the required thickness of a completed device. This is to allow a thin 100Å thick dielectric material of yttrium oxide to be incorporated in the middle of the phosphor layer, forming the named 'barrier layer' [7]. Following the

forming of the 'barrier layer', sputtering of the remaining phosphor layers was resumed until the targeted thickness was reached.

Structure of both the non barrier layer and the barrier layer ACTFEL devices are shown in figure 1.

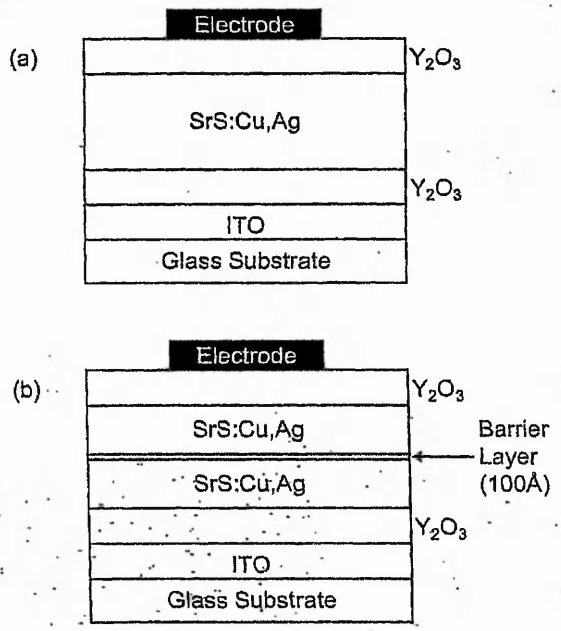


Figure 1: Schematic cross section of (a) conventional ACTFEL device; (b) barrier layer ACTFEL device of the same overall thickness

Laser annealing for both barrier layered and non barrier layered devices was performed prior to the deposition of the top insulating layer. A single fixed laser beam spot of 5x5 mm was incident on the phosphor with the laser fluences being varied from 1.0 to 1.8 J $cm^{-1}$. The laser annealing experiment configuration used is similar to that used for previous experiment on ZnS:Mn [8,9].

## RESULT AND DISCUSSION

The photoluminescence (PL) and the electroluminescence (EL) behaviour for both types of devices were investigated. Figure 2 shows the comparison of PL performance for thermally annealed, rapid thermal annealed and laser annealed devices.

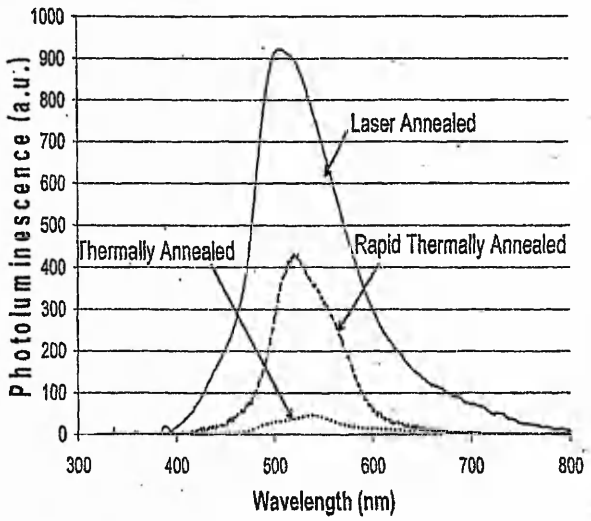


Figure 2: Photoluminescene of SrS:Cu,Ag by Laser Annealing, Rapid Thermal Annealing and Thermal Annealing

Clearly indicated by the figure, the laser annealed devices exhibited far greater performance, surpassing both the thermal and the rapid thermally annealed devices by at least a factor of 2. The PL luminance of the laser annealed devices reduces with the decrease of the applied laser fluence. Also from the figure, the luminances of the rapid thermally annealed devices are greater than those of the thermally annealed devices.

The effect of laser annealing is further enhanced when the annealing technique is applied on to barrier layered devices. There is no difference for PL performance between the barrier layered and non barrier layered devices. However, the electroluminescence of the barrier layered devices generally out performed equivalent non barrier layered devices when operated at comparable voltages. The results of laser annealing on barrier layer and non barrier layer devices are shown in figure 3.

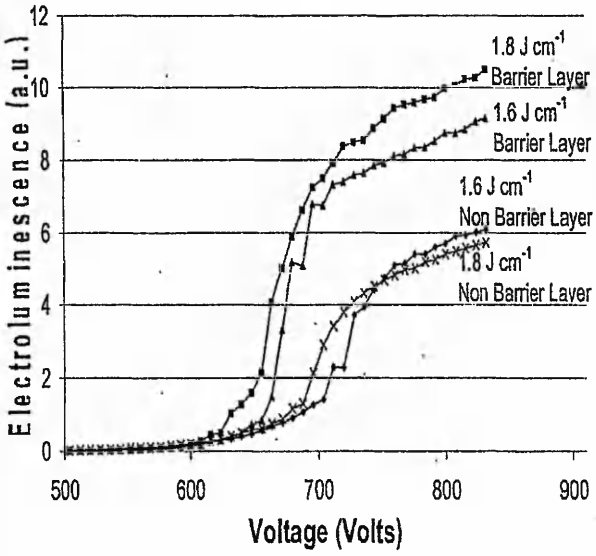


Figure 3: Luminance Vs Voltage Characteristics of equivalent laser annealed devices with and without barrier layers at the fluence indicated

The barrier layer devices also exhibit slightly sharper brightness Vs Voltage (B-V) characteristic as shown in figure 3, compared with devices without barrier layers.

The best performing barrier layered device typically in term of total luminance were obtained from devices that been laser annealed at high laser fluences. These results are comparable to that obtained from non barrier layered devices.

## CONCLUSION

SrS:Cu,Ag deposited with the incorporation of a thin barrier layer within the phosphor layer showing higher luminance and better electrical behaviour when compared with normal SrS:Cu,Ag thin film electroluminescent devices. In addition, the barrier layered devices also shows evidence of better device stability. The enhancement provided by the barrier layer is especially noticeable with the application of the novel laser annealing techniques.

## ACKNOWLEDGEMENTS

We are grateful to ESPRC for the loan of a KrF laser and one of us (S.C. Liew) thanks the University for the award of a scholarship.

## REFERENCES

[1] S. Tanaka, H. Yoshiyama, J. Nishiura, S. Ohshio, H. Kawakami, and H. Kobayashi, SID '88 Digest, pp. 293, 1988.

[2] E. Soininen, et al., Proc. 7th Workshop on Electroluminescence, Beijing, 1994.

[3] K.O. Velthous, B. Huttle, U. Tröppenz, R. Herman, and R.H. Mauch, SID '97 Digest, pp. 411, 1997.

[4] S.S. Sun, E. Dickey, J. Kane, and P. Yocom, SID '97 Digest, pp. 301, 1997.

[5] L. Neyts, and G. Stuyven, Applied Physics Letters, Vol. 75, Num. 17, pp. 2593-2595, 1999.

[6] S.S. Sun, 4th International Conference on the Science and Technology of Display Phosphor, Bend, Oregon, pp. 183-186, September 1998.

[7] C.B. Thomas, and W.M. Cranton, Appl. Phys. Lett., 63 (23), pp. 3119, 1993.

[8] E.A. Mastio, W.M. Cranton, C.B. Thomas, E. Fogarassy, and S. Unamuno, Applied Surface Science, 139, pp. 35, 1999.

[9] D.C. Koutsogeorgis, E.A. Mastio, W.M. Cranton, and C.B. Thomas, Thin Solid Films, 383, pp. 31-33, 2001.

# Laser annealing of inorganic thin film phosphors.

**D.C. Koutsogeorgis*, B. Nassuna, S.C. Liew, R.M. Ranson, W.M. Cranton and C.B. Thomas.**

The Nottingham Trent University, Centre for Creative Technologies, Burton St., Newton bldg, Nottingham, NG1 4BU, UK.

## ABSTRACT

Annealing has been proven to play an important role in the performance of inorganic phosphor thin films, by effectively incorporating the luminescent centre in the crystal lattice. Conventional annealing techniques, such as thermal annealing and rapid thermal annealing, are used extensively both in research and industry, but have limitations. To overcome these limitations a new annealing technique was introduced, making use of high power UV pulsed lasers. In this paper we are providing proof of laser annealing inflicting highly localised annealing and also we are presenting the effect of one or more laser annealing pulses, at various values of fluence, on the performance of ZnS:Mn thin films under photo- electro- and cathodo-luminescence.

## INTRODUCTION

Thin film technology can provide advantages over powder layers for phosphor applications. Some thin film applications have entered the market-place (Thin Film Electro-Luminescent TFEL displays) while for many other cases the introduction of thin film phosphors is expected to solve existing problems (photo-luminescent films for phosphor thermography, cathodo-luminescent films for Field Emission Displays FED). Some of the advantages provided by thin film phosphors are robustness, uniformity over large area, high density, transparency, stability (minimal out-gassing if any) and maybe the most important of all, thin film phosphors development is constantly enhanced by both the knowledge and the equipment/techniques of thin film technology developed for the semiconductor industry. The major disadvantage of phosphor thin films is that only a small volume of luminescent material is involved, limiting the number of luminescent centres available for producing light.

Industrially, the favourite deposition technique is sputtering (RF-magnetron) due to its characteristics : relatively fast, cheap and simple, therefore suitable for mass production and also enables conformal coating over patterned electrodes (e.g. ITO tracks). Unfortunately, however, sputtered thin films require post deposition annealing [1], typically carried out in a furnace at 500-600°C for at least an hour. Such a treatment not only restricts the type of substrate that can be used but also can be detrimental for other thin films that might be present. In previous studies [2] thermal annealing of ZnS:Mn thin films was investigated. In Figure 1 the results of thermal annealing are shown in terms of photo-luminescence and electro-luminescence, normalised to the as-deposited film performance. It was consistently found that higher temperatures improve the PL, whereas the EL is not significantly enhanced beyond 500°C. The investigation showed that the saturation in EL improvement with increasing the annealing temperature was a consequence of annealing the interfaces between the phosphor and the insulators. Although the phosphor itself has an improved efficiency, as the PL indicates, the overall performance of the same films in EL devices is limited due to the probable destruction of the interface states that act as donors of hot electrons for EL operation.

* Email : Demosthenes.koutsogeorgis@ntu.ac.uk

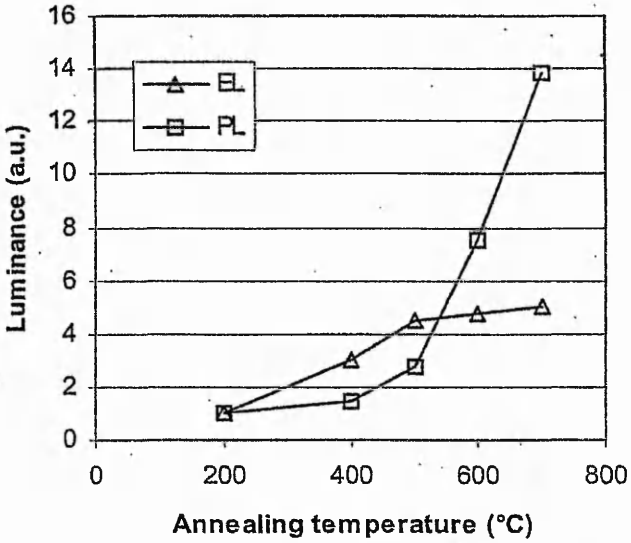


**FIG 1.** Photo-luminescence and electro-luminescence improvement with different thermal annealing temperatures, in vacuum for one hour. Both curves are normalised to the luminance at 200C which is the deposition temperature.

To overcome the above limitation laser annealing was proposed, with the intention to perform localised annealing of the phosphor layer only and not of the insulators and the interfaces between the two.

## EXPERIMENTAL DETAILS

For the purposes of laser annealing a KrF laser was used (Lambda Physik LPX 210, 248nm 20ns) and a pressure cell as described previously [3]. Various number of laser irradiations were used with the fluence varied from 0.3 to 1.5 J/cm$^2$, while the samples were in an overpressure of Ar (150 psi). For the PL measurements a UV laser (He-Cd, 326nm, 16mW) provided the excitation, an optical fibre collected the generated light and directed it to an Ocean Optics (S2000) spectrometer. The EL devices were characterised on a probe station located in a dark enclosure, driven by a sinusoidal wave at 5 kHz with a p-p voltage of 364Volts, and the generated light was collected by an optical fibre and fed to the spectrometer. Finally the CL was measured in a vacuum chamber with an electron beam at 6 kVolts and beam current 0.3mA with the generated light being collected and directed to the spectrometer via an optical fibre.

The ZnS:Mn thin films were 800nm thick deposited in a cluster magnetron sputtering system, in 3mTorr pressure of Ar and with RF power density of 2.6W/cm$^2$.

## RESULTS AND DISCUSSION

Initial experimentation involved only single laser annealing pulses and the resulting PL and EL improvement is shown in Figure 2. Both curves, demonstrating improvement, show the same trend, requiring a minimum fluence of ~0.5 J/cm$^2$ (threshold fluence) to induce any luminescence improvement. This is further enhanced with increasing the fluence until ~1.2J/cm$^2$ when the improvement is saturated. Compared with the results from thermal annealing shown in Figure 1, it is clear that laser annealing does not produce the inconsistency of the PL being further enhanced at high temperatures while the EL is saturated. Previously reported modelling of the laser annealing process [4] suggests that with laser annealing the front surface of the phosphor reaches temperatures in excess of 2000°C, for nanoseconds only, while the back

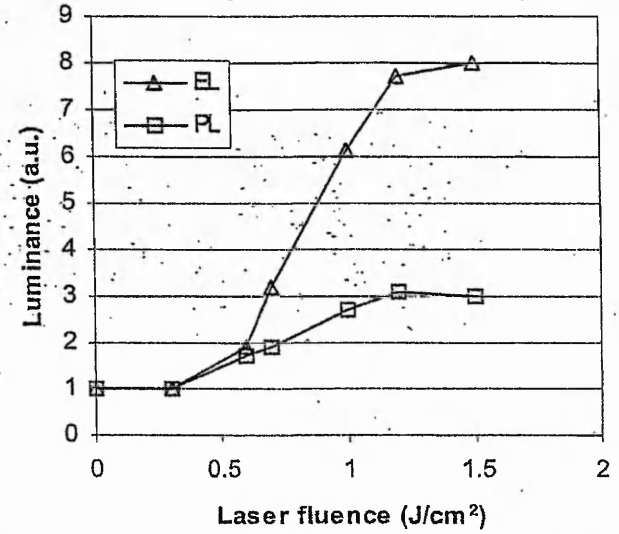


**FIG 2.** Photo-luminescence and electro-luminescence improvement with one laser annealing pulse. Both curves are normalised to the as deposited film performance.

surface, that forms the interface between the phosphor and the insulator, does not exceed ~500°C. Hence, the interface states that act as donors of hot electrons are preserved, since the critical temperature is not exceeded. The knee observed at 1.2J/cm$^2$ is attributed to reduction of the phosphor thickness due to probable ablation [5]. Therefore a laser pulse of adequate fluence can achieve highly localised annealing of the phosphor film only.

Further work in optimising the laser annealing process of ZnS:Mn films was extended to multiple pulses and the results were evaluated in terms of PL, EL and CL, shown in Figures 3, 4, and 5.

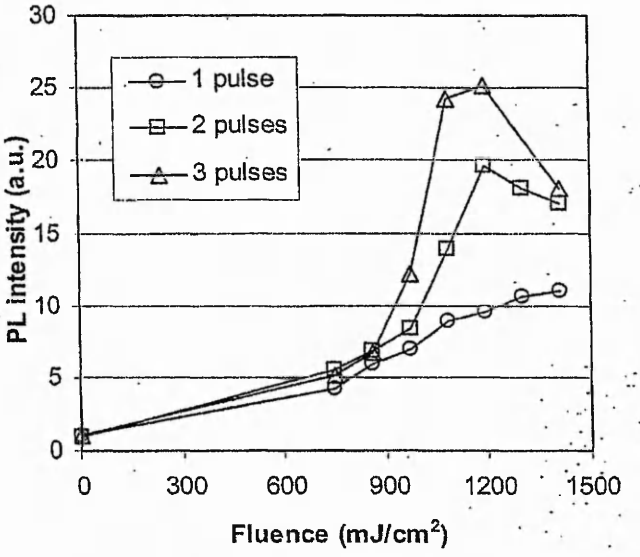


**FIG 3.** Photoluminescence improvement with one, two and three laser annealing pulses. Curves normalised to the performance of the as deposited films.

The photoluminescence showed substantial enhancement with one laser annealing pulse of high fluence. With two and three pulses further improvement is achieved at a lower fluence (~1.2J/cm$^2$), while ablation dominates above that value. More than three pulses did not show any further improvement.

For the case of electroluminescence again one pulse is beneficial but not as much as two pulses, that showed the best improvement at ~1.3J/cm$^2$. Three pulses have proven to be detrimental for

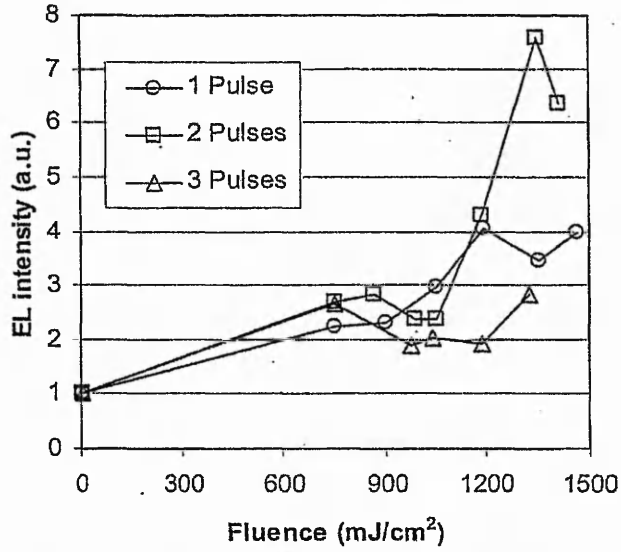


**FIG 4.** Electroluminescence improvement with one, two and three laser annealing pulses. Curves normalised to the as deposited films.

EL, suggesting that two pulses induce a heat treatment that does not reach the back surface of the phosphor, unlike three pulses, which also probably causes excessive ablation. In previous reports it has been shown that laser annealing can outperform thermal annealing, providing EL devices of higher luminance and better electrical characteristics [3, 6].

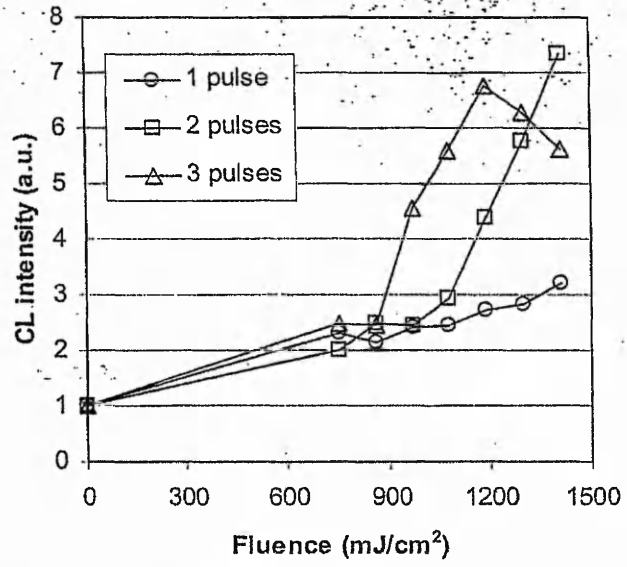


**FIG 5.** Cathodoluminescence improvement with one, two and three laser annealing pulses. Curves normalised to the as deposited films.

Finally, in cathodoluminescence one pulse is again beneficial, while two or three show further improvement. Double irradiation with higher fluence than 1.5J/cm$^2$ would possibly be beneficial, as well as more than three irradiations.

Currently, further work on laser processing of thin film phosphors is aimed at direct comparison of laser and thermal annealing for PL and CL, as well as applying laser annealing to other than ZnS:Mn inorganic phosphors, like SrS:Cu, SrS:Cu,Ag , ZnS:Cu and $Y_2O_3$ based phosphors. Also, combinations of both thermal and laser annealing are being investigated.

## ACKNOWLEDGEMENTS

We would wish to thank Lite-Array Inc. for financial support for part of this investigation and EPSRC, for the loan of a KrF laser from the CLF, in RAL. Also B.N. and S.C.L. are grateful to The Nottingham Trent University for the provision of scholarships.

## REFERENCES

1. M.R. Davidson, B. Pathangey, P.H. Holloway, P.D. Rack, S-S. Sun, and C.N. King. Sputter Deposition of Phosphors for Electroluminescent Flat Panel Displays. Journal of Electronics Materials, Vol. 26, No. 11, Nov. 1997, pp. 1355-1360.
2. W.M. Cranton, PhD thesis, University of Bradford, 1995.
3. D.C. Koutsogeorgis, E.A. Mastio, W.M. Cranton and C.B. Thomas. Pulsed KrF laser annealing of ZnS:Mn laterally emitting thin film electro-luminescent displays. Thin Solid Films, Vol. 383, No. 1-2, Feb. 2001, pp. 31-33.
4. E.A. Mastio, W.M. Cranton, C.B. Thomas, E. Fogarassy, S. de Unamuno. Pulsed KrF laser annealing of RF sputtered ZnS:Mn thin films. Applied Surface Science, Vol. 138-139, Jan. 1999, pp. 35-39.
5. E.A. Mastio, E. Fogarassy, W.M. Cranton, C.B. Thomas. Ablation study on pulsed KrF laser annealed electroluminescent ZnS:Mn/Y2O3 multilayers deposited on Si. Applied Surface Science, Vol. 1540-155, No. 1-4, Feb. 2000, pp. 35-39.
6. W.M. Cranton, E.A. Mastio, C.B. Thomas, C. Tsakonas, R. Stevens. Laser processing for enhanced performance thin film electroluminescent devices. Electronics Letters, Vol. 36, No. 8, Apr. 2000, pp. 754-756.

# Pulsed KrF Laser Annealing of R.F. Magnetron Sputtered SrS:Cu,Ag Thin Films.

**S.C. Liew, D.C. Koutsogeorgis, W.M. Cranton and C.B. Thomas**
The Nottingham Trent University, Centre For Creative Technologies, Burton Street, Newton Building, Nottingham NG1 4BU, United Kingdom

## ABSTRACT
A successful attempt has been made in post deposition annealing of the blue emitting RF magnetron sputtered SrS:Cu,Ag based thin film electroluminescent devices utilising pulsed KrF laser. By utilising this novel annealing method, the brightness of the thin film electroluminescent devices improve with the increase of the laser fluences. In fact, the brightness improvement of the laser annealed devices is generally greater than both the thermally annealed and rapid thermal annealed devices. Demonstrated also is the probability of fabricating blue emitting SrS:Cu,Ag devices without the need of applying high temperature post deposition annealing.

**Keywords:** Laser Annealing, SrS:Cu,Ag, Thin film electroluminescent, Inorganic Electroluminescent.

## INTRODUCTION
Although electroluminescence was first observed in silicon carbide by Captain Henry Joseph Round in 1907 [1] and first demonstrate by Destriau in 1936 [2], the search for a bright blue emitting thin film electroluminescent (TFEL) device is still the subject of many research groups around the world. This has create a huge disadvantage for TFEL in the ability to produce full colour devices, preventing electroluminescent (EL) displays from penetrating into the nowadays highly competitive display market. SrS:Ce was a promising blue TFEL phosphor since 1984 [3], however the emission spectrum was too small to meet the requirement. Fortunately, the recently developed SrS:Cu [4] and particularly SrS:Cu,Ag [5] shows a good colour gamut almost matching those of the hue of the CRT blue phosphor. Conversely, devices based on this phosphor generally required high post deposition annealing. We report a possibility of fabricating such devices with the absence of high temperature processes.

## DEVICE PREPARATION
The devices were of the basic thin film electroluminescent device, a phosphor layer (SrS:Cu,Ag) sandwiched between dielectric cladding layers ($Y_2O_3$) and electrodes (Al and polished silicon substrate). Both the phosphor layer and the dielectrics layer were rf magnetron sputtered with a fixed substrate temperature of 200°C. The phosphor was sputtered from a powder pressed target while the dielectric was sputtered from a solid target. The layers are 5000Åand 2000 Å thick respectively. Laser annealing of the phosphor thin film was carried out prior to the deposition of the top insulator. The laser annealing processes were performed utilising a similar arrangement as in previously reported work on ZnS:Mn [6,7]. Pulsed laser irradiation with a beam spot of 5x5 mm were 'shot' on to the substrate with a variant in laser fluences (0.4 ~ 1.8 J $cm^{-1}$), allowing the creation of test area/devices with different parameters. Finally, the top aluminium electrodes were deposited by evaporation through a patented shadow mask, forming individual test devices for electroluminescent (EL) measurement.

## EXPERIMENTATION
Photoluminescent (PL) and Electroluminescent (EL) emissions of the laser annealed SrS:Cu,Ag devices were investigated. PL measurement is one of the major methods employed for the study of luminance properties of SrS based blue phosphor. This is because the PL emission closely resembles that for the EL. For PL emission examination, a 1mW Helium Cadmium Ultraviolet laser was utilised as the source for excitation of the devices while the Ocean Optics Spec 2000 were used as the detector. EL emissions were also obtained utilising the same detector mentioned above.

## RESULT & DISCUSSION
Figure 1 shows the effects of laser fluences on the photoluminescent intensity of the laser annealed SrS:Cu,Ag. The figure clearly indicates that the PL intensity increases with the increase of the irradiated laser fluences. The highest PL intensity in term of peak intensity was achieved by devices that were irradiated with a laser fluence of 1.8 J $cm^{-1}$.

The PL emissions from the laser annealed devices were compared with rapid thermally annealed devices and thermally annealed devices. These results are presented in figure 2. From these results, the highest luminance was achieved by the laser annealed device. Generally, the laser annealed devices out performed the conventional annealed devices by almost a factor of 2.

For EL investigation, no emission can be observed for the conventional annealed devices as the films were either crazed or there was insufficient luminance for detection. The emissions for laser annealed films however, were easily obtained. Figure 3 shows the comparison between EL spectrum of the laser annealed


ISBN: 981-04-6983-7

devices and its relative PL measurement. No significant different can be observed between the spectrum of PL and EL.

## CONCLUSION

By applying this novel laser annealing techniques, high temperature post deposition annealing can be avoided. Hence, provided is a feasible path for low temperature fabrication of such devices. In addition, the improvement in luminance for SrS:Cu,Ag devices were generally far superior than those of rapid thermally annealed and thermally annealed devices particularly for high laser fluences. It is believed that laser annealing improves the crytallinity of the thin films.

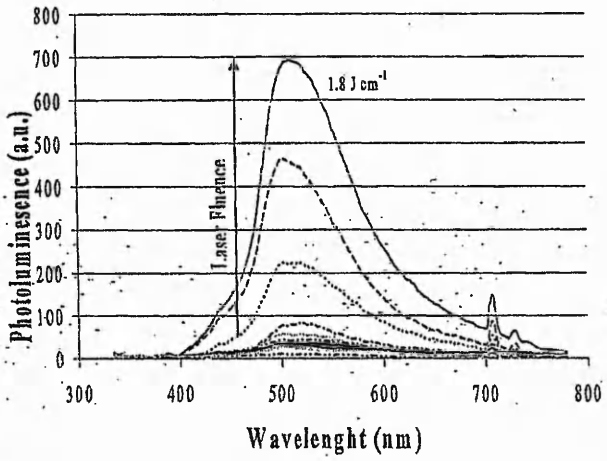


Figure 1: Effect of laser annealing on photoluminescent of SrS:cu,Ag thin films

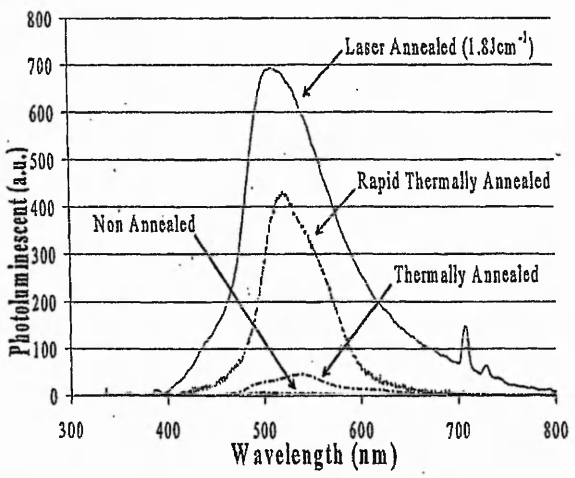


Figure 2: Photoluminescent of SrS:Cu,Ag by laser annealing, rapid thermal annealing and thermal annealing

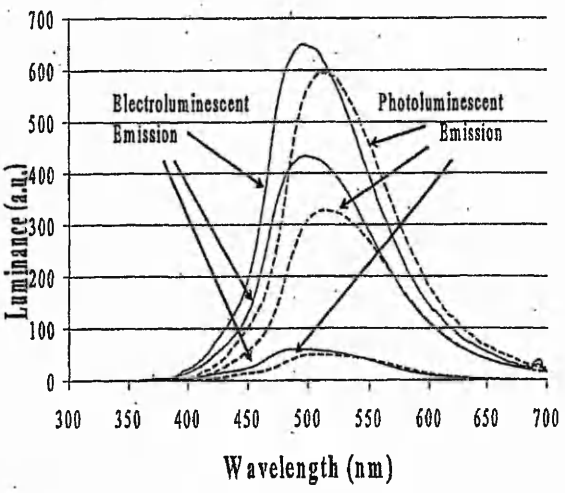


Figure 3: Comparison between PL and EL emission

## REFERENCES


1. Henry J. Round, "A Note on Carborundum", Electrical world, Vol. 19, pp. 309, 9 February 1907.
2. G.Destriau, "Recherches sur les scintillations des sulfures de zinc aux rayons", Journal de Chemie.Physique, vol. 34, pp. 587-625, 1936.
3. W.A. Barrow, R.E. Coovert and C.N. king, "Strontium Sulphide: The Host fro a New High-Efficiency Thin Film EL Blue Phosphor", SID'84 Digest, pp. 249, 1984.
4. S.S. Sun, E. Dickey, J. Kane, and P. Yocom, "A Bright and Efficient New Blue TFEL Phosphor", Conference Record of the 1997 International Display Research Conference, pp. 301, 1997.
5. S.S. Sun, "Blue Emitting SrS:Cu,Ag TFEL Devices", 4th International Conference on the Science and Technology of Display Phosphor, Extended Abstract, Bend, Oregon, pp. 183-186, September 1998.
6. E.A. Mastio, W.M. Cranton, C.B. Thomas, E. Fogarassy, and S. Unamuno, 'Pulsed KrF Laser Annealing of RF Sputtered ZnS:Mn Thin Films', Applied Surface Sciences, 139, pp. 35, 1999.
7. D.C. Koutsogeorgis, E.A. Mastio, WM. .Cranton, and C.B. Thomas, 'Pulsed KrF Laser Annealing Of ZnS:Mn Laterally Emitting Thin Film Electroluminecent Displays', Thin Solid Films, 383, pp. 31-33, 2001.

# I-20.4: Miniature Transverse TFEL Displays

**W.M. Cranton, C.B. Thomas, D.C. Koutsogeorgis, R.M. Ranson, S.C. Liew, C. Tsakonas, M.Sethu.**
School of Electronic Engineering
The Nottingham Trent University, UK
with
**R. Stevens**
Central Microstructure Facility, Rutherford Appleton Laboratory, UK.

*Email: wayne.cranton@ntu.ac.uk*

**Abstract**

*Materials processing and device engineering of thin film electroluminescent devices is discussed for high intensity miniature displays. Transverse light guiding in combination with barrier layers and laser annealing is used to provide high luminance laterally emitting thin film electroluminescent (LETFEL) devices emitting at > 5000fL.*

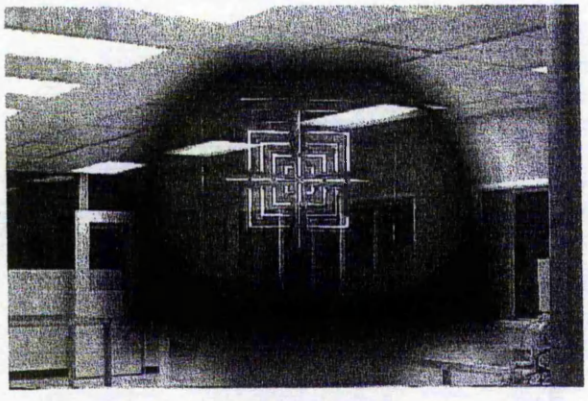

**Figure 1. Virtual image of LETFEL miniature display as seen via catadioptric HMD optics**

## 1. Introduction

Thin film electroluminescence (TFEL) is a mature flat panel emissive technology which is particularly suited for applications requiring ruggedness, reliability, high contrast, and high viewing angles; such as medical, transport, and military applications. In each of these applications, the display viewability and ruggedness is of more importance than the need for full colour, with the TFEL displays consequently based on the reliable yellow emitting ZnS:Mn thin film phosphor. The typical configuration of a TFEL device is a thin film structure deposited on a glass substrate with a ITO/dielectric/ZnS:Mn/dielectric/aluminium structure, which may include additional layers for contrast enhancement. *(For an excellent review of TFEL, see the book by Y. Ono [1]).*

In an alternative device configuration, reflected lateral emission from TFEL devices has been shown by our research to demonstrate the feasibility of high intensity luminous emission from fixed legend miniature displays[2]. These laterally emitting thin film electroluminescent (LETFEL) displays are intended for use in low cost see-through head mounted systems, where luminances in excess of 1000fL are required to provide life critical, or operational information. Realisation of these high luminances relies upon optimising both the internal light generation processes of TFEL devices and enhancing the optical out-coupling, both of which have been addressed by the work presented here. From a combined programme of materials enhancement and device engineering, the LETFEL display utilises the transverse light guiding in combination with novel phosphor processing to provide the basis for a series of high intensity miniature display devices, such as the example shown in Figure 1.

## 2. LETFEL Technology – Device Engineering

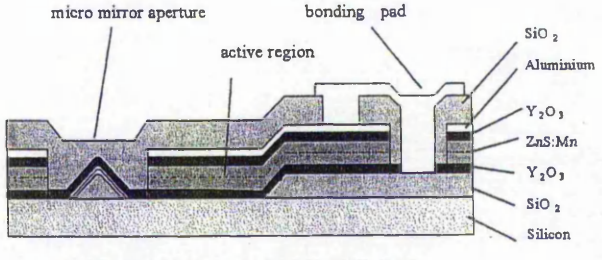


**Fig 2. Cross section of a LETFEL device**

Figure 2 illustrates the fundamental device technology which forms the basis for LETFEL displays. This structure is designed to utilise the inherent waveguiding attributes of TFEL thin films to produce devices with a typically four-fold increase in the emitted intensity as compared to conventional surface emission[3]. The improved emission occurs at the 'micro-mirror' aperture, where a reflecting microstructure is formed to convert the laterally

confined light into useful surface emission. Various geometries of light emitting devices have been fabricated using this principle, including the 4x4mm miniature fixed legend display shown in Figure 1.

The standard LETFEL design is based on a fabrication process which utilises a combination of magnetron sputtering and chemical vapour processes for the deposition of the various thin films onto silicon substrates, with dry etching used to pattern the layers and to form the micro-mirrors. Figure 3 illustrates the microstructure of an emitting pixel region, before and after etching to expose the emitting aperture.

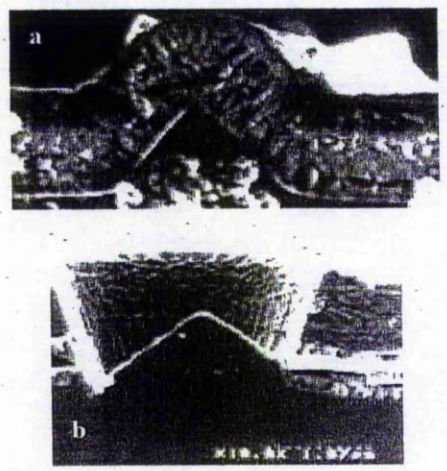


**Figure 3. SEM micrographs of the aperture region of a LETFEL device before (a) and after (b) etching**

For fixed legend displays of the type shown in Figure 1, each emitting line corresponds to a single aperture over a mirror which runs along the centre line, hence light is emitted from the passive region within an aperture, with the light generation occurring in the surrounding EL material. When a luminance in excess of 5000fL is required, a display design such as the cross-hairs of Fig 1 is ideal, since the geometry allows for a large active EL region to generate the light which is guided to and emitted from the aperture, hence maximising the benefit of the transverse light confinement.

Alternative display geometries which can incorporate legends meeting specific customer designs are possible with configurations where the micro-mirrors are distributed within the light emitting legend, as shown in Figure 4. For this type of LETFEL display, the mirrors are typically 3 microns wide, with legends (e.g. the letters 'TNTU') made up of arrays of mirrors spaced at 15 microns apart, with luminances in the range of 200 to 1000 fL, (driven at 5 kHz, 250V gnd to peak) depending on legend geometries. However, the display may incorporate a mixed design with higher intensity emission from specific highly critical legends, by utilising a higher ratio of light generating area to emitting area. The maximum intensity is produced by mirrors surrounded by > 100 microns of active ZnS:Mn phosphor.

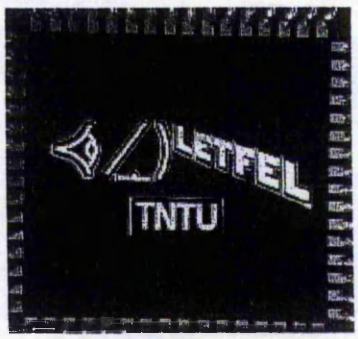


**Figure 4. 4mm x 4mm LETFEL display**

In summary, therefore, by utilising fabrication processes and techniques standard to the silicon device industry, LETFEL devices offer a potential low cost solution for applications requiring miniature symbology/fixed legend displays with high luminance, contrast and resolution plus the benefits of the all solid state TFEL technology.

### 3. Materials Engineering and Processing

Critical to the success of any TFEL device, including the LETFEL, is fine control over the materials properties of the various layers, and in particular the active phosphor layer. Hence, much research has been directed at improving both luminance and colour performance of these displays by adjusting the materials parameters of the phosphor layer during and after deposition. Two such techniques pioneered by the group at Nottingham Trent University *are pulsed laser annealing* and internal phosphor field modification via the incorporation of electron tunnelling layers, termed '*barrier layers*'. Both of these techniques are demonstrated to be effective at improving the performance of TFEL devices utilising yellow emitting ZnS:Mn, and SrS based blue emitting phosphors.

### 3.1 Materials Engineering – Barrier Layer Device

The accepted excitation mechanism of the ZnS:Mn TFEL system is one of direct impact excitation of luminescent centres by 'hot' electrons which have attained energies in excess of 2.2eV. In order to achieve these high energies via electron acceleration within the thin film phosphor, it is advantageous to

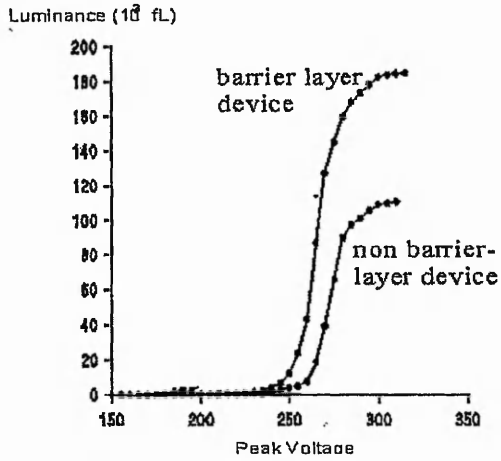


**Figure 5. Luminance vs edge emitting voltage characteristics of barrier layer TFEL devices**

produce a TFEL device with an operating field strength of the order of 2MVcm$^{-1}$. Work by the authors has demonstrated that this is possible by re-engineering the phosphor to alter the internal electric field and increase the percentage of 'hot' electrons. An example of this is the 'barrier-layer' phosphor [4], where thin (~10nm) dielectric layers are introduced within the phosphor during growth.

Figure 5 shows the luminance vs voltage characteristics from ZnS:Mn TFEL devices with and without the 'barrier-layer' phosphor. By fabricating a barrier layer of a dielectric material ($Y_2O_3$, $\varepsilon_r$=12) within the phosphor layer, a significant luminance gain is demonstrated for a device of identical dimensions to a non barrier-layer device. The mechanism of luminance enhancement is proposed via the energy band diagram of Figure 6 with the assumption that the barrier layer forms a potential barrier against electron conduction.

The observed increase in luminance is thus attributed to a net energy gain in the electron energy distribution due to electron tunnelling at the barrier layer. Without the barrier layer, the internal field attained in the phosphor, and thus the electron energy distribution, is determined by: i) the interface state density and profile at the phosphor/dielectric boundary, ii) defects and associated trapping states within the phosphor bulk, and c) space charge distribution. All of these factors are affected by deposition parameters, but we have found that the addition of a barrier layer within a ZnS:Mn phosphor consistently enhances the luminance by at least 50% and up to 100%, depending upon deposition parameters. The critical parameter is the barrier layer thickness.

In a series of experiments intended to indicate whether electron tunnelling was indeed occurring, devices were fabricated with barrier layers varying in thickness from 10nm to 40nm The results showed that at thicknesses > 10nm, the barrier layer effect is quenched, with the resultant device luminance equivalent to that of two back to back devices of half the phosphor thickness[5]. While not fully conclusive, these results serve to indicate that the barrier layer thickness is directly related to the improvement in luminance, and since the phosphor is the same in all cases, the only major difference would be in the electron transport properties, thus implying that electron tunnelling could be responsible, as indicated by Fig 6.

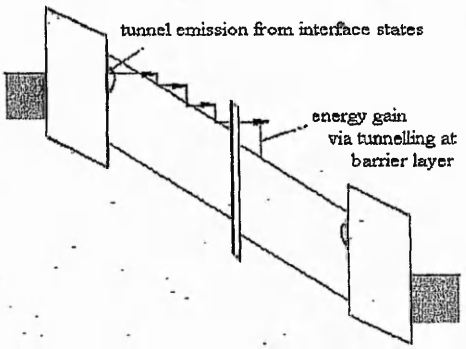


**Figure 6. Energy Band diagram illustrating the barrier layer effect in ZnS**

### 3. 2 Materials Processing – Laser Annealing

Perhaps the most significant series of results from recent work is the demonstration that the use of pulsed laser annealing (PLA) can produce major gains in luminance from TFEL devices[6]. This has application to both the miniature LETFEL displays discussed here, and also to conventional large area TFEL panels.

Critical to the luminescent efficiency of a TFEL device is an annealing treatment, which allows for the effective incorporation of luminescent dopant ions within the host lattice (activation). Commercial TFEL devices are typically fabricated on glass substrates and are subjected to a post deposition anneal at 500°C for ~ 1hr. The LETFEL device, however, is fabricated on a silicon substrate, which facilitates the investigation of higher annealing temperatures. We have observed that for our TFEL devices, there is no significant improvement in EL luminance beyond a 500°C anneal, even though the corresponding photoluminescent intensity is increasing. Modelling this behaviour based on the measured electro-optic characteristics indicates that the limitation in performance is due to a reduction of the interface state density at the phosphor / dielectric interface which becomes noticeable following annealing at > 500°C[7].

For optimum EL performance, therefore, the ideal interface would be the as-grown *disturbed* structure, such that the density of electron traps remains high, but where the luminescent quality of the thin film phosphor is optimised by annealing.

Based on these observations, it was proposed that an investigation of pulsed laser annealing (PLA) could provide a more effective means of heat treating the phosphor thin films of LETFEL devices. By irradiating the thin film phosphors at a wavelength with a high absorption coefficient, and by using high energy pulses of short duration, the research was designed to investigate the feasibility of optimising the devices by delivering energy to a localised surface region of the phosphor film, with minimal effect on the underlying interface. Since the band gap of ZnS is 3.65 eV, and that of SrS (a potential blue phosphor host) is 4.4 eV, the laser irradiation would ideally be at wavelengths < 343nm and 285nm respectively. For this study, therefore, KrF excimer lasers (emitting at 248nm) have been utilised.
TFEL and LETFEL devices were subjected to irradiation by 20ns pulses of KrF Excimer laser irradiation at 248nm. The optical systems used for beam delivery provided variable energy densities from 100-1500mJ/cm$^2$. At 248nm, the absorption coefficient of ZnS has been determined to be $3.33 \times 10^5$ cm$^{-1}$ for crystalline ZnS [8] and $3.15 \times 10^5$ cm$^{-1}$ for polycrystalline ZnS:Mn thin films[9], hence the energy absorption is contained within ~ 300nm of the thin film surface.

For TFEL device structures utilising either yellow emitting ZnS:Mn, or blue emitting SrS:Cu,Ag, the laser annealing process was performed prior to the deposition of the upper dielectric layer and electrode definition. Examples of the resultant improvements in EL performance for the SrS is are shown in figures 7. (the ZnS:Mn results are detailed in ref. [6] ). Clearly evident from these results is that a significant enhancement is possible for both ZnS and SrS based phosphors. In both cases, the effect is linked to measurable improvements in the crystallinity, which for ZnS:Mn based devices, is associated with a measurable phase change from predominantly cubic to predominantly hexagonal.

**Summary**
Demonstrated is that the use of transverse light confinement in the form of laterally emitting thin film electroluminescent devices is a viable technology for application to high luminance miniature display devices. The feasibility of fabricating fixed legend displays and application specific displays has been shown, in combination with the advances in materials processing knowledge that are required to ensure high efficiency TFEL phosphors.

**Acknowledgements**
The authors would like to thank UST Ltd. and the Engineering and Physical Sciences Research Council for providing the primary support for this work. We would also like to thank Graeme Hirst and his team at the Central Laser Facility, RAL for the support provided with laser annealing.

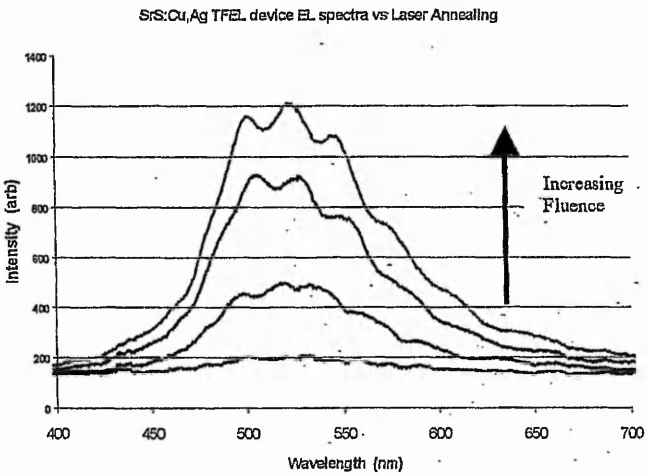


**Figure 7. EL emission spectra as a function of laser annealing with 248 KrF irradiation for SrS:Cu,Ag TFEL devices driven at 640 V pk-Pk**

**References:**

[1] Y. Ono; *Electroluminescent Displays*, World Scientific Press, (1995)
[2]CB Thomas, R Stevens, WM Cranton.; 1996 SID International Symposium. Digest of Technical Papers. First Edition. Soc. Inf. Display. 1996, pp.365-9.
[3] R. Stevens, C.B. Thomas, and W.M. Cranton, IEEE Electron Device Letters, Vol 15 No 3, (1994) 97.
[4] C B Thomas and W M Cranton; Appl Phys Letters 63 (1993) 3119
[5] W.M. Cranton, C.B. Thomas, R. Stevens; *1997 SID International Symposium. Digest of Technical Papers.* Soc. Inf. Display. Vol 28, page(s): 866-872.
[6]WM Cranton, EA Mastio, CB Thomas, C Tsakonas, R Stevens. Electronics Letters, vol.36, no.8, 13 April 2000, pp.754-6.
[7] W.M. Cranton, R.Stevens, C.B. Thomas, A.H. Abdullah, and M.R. Craven; Proc. IEE Colloquium on Materials for Displays (1995) 7/1.
[8] S. Ozaki and S. Adachi, Jpn. J. Appl. Phys. 32, 5008 (1993).
[9] P. M. Savani, M. Phil Thesis, University of Bradford, 1982, p. 97

# Laser Processing of Thin Film Phosphors for Flat Screen Displays

**W M Cranton, D Koutsogeorgis, S Liew, B Nassuna, R Ranson, C B Thomas**
*The Nottingham Trent University*

**Main contact email address:** *wayne.cranton@ntu.ac.uk*

## Introduction

The Displays Research Group at Nottingham Trent University has been working with the LSF since 1997 to investigate excimer laser processing of thin films suitable for use in flat screen display applications. Initial work, funded by the EPSRC, demonstrated the feasibility of using pulsed laser annealing to enhance the luminescence of thin film ZnS:Mn phosphors for use in miniature high intensity displays. Following this early work, the investigations have progressed to include thin film phosphors used in mid-size instrumentation display panels, with the result being the demonstration of a technique for phosphor processing that could be suitable for large volume manufacture. More recently, access to the NSL5 fluoride laser via the LSF Loan Pool has facilitated the investigation of laser processing for alternative wide band-gap thin film phosphors and cathodoluminescent phosphors. This report presents the initial results from the work performed at NTU using the Loan Pool NSL5 laser.

## Background

In the field of emissive flat panel displays, thin film electroluminescence (TFEL) is a technology that has been a subject of commercial and scientific interest for over 4 decades. Display panels based on this technology have been utilised where ruggedness, reliability, high contrast, and high viewing angles are required; such as in medical, transport, and military applications. In a novel TFEL device configuration, reflected lateral emission from TFEL devices has been shown by research at Nottingham Trent University (NTU) to demonstrate the feasibility of high intensity luminous emission from fixed legend miniature displays [1]. These laterally emitting thin film electroluminescent (LETFEL) displays are intended for use in low cost see-through head mounted systems, where luminances in excess of 3000cdm$^{-2}$ are required, but without the need for a full graphics display. Realisation of these high luminances relies upon optimising the internal light generation processes of TFEL devices by optimising the materials processing of the constituent thin films.

At the heart of these LETFEL, and indeed all inorganic emissive displays, is a light emitting layer composed of a wide band-gap polycrystalline phosphor. Phosphors under investigation at NTU include thin films of ZnS:Mn (3.68eV), SrS:Cu,Ag and SrS:Ce (4.4eV), and $Y_2O_3$:Eu (5.9eV). Each of these materials is of interest for TFEL display applications, although the primary research area for the $Y_2O_3$ based phosphor is for a light emitting thermographic sensor. In addition, thin films phosphors such as ZnS:Cu are under investigation for cathodoluminescent display applications - such as night vision and image intensifiers.

## Prior Work with The LSF

Critical to the luminescent efficiency of a TFEL device is an annealing treatment, which allows for the effective incorporation of luminescent dopant ions within the host lattice (activation). Commercial TFEL devices are typically fabricated on glass substrates and are subjected to a post deposition anneal at 500°C for ~ 1hr. Since 1997, EPSRC funded work at the LSF has demonstrated that pulsed laser annealing using a high energy flouride excimer laser is an effective means of activating the phosphor by achieving significantly higher temperatures localised to the phosphor thin film [2]. It is a combination of the higher processing temperatures attained and the localisation of the heat dissipation to within the phosphor layer that leads to a major enhancement in phosphor performance. This is due to the joint requirement for the phosphor layer to act as a light emitting material, and as the electron transport medium for luminescent excitation. High annealing temperatures are required to form an efficient phosphor, but the annealing process is detrimental to the electron emission process that provides the source of excitation. By localising the annealing effect to the light generating region, excimer laser processing has been demonstrated to be a viable means of spatially separating the optimisation of the light generating and electron emitting regions of a TFEL structure. Devices incorporating a ZnS:Mn thin film phosphor were subjected to 20ns pulses of KrF Excimer laser irradiation at 248nm. The optical systems used for beam delivery provided variable energy densities from 300-1500mJ/cm$^2$. At 248nm, the absorption coefficient of ZnS has been determined to be 3.33x10$^5$ cm$^{-1}$ for crystalline ZnS and 3.15x10$^5$ cm$^{-1}$ for polycrystalline ZnS:Mn thin films, hence the energy absorption is contained within ~ 300nm of the thin film surface. This initial work was undertaken at the x-ray laboratory of the LSF, with the help of Graeme Hirst and his team. Additional work on this system was used to demonstrate a potential scanning technique for larger area irradiation of ZnS:Mn based TFEL panels.

## Colour Displays

ZnS:Mn is an efficient EL phosphor, but is limited to broad-band yellow emission - hence it is used in the commercially successful monochrome TFEL displays. Achieving full colour has historically been a problem for these displays, due to the inefficiency of the blue phosphors. However, with the loan of the NSL5 laser to NTU, we have recently demonstrated that the laser annealing technique is also suitable for this wide band-gap phosphor.

## Experimental Technique

For the initial phase of the loan pool work, the phosphors investigated were ZnS:Mn (0.43%), and SrS:Cu,Ag (0.2%,0.4%). ZnS:Mn was investigated to ensure that the results obtained previously at the x-ray lab at RAL could confidently be repeated within the facility at NTU. The SrS:Cu,Ag phosphor is a potential blue emitting TFEL material. Phosphors were investigated for luminescence via photoluminescent (PL) excitation, electroluminescent (EL) excitation, and cathodoluminescent (CL) excitation as appropriate. The NSL5 laser (Lambda Physik LPX 205, 248nm/193nm 20ns) was installed within the clean-room facility at NTU and the optical arrangement was set up as described previously [2]. Samples of thin film phosphors were deposited by rf-magnetron sputtering and housed in a pressure cell during irradiation to minimise ablation. Various numbers of laser irradiations were used with the fluence varied from 0.3 to 1.5 J/cm$^2$, while the samples were in an overpressure of Ar (150 psi). For the PL measurements a UV laser (He-Cd, 326nm, 16mW) provided the excitation, an optical fibre collected the generated light and directed it to an Ocean Optics (S2000) spectrometer. The EL devices were characterised on a probe station located in a dark enclosure, driven by a sinusoidal wave at 5 kHz with a p-p voltage of 364Volts, and the generated light was collected by an optical fibre and fed to the spectrometer. Finally the CL was measured in a vacuum chamber with an electron beam at 6 kVolts and beam current 0.3mA with the generated light being collected and directed to the spectrometer via an optical fibre.

**Results and Discussion.**

Initial experimentation involved only single laser annealing pulses and the resulting PL and EL improvement for ZnS:Mn thin films is shown in Figure 1. Both curves, demonstrating improvement, show the same trend, requiring a minimum fluence of ~0.5 J/cm$^2$ (threshold fluence) to induce any luminescence improvement. This is further enhanced with increasing the fluence until ~1.2J/cm$^2$ when the improvement is saturated. These results are consistent with previous work, demonstrating the transferability of the technique between experimental systems. The previously reported modelling of the laser annealing process [3] suggests that with laser annealing the front surface of the phosphor reaches temperatures in excess of 2000°C, for nanoseconds only, while the back surface, that forms the interface between the phosphor and the insulator, does not exceed ~500°C. Hence, the interface states that act as donors of hot electrons are preserved, since the critical temperature is not exceeded. The knee observed at 1.2J/cm$^2$ is attributed to reduction of the phosphor thickness due to probable ablation [4]. Therefore a laser pulse of adequate fluence can achieve highly localised annealing of the phosphor film only.

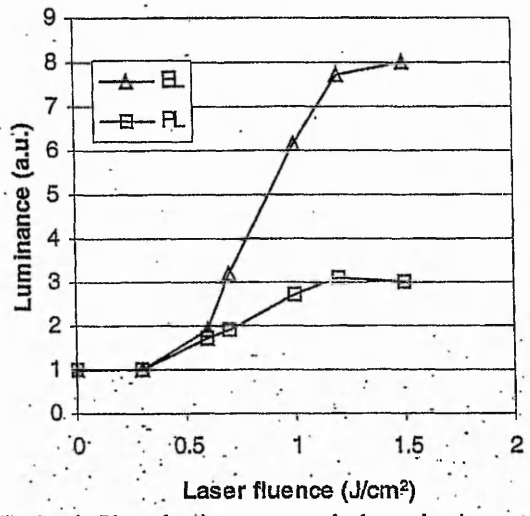


**Figure 1.** Photo-luminescence and electro-luminescence improvement for ZnS:Mn thin films with one laser annealing pulse. Both curves are normalised to the as-deposited film performance.

For the case of EL characterisation, multiple pulse irradiation experiments (Figure 2) show that one pulse is beneficial but not as significant as two pulses, which showed the best improvement at ~1.3J/cm$^2$. Three pulses have proven to be detrimental for EL, suggesting that two pulses induce a heat treatment that does not reach the back surface of the phosphor, unlike three pulses, which also probably causes excessive ablation. These results extend the information on the process that has been demonstrated to improve over thermal annealing, producing EL devices of higher luminance and better electrical characteristics.

Laser processing of SrS:Cu,Ag based TFEL devices was also successful - most critically as a viable annealing technique for rf-sputtered films of this phosphor, as compared to thermal and rapid thermal annealing which resulted in unusable films. Thin films were deposited and characterised initially for structural stability and also luminescence via photoluminescent excitation. With thermal annealing, at the temperatures reported as necessary for viable luminescence (up to 800°C [5]), crazing of the films prevented fabrication of EL devices. A detailed matrix of deposition and annealing parameters was investigated, varying the substrate temperature from 100°C to 400°C, and with annealing, both thermal and rapid thermal up to 800°C. The result of this study was that reliable films exhibiting luminescent behaviour were only achievable at low deposition temperatures, up to 200°C, and with no annealing. However for the TFEL devices produced from these films, the luminance was too weak to provide reliable measurements.

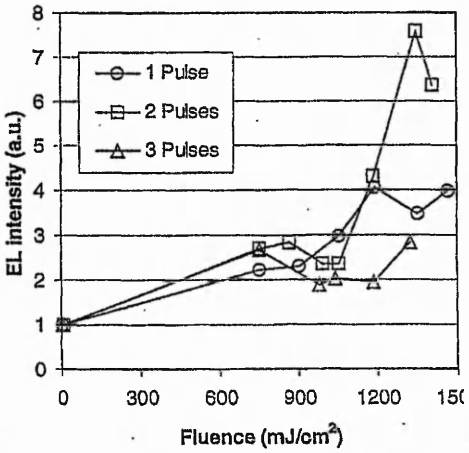


**Figure 2.** Electroluminescence improvement of ZnS:Mn based TFEL devices with one, two and three laser annealing pulses. Curves normalised to the as-deposited films.

For the laser annealing study, SrS:Cu,Ag thin films, grown at 200°C, onto 200nm thick layers of $Y_2O_3$, were exposed to 20ns pulsed irradiation at varying fluences using the KrF irradiation. Viable TFEL devices were obtained with single pulse irradiation fluences in the range of 0.4 –1.5 Jcm$^{-2}$. The effect of the higher fluence was to enhance the film crystallinity, as indicated by increased XRD intensity from the SrS (111) peak, which is consistent with the ZnS:Mn crystallinity enhancement demonstrated previously. Reproducible films for TFEL devices were obtained at the higher fluences, which were consequently used for the device fabrication used here. Figure 3 shows the blue/green emission spectrum of the EL devices fabricated using the laser processing technique.

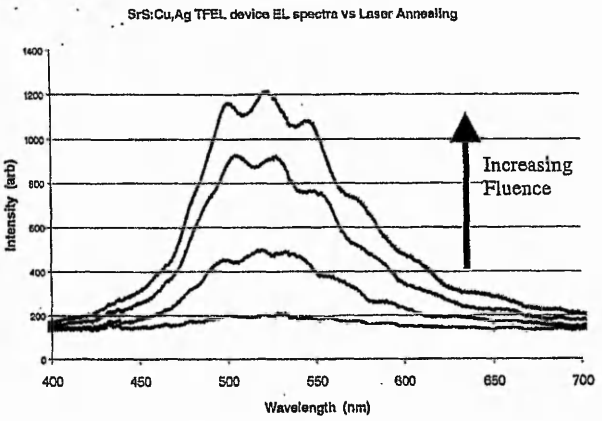


**Figure 3.** EL emission spectra as a function of laser annealing with 248 KrF irradiation for SrS:Cu,Ag TFEL devices driven at 640 V pk-Pk

Finally, laser processing of ZnS:Mn films on glass substrates for CL applications was investigated, with a similar result to the ZnS:Mn EL devices in that one pulse is again beneficial, while two or three show further improvement, although ablation effects dominate at higher fluences with three pulses. The results, shown in Figure 4 clearly demonstrate the enhancement

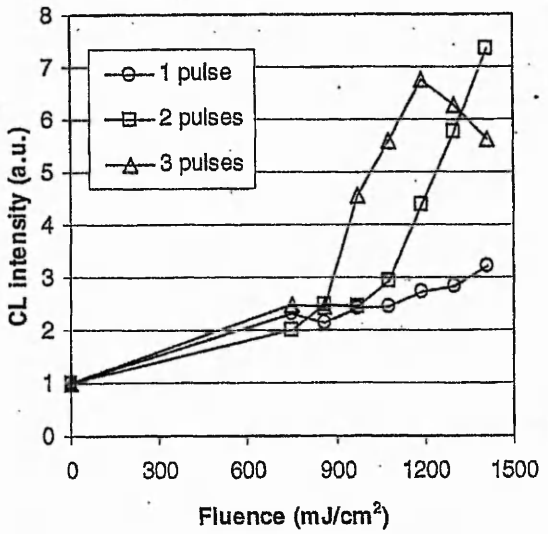


**Figure 4.** Cathodoluminescence improvement of ZnS:Mn thin films with one, two and three laser annealing pulses. Curves normalised to the as-deposited films.

in CL emission from these thin films as a result of the laser irradiation technique, hence highlighting the potential for application to a wide variety of flat screen display materials. Currently, films of ZnS:Cu phosphor are being investigated. This phosphor material is used as the CL screen in image intensifiers, and thin films are of interest for enhanced uniformity and reduced graininess in the final image which is a problem with powder based screens used. However, the luminous intensity from thin films has to date been insufficient for practical applications. Hence, the potential demonstrated here for luminescent enhancement via laser processing may help to solve this problem.

Additional work currently utilising the loan pool system is concerned with examining the use of the ArF 193nm emission for $Y_2O_3$ (5.9eV) based phosphors. Preliminary results are encouraging, once again highlighting the diverse potential of this materials processing technique.

**References**

1. C B Thomas, R Stevens, W M Cranton.; 1996 SID International Symposium. Digest of Technical Papers. First Edition. Soc. Inf. Display. 1996, pp.365-9.

2. D.C. Koutsogeorgis, E.A. Mastio, W.M. Cranton and C.B. Thomas. Thin Solid Films, 383, No. 1-2, Feb. 2001, pp. 31-33.

3. E.A. Mastio, W.M. Cranton, C.B. Thomas, E. Fogarassy, S. de Unamuno. Pulsed KrF laser annealing of RF sputtered ZnS:Mn thin films. Applied Surface Science, 138-139, Jan. 1999, pp. 35-39.

4. E.A. Mastio, E. Fogarassy, W.M. Cranton, C.B. Thomas. Ablation study on pulsed KrF laser annealed electroluminescent ZnS:Mn/Y2O3 multilayers deposited on Si. Applied Surface Science, 154-155, No. 1-4, Feb. 2000, pp. 35-39.

5. H.M. Menkara, W. Park, M.Chaichimansour, T.C. Jones, B.K. Wagner, C.J. Summers, and S.Sun; 4th Int. phosphor Conf. / 9th Int. Workshop on EL, Bend (Oregon) Extended Abstracts, p. 191 –194.

*Experiments:* We performed several experiments to generate beat-notes for applications ranging from high-speed communications (160 GHz) and microwave network (60 GHz) to THz waves. In the first set of experiments we fixed the main cavity FSR at 20 GHz (~7.5 mm bulk cavity optical length) by carefully tuning the PZT voltage. We tuned apart the two FBGs in 20 GHz steps from 40 to 200 GHz by stretching FBG1. Fig. 2 shows an example of the autocorrelation trace of a ~160 GHz beat-note signal, i.e. when the two FBGs were tuned apart by about eight times the main cavity FSR. A clean 60 GHz beat-note was also achieved.

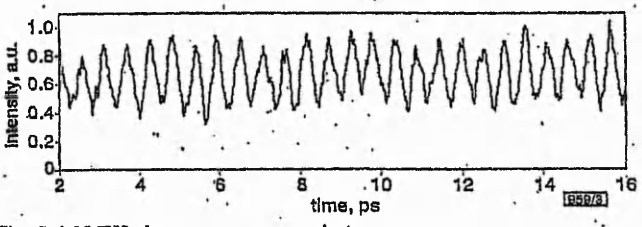


Fig. 3 *1.99 THz beat-note autocorrelation trace*

To increase the beat-note frequency to the THz range we performed a second set of experiments where we used a 1533.6 nm peak wavelength FBG as FBG2. We obtained a beat-note up to ~2.1 THz by using two FBGS centred at 1533.6 and 1550.4 nm. A 1.99 THz beat-note is shown in Fig. 3. The unresolved signal is due both to the limitation of our measurement setup and to the penalty discussed next.

The main issue of such a multi-wavelength approach is the intrinsic penalty due to partition noise. The problem can be detrimental because the antiphase dynamic generates an oscillating bias superimposed to the beat-note signal. To evaluate the partition noise we measured the relative-intensity-noise (RIN) of the laser by feeding a low noise photodiode. The electrical signal was recorded by a high-resolution electrical spectrum analyser (HP mod.3588). Measurements refer to the conditions of Fig. 3.

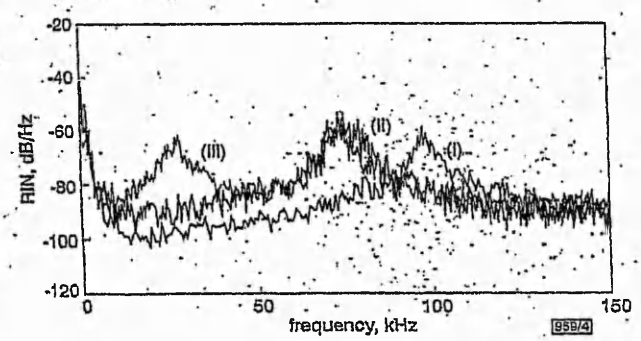


Fig. 4 *RIN spectra*

(i) single-frequency operation at 1534 nm
(ii) dual-frequency operation - total power
(iii) dual-frequency operation - power at 1534 nm

Fig. 4 shows the RIN spectra for three different conditions. Curve (i) shows the RIN spectrum of the laser operating in single-frequency operation at 1534 nm (FBG1 was absent). Curve (ii) shows the RIN spectrum of the total output power when dual-frequency operation at 1534 nm and at 1550 nm is obtained. Curve (iii) in Fig. 4 shows the RIN spectrum of the 1534 nm wavelength mode observed after filtering out the 1550 nm power by a tunable filter (Santec mod. TDS-820, ~133 GHz FWHM) centred at 1534 nm. From Fig. 4 it is apparent that RIN at around the relaxation oscillation frequency is unchanged but a large low frequency RIN peak is found. The extra noise is due to competition between the two lasing wavelengths and it can be seen, by observing curve (ii) in Fig. 4 where the total power does not exhibit the same feature, that the two modes behave in antiphase (when mode 1 has maximum power mode 2 has minimum power). In our case the antiphase dynamics superimpose on the sinusoidal beat-note a bias oscillating at ~27 kHz frequency. We believe the partition noise can be reduced by improving the mechanical stability of the main cavity to fibre focusing optics as well as by reducing the length of the fibres. The high RIN peak value, compared to other devices [7], is due to the limited pump power and to back reflections to the pump lasers that increase the laser diode RIN. An improved cavity design will be able to reduce the whole RIN spectrum.

*Conclusions:* We have proposed a simple cavity design to generate beat-note signals in the mm- to THz-frequency range. We have demonstrated that optical feedback from external cavity FBGs provide for reliable and discretely tunable beat-note signals. The antiphase dynamic noise induced by the dual-frequency operation has been investigated and it represents the main limitation of such a source for critical applications.


*26 September 2001*
*Electronics Letters Online No: 2001*
*DOI: 10.1049/el:2001*

S. Taccheo, G. Sorbello, G. Della Valle and P. Laporta (*INFM, Dipartimento di Fisica del Politecnico di Milano and CEQSE-CNR, Piazza Leonardo da Vinci 32, 20133 Milano, Italy*)

E-mail: stefano.taccheo@polimi.it

G. Karlsson and F. Laurell (*Department of Physics, Royal Institute of Technology, Lindstedtsv. 24, 10044 Stockholm, Sweden*)

W. Margulis (*ACREO, Electrum, 236, 16440 Stockholm, Sweden*)

S. Cattaneo (*IPG Fibertech, via Pisacane 46, 20025 Legnano, Italy*)

## References

1 SCHMUCK, H., HEIDEMANN, R., and HOFSTETTER, R.: 'Distribution of 60 GHz signals to more than 1000 base stations', *Electron. Lett.*, 1994, 30, pp. 59–60

2 MATSURA, S., TANI, M., ABE, H., SAKAI, K., OZEKI, H., and SATO, S.: 'High-resolution terahertz spectroscopy by a compact radiation source based on photomixing with diode lasers in a photoconductive antenna', *J. Mol. Spectrosc.*, 1998, 187, pp. 97–101

3 MAMYSHEV, V.P., CHERNIKOV, S.V., and DIANOV, E.M.: 'Generation of fundamental soliton trains for high-bit-rate optical fiber communications lines', *J. Quantum Electron.*, 1991, 27, pp. 2347–2455

4 MATSUI, Y., PELUSI, M.D., ARAHIRA, S., and OGAWA, Y.: 'Beat frequency generation up to 3.4 THz from simultaneous two-mode lasing operation of sampled-grating DBR laser', *Electron. Lett.*, 1999, 35, pp. 472–473

5 HIDAKA, T., MATSURA, S., TANI, M., and SAKAI, K.: 'CW terahertz wave generation by photomixing using two-longitudinal-mode laser diode', *Electron. Lett.*, 1997, 33, p. 2039

6 ALOUMI, M., BRUNEL, M., BRETENAKER, F., VALLET, M., and LE FLOCH, A.: 'Dual tunable wavelength Er:Yb: glass laser for terahertz beat frequency generation', *IEEE Photonics Technol. Lett.*, 1998, 10, pp. 1554–1556

7 TACCHEO, S., SORBELLO, G., LAPORTA, P., KARLSSON, G., and LAURELL, F.: '230-mW diode-pumped single-frequency Er:Yb laser at 1.5 μm', *IEEE Photonics Technol. Lett.*, 2001, 13, pp. 19–21

8 TACCHEO, S., LAPORTA, P., and SVELTO, C.: 'Widely tunable single-frequency erbium-ytterbium phosphate glass laser', *Appl. Phys. Lett.*, 1996, 68, pp. 2621–2623

# Optically transparent frequency selective window for microwave applications

C. Tsakonas, S.C. Liew, C. Mias, D.C. Koutsogeorgis, R.M. Ranson, W.M. Cranton and M. Dudhia

The microwave behaviour of a frequency selective windo consisting of a cascade of two optically transparent band-sto frequency selective surfaces (FSSs) made with highly conducti highly transparent thin-film indium tin oxide (ITO) investigated. The performance of the ITO FSS structure compared to a similar structure made from copper. Experimen results demonstrate the improved band-stop behaviour of double layer window over a single layer one.

*Introduction:* An optically transparent frequency selective surfa (FSS) made from a transparent conductor can be favoured m than a metal-based opaque FSS whenever the continuity of optical field of view through the FSS is required. This is true applications where aesthetic presentation can be important for

pleasing quality and inconspicuousness. The shielding effectiveness of an FSS structure depends on the good conductance of its metallic elements. Metals such as silver, gold and aluminium, when deposited in thin-film form on glass, are semi-transparent but more conductive than the traditional transparent conductive oxides such as indium tin oxide (ITO) and zinc oxide doped with aluminium (ZnO:Al). Unfortunately they are not resistant to weather conditions and deteriorate easily. Although some of the existing commercially available transparent metallic coatings on polymer substrates have low sheet resistance and good transparency (3 Ω/□ and 70%), they are also protected by a top surface layer with anticorrosive properties that renders any selective etching, in order to define FSS patterns, ineffective. This problem is more pronounced whenever etching of FSS structures with small geometrical patterns, operating at high frequencies, is required. Hence these coatings are only used in shielding applications where selective filtering is not an issue.

FSS structures with optically transparent conductive elements were first investigated by Parker *et al.* [1]. In this work the effect of conductivity on the performance of the FSS was presented. Frequency selective circular patch (band-stop) and slot ring (band-pass) surfaces were employed. These elements were arranged in a square lattice array. They were fabricated by using 4–8 Ω/□ sheet resistance thin-film silver deposited on thin polyester films. The performance of ITO (20 Ω/□ sheet resistance) was also investigated but the conductor was discounted due to its poor FSS behaviour resulting from its high sheet resistance. Results were presented that showed a 19 dB attenuation for the transparent silver band-stop FSS, at normal wave incidence, compared with > 30 dB attenuation for the copper FSS. It was subsequently concluded that it was feasible to construct optically transparent FSS provided the sheet resistance of the conductor is 4–8 Ω/□ or less. It was also suggested that cascading FSS structures would be more effective than single layer FSS.

In this Letter, we present for the first time results obtained from a double layer FSS structure based on highly conductive and highly transparent ITO deposited on 4 mm standard window glass substrate that shows high band-stop attenuation (> 25 dB).

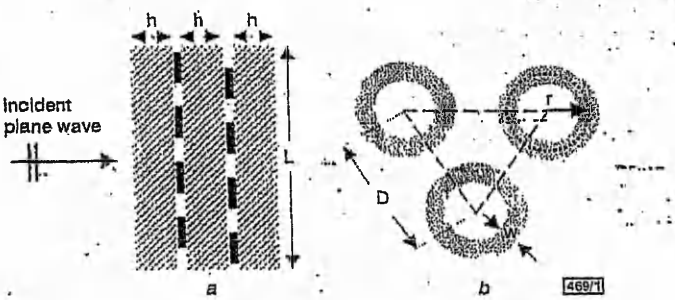


**Fig. 1** *Cross-section of double layer FSS window and triangular lattice pattern of each FSS*

*a* Cross-section
*b* Triangular lattice pattern

*Fabrication:* The in-house ITO was grown on standard glass wafers using RF magnetron sputtering at 280°C and 5 mTorr sputtering gas pressure, for 50 min. The RF power was 100 W. The sputtering gas consisted of 2% oxygen in argon. Each glass wafer has a diameter $L = 100$ mm and a thickness $h = 4$ mm (Fig. 1*a*). A commercially available ITO target was employed instead of a metallic indium target doped with tin. None of our films underwent post-annealing treatment. They showed excellent adherence to the glass and good stability.

The sheet resistance of our films was measured with a four-point probe station. The thickness is measured by a Dectak-Sloan profilometer and the transparency in the visual spectrum is measured using a spectrophotometer. The two films coated on the glass substrates, which were used to construct the double layer FSS structure, have a sheet resistance of 3.5 Ω/□ and ~90% transparency. Their resistivity was calculated to be $1.6 \times 10^{-4}$ Ωcm at a thickness of ~4500 Å. This compares well with one of the most conductive commercially available silver-based transparent conductive polymers that has a sheet resistance of 3 Ω/□ and optical transparency of 60–70%. The FSS pattern was created by dry physical etching.

*Results:* A double layer FSS window is created from two conductive FSS patterns which are sandwiched between three 4 mm thick glass substrates, (shown in Fig. 1*a*). Each FSS is made from a triangular lattice with ring patch elements. The period of the FSS is $D = 0.45$ mm, the mean radius of the ring element is $r = 0.15$ mm and the width of the ring element is $w = 1$ mm (Fig. 1*b*). The two FSS patterns overlap randomly, i.e. the individual elements of the two single layers do not coincide. The dimensions of the ring elements were estimated approximately by a heuristic formula that gives an estimate of the length of the mean radius of the ring element at the desired band-stop frequency of operation. The same FSS is used for both layers (Fig. 1*b*). The FSS structures were mounted onto the centre of a square metal plate (100 × 100 cm), which was covered with blocks of absorbers (184 × 184 cm in total). The measurements were carried out across three microwave spectral bands by using appropriately-sized horn antennas (12–18, 18–26 and 26–40 GHz). The transmitting and receiving antennas were each positioned, initially, at a distance of 113 mm from the FSS window. In Fig. 2, the co-polarisation transmission results of the double layer ITO FSS are compared with those of a copper FSS. Normal wave incidence is assumed. As expected, because of its lower sheet resistance, the copper structure has the best performance. The band-stop frequencies of the two-layer copper and ITO FSS coincide at about 26 GHz with an attenuation of 46 dB and 28 dB, respectively. Fig. 2 also illustrates the transmittance of the single layer copper and ITO FSS.

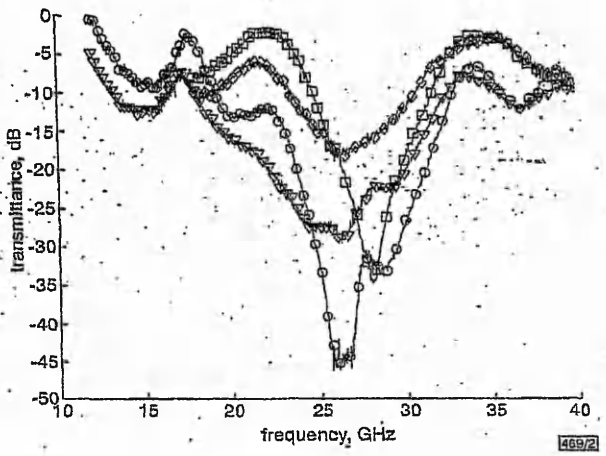


**Fig. 2** *Transmittance responses*

○ double layer copper FSS
▽ double layer ITO FSS
□ single layer copper FSS
◇ single layer ITO FSS

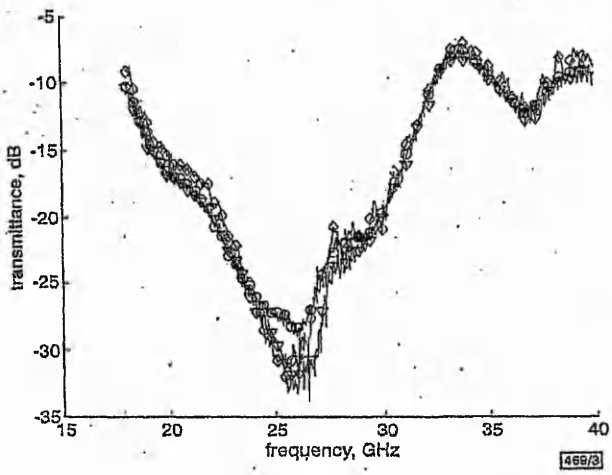


**Fig. 3** *Transmittance response for double-layer ITO FSS window when receiving antenna positioned at different distance R from sample*

◇ $R = 16$ mm
▽ $R = 66$ mm
○ $R = 113$ mm
Transmitting antenna positioned 113 mm from FSS window

It is established, by rotating one copper FSS layer relative to the other, that the transmittance response of the double layer FSS

is not significantly affected by the relative position of the two FSS layers.

The above position of the receiving antenna indicates that the measurements were made in the far field where the experimental results are the combination of aperture and FSS transmission. To investigate the effect of the aperture, the receiving antenna was placed closer to the FSS window at distances of 67 and 16 mm. The results, shown in Fig. 3, are not significantly altered by changing the receiver's position, Fig. 4 demonstrates the high optical transparency of the double layer ITO FSS window.


489/4

Fig. 4 *Double layer ITO FSS window on top of Radiocommunications Agency logo*

*Conclusion:* An optically transparent FSS structure based on highly conductive ITO is presented here for the first time. Comparative studies with a copper FSS structure showed that the performance of the ITO double layer FSS is very satisfactory and close to our 30 dB target. The current aim is to increase further the conductivity of the ITO. In general it is expected that any increase in the conductivity of the ITO would result in a concomitant decrease in its optical transparency. There are indications, based on in-house laboratory experiments and published literature, that the conductivity can be improved further without severely affecting the high optical transparency [2 – 4].

*Acknowledgments:* This work was performed under Radiocommunications Agency contract AY3365.


*11 September 2001*
*Electronics Letters Online No: 20010979*
*DOI: 10.1049/el:20010979*

C. Tsakonas, S.C. Liew, C. Mias, D.C. Koutsogeorgis, R.M. Ranson and W.M. Cranton (*School of Engineering, Division of Electrical and Electronic Engineering, The Nottingham Trent University, Burton Street, Nottingham, NG1 4BU, United Kingdom*)

E-mail: christos.mias@ntu.ac.uk

M. Dudhia (*Radiocommunications Agency, Radio Technology and Compatibility Group, Whyteleafe Hill, Whyteleafe, Surrey, CR3 0YY, United Kingdom*)

## References

1 PARKER, E.A., ANTONOPOULOS, C., and SIMPSON, N.E.: 'Microwave band FSS in optically transparent conducting layers: performance of ring element arrays', *Microw. Opt. Technol. Lett.*, 1997, **16**, (2), pp. 61–63

2 BELLINGHAM, J.R., PHILLIPS, W.A., and ADKINS, C.J.: 'Intrinsic performance limits in transparent conducting oxides', *J. Mater. Sci. Lett.*, 1992, **11**, pp. 263–265

3 RAY, S., BANERJEE, R., BASU, N., BATABYAL, A.K., and BARUA, A.K.: 'Properties of tin doped indium oxide thin films prepared by magnetron sputtering', *J. Appl. Phys.*, 1983, **54**, pp. 3497–3501

4 RAUF, I.A.: 'A novel method for preparing thin films with selective doping in a single evaporation step', *J. Mater. Sci. Lett.*, 1993, **12**, pp. 1902–1905

# Classification of vintages of wine by artificial nose using time delay neural networks

A. Yamazaki, T.B. Ludermir and M.C.P. de Souto

A pattern recognition system for an artificial nose is presented. It is composed of artificial neural networks with time delay taps on their inputs. For the classification of vintages of wine, it achieves better results (mean classification error of 4.32%) than those obtained by networks without delay taps (42.79%).

*Introduction:* The two main components of an artificial nose are the sensor and the pattern recognition systems. Each odorant substance presented to the sensor system generates a pattern of resistance values that characterises the odour. This pattern is often first preprocessed and then given to the pattern recognition system, which in its turn classifies the odorant stimulus [1]. Sensor systems have often been built with polypyrrole-based gas sensors. Some advantages of using such a kind of sensor are [2]: (i) rapid adsorption kinetics at the environment temperature; (ii) low power consumption, as no heating element is required; (iii) resistance to poisoning; and (iv) the possibility of building sensors tailored to particular classes of chemical compounds. Artificial neural networks (ANNs) have been widely applied as pattern recognition systems in artificial noses [1]. Implementing the pattern recognition system with ANNs has advantages such as [3]: (i) the ability to handle nonlinear signals from the sensor array; (ii) adaptability; (iii) fault and noise tolerance; and (iv) inherent parallelism, resulting in high speed operation. The type of neural network most commonly used for odour classification in artificial noses has been the multi-layer perceptron (MLP), together with the backpropagation learning algorithm [4]. Such networks are usually constrained to deal only with static patterns. In contrast, in this Letter we propose an odour recognition system for artificial noses, which takes into account the temporal properties of the sensor signals. This is accomplished by using ANNs with time delay taps on their inputs.

*Problem and data description:* The aim is to classify odours from three different vintages (years 1995, 1996 and 1997) of the same wine (Almadém, Brazil). A prototype of an artificial nose was used to acquire the data. This prototype is composed of six distinct polypyrrole-based gas sensors, built by electrochemical deposition of polypyrrole using different types of dopants. Three disjointed data acquisitions were performed for every vintage of wine, by recording the resistance value of each sensor at every half second during a five minute interval. Therefore, this experiment yielded three data sets with equal numbers of patterns: 1800 patterns (600 from each vintage). A pattern is a vector of six elements representing the values of the resistances recorded by the sensor array. The patterns in every set of vintage have been ordered according to the sequence in which they were obtained. Thus there is a curve (resistance against time) associated with each sensor.

*Experiments:* In this Letter, a pattern recognition system for a artificial nose is proposed. The system comprises a time delay neural network (TDNN) [5], which allows for the handling of th temporal features in the signals generated by the sensors.

The data for training and testing the network were divided a follows: the first data acquisition was assigned to the training se the second to the validation set, and the last was reserved to te the network. This partitioning has been chosen so that the temp ral behaviour of the patterns within each set could be kept, allo ing the presentation of these patterns in the same order as th originally occurred. The patterns were normalised to the range [- +1], for all network processing units implemented by hyperbo tangent activation functions. All networks analysed were TDN with only a single hidden layer, but with different numbers of t delay lines and hidden nodes. The first group of TDNNs had units in the input layer: one for each sensor – in fact this group topologies had no delays, for the classification is based on o the current input. Conversely, the second group of TDNNs h twelve units in the input layer: six units representing the patt currently presented and the other six units for the pattern sho at the previous time step. For both groups of topologies, the n work output was represented by a 1-of-$m$ code – one unit for e

# 4.10: Materials Processing and Device Engineering for Laterally Emitting Thin Film Electroluminescent Miniature Displays

**W.M. Cranton, C.B. Thomas, D. Koutsogeorgis, E. Mastio, M. Craven, R. Stevens, R.Ranson, M.Sethu, J. Rudiger, S. Barros, A.Liew, and P. Theng**

Department of Electrical and Electronic Engineering
The Nottingham Trent University, UK
*Email: wayne.cranton@ntu.ac.uk*

**Abstract**

*Miniature emissive displays utilising laterally emitting thin film electroluminescence are discussed in terms of the device engineering and materials processing required to fabricate high intensity, high resolution fixed legend displays.*

## 1. Introduction

In the field of emissive flat panel displays, thin film electroluminescence (TFEL) is a technology that has been a subject of commercial and scientific interest for over 4 decades. Display panels based on this technology have been utilised where ruggedness, reliability, high contrast, and high viewing angles are required; such as in medical, transport, and military applications. It is the solid state thin film structure at the heart of TFEL displays that provides the inherent ruggedness and potential for low cost manufacture, and as demonstrated by Planar, can be configured to provide high resolution miniature emissive displays[1].

In an alternative device configuration, reflected lateral emission from TFEL devices has been shown by our research to demonstrate the feasibility of high intensity luminous emission from fixed legend miniature displays[2]. These laterally emitting thin film electroluminescent (LETFEL) displays are intended for use in low cost see-through head mounted systems, where luminances in excess of 3000cdm$^{-2}$ are required, but without the need for a full graphics display. Realisation of these high luminances relies upon optimising both the internal light generation processes of TFEL devices and enhancements in the optical out-coupling. Presented in this paper is a brief review of the materials and device engineering research that has resulted in a fabrication route for miniature fixed legend LETFEL displays based on this technology.

## 2. LETFEL Technology – Device Engineering

Figure 1 illustrates the fundamental device technology which forms the basis for LETFEL displays. This structure is designed to utilise the inherent waveguiding attributes of TFEL thin films to produce devices with a typically four-fold increase in the emitted intensity as compared to conventional surface emission[3]. The improved emission occurs at the 'micro-mirror' aperture, where a reflecting microstructure is formed to convert the laterally confined light into useful surface emission. Various geometries of light emitting devices have been fabricated using this principle, including the 4x4mm miniature fixed legend display shown in Figure 2.

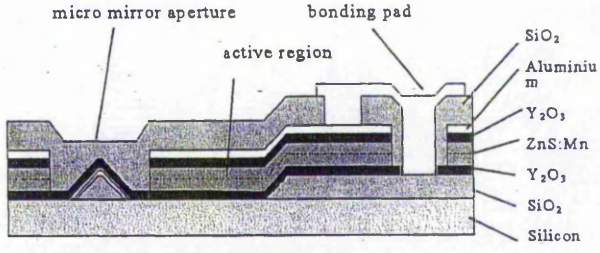


Fig 1. Cross section of a LETFEL device

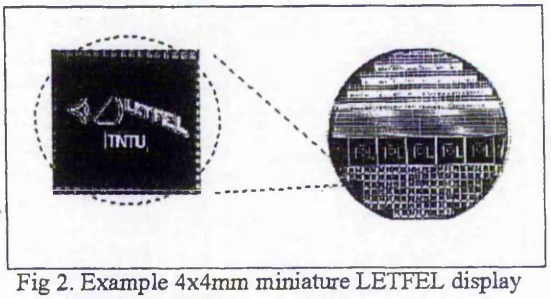


Fig 2. Example 4x4mm miniature LETFEL display and 4" Silicon substrate

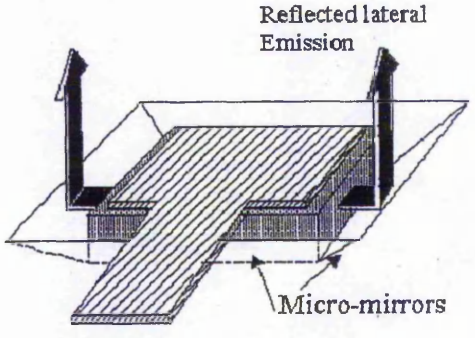


Fig 3. Schematic of LETFEL display pixel

The standard LETFEL design is based on a fabrication process which utilises a combination of magnetron sputtering and chemical vapour processes for the deposition of the various thin films onto silicon substrates, with dry etching used to pattern the layers and to form the micro-mirrors. Figure 3 illustrates the microstructure of an emitting pixel region, where the mirrors are arranged around the periphery of an active pixel region. This would be a configuration suitable for matrix displays, with the mirror boundary also preventing optical cross-talk between pixels.

For fixed legend displays of the type shown in Figure 2, arrays of micro-mirrors are distributed within the light emitting legend as shown in Figure 4. The mirrors are typically 3 microns wide, with legends (e.g. the letters 'TNTU') made up of arrays of mirrors spaced at 15 microns apart. For higher intensity emission, a higher ratio of light generating area to emitting area is required, which may affect the flexibility on legend design. The luminance from a display of the type shown in Fig 1 is between 500 and 3000 $cdm^{-2}$, (driven at 5 kHz, 250V gnd to peak) depending on legend geometries. The maximum intensity is produced by mirrors surrounded by > 100 microns of active ZnS:Mn phosphor.


Fig 4. LETFEL display legend showing arrays of mirror apertures within active EL regions

For each of these displays, the full fabrication process requires a dedicated set of photolithographic masks with each design. However, in a recent series of experiments, the possibility of fabricating low cost Application Specific Displays from a generic micro-mirror substrate was examined. In the application specific configuration – illustrated by an example in Figure 5 – only the upper electrode mask is changed for each design, generating the required features by linking individual pixels from a common base array.

In summary, therefore, by utilising fabrication processes and techniques standard to the silicon device industry, LETFEL devices offer a potential low cost solution for applications requiring miniature symbology/fixed legend displays with high luminance, contrast and resolution plus the benefits of the all solid state TFEL technology.

Fig. 5 Application Specific LETFEL display.

### 3.1 Materials Processing – Barrier Layer

To obtain the target luminances of ~ 3000$Cdm^{-2}$, enhancement of the TFEL light generating process is required in addition to the device engineering. This was achieved via the restructuring of the phosphor layer by the incorporation of a thin (100Å) field modifying 'barrier layer' of yttrium oxide.[4] For yellow emitting ZnS:Mn devices with this

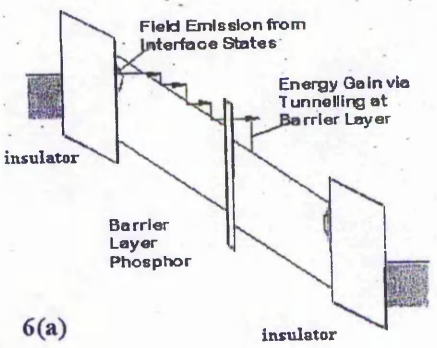


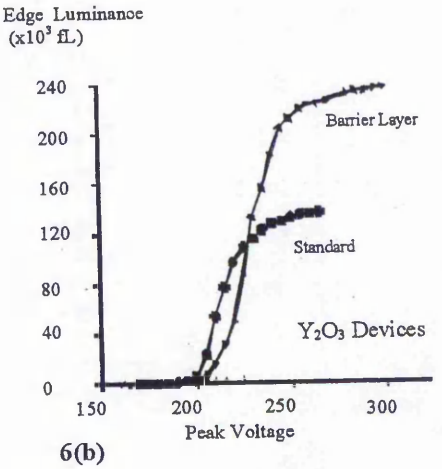


Fig 6 – Barrier Layer TFEL phosphor: (a) energy band diagram, (b) LV characteristics for edge emitting devices.

modification, the luminance Vs voltage characteristics show significant improvements, which are attributed to an electron tunnelling effect leading to a higher excitation efficiency, as explained by Figure 6. The effect is currently being investigated for the blue emitting SrS:Ce and SrS:Cu,Ag phosphors.

### 3. 2 Materials Processing – Laser Annealing

Perhaps the most significant series of results from recent work is the demonstration that the use of pulsed laser annealing (PLA) can produce up to four-fold increases in luminance from TFEL devices[5]. This has application to both the miniature LETFEL displays discussed here, and also to conventional large area TFEL panels.

Critical to the luminescent efficiency of a TFEL device is an annealing treatment, which allows for the effective incorporation of luminescent dopant ions within the host lattice (activation). Commercial TFEL devices are typically fabricated on glass substrates and are subjected to a post deposition anneal at 500°C for ~ 1hr. The LETFEL device, however, is fabricated on a silicon substrate, which facilitates the investigation of higher annealing temperatures. Via a programme funded by the Engineering and Physical Sciences Research Council in the UK, we have demonstrated that PLA is an effective means of activating the phosphor by achieving higher temperatures localised to the phosphor thin film .

The luminescent properties of LETFEL devices as a function of annealing temperature are shown in Figure 7. From the Photoluminescence (PL) results it is clear that the quality of the ZnS:Mn thin films is improving with increased temperature. This is indicative of improved incorporation of the luminescent Mn centres into the host lattice, which is the premise behind the standard TFEL annealing process. Under EL excitation, however there is no significant improvement in EL luminance beyond 500°C, even though the corresponding PL intensity is increasing.

Modelling this behaviour based on the measured electro-optic characteristics indicates that the limitation in performance is due to a reduction of the interface state density at the phosphor / dielectric interface which becomes noticeable following annealing at > 500°C[6]. For optimum EL performance, therefore, the ideal interface would be the as-grown *disturbed* structure, such that the density of electron traps remains high, but where the luminescent quality of the thin film phosphor is optimised by annealing.

Based on these observations, it was proposed that an investigation of pulsed laser annealing (PLA) could provide a more effective means of heat treating the phosphor thin films of LETFEL devices. By irradiating the thin film phosphors at a wavelength with a high absorption coefficient, and by using high energy pulses of short duration, the research was designed to investigate the feasibility of optimising the devices by delivering energy to a localised surface region of the phosphor film, with minimal effect on the underlying interface. Since the band gap of ZnS is 3.65 eV, and that of SrS (a potential blue phosphor host) is 4.4 eV, the laser irradiation would ideally be at wavelengths < 343nm and 285nm respectively. For this study, therefore, KrF excimer lasers (emitting at 248nm) have been utilised.

TFEL and LETFEL devices were subjected to irradiation by 20ns pulses of KrF Excimer laser irradiation at 248nm. The optical systems used for beam delivery provided variable energy densities from 100-1500mJ/cm$^2$. At 248nm, the absorption coefficient of ZnS has been determined to be $3.33 \times 10^5$ cm$^{-1}$ for crystalline ZnS [7] and $3.15 \times 10^5$ cm$^{-1}$ for polycrystalline ZnS:Mn thin films[8], hence the energy absorption is contained within ~ 300nm of the thin film surface.

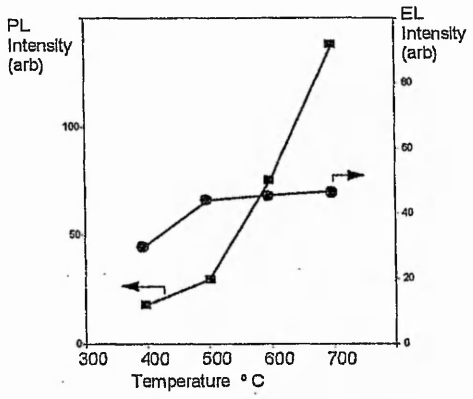


Fig. 7. PL and EL intensity of LETFEL devices Vs thermal annealing temperature.

For TFEL/LETFEL device structures, the laser annealing process was performed prior to the deposition of the upper dielectric layer and electrode definition. Examples of the resultant luminance Vs drive voltage characteristics of these devices are shown in figures 8 and 9. Clearly evident from these results is that a significant enhancement in EL performance is possible for both conventional surface emitting TFEL devices and LETFEL miniature

display structures employing opaque upper electrodes and micro-mirrors, although the relative improvement is greater for the surface emitting TFEL device. The enhancement in performance for ZnS:Mn based devices is associated with a measurable phase change in the crystalline structure of the thin film from predominantly cubic to predominantly hexagonal [9], which may be reducing the lateral transmission of light and enhancing the surface emission. Under investigation, therefore, is the combination of surface and lateral emission LETFEL devices, using ITO electrodes to obtain the maximum benefit from combining laser annealing and barrier layers with the reflecting LETFEL device structure.

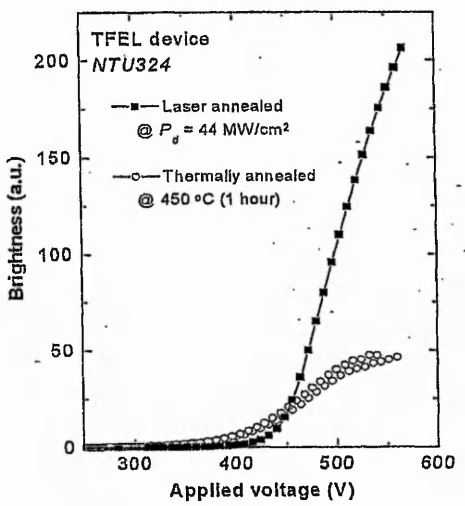


Figure 8. luminance Voltage characteristics of a TFEL device showing effect of laser annealing

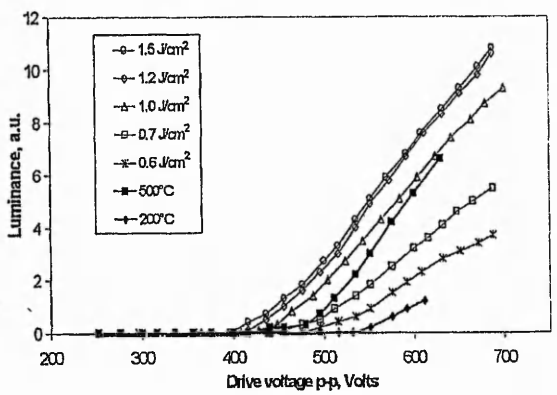


Fig. 9. LV characteristics for LETFEL devices following laser annealing at the fluences indicated, compared to thermal annealing.

**Summary**

Demonstrated is that laterally emitting thin film electroluminescence is a viable technology for application to high luminance miniature display devices. The feasibility of fabricating fixed legend displays and application specific displays has been shown, in combination with the advances in materials processing knowledge that are required to ensure high efficiency TFEL phosphors.

**Acknowledgements**

The authors would like to thank the Engineering and Physical Sciences Research Council for providing the primary support for this work.

**References:**

[1] Arbuthnot L, Aitchison B, Carlsen C, King C, Larsson T, Nguyen T. SPIE-Int. Soc. Opt. Eng. Proceedings of Spie - the International Society for Optical Engineering, vol.3689, 1999, pp.260-8. USA.

[2]Thomas CB, Stevens R, Cranton WM.; 1996 SID International Symposium. Digest of Technical Papers. First Edition. Soc. Inf. Display. 1996, pp.365-9.

[3] R. Stevens, C.B. Thomas, and W.M. Cranton, IEEE Electron Device Letters, Vol 15 No 3, (1994) 97.

[4]Patents: US08293540, EP0639937

[5]Cranton WM, Mastio EA, Thomas CB, Tsakonas C, Stevens R. Electronics Letters, vol.36, no.8, 13 April 2000, pp.754-6.

[6] W.M. Cranton, R.Stevens, C.B. Thomas, A.H. Abdullah, and M.R. Craven; Proc. IEE Colloquium on Materials for Displays (1995) 7/1.

[7] S. Ozaki and S. Adachi, Jpn. J. Appl. Phys. **32**, 5008 (1993).

[8] P. M. Savani, M. Phil Thesis, University of Bradford, 1982, p. 97

[9]Mastio EA, Craven MR, Cranton WM, Thomas CB, Robino M, Fogarassy E. Journal of Applied Physics, vol.86, no.5, 1 Sept. 1999, pp.2562-70.

# Highly Conductive ITO Coating For Frequency Selective Structures

**C. Tsakonas, C. Mias, S. C. Liew, C. Oswald, D. C. Koutsogeorgis and W. Cranton**
**Nottingham Trent University**
**M. Dudhia**
**Radiocommunications Agency**

## 1. INTRODUCTION

The frequency selective surfaces (FSS) are periodic arrays of conductive elements which perform a filter operation (see Fig. 1). They can be used for shielding applications at specific frequencies. The best conductive materials are usually opaque. Recently work was published indicating that, transparent conductors such as ITO and thin silver or gold films may also be used [1,2]. The transparency of silver and gold (which was shown to be the best conductive material) is not as good as that of the ITO. We report the use of highly conductive ITO (better in transparency and conductivity than the currently available thin silver films) in FSS structures.

We also compare the performance characteristics of an FSS structure with elements made from different conductive materials. The main aim is to show how the conductivity of the particular material affects the performance of the FSS. This result will in turn show how effective an enhanced conductivity ITO based FSS is in a shielding application.

## 2. FSS WITH TRANSPARENT CONDUCTORS

To the best of our knowledge, there is only one paper on optically transparent conductor FSS[1]. In this paper, the details of the effect of conductivity on the performance of optically transparent conductor FSS situated on opaque dielectric substrates are described. Different FSS structures were fabricated using 20Ω/□ Indium Tin Oxide (ITO) and 4-8Ω/□ Silver-based thin film (Ag) deposited on polymer substrate. Both films were attached on non-transparent substrates. By comparing the performance of the transparent conductor FSS with copper FSS it was concluded that it is feasible to construct optically transparent FSS provided that the conductivity of the conductor is approximately 4-8Ω/□ or less.

We used three different materials to assess the performance of the in-house fabricated FSS structure. These were copper, gold coated flexible polymer sheet, and ITO covered standard glass. The same FSS pattern was replicated on each of the three different materials by following the consecutive steps of established etching procedures. The final etching step of the FSS patterns was achieved by using dry or wet chemical etching.

For the copper FSS structure a thin sheet of copper was used which was attached to a standard glass after the FSS pattern had been etched. For the second FSS structure a commercially available gold-coated polymer sheet was used which it was also attached on a standard glass substrate. The gold surface resistance is 1-2 Ω/□ and it is about 20-35% transparent in the visual spectrum. The uniformity of the gold film across the polymer substrate was very good.

A triangular lattice with ring elements was chosen as the particular type of FSS for all the materials. The structure can be seen in Fig. 1. The period, D, of the FSS is equal to 0.45 mm and the mean diameter, r, of the ring element is equal to 0.15mm.

## 3. IN-HOUSE FABRICATION AND CHARACTERISTICS OF THE ITO

The in-house ITO was grown on glass wafers 100 mm in diameter and 2 mm in thickness, by using RF magnetron sputtering at 280°C and 5 m Torr sputtering gas pressure, for 50 min. The RF power was varied from 100 watt to 200 Watt in order to get optimum quality ITO films. Samples grown at higher temperatures were also examined. The sputtering gas consisted of 2% oxygen in argon. A 13.56 MHz RF power supply was used. A commercially available ITO ceramic target was employed instead of a metallic indium and tin target.

The best ITO in terms of combined transparency and surface resistance that has been achieved in our lab is around 1.6 Ω/□. With optical transparency around 90% and thickness 8000 Å it has a resistivity of $1.28 \times 10^{-4}$ Ωcm. None of our films has undergone post-annealing treatment. They are slightly stressed but they show excellent adherence to the glass, good stability and good performance with varying environmental factors. This resistivity is among the lowest reported to date[3,4]. An elevated deposition temperature was used because the ITO resistivity is abruptly increasing below 250°C.

Current investigation is focused on optimising the deposition, growing ITO at lower temperatures without affecting the achieved conductivity and using different techniques for improving further the conductivity without compromising the optical transparency. There are indications (from our lab experiments and in literature) that the conductivity can be improved further without affecting much the high optical transparency[5,6].

The sheet resistance of our films was measured with a four-point probe station. The resistivity is estimated by multiplying the sheet resistance by the thickness of the film. The thickness is measured by a Dectak-Sloan profilometer over an edge of the film. The transparency in the visual spectrum is measured with the aid of a spectro-photometer. It is calculated as the ratio of the transmitted light intensity through the film to the transmitted light intensity through the glass substrate only. A standard incandescent source is used to provide the incident white light. The comparison in terms of transparency between the thin gold film and one of our ITO samples can be seen in Fig. 2.

Wet chemical etching (for all types of materials) or dry physical etching (for the in-house grown ITO) was used to define the FSS pattern on the different substrates. Regarding the wet etching, both the gold-based and the ITO films were etched by using a standard gold etch, whereas for the copper film a solution of ferric chloride hexahydrate was employed instead. Preliminary results indicate differences in the performances between .1U.1Uthe dry and etched ITO. Future investigation will aim to characterise the two etching processes.

## 4. EXPERIMENTAL PROCEDURE AND RESULTS

The FSS structures were mounted onto a square metal plate (280 × 280mm), which was covered with absorbers (600 × 490mm) for protection against any diffraction phenomena as seen in Fig 3. The metal plate has a hole of 100 mm in the middle in order to accommodate the sample. The whole structure has the capability of rotational motion. Measurements were carried out with and without the absorbers at different angles. It was established that the use of absorbers was necessary in order to have any meaningful results. We anticipate, however that diffraction might occur and we are in the process of minimising its effects. The structures have two different interfaces, glass and air as shown in Fig.1. An open-ended $K_A$ band rectangular waveguide was used for the production of the incident plane wave, and it was

positioned at 463 mm away from the structure. A horn antenna was used as the receiver, and was position 214 mm away from the back of the FSS. The transmission coefficient ($S_{21}$ parameter) was obtained with the aid of a HP 8722D vector network analyser. The permittivity of the glass substrate was obtained by two approximate methods: i) by matching the experimental free space data of the transmission of a plane wave through a glass sheet with the theoretical results generated by analytically solving the ideal case, and ii) by a HP87050C open-ended coaxial probe. For a standard glass the first method gave a figure of $\varepsilon_r$ = 6.6 and the second that of $\varepsilon_r$ = 7. Fig. 4 presents the co-polarisation transmission results of the triangular lattice FSS made with different conducting materials. It can be seen that the copper structure has the best performance as expected, while the ITO is visibly superior to the gold film of comparable surface resistance. The copper FSS has a resonant frequency at almost 32 GHz with an attenuation of –30 dB. This has been confirmed by independent measurements at the Radiocommunications Agency and at The Nottingham Trent University. The gold FSS has a resonance frequency greater than the copper and an attenuation of –16 dB. In contrast to both of these materials the ITO FSS has a resonant frequency at 29 GHz and an attenuation of –25 dB. We believe that this shift can be attributed to the finite size of our aperture and can be eliminated if more ring elements are used. Further investigation is being carried out to clarify this matter. It was further established that the orientation of the FSS structures did not affect the experimental results at the angle $\theta$=0°. However this is not true for larger angles. It is not also clear why the gold and ITO FSS differs so much in the frequency of the maximum attenuation despite the fact that they have comparable surface resistances. Further work is needed to clarify this discrepancy. Fig. 5 shows how the angle of plane wave incidence affects the performance of the co-polarisation transmission of the ITO structure. It can be seen that the resonance frequency changes only a little with the angle of rotation. This stable behaviour is attributed to the particular FSS structure that has been selected for this work. Fig. 6 shows how the performance of ITO compares with that of copper at 30° plane wave incidence. The attenuation around 35 and 37 GHz is caused by the particular orientation of the structure. This was verified by measuring the response of a substrate of larger dimensions (270mm × 200mm) with copper based FSS.

## 5. CONCLUSIONS

We have showed that in order to have 'good' screening performance (better than -20db) the transparent conducting material should be around 1-2 Ω/□ or even lower if this is possible without compromising the transparency. It is our contention that lower ITO conductivity is achievable and future investigation will establish how cost effective this can be.

## 6. REFERENCES


1. E.A. Parker, C. Antonopoulos and N.E. Simpson , "Microwave Band FSS in Optically Transparent Conducting Layers: Performance of ring element arrays", Microwave and Optical Technology Letters, vol. 16, no. 2, October 1997, pp. 61-63.
2. C. Mias, C. Tsakonas, N. Prountzos, D.C. Koutsogeorgis, S.C. Liew, C. Oswald, R. Ranson, W.M. Cranton and C.B. Thomas, "Optically transparent microstrip antennas", Proceedings of the IEE Colloquium on Antennas for Automotive Applications, 10 March 2000, London, pp. 8/1-8/5.
3. I. Hamberg, C. G. Granvist, "Evaporated Sn-doped $In_2O_3$ films:Basic optical properties and applications to energy efficient windows", J. Appl. Phys., vol 60, 1983, pp. R123-R159
4. A.L. Dawar, J.C. Joshi, "Review Semiconducting transparent thin films:their properties and applications", J. Mater. Sci., vol 19, 1984, pp.1-23
5. J.R. Bellingham, W.A. Phillips, C.J. Adkins. "Intrinsic performance limits in transparent conducting oxides", J Mater. Sci. Lett., vol 11, 1992, pp. 263-265
6. S. Ray, R. Banerjee, N. Basu, A.K. Batabyal, A.K. Barua, "Properties of tin doped indium oxide thin films prepared by magnetron sputtering", J. Appl. Phys., vol 54, 1983, pp. 3497-3501

## 7. ACKNOWELEDGEMENTS

This work was funded by the Radiocommunications Agency.

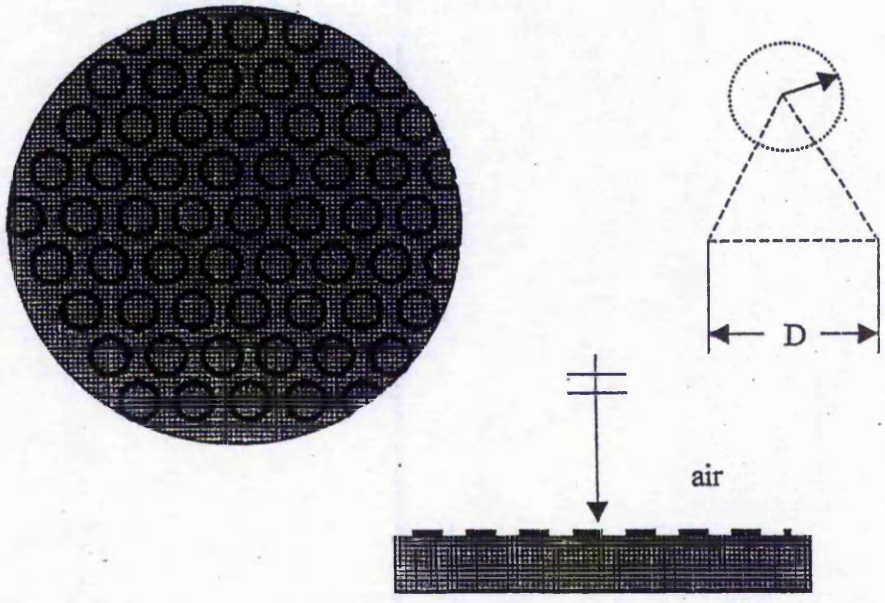


Fig 1 Top and side view of the FSS structure that has been used with D = 0.45 mm and r = 0.15 mm

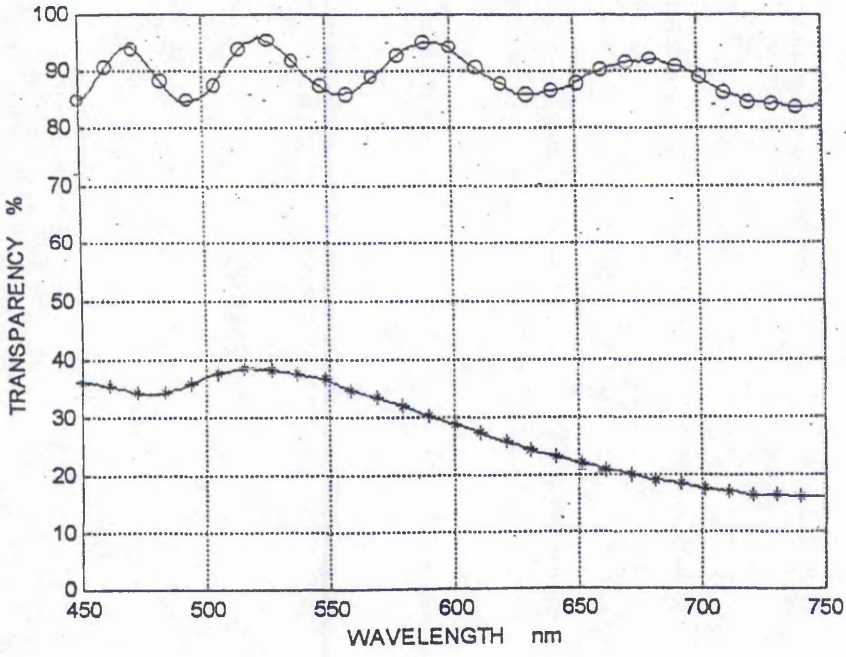


Fig 2 The optical transparencies of the in-house ITO (o) and the commercially available gold thin film (*).

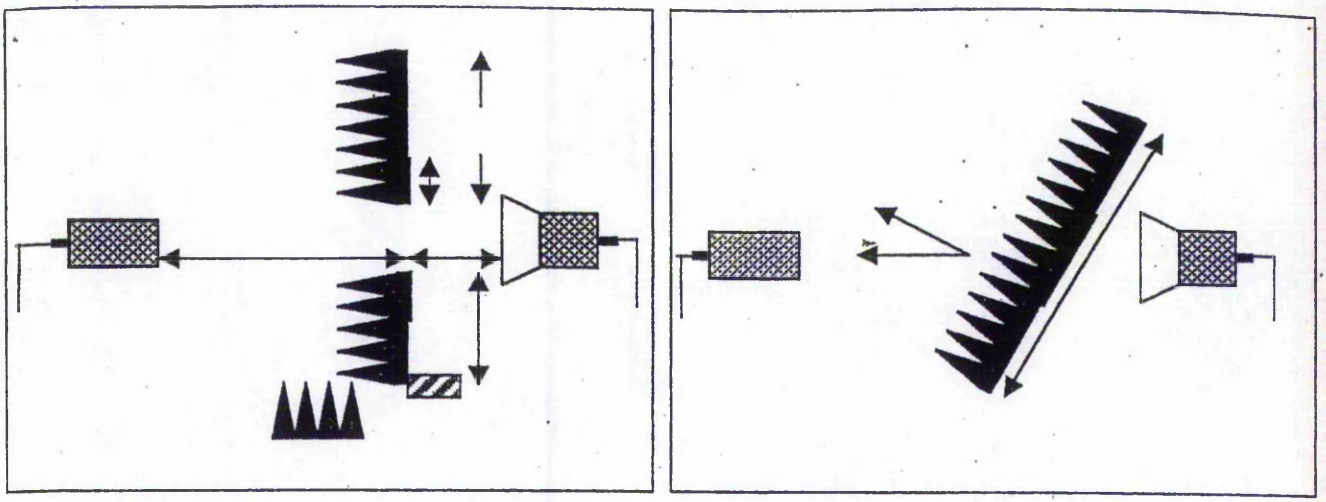

Fig 3 The dimensions of the set up used in this experiments. The width of the absorber block is W= 600 mm.

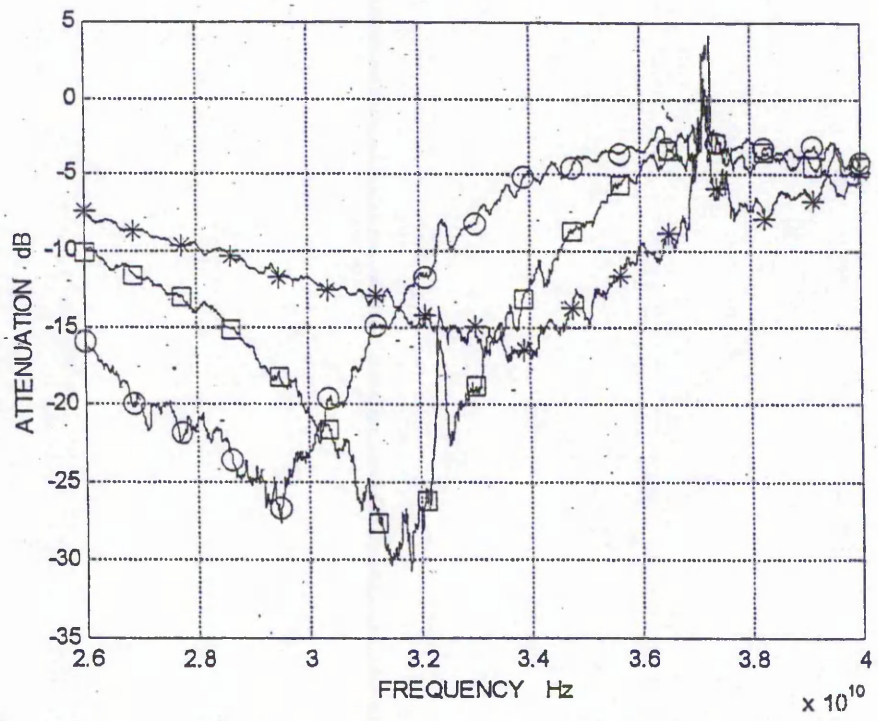


Fig 4 Co-polarisation transmission graphs graphs of Copper FSS (□), ITO FSS (O) and thin Gold film FSS (*).

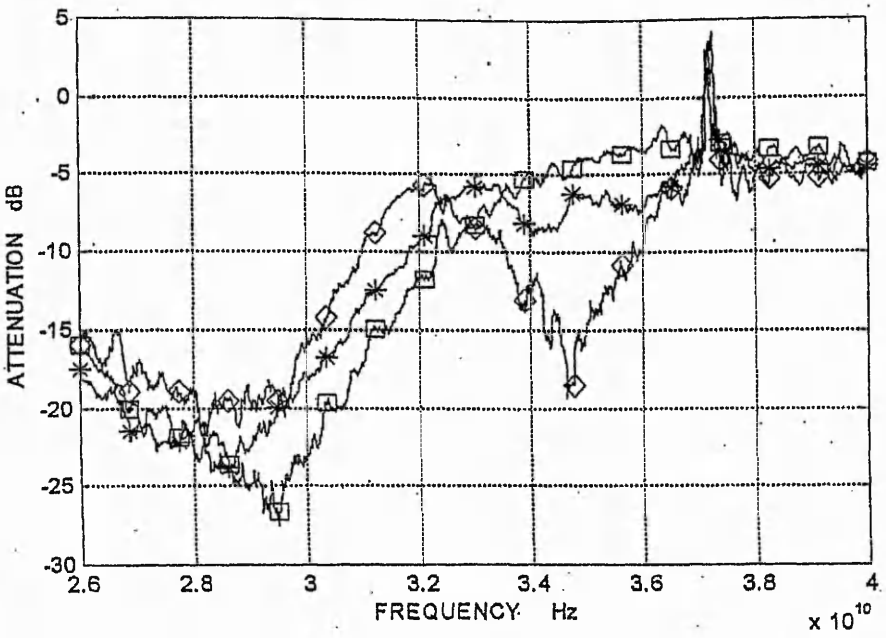


Fig 5 Co-polarisation transmission graphs of ITO FSS at different angles of plane wave incidence: θ=0° (□), θ=15° (*), θ=30° (◊).

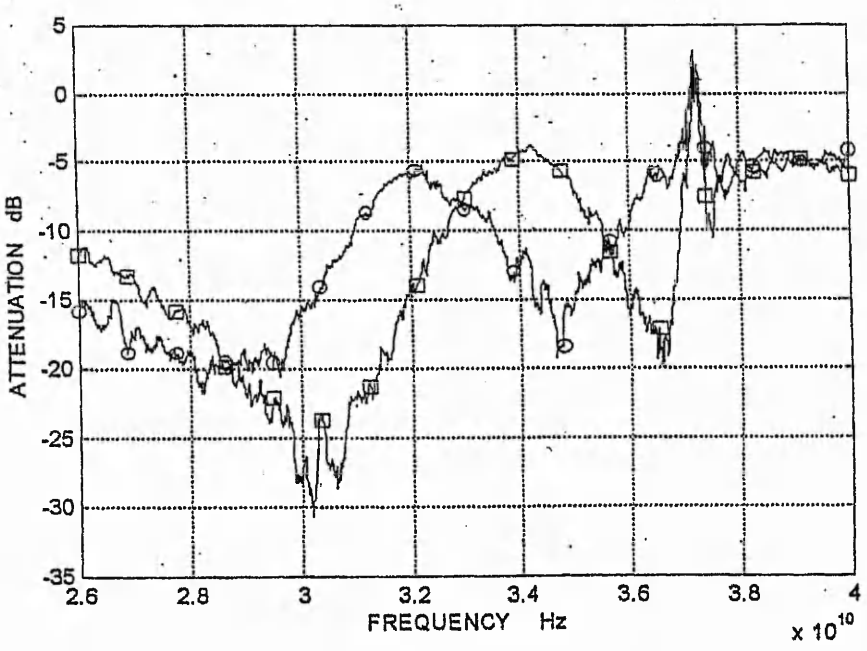


Fig 6 Co-polarisation transmission graphs for Copper (□) and ITO (O) at θ=30° of plane wave incidence.

# OPTICALLY TRANSPARENT MICROSTRIP ANTENNAS

C. Mias, C. Tsakonas, N. Prountzos, D.C. Koutsogeorgis, S.C. Liew, C. Oswald, R. Ranson, W.M. Cranton and C.B. Thomas

## Introduction

Optically transparent antennas have potential applications as receivers/transmitters for wireless automotive applications. They can be incorporated in the car's window or light panels thus preserving car aesthetics. These antennas could also be incorporated in the displays of wireless communications electronic equipment.

To fabricate these antennas, an optically transparent conductor is required with, ideally, conductivity comparable to that of copper and transparency comparable to that of glass. This paper describes a feasibility study carried out on the performance of antennas made from different transparent conductors. These antennas are compared to conventional copper-based antennas and an antenna made from (non-transparent) thin film aluminium. The antenna type chosen was that of a microstrip dipole on a glass substrate (shown in Fig. 1).

The paper considers the fabrication of microstrip antennas made from in-house and commercially available transparent conductors. Measurements of the antennas' radiation pattern, input impedance and VSWR coefficient are presented for comparison purposes.

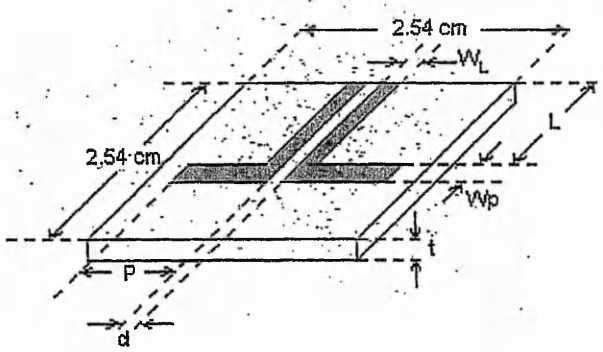


Figure 1: The geometry of the microstrip dipole antenna.

## Fabrication

Five different materials were used in the preparation of the dipole antenna: copper (Cu), aluminium (Al), Indium Tin Oxide (ITO), silver (Ag) and gold (Au). Whether a coating is transparent or not largely depends on its thickness. All dipoles are situated on a glass substrate of thickness t=0.7 mm. The relative permittivity and loss tangent of the glass at 1MHz (manufacturer's data) are 5.84 and 0.001 respectively.

Department of Electrical and Electronic Engineering, Nottingham Trent University, Burton Street, Nottingham, NG1 4BU, UK

Although copper is not a transparent material it was included for comparison and evaluation purposes since it gives the best characteristics due to its high conductivity. Two copper antennas were generated using a cut and paste technique and an etch-resist transfer technique. In the latter case the antenna was generated from a copper foil which was attached to the glass substrate. A third copper antenna was fabricated using a standard printed circuit board (PCB) etching technique on a glass fabric epoxy resin substrate of relative permittivity 2.7 and loss tangent 2.7 at 1 MHz (according to the manufacturer's data sheet). The dimensions of this substrate are close to those of the glass substrate.

The in-house aluminium antenna was prepared in the optoelectronics lab using the thermal evaporation method. An aluminium wire is placed in a tungsten basket in a vacuum chamber. Passing a current through the tungsten basket leads to the thermal evaporation of aluminium. The glass substrate is positioned above the basket thus ensuring deposition of a thin film. Film thickness is controlled with the aid of a crystal thickness monitor. No subsequent heat treatment of the film is performed. The microstrip aluminium antenna geometries are produced using two methods. The first involves a polyester mask being placed on top of the glass substrate, allowing deposition only at the desired surface area. Wet chemical etching (outlined below) is the second method. The aluminium antenna referred to in this paper was produced by the latter technique.

Transparent ITO antennas are produced from in-house and commercially available ITO coatings using an in-house aperture mask and wet chemical etching respectively. Both ITO coatings are generated by a sputtering method. The in-house ITO fabrication process begins with loading the glass substrate into the main chamber through a load arm. The chamber is kept at a constant low pressure to minimise contamination. An ITO target is situated on the magnetron electrode. A RF voltage is applied between the electrode and the substrate. A non-reactive gas is used to provide positively charged ions which are accelerated in the applied field. The charged ions, upon hitting the target, transfer their momentum to the constituent atoms of the target which are ejected forcibly. The target atoms are subsequently deposited on the glass substrate situated opposite.

The gold and silver transparent films are produced, commercially, by sputtering. Both films were patterned using wet chemical etching as in the case of the ITO above. The wet chemical etching process involves depositing a positive photoresist on the coating and spinning the latter to achieve a uniform photoresist layer. The sample is baked in order to dry the resist for proper ultraviolet exposure. Post exposure bake is performed to harden the desired pattern so as to prevent it being 'washed' away during the development process. After the development process, the sample is baked again to further strengthen the desired photoresist pattern. An acidic etch is then employed to remove the unnecessary coating. The thin film pattern of the commercial coatings is coated on a synthetic material and is subsequently attached to the glass substrate.

**Antenna measurements**

Ideally, the conductivity of the transparent conductors should be measured at 10 GHz. Currently, we present typical values of the direct current left and right arm resistance of the dipoles. These are listed in Table 1. The resistance values include the coaxial connector and bonding resistance. Table 1 also depicts approximate values of the thickness of the thin film antennas that we measured using a diamond tipped profilometer. The optical transparency of the various transparent coatings employed is shown in Fig. 2. It was obtained using an optical spectrometer that sweeps over the 200nm-1100nm wavelength range. The first sweep is done over the free space (or glass) and the second sweep is done with the specimen in place between transmitter and receiver. From both measurements a percentage value of the optical transparency of the coatings is obtained. The microstrip dipole antenna under investigation has the following dimensions (see Fig.1): P=8.43mm, $W_p$=1.22mm, $W_L$=1.22mm, L=13.48mm, d=0.9mm. The dimensions were chosen in an attempt to have an antenna with operation around the 10 GHz region. Only the in-house ITO antenna is not fitting these

dimensions because of inaccuracies in the in-house aperture mask (P=8.7mm, $W_p$=1.5mm, $W_L$=1.5mm, L=15.3mm, d=1.1mm). The latter antenna also contained a defect in one of its arms. It was decided though to be included in the results due to its satisfactory performance. Note also that, in bonding the coaxial connector to each transparent antenna, part of the antenna's feeding

Table 1: Transparent antenna parameters

| Material | Film Thickness (Å) | Arm resistance (Ω) |
|---|---|---|
| ITO-IH | 850 | L:193, R:110 |
| ITO | 850 | L:720, R:740 |
| Silver | 530 | L:75, R:68 |
| Gold | 500 | L:158, R:213 |

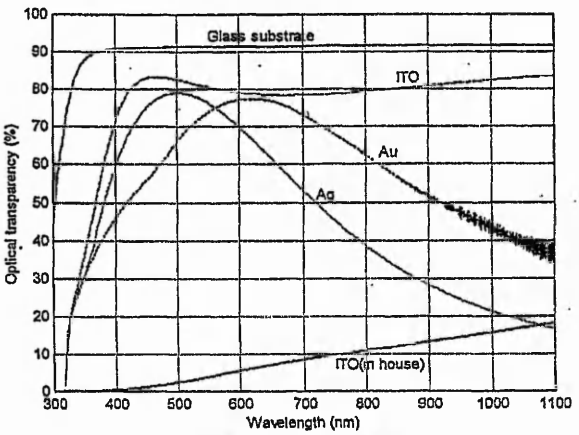


Figure 2: Film Transparency.

line was replaced by a better (than the coating) conductor. In the future we will aim to standardise this conductor's length. A network analyser was used to obtain the VSWR and input impedance results plotted in Figs. 3 and 4. All antennas exhibited a minimum VSWR close to 10GHz. Evaluation of the power loss due to the glass substrate and the conductivity of the transparent coatings at 10GHz require further investigation. In an attempt to identify the amount of radiating power from the antennas, the far-field (40 cm) radiation patterns were obtained at the frequency of minimum VSWR of each antenna. The measurements were made using an in-house built measurement setup. The preliminary measurements of the E- and H-plane co-polarisation antenna power radiation patterns [1] are shown in Figures 5 and 6. Figure 7 shows the cross-polarisation antenna power radiation pattern. In the radiation pattern plots, the reference level is –65dBm (thus the correct value is the value indicated in the plots minus 65dBm).

## Conclusion

The E-plane result is expected to have the boresight direction along the $\theta=90^\circ$ axis. Instead, the maximum of the lobe is roughly at $30^\circ$ to the right of that axis. Thus, the issue of balanced antenna operation [1] must be addressed as well as the need to perform more accurate radiation pattern measurements. Consequently, the (H-plane) difference in the transmitted power between the ITO antennas and the copper/aluminium antennas is, at certain angles, significant. However, for the Au and Ag coatings, measurements are very close to those of the copper antennas. One may therefore conclude that the transparent coatings (especially Au and Ag) have the potential to be used in antenna production. Continuation of this work concentrates (apart from the issues raised above) on the optimisation of the etching process, the improvement (in conductivity and transparency) of the in-house developed ITO and the development of transparent aluminium and Zinc Oxide.

## References

[1] W.L. Stutzman and G.A. Thiele, *Antenna Theory and Design*, 2nd ed., Wiley, 1998.

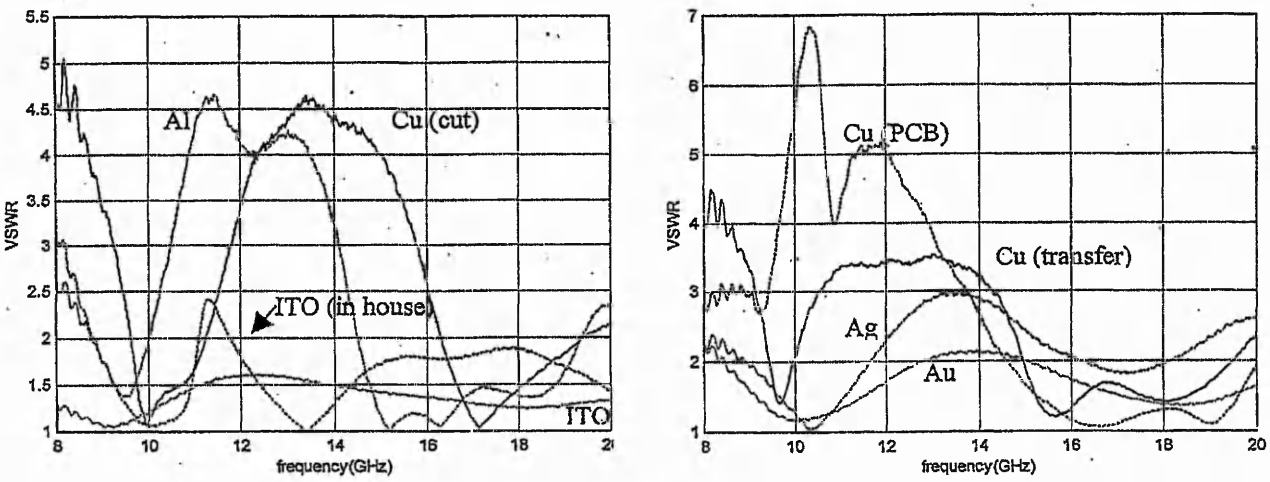


Figure 3: Antenna VSWR versus frequency.

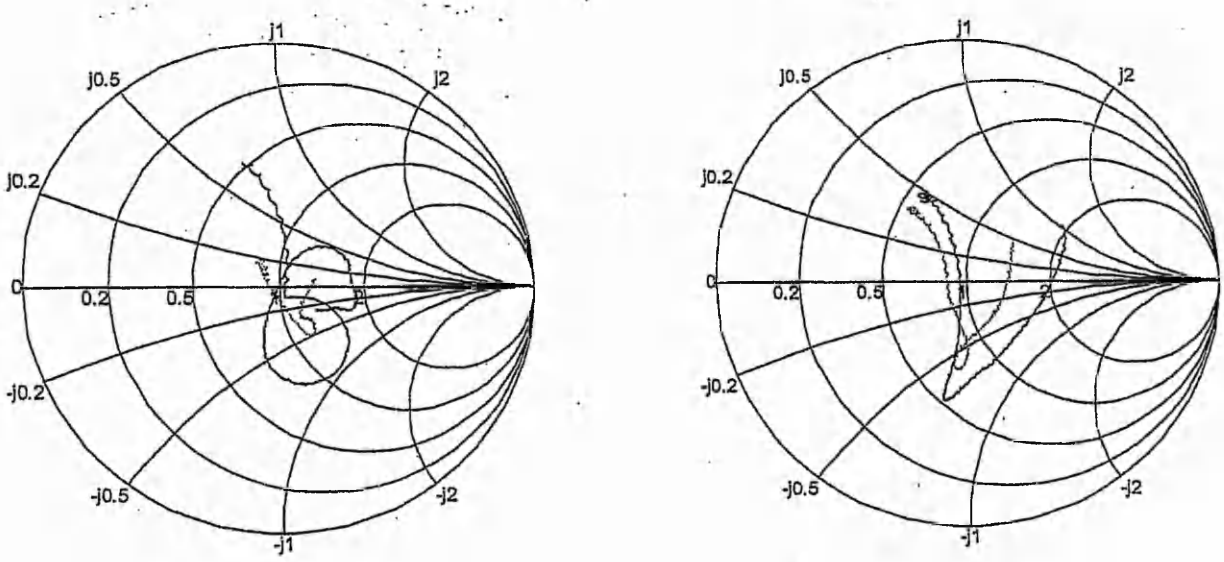


ITO: dashed line
ITO (in house): solid line

Au: dashed line
Ag: solid line

Figure 4: Smith Chart representation of the antenna input impedance for the frequency range 8-20 GHz.

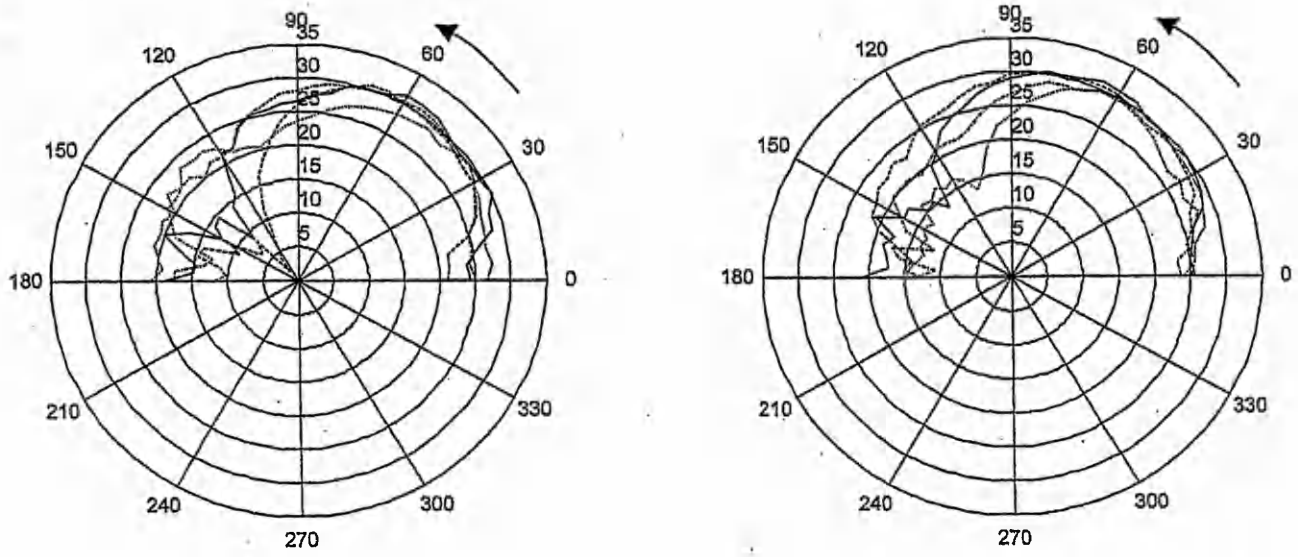


Cu (cut): solid line
Al: dash-dot line
ITO: long-dash line
ITO (in house): short-dash line

Cu (transfer): solid line
Ag: dash-dot line
Cu (PCB): long-dash line
Au: short-dash line

Figure 5: E-plane antenna power radiation pattern. Radiation pattern units in dBm with a reference level of –65 dBm.

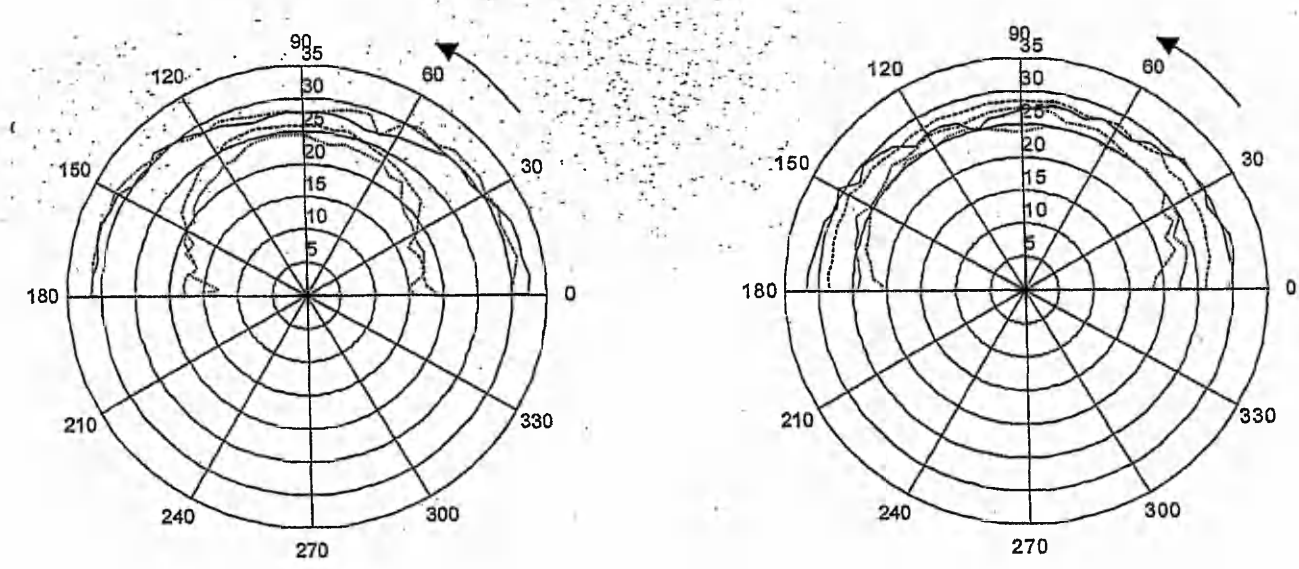


Cu (cut): solid line
Al: dash-dot line
ITO: long-dash line
ITO (in house): short-dash line

Cu (transfer): solid line
Ag: dash-dot line
Cu (PCB): long-dash line
Au: short-dash line

Figure 6: H-plane antenna power radiation pattern. Radiation pattern units in dBm with a reference level of –65 dBm.

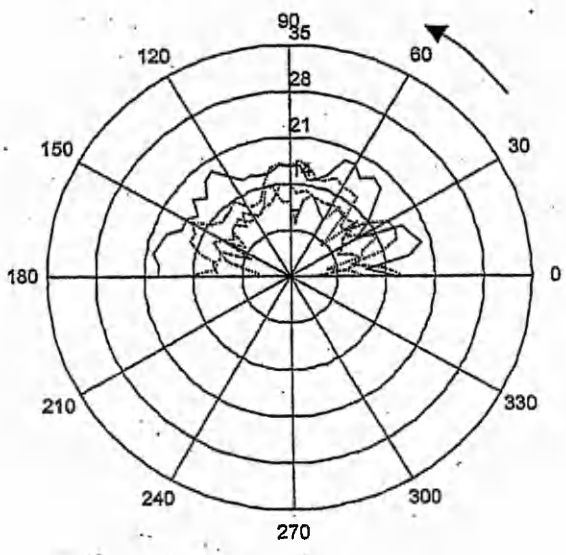


Cu (cut): solid line
Al: dash-dot line
ITO: long-dash line
ITO (in house): short-dash line

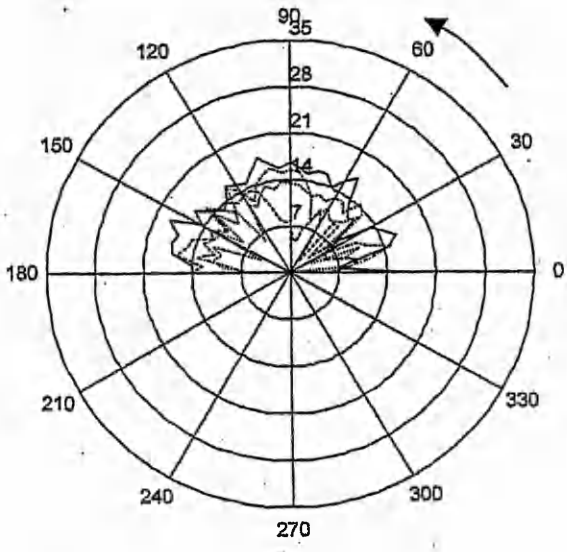


Cu (transfer): solid line
Ag: dash-dot line
Cu (PCB): long-dash line
Au: short-dash line

Figure 7: Cross-polarisation antenna power radiation pattern. Radiation pattern units in dBm with a reference level of –65 dBm.